



Intracellular Microenvironment Triggered Co-delivery of Anticancer Drugs and Genes

Seonho Yun

Master of Engineering (Chemical)

A thesis submitted for the degree of Doctor of Philosophy

School of Chemical Engineering and Advanced Materials
Faculty of Engineering, Computer and Mathematical Sciences
The University of Adelaide

July 2019

I dedicate this thesis to my beloved wife Younsun Joelle Lee.

Table of Contents

Table of Contents	iii
List of Tables	ix
List of Schemes	x
List of Figures.....	xi
List of Supporting Figures	xv
Abstract.....	xviii
Declaration.....	xx
Acknowledgement.....	xxi
Chapter 1. Introduction	1
1.1 Background	1
1.2 Aim and Objectives.....	3
1.3 Thesis outline	3
1.4 Key contributions of this thesis	5
Chapter 2. Rationale design of doxorubicin and gene drug co-delivery systems for enhanced anticancer efficacy and efficiency.....	8
Abstract	11
2.1 Introduction	13
2.2 DOX as an anticancer drug	14
2.2.1 Merits of DOX in anticancer therapy	14
2.2.2 Defects of DOX in anticancer therapy	18
2.3 Supplementary gene drugs	23
2.3.1 microRNA-21 inhibitor as a sub-drug.....	24
2.3.2 ATP aptamer as a sub-drug	25
2.4 Enhance therapeutic efficiency using delivery carriers.....	25

2.4.1 Before administration	28
2.4.2 Blood circulation	35
2.4.3 Extracellular microenvironment	39
2.4.4 Intracellular microenvironment	44
2.4.5 Traceability over delivery course	53
2.5 Summary and Future perspectives	55
Acknowledgement.....	56
References	57
Chapter 3. Microenvironment-degradable multifunctional microgels for selective co-delivery of DOX and miRNA-21 inhibitor for enhanced anticancer therapy	73
Abstract	76
3.1 Introduction	77
3.2 Methods.....	80
3.2.1 Materials	80
3.2.2 Synthesis of PSeH microgels.....	81
3.2.3 Co-drug loading and release	83
3.2.4 <i>Ex vivo</i> multi-function assays	84
3.2.5 Cell culture	86
3.2.6 Cellular uptake assays	86
3.2.7 <i>In vitro</i> biocompatibility assays of microgels without co-drugs	87
3.2.8 <i>In vitro</i> cell viability assays for the efficacy of PSeHD/miR-21i/HA.....	88
3.3 Results and Discussion.....	88
3.3.1 Synthesis of PSeH microgels.....	88
3.3.2 Controlled loading and releasing of DOX and miR-21i.....	91
3.3.3 <i>Ex vivo</i> multi-function assays	95
3.3.4 Cellular uptake assays	97

3.3.5 Biocompatibility evaluation	99
3.3.6 Synergistic therapeutic effect on metastatic breast cancer cells	101
3.4 Conclusion.....	105
Acknowledgement.....	106
References	107
Supporting Information	113
Chapter 4 Design of dual-locked smart microgels for effective co-delivery of DOX and miRNA-21 inhibitor to multidrug resistant cancer cells	122
Abstract	125
4.1 Introduction	126
4.2 Material and methods	128
4.2.1 Materials	128
4.2.2 Synthesis of DOX loaded microgels (PSeHD-SeSeP)	130
4.2.3 <i>Ex vivo</i> DOX releasing assays	133
4.2.4 miR-21i loading and <i>ex vivo</i> releasing assay	134
4.2.5 Characterization of PSeHD-SeSeP/miR-21i/HA delivery systems	134
4.2.6 Culture of cell lines (HEK293T, MDA-MB-231-S, MDA-MB-231-R)	135
4.2.7 Cellular uptake assays	136
4.2.8 Biocompatibility evaluation	137
4.2.9 Viability assays on DOX sensitive or resistant cancer cells.....	138
4.3 Results and Discussion.....	139
4.3.1 Synthesis of DOX loaded microgels (PSeHD-SeSeP)	139
4.3.2 Exceptional control of DOX release.....	141
4.3.3 miR-21i loading and <i>ex vivo</i> releasing assay.....	144
4.3.4 Characterization of PSeHD-SeSeP/miR-21i/HA delivery system	145
4.3.5 DOX resistance of MDA-MB-231-R	147

4.3.6 Cellular uptake assays	148
4.3.7 Evaluation on side effect of co-delivery system.....	150
4.3.8 Comparison on viability of PSeHD-SeSeP/miR-21i/HA on DOX sensitive and resistant cancer cells	153
4.4 Conclusion.....	155
Acknowledgement.....	156
References	157
Supporting information	161
Chapter 5 Developing traceable nanomedicines of doxorubicin, miR-21 inhibitor and ATP aptamer for enhanced therapeutic treatment on multidrug resistant cancers	167
Abstract	170
5.1 Introduction	171
5.2 Experimental	175
5.2.1 Materials	175
5.2.2 Synthesis of DOX loaded microgels (PSeSeD).....	175
5.2.3 <i>Ex vivo</i> DOX release and biodegradation.....	178
5.2.4 miR-21i and Apt loading (PSeSeD/miR-21i/Apt) and release.....	178
5.2.5 HA coating (PSeSeD/miR-21i/Apt/HA) and characterization	179
5.2.6 Cell culture	179
5.2.7 Intracellular uptake of PSeSeD/FAM-miR/Apt/HA and localization of DOX	180
5.2.8 Biocompatibility of PSeSe microgels and PSeSeD/miR-21i/Apt/HA	181
5.2.9 Anticancer efficacy PSeSeD/miR-21i/Apt/HA against MDA-MB-231 cell lines	182
5.2.10 ATP aptamer efficacy	183
5.2.11 Anticancer synergy of PSeSeD/miR-21i/Apt/HA on cancer cells with MDR	184
5.3 Results and Discussion.....	184
5.3.1 Synthesis of PSeSeD microgels.....	184
5.3.2 Cytosol responsive DOX release and biodegradation of PSeSeD.....	187

5.3.3 miR-21i and Apt loading (PSeSeD/miR-21i/Apt) and release	188
5.3.4 HA surface coating to produce PSeSeD/miR-21i/Apt/HA.....	190
5.3.5 Cellular uptake of PSeSeD/FAM-miR/Apt/HA and release of therapeutic agents	190
5.3.6 Cytotoxicity of PSeSeD/miR-21i/Apt/HA with normal cells.....	193
5.3.7 Therapeutic effect of PSeSeD/miR-21i/Apt/HA on metastatic breast cancer cells	195
5.3.8 Effect of ATP on therapeutic effects on multidrug resistant cancer cells	196
5.3.9 Therapeutic synergy on multidrug resistance cancer cells by PSeSeD/miR-21i/Apt/HA	200
5.4 Conclusion.....	202
Acknowledgement.....	203
References	204
Supporting information	208
Chapter 6 DEVDC peptide conjugated microgels for intracellular-responsive sequential releasing of miRNA-21 inhibitor and doxorubicin for enhanced therapy to multidrug resistant cancers	215
Abstract	218
6.1 Introduction	219
6.2 Experimental	224
6.2.1 Materials	224
6.2.2 Synthesis of PSeDEVDCD complexes.....	225
6.2.3 <i>Ex vivo</i> release of DOX and miR-21i	227
6.2.4 HA receptor mediated endocytosis.....	229
6.2.5 <i>In vitro</i> cell viability assays on normal and cancer cells	231
6.2.6 <i>In vitro</i> trace of miR-21i and DOX sequential release	231
6.2.7 Therapeutic effect of PSeDEVDCD/miR-21i/HA on multidrug-resistant MDA-MB-231-R cancer cells	232
6.3 Results and Discussion.....	233

6.3.1 Synthesis of PSeDEVDCD.....	233
6.3.2 <i>Ex vivo</i> releasing of DOX and miR-21i.....	236
6.3.3 HA receptor mediated endocytosis.....	239
6.3.4 <i>In vitro</i> cell viability assays on normal and DOX sensitive cancer cells	241
6.3.5 MDR reverse-triggered sequential releasing.....	243
6.3.6 Therapeutic effects on multidrug-resistant cancer cells	247
6.4 Conclusion.....	250
Acknowledgement.....	251
References	252
Supporting Information	256
Chapter 7. Conclusion and Recommendation.....	265
7.1 Conclusion.....	265
7.2 Future directions.....	267

List of Tables

Table 2.1 Summary of required essential factors and functional conditions of ideal delivery vectors	27
Table 3.S1 Comparison on the DOX and miR-21i loading capability of various complexes, PSeH5%D, PSeH10%D (PSeHD), PSeH20%D ($P < 0.05$).....	114
Table 3.S2 Comparison on the anticancer therapeutic performance of various DOX systems from their relative IC_{50} values on MDA-MB-231 cells.	114
Table 5.S1 Characterizations of synthesized microgels of PSeSeD, PSeSeD2X, PSeSeDBHQ, PSeSe, and Degrade-P.	209
Table 6.S1 Comparison on the therapeutic efficiency of sequential and simultaneous release of miR-21i and DOX in various co-drug delivery systems via relative IC_{50} value of free DOX to co-delivery system on MDA-MB-231-R cells.....	257
Table 6.S2 Comparison on the anticancer efficiency of various therapeutic systems via relative IC_{50} value of free DOX to therapeutic system on MDA-MB-231-R cells	258

List of Schemes

- Scheme 3.1** Schematic representation of the developed microenvironment-degradable multifunctional PSeHD/miR-21i/HA for selective delivery of DOX and miR-21i..... 79
- Scheme 3.2** (A) Synthesis of PSeH microgels as co-delivery carriers, (B) loading of DOX (PSeHD), miR-21i (PSeHD/miR-21i) and HA (PSeHD/miR-21i/HA) to PSeH microgels.... 90
- Scheme 4.1** Scheme description for the DOX and miR-21i co-loading and co-delivery to cancer cells: (A) DOX-conjugated PEI microgel via diselenide and hydrazone bonds (PSeHD-SeSeP) and miR-21i loading and HA surface coating to the PSeHD-SeSeP, (B) co-delivery system of PSeHD-SeSeP/miR-21i/HA, (C) HA receptor-mediated endocytosis, (D) PSeHD-SeSeP/miR-21i/HA in endosome/lysosome, (E) hydrazone bond cleaved in acidic lysosome and endosomal escape, and (F) diselenide bond cleaved in glutathione-concentrated cancer cytosol and release of DOX and miR-21i. 129
- Scheme 4.2** Scheme of diselenide crosslinked PEI800 microgels with DOX loading via dual-locks of hydrazone and diselenide bonds..... 133
- Scheme 5.1** (A) Scheme for entire process of the traceable tri-delivery system, PSeSeD/miR-21i/Apt/HA: synthesis, HA receptor-mediated endocytosis, GSH-triggered nanomedicine degradation in cytosol to release loaded DOX, miR-21i and Apt, isolating ATP by Apt, and inhibiting miR-21 by miR-21i. (B) Scheme for tracing intracellular DOX localization by quenching the fluorescence in PSeSeDBHQ but emitting fluorescence in GSH-rich cytosol. 174
- Scheme 5.2** Synthesis of PSeSeD by crosslinking PEI800 and DOX with –SeSe- 186
- Scheme 6.1** (A) Scheme on the synthesis of PSeDEVDCD as a co-delivery carrier of DOX and miR-21i and the release of cysteine-DOX in the presence of caspase-3, (B) Scheme on the synthesis of PSeBHQDEVDCD as a traceable co-delivery carrier before and after releasing cysteine-DOX, where DOX fluorescence is quenched before release and is recovered after release. 222
- Scheme 6.2** Schematic representation of PSeDEVDCD/miR-21i/HA as effective nanomedicines for intracellular sequential release of miR-21i being triggered by the cytosol GSH of MDR cells and DOX release to re-sensitized MDR cells with activated caspase-3. MDR cell is reversed to re-sensitized cells through the inhibition of miR-21 by miR-21i... 223

List of Figures

- Figure 2.1** Chemical structure of doxorubicin (DOX) consisting of a tetracyclic ring, a glycoside-linked daunosamine sugar and functional groups. 14
- Figure 2.2** DOX-induced apoptotic pathways. The intrinsic pathway indicates the mitochondrial pathway initiated by Topo II intercalation or ROS-induced DNA damage in the nucleus. The extrinsic pathway indicates the death receptor-mediated pathway that is initiated by ROS production by DOX in cytosol. Casp represents caspase..... 17
- Figure 2.3** Pro-survival pathways: PI3K/Akt/mTOR, RAS/RAF/MAPK and JAK/STAT, and roles of miRNA-21 (miR-21) in downregulating multiple inhibitors of the survival pathways. 20
- Figure 2.4** Cellular uptake of free DOX without any carrier to normal organs and tumors via systemic administration, reproduced from [50] with copyright..... 23
- Figure 2.5** Schematic description of the delivery course of MSNs loaded with DOX and gene via IV injection: loading, blood circulation, extravasation, active target-mediated endocytosis, endosomal escape, and controlled release of the drugs, reused from [128] with copyright. ... 26
- Figure 2.6** Illustration of types of non-viral vectors and a rough mechanism of loading and release of anticancer drugs via liposome, reused from [75] with copyright. 29
- Figure 2.7** Schematic DOX loading mechanisms. Upper left: electrostatic interaction with DOX and HA as well as miRNA and chitosan, reused from [78] with copyright. Lower left: hydrophobic interaction of DOX with the hydrophobic core of polymer micelles, reused from [116] with copyright. Right: physical adsorptions of DOX to AuNPs, reused from [112] with copyright. 32
- Figure 2.8** Intracellular stimuli-cleavable linkers. Upper left: acid-cleavable hydrazone bond and lysosomal enzyme cathepsin B-cleavable GFLG peptide linker, reused from [122] with copyright. Upper right: acid-cleavable acetal crosslinker, cited from [194] (<https://pubs.acs.org/doi/10.1021/mz5004097>) with copyright, further permission directed to ACS. Lower left: weak acid-cleavable benzoic imine bond used in self-gatekeeping, reused from [196] with copyright. Lower right: disulfide bond crosslinkers, reused from [200] with copyright. 47
- Figure 2.9** Methods to trace carriers and drug release. Left: label-free autofluorescent polymer nanogels and degradation-induced fluorescence-off, reused from [212] with copyright. Upper right: FRET-on between QDs loaded with DOX and FRET-off when DOX is released, reused from [216] with copyright. Lower right: quenching of DOX via ACQ when conjugated to TPE and fluorescence-on of DOX after cleaving the hydrazone bond, reused from [217] with copyright. 52

Figure 3.1 (A) Hydrazone bond cleavage to determine DOX release from PSeHD microgels at pH 5.0, 6.5 and 7.4 buffer solutions after 48 h. ($P < 0.05$, $n = 3$), (B) Loading of miR-21i to PSeHD at different N/P ratios (1, 2, 4 and 6), PEI25K as the reference, (C) Comparison of miR-21i release after incubation in 20 mM GSH for 24 h.....92

Figure 3.2. (A) Zeta potentials of PSeHD, PSeHD/miR-21i at 10 N/P and PSeHD/miR-21i/HA at 5 w/w ratio of HA to miR-21i ($P < 0.05$, $n = 3$). (B) Protein adsorption by PSeHD/miR-21i/HA (5 w/w ratio of HA to miR-21i) against BSA with PEI800 and Lipofectamine2000 as controls ($n = 3$), (C) *ex vivo* biodegradability of PSeHD/miR-21i/HA by measuring hydrodynamic sizes in PBS 7.4 with 0 M, 10 μ M and 20 mM GSH over 168 h. ($n = 3$)94

Figure 3.3 Qualitative cellular uptake under a confocal laser scanning microscope (CLSM): (A) MDA-MB-231 cells without delivery carriers, (B) MDA-MB-231 cells with delivery carriers loaded with FAM-miR and DOX (PSeHD/FAM-miR/HA), (C) HA pre-treated MDA-MB-231 cells with the delivery carriers loaded with FAM-miR and DOX (PSeHD/FAM-miR/HA), scale bar 15 μ m.....98

Figure 3.4 Cell viability, (A) HEK293T survival rate against various carriers (PEI800, PSeH, lipofectamine2000 and PEI25k) before loading DOX ($n = 4$), (B) HEK293T survival rates against free DOX and DOX loaded PSeHD and PSeHD/miR-21i (10 N/P) ($n = 4$), (C) HEK293T survival rates against PEI800, PSeH and degraded fragments of PSeH after incubation in 20 mM GSH for 24 h ($P < 0.05$, $n = 4$), (D) MDA-MB-231 survival rate against free DOX, PSeHD and PSeHD/miR-21i (10 N/P) ($n = 4$), (E) Comparison of cell survival rates of HEK293T cells and MDA-MB-231 cells against PSeHD/miR-21i and PSeHD/miR-21i/HA ($n = 3$) (10 N/P and 5 w/w ratio of HA to miR-21i), and (F) IC_{50} values (μ g mL⁻¹) of free DOX, PSeHD and PSeHD/miR-21i/HA. ($P < 0.0001$, $n = 4$) 103

Figure 4.1 *ex vivo* DOX releasing assays, DOX releasing from (A) PSeHD at pH 7.4, 6.5, and 5.0 with 0 M GSH over 48 h, (B) PSeHD-SeSeP at pH 7.4, 6.5, and 5.0 with 0 M GSH, (C) PSeHD-SeSeP at pH 7.4 with 0 M GSH, 10 μ M GSH, and 20 mM GSH over 48 h, and (D) PSeHD-SeSeP at pH 7.4 with 0 M GSH and at sequential condition of 0 M GSH at pH 5.0 for 6 h then 20 mM GSH at pH 7.4, ($P < 0.05$, $n = 3$)..... 143

Figure 4.2 Agarose gel retardation assays for (A) miR-21i loading to PSeHD-SeSeP at N/P ratios from 1 to 6, where naked miR-21i and its polyplexes with PEI25k at the N/P ratio 1 are used as negative control and positive control. (B) miR-21i releasing profiles from the PSeHD-SeSeP/miR-21i at a N/P ratio 10 after incubation with 20 mM GSH for 48 h and 72 h. 144

Figure 4.3 (A) Comparison on the zeta potentials of PSeHD-SeSeP, PSeHD-SeSeP/miR-21i and PSeHD-SeSeP/miR-21i/HA, ($n=4$), (B) Hydrodynamic sizes of PSeHD-SeSeP/miR-21i/HA at pH 7.4 with different GSH concentrations of 0, 10, and 20 mM, and the sequential condition of pH 5.0 and 0 M GSH for 4 h then pH 7.4, 20 mM GSH, ($n=4$)..... 146

Figure 4.4 MDA-MB-231 cellular uptake assays of PSeHD-SeSeP/FAM-miR/HA system by confocal laser scanning microscopy (CLSM), (A) Cells only without the PSeHD-SeSeP/FAM-miR/HA, (B) Cells with PSeHD-SeSeP/FAM-miR/HA system in low magnification and (C) in high magnification, and (D) HA pre-treated cells with the PSeHD-SeSeP/FAM-miR/HA. . 149

Figure 4.5 Cell viability, (A) HEK293T survival rate against microgel carriers without loading DOX (PSeSe, PSeH and degraded microgel fracture products), PEI25k as a negative control and Lipofectamine2000/PEI800 as positive controls, (n = 4), (B) HEK293T survival rate against delivery carriers with DOX loading (PSeHD-SeSeP, PSeHD-SeSeP/miR-21i and PSeHD-SeSeP/miR-21i/HA) and free DOX as a negative control, (n = 12), (C) MDA-MB-231-S survival rate against free DOX, PSeHD-SeSeP/HA and PSeHD-SeSeP/miR-21i/HA, (n = 12), (D) MDA-MB-231-R4w survival rate against free DOX, PSeHD-SeSeP/HA and PSeHD-SeSeP/miR-21i/HA, (n = 4), (E) MDA-MB-231-R12w survival rate against free DOX, PSeHD-SeSeP/HA and PSeHD-SeSeP/miR-21i/HA, (n = 8), and (F) IC50 value, DOX concentration for half cell death, of free DOX, PSeHD-SeSeP/HA and PSeHD-SeSeP/miR-21i/HA against MDA-MB-231-S, MDA-MB-231-R4w, and MDA-MB-231-R12w cells, (n = 4). 152

Figure 5.1 (A) DOX releasing profiles from PSeSeD at pH 7.4 and different concentrations of GSH over 144 h (n = 4). (B) Hydrodynamic size distributions of PSeSeD at pH 7.4 and various GSH concentrations (n = 4). Gene of miR-21i and Apt loading assay via agarose gel electrophoresis for (C) PSeSeD at N/P ratios of 1, 2, 4, 6 and 8 with naked gene as a control, and (D) PEI25kDa (P25k) at N/P ratios (0.5, 1, 2 and 3) and PEI800Da (P800) at N/P ratios (4, 6, 8 and 10) as the references. (E) Gene of miR-21i and Apt releasing profiles of the PSeSeD/miR-21i/Apt (N/P 10) after incubation with 20 mM GSH at pH 7.4 for 72 h..... 188

Figure 5.2 Tracing cell intake of PSeSeD/FAM-miR/HA via CLSM imaging of (A) MDA-MB-231 cells without PSeSeD/FAM-miR/HA (scale bar 20 μm), (B) MDA-MB-231 cells with PSeSeD/FAM-miR/HA (scale bar 15 μm), (C) HA pre-treated MDA-MB-231 cells with PSeSeD/FAM-miR/HA (scale bar 10 μm). Cellular uptake tracing via flow cytometer of (D) MDA-MB-231 cells without PSeSeD/FAM-miR/HA as a control and (E) MDA-MB-231 cells with PSeSeD/FAM-miR/HA. (F) Tracing DOX release from PSeSeDBHQ/FAM-miR/HA to MDA-MB-231 cells via flow cytometer over 4 and 12 h, (MDA-MB-231 cells without PSeSeDBHQ/FAM-miR/HA as a control). 192

Figure 5.3 (A) Cell viability assays of PEI25k as negative control, PEI800 as positive control, PSeSe and Degrade-P on HEK293T cells after administration for 48 h (n = 4). (B) Cell viability assays of PSeSeD/miR-21i/Apt/HA on HEK293T after 48 h administration (n = 8) with free-DOX as negative control. (C) Anticancer effects of PSeSeD/miR-21i/Apt/HA on MDA-MB-231 after 48 h administration (n = 12) 195

Figure 5.4 (A) Cell viability assay of DOX with diverse concentrations on multidrug-resistant MDA-MB-231-R cells with various culturing periods of 4 weeks (4 W), 8 weeks (8 W) and 12 weeks (12 W), and DOX-sensitive MDA-MB-231 (231-S) cells, DOX-resistant MDA-MB-231-R (231-R) cells and those cells with ATP aptamer treatment (231-S/Apt and 231-R/Apt), via a spectrofluorophotometer, (n = 3). Tracing MDA-MB-231-R cell localization of DOX released from (C) PSeSeDBHQ/HA for 24 h (scale bar 30 μm), (D) PSeSeDBHQ/HA for 48 h (scale bar 20 μm), (E) PSeSeDBHQ/Apt/HA for 24 h (scale bar 50 μm), (F) PSeSeDBHQ/Apt/HA for 48 h (scale bar 20 μm). Colors of red, cyan, blue and overlaps in the low from 1 to 4 of CLSM images are cell membrane, cell nucleus, DOX and the merged. 198

Figure 5.5 Cell viability assay on anticancer effects of free-DOX, PSeSeD/HA, PSeSeD/Apt/HA, PSeSeD/miR-21i/HA and PSeSeD/miR-21i/Apt/HA on multidrug resistant MDA-MB-231-R cells with (A) the cell survival rate to DOX loaded concentrations (n = 12) and (B) DOX concentration for one half cell death, IC₅₀ value.....201

Figure 6.1 (A) DOX release from the PSeDEVDCD in the presence/absence of caspase-3 (n = 3), (B) ex vivo degradation of PSeDEVDCD via hydrodynamic size measurement in HEPES buffer at pH 7.4 and 0 M GSH, 10 μM and 20 mM GSH (n = 3), (C) miR-21i loading to PSeDEVDCD at various N/P ratios (1, 2, 4, 6 and 8), PEI25k (P25k) N/P of 1 as a positive control and naked miR-21i as a negative control, (D) miR-21i release from the PSeDEVDCD/miR-21i at a 10 N/P in 20 mM GSH after 72 h incubation (right), PSeDEVDCD/miR-21i at a 10 N/P without GSH as positive control (middle) and naked miR-21i as negative control (left).237

Figure 6.2 Cellular uptake images from a CLSM: (A) MDA-MB-231 cells without PSeDEVDCD/FAM-miR/HA (scale bar 30 μm), (B) MDA-MB-231 cells with PSeDEVDCD/FAM-miR/HA (scale bar 20 μm), (C) HA receptor-blocked MDA-MB-231 cells with PSeDEVDCD/FAM-miR/HA (scale bar 20 μm). The low from 1 to 4 are FAM-miR, cell membrane, DOX and the merged.....240

Figure 6.3 Cell viability against free DOX, PSeDEVDCD/HA and PSeDEVDCD/miR-21i/HA (10 N/P) (A) HEK293T survival rates (n = 12) and (B) MDA-MB-231 survival rates (n = 8).242

Figure 6.4 Tracing release of quenched FAM-miR and DOX from PSeBHQDEVDCD/FAM-miR/miR-21i/HA to MDA-MB-231-R cells: (A) CLSM images after 4 h incubation (scale bar 10 μm), (B) CLSM images after 8 h incubation (scale bar 30 μm), and (C) CLSM images after 12 h incubation (scale bar 20 μm). The low from 1 to 4 are FAM-miR, cell membrane, DOX and the merged. (D) quantitative release via flow cytometer, MDA-MB-231-R without PSeBHQDEVDCD/FAM-miR/miR-21i/HA as a control, and MDA-MB-231-R incubated with PSeBHQDEVDCD/FAM-miR/miR-21i/HA for 4, 8, 12 and 24h (FL1 for FAM and FL2 for DOX), (E) graphic presentation of cumulative release of FAM-miR, miR-21i and DOX from PSeBHQDEVDCD/FAM-miR/miR-21i/HA to MDA-MB-231-R cells for 24 h incubation (n = 3).246

Figure 6.5 Viability of multidrug resistant cancer cells MDA-MB-231-R24w in the presence of free DOX, PSeDEVDCD/HA and PSeDEVDCD/miR/HA: (A) cell survival rate (n = 12) (B) IC₅₀ values (n = 12).249

List of Supporting Figures

Figure 3.S1 Raman spectrum of the synthesized diselenide crosslinker (-SeSe-).....	115
Figure 3.S2 FTIR spectra of 3-chloropropionic acid, diselenide crosslinker of (-SeSe-), branched PEI800, and diselenide crosslinked PEI800 microgels (PSeSe).....	115
Figure 3.S3 Conductivity and pH titrations for (A) PEI800 (10 mg) and (B) PSeSe (2.4 mg) at room temperature.....	116
Figure 3.S4 Time dependent size distributions of PSeH microgels in 25 mM DTT aqueous solution at room temperature (n = 3)	116
Figure 3.S5 UV-vis calibration curve of DOX aqueous solutions at the wavelength of 479.5 nm at room temperature.....	117
Figure 3.S6 UV-vis absorbance at 479.5 nm of feed DOX and unloaded DOX after conjugation to PSeH microgels.....	117
Figure 3.S7 Conductivity and pH titration of PSeHD microgels (1.4 mg) at room temperature.....	118
Figure 3.S8 Loading assays of miR-21i (miR) to PSeH20%D at different N/P ratios from 1 to 10, PEI25K at the N/P of 1 as the reference, images from agarose gel electrophoresis.....	118
Figure 3.S9 UV-vis calibration curve for bovine serum albumin (BSA) absorbance at 280 nm and room temperature.....	119
Figure 3.S10 Flow cytometry for quantitative cellular uptake of PSeHD/miR/HA, (A) MDA-MB-231 cells without PSeHD/miR/HA, as a control, (B) MDA-MB-231 cells with PSeHD/miR/HA, and (C) HA pre-treated MDA-MB-231 cells with PSeHD/miR/HA, FL1 and FL2 indicate FAM and DOX respectively.....	119
Figure 3.S11 Ex vivo DOX release in pH 7.4 PBS from PSeHD and PSeHD/miR. (n = 3)	120
Figure 4.S1 Raman spectrum of the diselenide bond crosslinker (-SeSe-).....	162
Figure 4.S2 FTIR spectra of diselenide crosslinker (-SeSe-), branched polyethyleneimine 800 (PEI800), and PEI800 microgels via crosslinking PEI800 with -SeSe-	162
Figure 4.S3 Characterizations of diselenide bond (-SeSe-) crosslinked PEI800 microgels (PSeSe) with (A) zeta potential to compare with that of PEI25k as a golden standard for gene delivery vector and (B) size to confirm diselenide bond cleavage under various glutathione (GSH) concentrations of 0 M, 10 μ M, and 20 mM	163
Figure 4.S4 Conductivity and pH titrations for (A) PSeSe (2.4 mg) and (B) PSeHD-SeSeP (2.65mg), measured at room temperature	163

Figure 4.S5 DOX calibration curve: light absorbance at 479.5 nm wavelength to DOX concentrations	164
Figure 4.S6 Agarose gel retardation assay for miR-21i loading to PSeHD.....	164
Figure 4.S7 Cell viability assays for doxorubicin (DOX) resistance of metastatic breast cancer cells, MDA-MB-231, at every 4 week during incubation with DOX over 12 weeks.....	165
Figure 4.S8 Quantitative MDA-MB-231 cellular uptake assay of PSeHD-SeSeP/FAM-miR/HA delivery systems using flow cytometer, (A) cells without the delivery systems as a control, (B) cells with the delivery systems, and (C) HA-pretreated cells with the delivery systems, FL1 and FL2 represent FAM and DOX	166
Figure 5.S1 Raman spectrum of diselenide crosslinker of –SeSe-	210
Figure 5.S2 FTIR spectra of PEI800, synthesized microgels of PSeSe and PSeSeD.....	210
Figure 5.S3 Calibration curve of free DOX via absorbance at 479.5 nm to various concentrations, observed in UV-vis spectrophotometer	211
Figure 5.S4 Absorbance spectra of PSeSeD and PSeSeDBHQ from 400 to 800 nm wavelength, and their aqueous solution colors in visible light.....	211
Figure 5.S5 Hydrodynamic size measurement of PSeSe microgels in the process of Degrade-P production at pH 7.4 buffer solutions with 20 mM GSH over 72 h and with 0 M GSH as negative control.....	212
Figure 5.S6 Amine content assays via conductivity and pH titration of (A) PSeSeD microgels (2.5 mg) and (B) PSeSe microgels (2.4 mg)	212
Figure 5.S7 Zeta potentials of PSeSeD, PSeSeD/miR/Apt (N/P 10), and PSeSeD/miR/Apt/HA (N/P 10 and 1.5 wt. of HA to PSeSeD), measured in 10 mM NaCl solution at pH 7.4	213
Figure 5.S8 Gene of miR-21i and Apt loading assay via agarose gel electrophoresis for (A) PSeSeD2X, (B) PSeSeDBHQ, and (C) PSeSe microgels	213
Figure 5.S9 Calibration curve of fluorescence intensity of luciferin (ex. 350 and em. 530 nm wavelength) to ATP concentrations, which is detected in a spectrofluorophotometer.....	214
Figure 5.S10 Fluorescence spectra of luciferin with/without ATP in presence of luciferase, measuring a spectrofluorophotometer with excitation at 350 nm wavelength	214
Figure 6.S1 FTIR spectra of diselenide crosslinked PEI microgels (PSeSe), azide group contained PEI microgels (PSeN ₃), DOX conjugated alkyne-ended peptide linker (DEVDCDOX), and DOX conjugated microgels via DEVDC peptide linker (PSeDEVDCD)	259
Figure 6.S2 UV-vis calibration curve of (A) DOX and (B) DEVDCDOX in aqueous solution at the equivalent wavelength of 479.5 nm at room temperature.....	259

Figure 6.S3 UV-vis absorbance spectra and aqueous solution color of (A) DOX·HCl, (B) DEVDCDOX, (C) PSeN₃ microgels, (D) Triethylenetetramine (Trien), (E) mixture of Trien and DEVDCDOX, (F) mixture of Trien and PSeN₃, (G) copper, (H) mixture of copper and PSeDEVDCD, (I) mixture of copper and Trien, (J) mixture of copper, Trien and DEVDCDOX, (K) mixture of copper, Trien and PSeN₃, (L) mixture of copper, Trien and PSeDEVDCD, (M) gentisic acid, (N) mixture of copper, Trien, gentisic acid and PSeDEVDCD, and (O) PSeDEVDCD at room temperature260

Figure 6.S4 UV-vis absorbance spectra of DOX·HCl, BHQ2 conjugated peptide (BHQDEVDC), DOX and BHQ2 conjugated peptide linker (BHQDEVDCDOX), and DOX and BHQ2 conjugated PEI microgels (PSeBHQDEVDCD) at room temperature.....261

Figure 6.S5 Colors of aqueous solution: (A) PSeDEVDCD and (B) PSeBHQDEVDCD, (1) with copper and gentisic acid at the end of copper catalyzed click reaction, (2) with addition of Trien to the mixture of (1), and (3) after purification261

Figure 6.S6 Conductivity and pH titration of PSeDEVDCD microgels (4.5 mg) at room temperature262

Figure 6.S7 Zeta potentials of PSeN₃, PSeDEVDCD, PSeDEVDCD/miR at 10 N/P and PSeDEVDCD/miR/HA at 4-folds weight of HA to miR-21i (miR) (n = 3).....262

Figure 6.S8 DOX resistance of MDA-MB-231-R cells via viability against free DOX after culturing in diluted DOX-incorporated culture medium for 4 W, 8 W, 12 W and 24 W, and 0 W indicates DOX sensitive MDA-MB-231 cells. (n = 12)263

Abstract

Currently, infallible cancer treatment has not been achieved. Doxorubicin (DOX), an active anticancer drug, initiates the apoptotic signaling pathway by intercalating topoisomerase-II, resulting in DNA replication disorder and producing reactive oxygen species that can damage DNA and activate cell death receptors. However, long-term DOX administration is always accompanied with serious multidrug resistance (MDR) and adverse side-effects. Therefore, delivery systems for DOX and gene drug, such as miRNA-21 inhibitor (miR-21i) which mitigates MDR, have been developed to reduce side-effects caused by non-selective cellular uptake of co-drugs in the absence of suitable delivery systems. However, difficulties in designing delivery systems for different types of drugs to achieve both high therapeutic efficacy and low side-effects have been reported.

In this thesis, various biodegradable and biocompatible smart microgels are developed for DOX and gene co-delivery to achieve maximal anticancer performance and minimal side-effects. The microgel delivery carriers are prepared by crosslinking biocompatible low molecular weight polyethyleneimine (PEI800) using glutathione-cleavable diselenide crosslinkers. To the carriers, DOX is conjugated via various intracellular microenvironment sensitive linkers, and genes are electrostatically loaded to glutathione-cleavable polyethyleneimine. Finally, anionic hyaluronic acid (HA) surface coating is able to inhibit serum protein adsorption during blood circulation and promote HA receptor-mediated endocytosis for selective metastatic cancer cells. The hydrodynamic sizes of resulting nano-drugs at 100–200 nm allow prolonged circulation. The developed nano-drugs degrade into less than 10 nm fragments in the glutathione-rich cytosol of cancer cells by cleaving diselenide crosslinkers, allowing intensive gene release and complete urinary excretion. Real-time tracks of release profiles are developed using fluorescence quenching technique.

On the other hand, to eliminate premature release, DOX is conjugated to microgel carriers through various linkers for efficiently controlled spatiotemporal release in cancer lysosomes, such as acid-responsive hydrazone linkers, glutathione-cleavable diselenide linkers and enzyme-cleavable peptide linkers. The system comprising of DOX with a hydrazone bond demonstrates 4.4-fold higher *in vitro* anticancer performance on MDA-MB-231 cell line than free DOX. The nano-drug system of miR-21i and conjugated DOX via hydrazone and diselenide dual bonds completely surpasses DOX premature leakage in physiological condition and results in a high survival rate of over 95 % for HEK293T kidney cell line at a DOX concentration of $2.5 \mu\text{g mL}^{-1}$, but it reveals 3.2-fold increase in therapeutic effect on the multidrug-resistant cancer cell line of MDA-MB-231-R12w compared with free DOX. To simplify DOX loading process, diselenide crosslinkers can be used for both microgel synthesis and DOX conjugation to produce a simultaneous release system of gene and DOX in cytosol. The introduction of ATP aptamer to the miR-21i and DOX co-delivery system further increases intracellular DOX accumulation in MDA-MD-231-R12w cells with 4.2-fold higher anticancer performance than free DOX but with low cytotoxicity to healthy cells. To achieve sequential release, the nano-drug system of miR-21i and conjugated DOX with a caspase-3-cleavable DEVDC peptide linker enables the step release of miR-21i followed by DOX. Compared with free DOX, this systems demonstrates a 7.3-fold increase in anticancer effect on MDA-MB-231-R24w and negligible side effects.

In summary, we have developed various smart nano-drugs with outstanding advantages of low cytotoxicity, complete biodegradability, targeting and selective delivery and high anticancer performance to MDR cells. Our approach suppresses traditional gene and drug delivery concepts, and advances knowledge for successive design of delivery systems in clinical applications.

Declaration


I certify that this work contains no material which has been accepted for the award of any other degree or diploma in my name, in any university or other tertiary institution and, to the best of my knowledge and belief, contains no material previously published or written by another person, except where due reference has been made in the text. In addition, I certify that no part of this work will, in the future, be used in a submission in my name, for any other degree or diploma in any university or other tertiary institution without the prior approval of the University of Adelaide and where applicable, any partner institution responsible for the joint-award of this degree.

I acknowledge that copyright of published works contained within this thesis resides with the copyright holder(s) of those works.

I also give permission for the digital version of my thesis to be made available on the web, via the University's digital research repository, the Library Search and also through web search engines, unless permission has been granted by the University to restrict access for a period of time.

I acknowledge the support I have received for my research through the provision of an Australian Government Research Training Program Scholarship.

Name : Seonho Yun

Signature : 

Date : 20/05/2019

Acknowledgement

First, I extremely appreciate and respect my supervisor Professor Sheng Dai for his guidance and encouragement during my PhD candidate. His continuous helpful advice and valuable discussion from my master degree up to now opens my eyes on research and allows me to critically think.

I also express my deepest gratitude to my co-supervisors, Associate Professor Jingxiu Bi and Professor Hu Zhang, for their invaluable guidance and support on academic experience and critical discussion on the projects.

I would like to appreciate Professor Bo Jin for his support on academic experience. I would like to thank Associate Professor Zeyad Alwahabi for kinds of supports. I also appreciate all staffs at School of Chemical Engineering, the University of Adelaide for invisible supporting.

I would like to thank all group members, Dr. Yusak Hartanto, Dr. Xiaolin Cui, Jiabin Zhang, Hesamoddin Rabiee, Mahdhir Bin Amat Tugiman, Bingyang Zhang, Sunjin Nam, Heng Wang, Qi Bi, Umar Azhar, Afshin karami, Foad Farivar, Yechuan Zhang, Yiran Qu, Shuang Yin, Nhat Hoang Huynh, and Thai Thao Ly, for their collaboration, support and friendship during my PhD journey at the University of Adelaide.

I appreciate the University of Adelaide for giving me a chance and scholarship for PhD degree. I also acknowledge Australian Research Council for research grant.

I also thank Wookyeong Lee and Byeongjun An for assisting schematic drawings.

Lastly, I must give my greatest grateful to my parents, sisters, brother in law and my wife Younsun Joelle Lee, for their endless love, love and love throughout my life.

Chapter 1. Introduction

1.1 Background

To date, cancer is one of the highest causes of human death, but cancer treatment remains an unsolved task because of the unusual growth patterns of cancer cells. Opposed to healthy cells, cancer cells lose apoptotic functions and grow rapidly [1]. The abnormally growing cells undergo epithelial to mesenchymal transition (EMT) that induces the loss of cell adhesion and polarity [2], and the mesenchymal stem cells then accumulate to form an abnormal cell mass being referred to as tumor. Tumor cells secrete vascular endothelial growth factor (VEGF), which stimulates tumor vasculature formation [3]. The tumor cells metabolize and transport blood and nutrients to newly generated tumor cells through the tumor vasculature. The tumor cells utilize the vasculature for invasive migration into other tissues, becoming a malignant tumor being termed as cancer [4].

Anticancer chemotherapy targets the abnormalities of cancer cells such as apoptotic function loss, EMT and tumor angiogenesis [5-7]. However, long-term administration is accompanied with serious multidrug resistance (MDR) and dose-dependent side-effects. MDR mechanisms are the source of multiple self-defense systems of cancer cells, including target alteration, detoxification, activation of pro-survival pathways, and overexpression of ATP-binding cassette (ABC) transporters [8-11]. The MDR-induced reduction of therapeutic effect prompts the increased dosage of anticancer drugs, causing severe side-effects such as cardiotoxicity, hepatotoxicity and nephrotoxicity [12-14].

Co-drug therapy with chemotherapeutic and gene drugs exerts synergistic effects on anticancer treatment by reversing MDR and reducing dosage. Recent genetic drug developments include microRNAs (miRNAs), which are small non-coding RNAs of approximately 22 nucleotides

[15]. The miRNAs can target multiple messenger RNAs (mRNAs) to regulate gene expression associated with apoptosis, EMT, angiogenesis, and MDR in malignant tumor cells [16-19]. miRNA-21 (miR-21), a cancer-promoting oncogenic miRNA, downregulates tumor suppressor genes that inhibit the pro-survival pathways in cancer cells [20]. miR-21 inhibitor (miR-21i) hinders the activity of miR-21 and upregulates the tumor suppressor genes. Aptamers are short single-stranded oligonucleotides that strongly bind specific molecules such as adenosine triphosphate (ATP) [21]. The ATP aptamer (Apt) may act as a gene drug to isolate ATP, which is a driving force of the ABC transporters involved in MDR.

On the other hand, non-selective cellular uptake of co-drugs in the absence of suitable delivery systems leads to side-effects as well [22]. The demands to enhance therapeutic efficiency and minimize side effects have prompted the development of co-delivery systems. Delivery systems have been developed with improved functional conditions to satisfy some of the essentially required factors in the course of systemic administration such as non-toxic materials, effective loading of co-drugs, degradation avoidance, prolonged blood circulation, passive and active targeting, effective cellular uptake, endosomal escape, control of spatiotemporal release, complete urinary excretion of the drug-released carriers from patients' body, and traceability of their biodistribution [23, 24]. However, the functional conditions of the delivery systems that are required to achieve all the factors can be in conflict with each other, such as charges, sizes, and mechanisms of co-drug loading and release, resulting in inefficient therapeutic effects or less biocompatibility. Moreover, both anticancer synergy and biocompatibility require the effective control of the spatiotemporal release of co-drugs. In this thesis, we propose advanced multifunctional polymer microgels to selectively and efficiently deliver doxorubicin (DOX) and gene drugs to multidrug-resistant cancer cells by satisfying all the above factors. A series of intracellular stimuli-cleavable linkages for DOX conjugation was designed to enhance controllability of the spatiotemporal release for both exceptionally high anticancer effects and

negligible side effects and is presented in this thesis to confirm its potential for the further therapeutic applications.

1.2 Aim and Objectives

This thesis aims to develop novel multifunctional microgels as the co-drug delivery carriers of a model drug DOX and a model microRNA (miR-21i) to maximize their anticancer performance and minimize relevant side-effects. The detailed objectives are

1. To produce low-toxic and biodegradable microgel-based delivery carriers through the reaction of diselenide crosslinkers and low molecular weight branched polyethyleneimine (PEI800).
2. To load the model anticancer drug of DOX to the microgel carriers through conjugation via different intracellular stimuli-responsive linkers and load miR-21i and/or Apt via electrostatic interaction.
3. To handle surface modification via hyaluronic acid (HA) coating to eliminate serum protein adsorption and promote receptor-mediated endocytosis.
4. To evaluate the performance of resulting nano-drugs such as controlled release of DOX and miR-21i *ex vivo* and *in vitro*, biocompatibility with normal cell line HEK293T, and anticancer effects on metastatic breast cancer cell line MDA-MB-231 and multidrug resistant cancer cell line MDA-MB-231-R.
5. To further improve synergetic anticancer efficacy by introducing Apt for the inhibition of ABC transporters, or developing sequential release systems of miR-21i and DOX.

1.3 Thesis outline

This thesis has seven chapters. [Chapter 1](#) introduces the background of cancer treatment strategic approaches. After highlighting research gaps, aim and objectives of the thesis is

defined. [Chapter 2](#) reviews the rationale for co-delivery system design on cancer treatment after understanding DOX-induced apoptotic pathway, MDR, side-effects and co-drug synergies of miR-21i and Apt. Current difficulties in designing co-delivery systems before administration, in blood circulation, in extracellular/intracellular microenvironment, and over the delivery course are critically analyzed. [Chapter 3](#) proposes smart multifunctional microgels with HA surface coating for selective co-delivery of DOX and miR-21i to enhance anticancer effects. Synthesis of microgels utilizing low cytotoxic PEI800 and diselenide crosslinkers allows to load miR-21i electrostatically and release in GSH-rich cancer cytosol, and DOX conjugation via a hydrazone bond enables the release of DOX in endosome/lysosome of cancer cells. [Chapter 4](#) proposes advanced microgels with dual-lock conjugated DOX and electrostatically interacted miR-21i to further improve their biocompatibility with normal cells and achieve anticancer synergy in multidrug-resistant cancer cells. Conjugation of DOX to microgels via hydrazone and diselenide dual-lock suppresses premature leakage under mimicked physiological conditions and promotes intensive release in a mimicked sequential route of lysosome and cytosol. [Chapter 5](#) develops traceable nanomedicines of DOX, miR-21i, and Apt for further enhancement of the therapeutic effects on cancer cells with MDR by inhibiting miR-21 and ABC transporters. DOX conjugation to the microgels via diselenide bond enables DOX release in cancer cell cytosol with GSH, and BHQ2 conjugation to the microgels allow to monitor DOX release *in vitro*. [Chapter 6](#) proposes smart microgels containing DEVDC peptides for the sequential release of miR-21i followed by DOX to maximize therapeutic effects on multidrug-resistant cancer cells and minimize side effects. DOX conjugation to the microgels via peptide linkers containing DEVDC allows to release DOX in the presence of activated caspase-3 enzyme after reversing MDR by formerly released miR-21i in MDA-MB-231-R cells. [Chapter 7](#) concludes key scientific contribution from the thesis and future research directions are recommended.

1.4 Key contributions of this thesis

This thesis demonstrates the strategic development of anticancer drug/gene co-delivery carriers based on a deep understanding of pro-apoptotic and pro-survival pathways for a high feasibility of complete therapeutic effects and negligible side effects. The research outcomes directly contribute to the development of low toxic intracellular stimuli-responsive drug and gene co-delivery systems. An outline of key contributions is presented below:

1. For the first time, we designed a series of nano-drugs from our developed biocompatible and biodegradable low-toxic smart microgels to achieve high drug co-loading ability, no premature leakage and protein adsorption with blood circulation, selective cellular uptake to target cancer cells, low toxic to healthy cells and high anticancer effects to MDR cells.
2. For the first time, we developed nanomedicines by introducing Apt as a supplementary gene drug to inhibit ABC transporters in multidrug resistant cancer cells.
3. For the first time, we developed the sequential release approach of miR-21i and DOX from the co-delivery systems.
4. For the first time, we chemically conjugated BHQ2 to the microgels to provide real-time tracing of DOX release profiles and crucial information concerning the synergetic interaction between DOX and supplementary gene drugs of miR-21i or Apt.

References

- [1] S.W. Lowe, A.W. Lin, Apoptosis in cancer, *Carcinogenesis*, 21 (2000) 485-495.
- [2] E. Buck, A. Eyzaguirre, S. Barr, S. Thompson, R. Sennello, D. Young, K.K. Iwata, N.W. Gibson, P. Cagnoni, J.D. Haley, Loss of homotypic cell adhesion by epithelial-mesenchymal transition or mutation limits sensitivity to epidermal growth factor receptor inhibition, *Mol. Cancer Ther.*, 6 (2007) 532-541.
- [3] P. Carmeliet, R.K. Jain, Molecular mechanisms and clinical applications of angiogenesis, *Nature*, 473 (2011) 298.
- [4] J. Folkman, R. Kalluri, Cancer without disease, *Nature*, 427 (2004) 787.
- [5] G. Minotti, P. Menna, E. Salvatorelli, G. Cairo, L. Gianni, Anthracyclines: Molecular Advances and Pharmacologic Developments in Antitumor Activity and Cardiotoxicity, *Pharmacol. Rev.*, 56 (2004) 185-229.
- [6] F.M. Davis, T.A. Stewart, E.W. Thompson, G.R. Monteith, Targeting EMT in cancer: opportunities for pharmacological intervention, *Trends Pharmacol. Sci.*, 35 (2014) 479-488.
- [7] J. Yinghua, Q. Ping, W. Zhiwei, S. Qirong, W. Jian, Z. Weige, S. Hongrui, 3D-QSAR Study of Combretastatin A-4 Analogs Based on Molecular Docking, *Molecules*, 16 (2011) 6684-6700.
- [8] C. Leontiou, J.H. Lakey, C.A. Austin, Mutation E522K in Human DNA Topoisomerase II β Confers Resistance to Methyl N-(4'-(9-acridinylamino)-phenyl)carbamate hydrochloride and Methyl N-(4'-(9-acridinylamino)-3-methoxy-phenyl) methane sulfonamide but Hypersensitivity to Etoposide, *Mol. Pharmacol.*, 66 (2004) 430-439.
- [9] J. Deng, D. Coy, W. Zhang, M. Sunkara, A.J. Morris, C. Wang, L. Chaiswing, D. St Clair, M. Vore, P. Jungsuwadee, Elevated glutathione is not sufficient to protect against doxorubicin-induced nuclear damage in heart in multidrug resistance-associated protein 1 (Mrp1/Abcc1) null mice, *J. Pharmacol. Exp. Ther.*, 355 (2015) 272-279.
- [10] T.A. Buchholz, X. Tu, K.K. Ang, F.J. Esteva, H.M. Kuerer, L. Pusztai, M. Cristofanilli, S.E. Singletary, G.N. Hortobagyi, A.A. Sahin, Epidermal growth factor receptor expression correlates with poor survival in patients who have breast carcinoma treated with doxorubicin-based neoadjuvant chemotherapy, *Cancer*, 104 (2005) 676-681.
- [11] K.P. Locher, Review. Structure and mechanism of ATP-binding cassette transporters, *Philos. Trans. R. Soc. Lond. B Biol. Sci.*, 364 (2009) 239-245.
- [12] A. Ghigo, M. Li, E. Hirsch, New signal transduction paradigms in anthracycline-induced cardiotoxicity, *Biochim. Biophys. Acta*, 1863 (2016) 1916-1925.
- [13] Y. Zen, M.M. Yeh, Hepatotoxicity of immune checkpoint inhibitors: a histology study of seven cases in comparison with autoimmune hepatitis and idiosyncratic drug-induced liver injury, *Mod. Pathol.*, 31 (2018) 965-973.
- [14] H. Izzedine, M.A. Perazella, Anticancer Drug-Induced Acute Kidney Injury, *Kidney Int. Rep.*, 2 (2017) 504-514.

- [15] D.P. Bartel, *MicroRNAs: Genomics, Biogenesis, Mechanism, and Function*, Cell, 116 (2004) 281-297.
- [16] H. Park, X. Huang, C. Lu, M.S. Cairo, X. Zhou, MicroRNA-146a and MicroRNA-146b Regulate Human Dendritic Cell Apoptosis and Cytokine Production by Targeting TRAF6 and IRAK1 Proteins, *J. Biol. Chem.*, 290 (2015) 2831-2841.
- [17] X. Peng, W. Guo, T. Liu, X. Wang, X.a. Tu, D. Xiong, S. Chen, Y. Lai, H. Du, G. Chen, G. Liu, Y. Tang, S. Huang, X. Zou, Identification of miRs-143 and -145 that Is Associated with Bone Metastasis of Prostate Cancer and Involved in the Regulation of EMT, *PLoS One*, 6 (2011) e20341.
- [18] P.N. Plummer, R. Freeman, R.J. Taft, J. Vider, M. Sax, B.A. Umer, D. Gao, C. Johns, J.S. Mattick, S.D. Wilton, V. Ferro, N.A.J. McMillan, A. Swarbrick, V. Mittal, A.S. Mellick, MicroRNAs Regulate Tumor Angiogenesis Modulated by Endothelial Progenitor Cells, *Cancer Res.*, 73 (2013) 341-352.
- [19] T. Yang, Z.-m. Zheng, X.-n. Li, Z.-f. Li, Y. Wang, Y.-f. Geng, L. Bai, X.-b. Zhang, MiR-223 modulates multidrug resistance via downregulation of ABCB1 in hepatocellular carcinoma cells, *Exp. Biol. Med.*, 238 (2013) 1024-1032.
- [20] Y.H. Feng, C.J. Tsao, Emerging role of microRNA-21 in cancer, *Biomed. Rep.*, 5 (2016) 395-402.
- [21] P. Yu, X. He, L. Zhang, L. Mao, Dual Recognition Unit Strategy Improves the Specificity of the Adenosine Triphosphate (ATP) Aptamer Biosensor for Cerebral ATP Assay, *Anal. Chem.*, 87 (2015) 1373-1380.
- [22] Z. Liu, A.C. Fan, K. Rakhra, S. Sherlock, A. Goodwin, X. Chen, Q. Yang, D.W. Felsher, H. Dai, Supramolecular Stacking of Doxorubicin on Carbon Nanotubes for In Vivo Cancer Therapy, *Angew. Chem. Int. Ed.*, 48 (2009) 7668-7672.
- [23] S. Hossen, M.K. Hossain, M.K. Basher, M.N.H. Mia, M.T. Rahman, M.J. Uddin, Smart nanocarrier-based drug delivery systems for cancer therapy and toxicity studies: A review, *J. Adv. Res.*, 15 (2019) 1-18.
- [24] S.H. Ku, K. Kim, K. Choi, S.H. Kim, I.C. Kwon, Tumor-Targeting Multifunctional Nanoparticles for siRNA Delivery: Recent Advances in Cancer Therapy, *Adv. Healthc. Mater.*, 3 (2014) 1182-1193.

Chapter 2. Rationale design of doxorubicin and gene drug co-delivery systems for enhanced anticancer efficacy and efficiency

*Seonho Yun, Hu Zhang, Jingxiu Bi, Sheng Dai**

S. Yun, Prof. H. Zhang, Prof. J. Bi, Prof. S. Dai

School of Chemical Engineering, the University of Adelaide, Adelaide, SA 5005, Australia

Prof. H. Zhang

Amgen Bioprocessing Centre, Keck Graduate Institute, 535 Watson Drive, Claremont, CA
91711

Prof. S. Dai

Department of Chemical Engineering, Brunel University London, Uxbridge, UB8 3PH,
United Kingdom

sheng.dai@brunel.ac.uk

Statement of Authorship

Title of Paper	Rationale design of doxorubicin and gene drug delivery systems for enhanced anticancer efficacy and efficiency
Publication Status	<input type="checkbox"/> Published <input type="checkbox"/> Accepted for Publication <input type="checkbox"/> Submitted for Publication <input checked="" type="checkbox"/> Unpublished and Unsubmitted work written in manuscript style
Publication Details	In preparation for submission

Principal Author

Name of Principal Author (Candidate)	Seonho Yun		
Contribution to the Paper	Reviewed the research papers and wrote manuscript		
Overall percentage (%)	80 %		
Certification:	This paper reports on the original research I conducted during the period of my Higher Degree by Research candidature and is not subject to any obligations or contractual agreements with a third party that would constrain its inclusion in this thesis. I am the primary author of this paper.		
Signature		Date	20/05/2019

Co-Author Contributions

By signing the Statement of Authorship, each author certifies that:

- i. the candidate's stated contribution to the publication is accurate (as detailed above);
- ii. permission is granted for the candidate to include the publication in the thesis; and
- iii. the sum of all co-author contributions is equal to 100% less the candidate's stated contribution.

Name of Co-Author	Hu Zhang		
Contribution to the Paper	Proof read the manuscript and evaluation		
Signature		Date	24/02/2019

Name of Co-Author	Jingxiu Bi		
Contribution to the Paper	Proof read the manuscript and evaluation		
Signature		Date	25/02/2019

Name of Co-Author	Sheng Dai		
Contribution to the Paper	Proof read the manuscript, evaluation and corresponding author		
Signature		Date	20/05/2019

Abstract

Infallible cancer treatment has yet to be achieved. Doxorubicin (DOX) as an active anticancer drug causes apoptosis as well as serious multidrug resistance and adverse side effects. The merits and defects of DOX are reviewed in the scope of its interaction with physiological mechanisms and signaling pathways. Co-therapy using supplementary drugs such as miRNA-21 inhibitor or adenosine triphosphate aptamer is reviewed to devise a strategy to enhance therapeutic efficacy by mitigating the side effects caused by long-term DOX administration. We also review detailed mechanisms for adverse side effects caused by non-selective delivery of co-drugs to normal cells. The development of modern delivery systems with multifunctional conditions to satisfy all essential factors during the delivery course of before administration, in blood circulation, in extracellular/intracellular microenvironment and overall the delivery course is analyzed to provide guidance on rationale design of potential co-drug delivery systems with enhancing therapeutic efficiency and minimizing side effects.

Contents

2.1 Introduction	13
2.2 DOX as an anticancer drug	14
2.2.1 Merits of DOX in anticancer therapy	14
2.2.2 Defects of DOX in anticancer therapy	18
2.2.2.1 MDR	18
2.2.2.2 Side effects.....	22
2.3 Supplementary gene drugs	23
2.3.1 microRNA-21 inhibitor as a sub-drug	24
2.3.2 ATP aptamer as a sub-drug	25
2.4 Enhance therapeutic efficiency using delivery carriers	25
2.4.1 Before administration	28
2.4.1.1 Low-toxic materials	28
2.4.1.2 Effective DOX loading	31
2.4.1.3 Effective gene loading	33
2.4.2 Blood circulation	35
2.4.2.1 Avoiding nuclease degradation.....	35
2.4.2.2 Avoiding RES clearance	36
2.4.2.3 Avoiding renal clearance	38
2.4.2.4 Effective extravasation.....	38
2.4.3 Extracellular microenvironment	39
2.4.3.1 Effective cell internalization	39
2.4.3.2 Selective cell internalization	42
2.4.4 Intracellular microenvironment	44
2.4.4.1 Effective endosomal escape	44
2.4.4.2 Spatiotemporal release	44
2.4.4.3 Complete excretion	51
2.4.5 Traceability over delivery course	53
2.5 Summary and Future perspectives	55
Acknowledgement	56
References	57

2.1 Introduction

Because of the abnormal growth of cancer cells, complete treatment of cancers has not been achieved. Cancer growth is rapid and widespread, and anticancer chemotherapy is a relatively less invasive treatment method than therapeutic radiation and local surgery. The initial anticancer effects from chemotherapy decline with the increased rounds of chemotherapy that accompany the recurrence and resistance of cancer cells. Thus, patients suffer from the recurred cancer as well as dose-dependent side effects. Delivery carrier-mediated co-drug therapy with combined anticancer chemotherapeutic and nucleic acid drug has great potential for enhancing the anticancer effects and minimizing side effects.

This review aims to provide a crucial rationale to encourage the successive design of the above-mentioned co-drug delivery systems. In detail, the advantages and disadvantages of DOX (doxorubicin) -based chemotherapy are reviewed against the scope of intracellular signaling pathways to support therapeutic strategies. To enhance its anticancer efficacy, co-therapy of DOX and different gene drugs, including microRNA 21 inhibitor (miR-21i) and adenosine triphosphate (ATP)-aptamer (Apt), is further analyzed with an explanation of their synergistic effects on signaling pathways to mitigate DOX-induced multidrug resistance (MDR). Strategies for increasing therapeutic efficiency with new delivery carriers by overcoming the causes of side effects will be reviewed for each delivery course. The mismatches between the essential factors in an ideal delivery course and functional conditions of the delivery systems will be discussed to outline current research gaps and significant information for the feasibility of the systems in potential clinical application.

2.2 DOX as an anticancer drug

2.2.1 Merits of DOX in anticancer therapy

DOX is one of the most effective anticancer drugs against many types of cancers, such as breast cancer [1], gastric cancer [2], non-small-cell lung cancer [3], ovarian cancer [4], and bladder cancer [5]. DOX was the first anthracycline [6], consisting of a hydrophobic tetracyclic ring and a glycoside-linked daunosamine sugar (Figure 2.1).

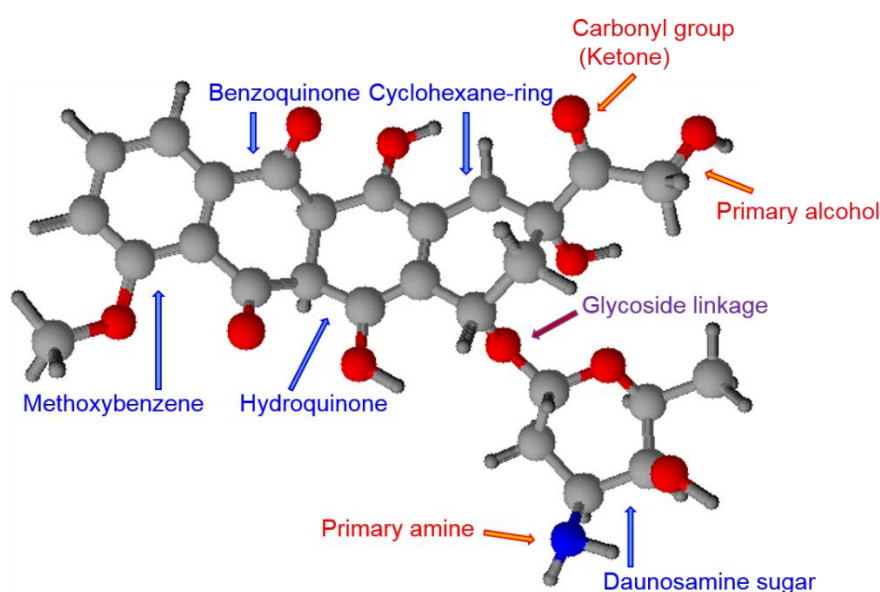


Figure 2.1 Chemical structure of doxorubicin (DOX) consisting of a tetracyclic ring, a glycoside-linked daunosamine sugar and functional groups.

In DOX, the tetracyclic ring is an aligned structure of a methoxybenzene, benzoquinone, hydroquinone, and cyclohexane ring. A short side chain of the cyclohexane ring contains a carbonyl group and a primary alcohol. A primary amine group is located at the sugar moiety. The DOX morphology causes an active anticancer effect initiated by intercalation with topoisomerase II (Topo II) and the production of reactive oxygen species (ROS) (Figure 2.2).

On the one hand, DOX acts as an initiator in the Topo II intercalation-induced anticancer pathways. Topo II is a key enzyme for the transcriptional activity of DNA via unwinding of

the twisted DNA double helix without altering its sequence [7]. The hydrophobic tetracyclic ring of DOX allows intermediate intercalation with both a Topo II active site and DNA bases in nucleus, forming a stable Topo II-DOX-DNA ternary complex that inhibits Topo II activity in DNA replication [7]. The Topo II intercalation-induced DNA damage promotes p53 activation, which stimulates tumor-suppressing pathways [8]. The nuclear transcription factor p53 is involved in tumor cell cycle arrest. p53 negatively affects the activity of proto-oncogene c-Jun as a subunit of activator protein 1 transcription [9]. The inhibition of c-Jun activity assists in hindering the cell cycle progression from G1- to S-phase and tumor cell proliferation, resulting in cancer cell cycle arrest [10]. Furthermore, p53 activation caused by DNA damage drives the mitochondrial apoptotic pathway in tumor cells via upregulation of B-cell lymphoma-2 (Bcl-2)-associated X protein (Bax), a pro-apoptotic regulator in the Bcl-2 protein family [11]. The relative expression of Bax to the anti-apoptotic protein Bcl-2 contributes to the apoptotic pathway. Both Bax-Bcl-2 heterodimers and Bax homodimers allow mitochondria to release the pro-apoptotic factor cytochrome c (cyt c) while Bcl-2 homodimers inhibit its release [12]. Cytoplasmic cyt c interacts with both apoptotic peptidase activating factor-1 and procaspase-9 to form an apoptosome and activate caspase-9 [13]. The active caspase-9 subsequently activates caspase-3, and the caspase cascade culminates with apoptosis in tumor cells via a number of protein cleavage and DNA fragmentation mechanisms [11].

On the other hand, DOX acts as a free radical intermediate to stimulate ROS production-induced anticancer pathways. Reduced nicotinamide adenine dinucleotide phosphate (NADPH) in the cytosol acts as a cellular anti-oxidative defense system [14]. The NADPH transfers one electron to DOX in a metabolic process by reducing quinone in the tetracyclic ring of DOX to a semiquinone moiety [15]. The semiquinone is promptly oxidized back to quinone by reducing oxygen as an electron acceptor, thereby generating ROS such as superoxide anion and hydrogen peroxide [6]. The semiquinone is also oxidized to its parent quinone by reducing the

glycosidic linkage of DOX between a daunosamine sugar and a cyclohexane ring in an anaerobic state and generating 7-deoxyaglycone [16]. The removal of the sugar moiety from DOX increases the lipid solubility of the 7-deoxyaglycone metabolite, which intercalates with the inner mitochondrial membrane and results in ROS production [16]. During the redox cycling, DOX can form a complex with intracellular iron, and the complex transforms superoxide anion and hydrogen peroxide to more reactive hydroxyl radicals as more toxic ROS [15].

The higher production of ROS than the cellular anti-oxidative defense systems brings about oxidative stress that can induce cell death via two routes. The oxidative stress can directly damage DNA or mitochondria to stimulate apoptotic signaling pathways initiating from p53 or Bax to cause caspase-9/caspase-3 activation, resulting in cell death [17]. The other is the death receptor-induced apoptotic pathway. ROS over-production can activate the transmembrane death receptors of the tumor necrosis factor (TNF) receptor superfamily, including Fas, TNF receptor 1 (TNF-R1), and TNF-related apoptosis-inducing ligand receptor 1/2 [18]. This activation can recruit Fas-associated protein with death domain, which is an adaptor protein, and procaspase-8 to form death-inducing signaling complex, which activates caspase-8 and its downstream caspase-3, thereby resulting in cell death. Caspase-8 can interconnect the two death pathways. Caspase-8 stimulates the production of truncated BH3 interacting death domain (tBid) that inhibits the activity of Bcl-2 in mitochondria [18]. Inhibition of Bcl-2 facilitates the mitochondria-mediated caspase-9 activation required for apoptosis.

Work carried out by Pilco-Ferreto and Calaf well supports the DOX-induced apoptotic pathways in different types of breast cancer cell lines, MCF-10F, MCF-7, and MDA-MB-231 [19]. DOX administration leads to upregulation of caspase-9 and caspase-3 in all of the cell lines, indicating activation of the mitochondrial apoptotic pathway. Hydrogen peroxide production and upregulation of caspase-8 protein are also observed in MCF-10F and MDA-

MB-231 as evidence of the death receptor-mediated pathway. Bcl-2 downregulation and Bax upregulation by DOX in the cancer cells proves the crosstalk between the two pathways. Thus, these results indicate that DOX effectively activates apoptosis via two signaling pathways starting from nucleus and cytosol of the cell lines.

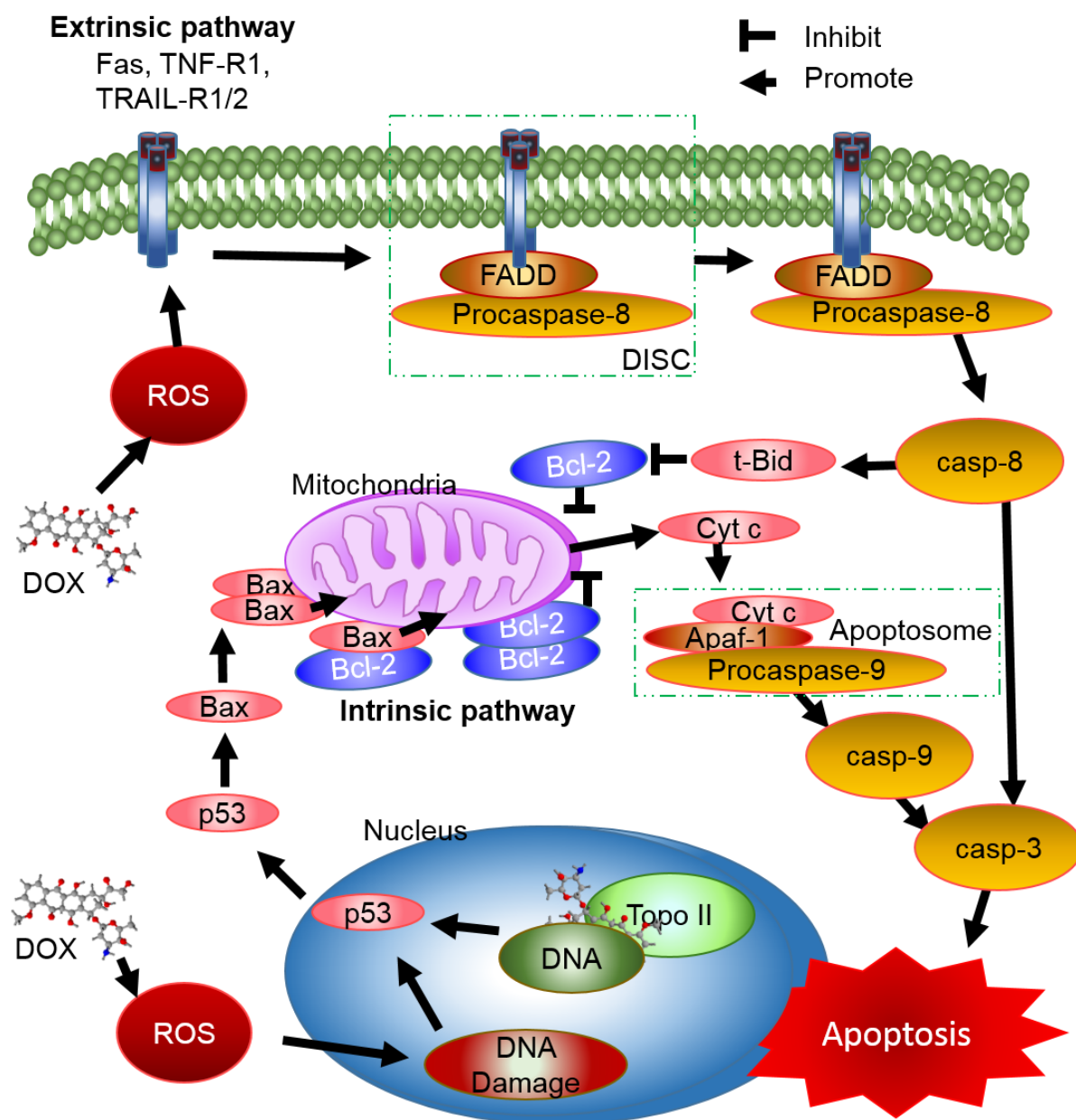


Figure 2.2 DOX-induced apoptotic pathways. The intrinsic pathway indicates the mitochondrial pathway initiated by Topo II intercalation or ROS-induced DNA damage in the nucleus. The extrinsic pathway indicates the death receptor-mediated pathway that is initiated by ROS production by DOX in cytosol. Casp represents caspase.

2.2.2 Defects of DOX in anticancer therapy

Despite the wide clinical utilization of DOX for its merits, long-term administration brings about clinical defects. The culture of cancer cell lines in a DOX-incorporated culture medium for > 3 months has demonstrated that the cell lines gain gradual tolerance to the chemotherapeutic agent with a decreasing cell death rate following identical doses of the agent [20, 21]. The surviving cancer cells enhance their self-defense systems, known as multidrug resistance (MDR), which resultantly increases drug dosage and dose-dependent side effects.

2.2.2.1 MDR

Long-term administration-induced MDR to DOX causes target alteration, detoxification, activation of pro-survival pathways, and overexpression of ATP-binding cassette (ABC) transporters.

2.2.2.1.1 Target alteration and detoxification

Tumor cells can avoid the effects of DOX treatment by alteration of the DOX target, Topo II, via mutations or reducing its expression [12, 22]. To counterbalance the role of Topo II, topoisomerase I is overexpressed in cells lacking Topo II [23].

Increasing levels of glutathione (GSH) and glutathione S-transferase have been observed in tumor cells following the administration of low-dose DOX [24, 25]. The thiol molecules are involved in detoxifying free radicals and ROS as anti-oxidative defense systems.

2.2.2.1.2 Pro-survival pathways

Importantly, the exposure of DOX to tumor cells can activate a number of pro-survival pathways to inhibit apoptosis and rather promote survival, cell growth, angiogenesis, invasion, and metastasis (Figure 2.3). Following chemotherapy, Bcl-2 expression in a DOX-resistant myeloid leukemia cell line, HL-60-DOX, decreases far less than that in DOX-sensitive HL-60 [26]. An abundant amount of the anti-apoptotic Bcl-2 proteins can interrupt the activity of pro-

apoptotic Bax proteins in the formation of pores on the outer membrane of mitochondria [13]. Since cyt c can be released through these pores, Bcl-2 upregulation can inhibit the mitochondria-mediated apoptotic pathway.

DOX-based chemotherapy is accompanied by overexpression of the epidermal growth factor receptor (EGFR) family, which enhances chemotherapeutic resistance [27]. The EGFR family is a transmembrane tyrosine kinase receptor family, and their cytoplasmic domains can activate downstream signaling pathways such as the phosphatidylinositol-3-kinase (PI3K)/Akt pathway, rat sarcoma (RAS)/rapidly accelerated fibrosarcoma (RAF)/mitogen-activated protein kinase (MAPK) pathway, and Janus kinase (JAK)/signal transducers and activators of transcription (STAT) pathway [28].

PI3K/Akt pathway

The PI3K/Akt pathway is associated with cancer cell survival via apoptosis inhibition and supporting the cancer cell cycle and angiogenesis. The PI3K/Akt pathway inactivates the proapoptotic protein of Bcl-2-associated agonist of cell death and procaspase-9 [29]. Blocking the apoptotic pathway for caspase-9 activation encourages cancer cell survival. Akt in the pathway downregulates p53 in the nucleus by phosphorylating a proto-oncogene of mouse double minute 2 homolog [29]. Loss of p53 inhibits apoptosis. The PI3K/Akt pathway hinders the role of p21 and p27 in inhibiting the cell cycle the G1 phase. Phosphorylation of p21 and p27 by the PI3K/Akt pathway impairs their nuclear localization from cytoplasm, resulting in progression of the cancer cell cycle and cancer growth [30]. Activation of mammalian target of rapamycin (mTOR), a downstream pathway of PI3K/Akt, transmits a signal to increase the secretion of vascular endothelial growth factor (VEGF) and accelerates tumor angiogenesis and therapeutic resistance [31].

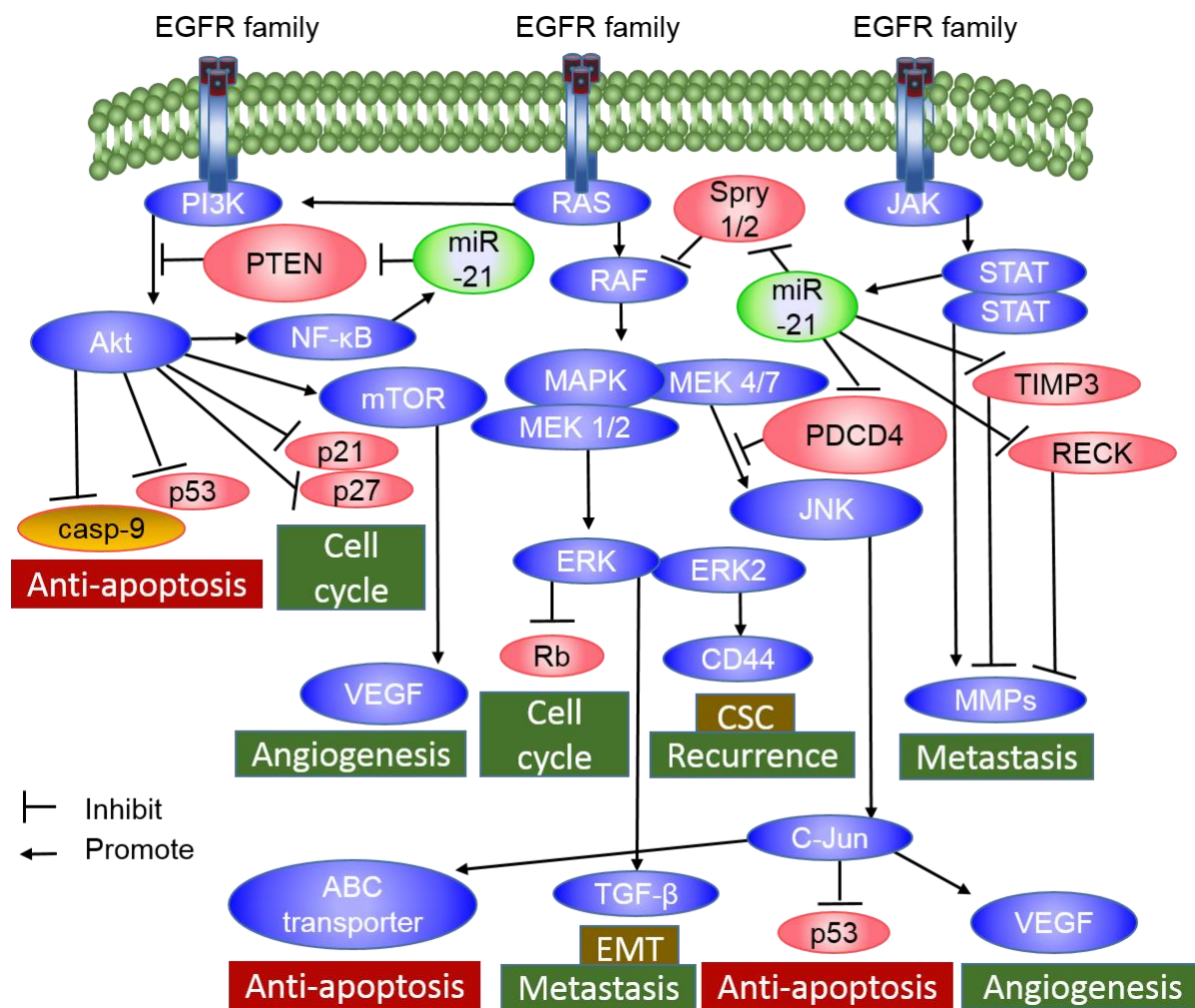


Figure 2.3 Pro-survival pathways: PI3K/Akt/mTOR, RAS/RAF/MAPK and JAK/STAT, and roles of miRNA-21 (miR-21) in downregulating multiple inhibitors of the survival pathways.

RAS/RAF/MAPK pathway

The RAS/RAF/MAPK pathway is another downstream signaling pathway of the cytoplasmic tyrosine kinase domain [32]. The MAPK pathway includes extracellular signal-regulated kinase (ERK), which promotes cell cycle progression from G1- to S-phase by inhibiting the activity of retinoblastoma tumor suppressor protein (Rb) [33]. The ERK in the MAPK pathway is also involved in the secretion of transforming growth factor β (TGF- β) that induces epithelial to mesenchymal transition (EMT), a process whereby cancer cells lose adhesion to their surroundings and subsequently migrate as a metastasis [34]. Notably, ERK2 activates EMT

transcription factors as well as CD44 overexpression as a biomarker of cancer stem cells (CSCs) in breast cancer cell line MCF-10A [35]. Cancer cells include a small percentage of CSCs, which are capable of recurrence, invasive metastasis, heterogeneous tumorigenesis, and resultant resistance to chemotherapy [36].

Environmental stress induces a MAPK pathway downstream of the c-Jun N-terminal kinases (JNK) pathway that plays roles in cancer as both a tumor suppressor and a stimulator of oncogenesis [37]. While JNK activation assists apoptosis by phosphorylating Bcl-2 protein and activating Bax [38], the JNK pathway rather encourages drug resistance by downregulation of p53 expression through its downstream effector c-Jun [9]. In addition to p53 regulation, c-Jun activation directly influences VEGF expression and angiogenesis in invasive breast cancer [10]. Importantly, the JNK signaling pathway maintains the mesenchymal properties of human epidermoid carcinoma cells via the downstream transcriptional factors of snail and twist 1 [39]. Such angiogenesis and sustainable mesenchymal properties allow cancer cells to avoid the effects of chemotherapy.

JAK/STAT pathway

In the JAK/STAT pathway downstream of the EGFR family, JAK stimulates the formation of STAT dimers by phosphorylating tyrosine residues, and the dimers translocated in the nucleus activate matrix metalloproteinase-1 (MMP-1) [40]. MMP-1 is a collagen-digesting enzyme that is essentially required to break down the extracellular matrix for the migration of human bone marrow-derived mesenchymal stem cells and myoblasts [41, 42]. This suggests that activation of the JAK/STAT pathway in cancer cells may promote their migration and chemotherapeutic resistance.

2.2.2.1.3 ABC transporter

DOX administration significantly increases ABC transporters in invasive cancer cell lines MDA-MB-231 and MDA-MB-435 via upregulation of EMT markers [43]. Activation of a JNK/c-Jun signaling pathway is also correlated with ABC transporter overexpression in human colon cancer cell line SW1116/HCPT [44]. The ABC transporters are a superfamily of bifunctional transmembrane proteins that import hydrophilic nutrients into the cytoplasm and export hydrophobic substrates (including cancer drugs, lipids, and antigenic peptides) out of the cytoplasm [45]. ATP hydrolysis via a pair of cytoplasmic nucleotide-binding domains converts the structure from a pair of transmembrane domains in the transporters facing inward to an outward-facing direction when transporting hydrophobic anticancer drugs [45]. The overexpression of ABC transporters in cancer cells plays a key role in MDR as DOX exporters, thereby reducing the intracellular accumulation of DOX and the demand for an increased dosage.

2.2.2.2 Side effects

MDR allows cancer cells to tolerate constant chemotherapy and confers a high probability of survival, which correspondingly requires higher dosages of anticancer drugs to compensate for the loss of treatment effectiveness. Long-term DOX administration induces dose-dependent side effects such as heart failure, liver injury, chronic kidney dysfunction, and skeletal muscle function loss [46-49].

As presented in [Figure 2.4](#), in addition to the side effects, administration of free DOX without any carrier demonstrates a far lower cellular uptake by tumors compared with that of other normal organs such as the spleen, kidneys, liver, lung, heart, and intestine [50]. The hydrophobicity of protonated free DOX in the slightly acidic extracellular cancer environment can limit its interaction with the lipid cellular membrane, whereas the hydrophobicity of unprotonated free DOX at the neutral pH of normal extracellular conditions can promote higher

transmembrane permeation [51]. Eksborg's partition experiments demonstrate that dimer and tetramer formation with protonated DOX in the acidic extracellular aqueous phase could be the cause of poor diffusion to intracellular organic phase and the reduced cellular uptake by tumors [52].

Such side effects that negatively compensate the anticancer effects of DOX promote the development of diverse strategies to enhance therapeutic efficacy via mitigation of MDR and increase efficiency using delivery carriers.

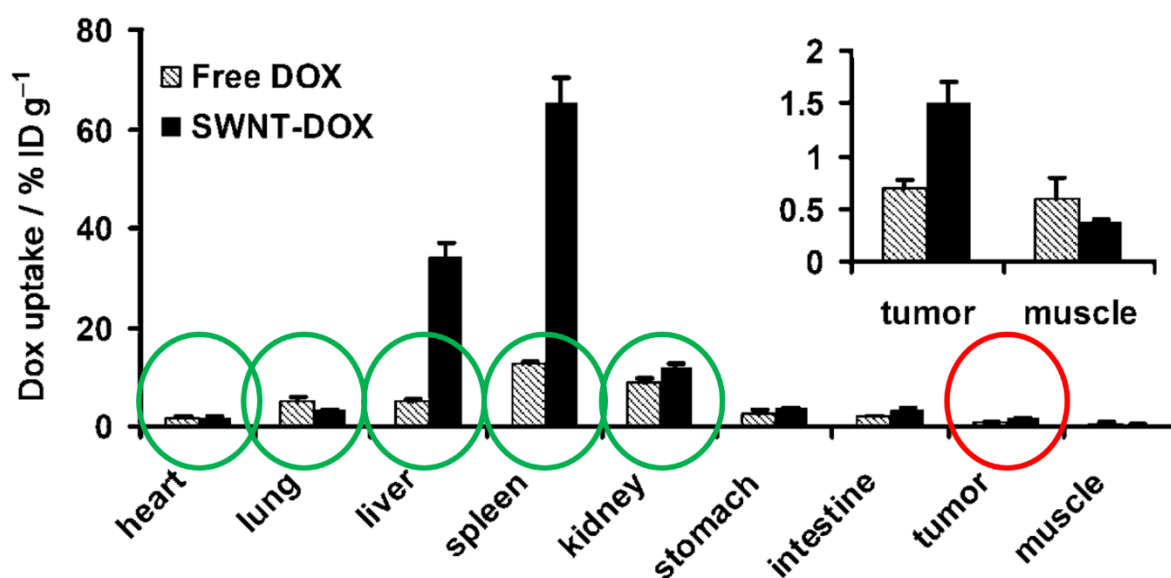


Figure 2.4 Cellular uptake of free DOX without any carrier to normal organs and tumors via systemic administration, reproduced from [50] with copyright.

2.3 Supplementary gene drugs

There have been some strategies to achieve higher therapeutic efficacy via MDR suppression, such as co-therapy with supplementary gene drugs like miR-21i or Apt in DOX-based chemotherapy.

2.3.1 microRNA-21 inhibitor as a sub-drug

A microRNA (miRNA) is a small, non-coding RNA of approximately 22 nucleotides that negatively regulates messenger RNAs (mRNAs) of target genes at the posttranscriptional level [53]. A diverse range of miRNAs are directly or indirectly involved in the creation or maintenance of MDR in cancer cells [54]. miRNA-21 (miR-21) critically modulates the resistance of cancer cells to DOX-based chemotherapy [55] by targeting multiple inhibitors of pro-survival signaling pathways to support MDR (Figure 2.3).

DOX-induced DNA damage promotes Akt activation that upregulates I κ B kinase as a regulator of nuclear factor kappa B (NF- κ B), which expresses miR-21 [29, 56]. The upregulated miR-21 facilitates cancer cell growth, invasion, and resultant survival by inhibiting phosphatase and tensin homolog (PTEN) that restricts the PI3K/Akt/mTOR signal transduction pathway [57, 58]. miR-21 can also be regulated by oxidative stress-induced NF- κ B and VEGF-related STAT3 activation [19, 59]. The overexpression of miR-21 maintains cancer cell survival, metastasis, and resistance to apoptosis by inhibiting programmed cell death 4 to block the JNK/c-Jun signaling pathway [60]. Additionally, miR-21 also downregulates tumor suppressor genes, such as Sprouty homolog 1/2, as an inhibitor of the MAPK pathway and tissue inhibitor of metalloproteinase 3 and reversion-induced cysteine-rich protein with Kazal motifs (RECK) as inhibitors of MMPs [61].

Therefore, disturbance of miR-21 activity in the protection of such diverse pro-survival signaling pathways from their inhibitors becomes a strategy to enhance therapeutic efficacy. The introduction of a miR-21i with DOX in human glioblastoma cell lines demonstrates synergistic increase of anticancer effects via upregulation of E-cadherin, RECK, PTEN, and p21 for the successful reversal of MDR [62]. Importantly, miR-21i administration in multidrug-resistant breast cancer cell line MCF-7/ADR causes a 45% reduction in the expression P-glycoprotein (P-gp), an ABC transporter family [63]. Such recovery of chemosensitivity via

inhibition of miR-21 activity by its inhibitors has been observed in many tumors such as renal carcinoma, bladder cancer, non-small cell lung carcinoma, and human breast cancer [64-67].

2.3.2 ATP aptamer as a sub-drug

Aptamers are short single-stranded oligonucleotides that selectively bind their target molecules with strong affinity [68]. Apt, an aptamer to selectively detect ATP, has been developed as a biosensor to recognize intracellular ATPs [69, 70]. ATP is a driving force of ABC transporters that export intracellular hydrophobic drugs such as DOX [45]. A study on mice carrying the colon carcinoma cell line HCT-8/T has shown that depletion of ATP is directly correlated to the downregulation of P-gp [71]. Mo *et al.* have employed Apt in ATP-responsive DNA scaffolds or DNA-graphene hybrid nanoaggregates for DOX delivery systems [72, 73]. However, the utilization of Apt as a supplementary drug requires further elucidation and could be another strategy to enhance therapeutic efficacy by inhibiting ABC transporters via isolation of their driving force.

2.4 Enhance therapeutic efficiency using delivery carriers

Although co-therapy with DOX and supplementary gene drugs and their sequential therapy have great potential to improve therapeutic efficacy against multidrug-resistant cancers, the systemic administration of DOX and gene drugs without any delivery carrier can unselectively deliver them to both cancer and normal cells [50]. In addition, gene drugs might be de-functionalized associated with blood circulation. The off-target delivery of anticancer drugs causes direct damages and metabolic alterations to normal cells as well as dose-dependent side effects by reducing therapeutic efficiency [47, 74]. Therefore, suitable delivery carriers are crucial to selectively deliver co-drugs to target cells for enhancing therapeutic efficiency and minimizing side effects.

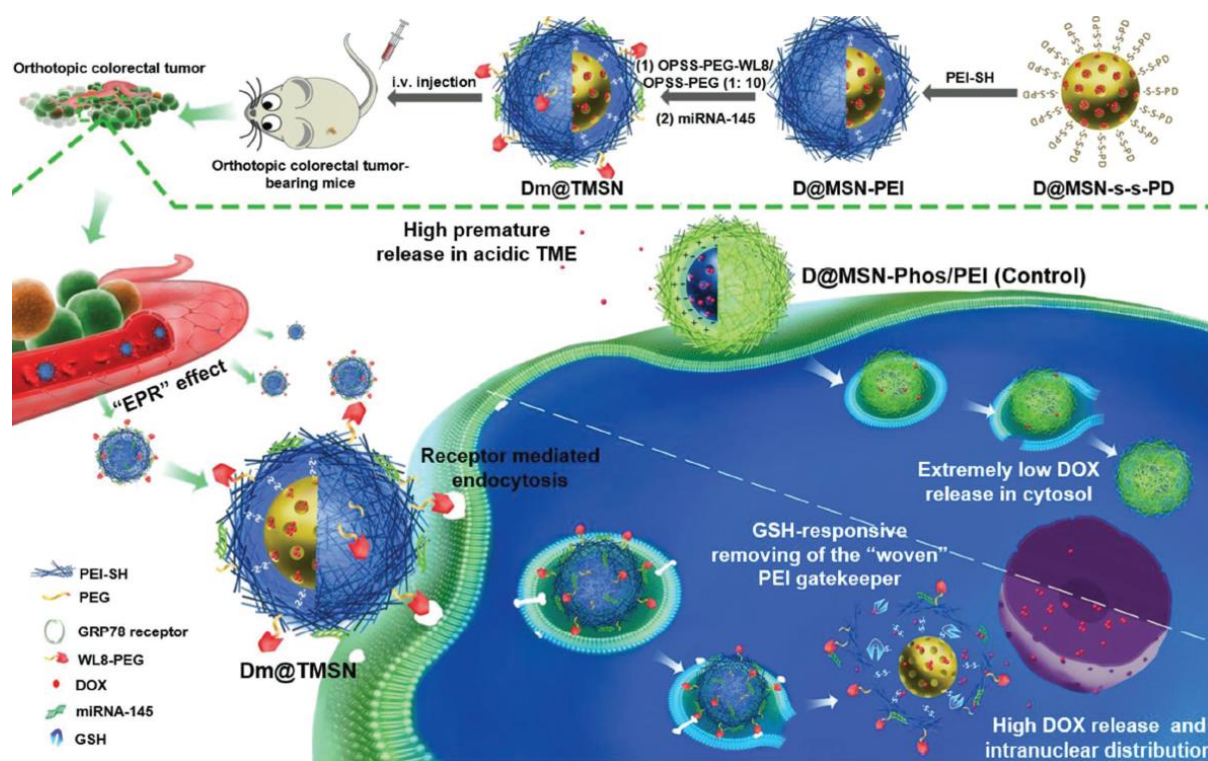


Figure 2.5 Schematic description of the delivery course of MSNs loaded with DOX and gene via IV injection: loading, blood circulation, extravasation, active target-mediated endocytosis, endosomal escape, and controlled release of the drugs, reused from [128] with copyright.

The successive design of co-delivery carriers to increase therapeutic efficiency should satisfy all essentially required factors in the delivery course, summarized in Table 2.1 and Figure 2.5. Before administration, there are basic factors of delivery carriers, such as choosing low-toxic materials with effective loading ability of DOX and genes [75, 76]. The delivery vectors should effectively load the diverse properties of anionic genes and either hydrophobic DOX or cationic DOX hydrochloride (DOX·HCl) without premature leakage [77, 78]. After systemic administration, the delivery carriers in the blood vessels should avoid serum nuclease degradation, reticuloendothelial system (RES) clearance, and renal clearance to achieve prolonged circulation and effectively extravasate to the tumor site via the pores of tumor vasculature [79]. Importantly, the carrier should be able to selectively deliver the co-drugs to cancer cells via active targeting and effective endocytosis from the extracellular microenvironment [80]. In the intracellular microenvironment setting, the carriers loaded with

the drugs should enable endosomal escape and drug release in a spatiotemporal manner as well as their complete urinary excretion [81-83]. Over the delivery course, traceability of the carriers is also fundamental to monitor the invisible and non-harmful delivery process [84, 85]. Therefore, ideal delivery vehicles should be designed to fulfill these essential required factors in the order of delivery course.

Table 2.1 Summary of required essential factors and functional conditions of ideal delivery vectors

Delivery course	Required factor(s)	Functional condition(s)	References
Before administration	Low-toxic materials	Natural polymers	[89]
		Degradable polymers	[90], [94]
		Negative charge	[92]
		Lipids	[95]
		Biocompatible inorganics	[98-105]
	Effective DOX loading	Effective gene loading	Physical adsorption
Chemical conjugation			[120-123]
Blood circulation	Avoiding nuclease degradation	Positive charged carriers	[129], [78] [125-128]
		Steric hindrance	[71], [118], [132-133]
	Negative charges	[138]	
	Avoiding RES clearance	Size < 200 nm in diameter	[144-145]
	Avoiding renal clearance	Size > 20 nm in diameter	[150]
Effective extravasation	Size < 500 nm in diameter	[80]	
Extracellular microenvironment	Effective cell internalization	Size < 50 nm in diameter for penetration	[156-157]
		CPPs or pHLIPs for penetration	[158-159], [162]
		Size 50–200 nm in diameter for endocytosis	[163-166]
		Positive charge for endocytosis	[169-170]
		Receptor mediation for endocytosis	[163]
	Selective cell internalization	Targeting ligands	[68], [172-173], [175-176], [179]

Intracellular microenvironment	Effective endosomal escape	Amine group-induced pH buffering	[182-184]
		Spatiotemporal release	Thermal responsive moiety
	Magnetic field responsive moiety		[188]
	Ultrasound responsive moiety		[189]
	NIR responsive moiety		[129], [191]
	pH responsive moiety		[115], [118], [122], [194-196]
	Enzyme responsive moiety		[197-198]
	GSH responsive moiety		[88], [125], [200-201]
	Complete excretion		Size < 6 nm in radius
		Biodegradation	[94], [208]
Overall delivery course	Tracing carrier biodistribution	Optical inorganics	[209-211]
		Label-free polymer nanogel	[212]
		Carrier loaded with fluorescent drugs	[213-215]
	Tracing drug release	FRET between fluorophores	[216]
		Aggregation-caused quenching	[217]
		BHQ2-mediated quenching	[219]
		Distance < 10 nm between fluorophores	[218]

2.4.1 Before administration

Consideration of the basic factors to produce a successful co-delivery vector begins before systemic administration. This includes how to enhance DOX and gene loading to their low-toxic co-delivery vectors.

2.4.1.1 Low-toxic materials

The use of low-toxic and biocompatible co-delivery vector materials is an obvious choice due to the requirement of clinical purpose and prevention of activating host immune systems. As viral vectors are unsuitable for DOX loading [86], the scope of co-delivery carriers is limited to non-viral vectors consisting of polymer-, lipid-, or inorganic-based materials (Figure 2.6).

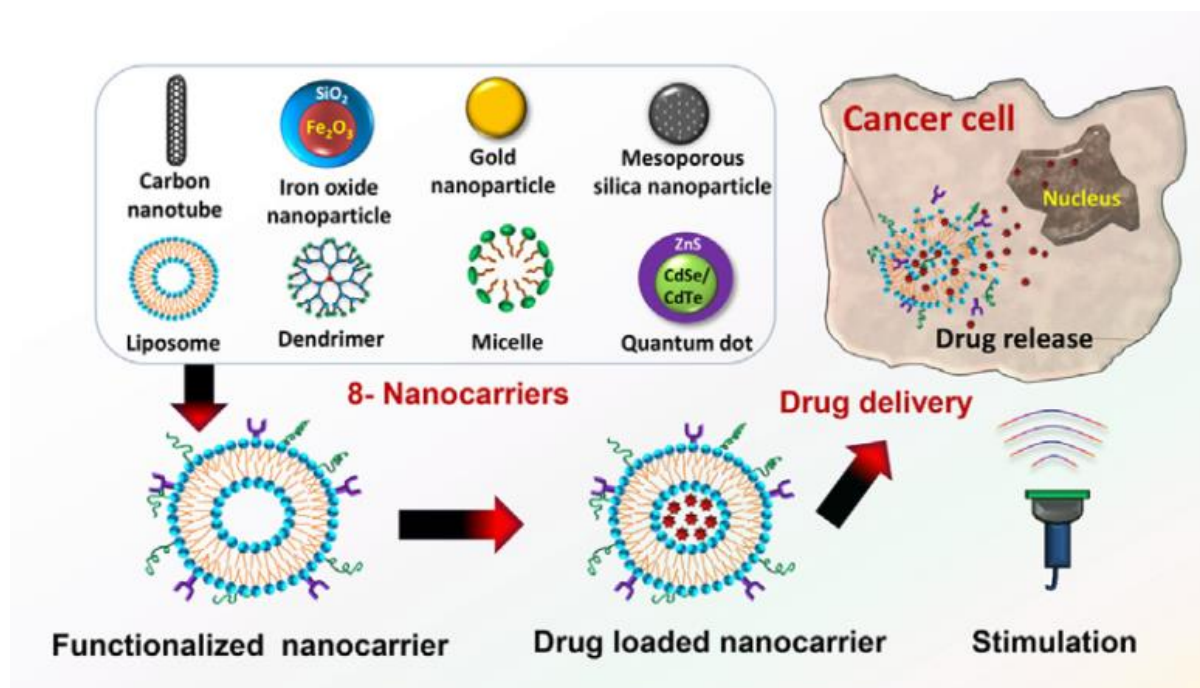


Figure 2.6 Illustration of types of non-viral vectors and a rough mechanism of loading and release of anticancer drugs via liposome, reused from [75] with copyright.

Polymer-based materials are widely employed in medical applications, such as regenerative medicine and drug delivery carriers due to their excellent functional modifications and biocompatibility [87, 88]. Naturally produced polymers, such as collagen, chitosan, and hyaluronic acid (HA), exhibit inherent biocompatibility via enzymatic biodegradation but perform at a relatively low transfection efficiency [89]. The weakness of the natural polymers promotes the development of synthetic polymers for both biocompatibility and delivery efficiency. A representative biocompatible synthetic polymer is poly(lactide-co-glycolide) (PLGA) due to its hydrolysis into easily eliminated monomers of lactic acid and glycolic acid and its hydrophobicity for effective loading of hydrophobic DOX [90]. However, the limitation of hydrophobic PLGA in binding with negatively charged genes contributes to the use of positively charged synthetic polymers. High molecular weight polyethyleneimine (PEI) and polyamidoamine (PAMAM) dendrimer not only exhibit effective gene binding but also disrupt plasma membrane integrity to cause mitochondria and lysosome damages in normal cells [91-

93]. Surface modification with anionic succinamic acid or neutral aminoethanol on Generation 6 (G6) PAMAM did not cause severe cell mortality compared with non-modified G6 PAMAM [92]. Moreover, the use of biodegradable dendrimers, such as polyester, polyacetal, or other types of dendrimers, can avoid accumulation-induced cytotoxicity [94]. The amphiphilic property of lipid molecules, which consist of fatty acid hydrophobic tails and hydrophilic phosphate heads, in cell membranes is incorporated in liposome, micelle, nanoemulsion, and solid lipid nanoparticle delivery vectors [95]. The lipid-based vectors are beneficial for the sufficient loading of different types of multiple drugs, the control of carrier size, the simple modification of functions, and their minimal carrier-induced cytotoxicity [95]. However, lipid-based delivery vectors still face some drawbacks, such as instability of the loaded drugs, positive charge surface-induced toxicity, and uncontrolled drug precipitation [96].

Non-toxic or less toxic inorganic materials are key components for biocompatible delivery systems, such as mesoporous silica nanoparticles (MSNs), gold nanoparticles (AuNPs), carbon nanotubes (CNTs), quantum dots (QDs), and iron oxide nanoparticles (IONPs). Although silicone dioxide or silica is approved as biocompatible by the Food and Drug Administration (FDA) of the United States, MSNs are in conflict due to *in vivo* toxicity depending on the diversity of size, shape and surface charge, and ROS production from their surface [97]. Renal-clearable and optical nanoparticles, such as AuNPs, CNTs, and QDs, have not been observed *in vivo* or assessed for *in vitro* cytotoxicity and immunological toxicity, but deposition has been monitored in the liver, spleen, and lungs with possible long-term toxicity [98-105]. Although the biocompatibility of IONPs is approved for wide clinical use as a magnetic resonance (MR) imaging contrast agent and they are biodegraded into iron and iron ions, immune response by ROS production and the accumulation of large amounts in the spleen and liver have been observed [106-109].

The current trend of non-toxic materials for delivery vectors is a modified mixture of materials depending on the enhancement of specific functional conditions and biocompatibility.

2.4.1.2 Effective DOX loading

Drug delivery carriers have been developed to enhance the loading efficiency of a tunable solubility of DOX, such as cationic DOX·HCl and hydrophobic DOX (Figure 2.7). The conventional method of DOX loading is the physical adsorption of cationic DOX·HCl to the delivery carriers. For example, cationic DOX·HCl and another cationic chitosan can assemble nanoparticles with anionic HA, tripolyphosphate, and miR-34a via electrostatic interaction in aqueous media, expressing >40% encapsulation efficiency [78]. The hydrophilic DOX·HCl has been encapsulated in the internal aqueous cavity of a liposome, a phospholipid bilayer, producing the clinical product Doxil® [110]. The cationic DOX·HCl can also be loaded in the internal pores of anionic MSNs via electrostatic interaction, with possible leakage via the open pores [111].

Curry *et al.* produced citrate-capped AuNPs to effectively load DOX [112]. AuNPs incorporate four different mechanisms in DOX loading, namely, cation- π interaction between the cationic AuNP surface and tetracyclic ring of DOX, coordination chemistry between the AuNP surface and carbonyl moieties of DOX, electrostatic interaction between a protonated amine group in DOX and anionic citrate, and hydrogen bonding between DOX molecules. Runnim *et al.* loaded DOX·HCl to CNTs via π - π stacking interaction and encapsulation in the inner cavity with subsequent wrapping by deprotonated chitosan at pH 7.4 to protect leakage [113]. Hollow magnetic colloidal nanocrystal, a type of IONP, can effectively load DOX via nanoprecipitation to its inner large pore volume [114]. A zeolitic imidazolate framework (ZIF-8), a class of metal organic frameworks (MOFs), can encapsulate DOX·HCl in its large volume of pores via nanoprecipitation in a one-pot process with >40% loading capability [115].

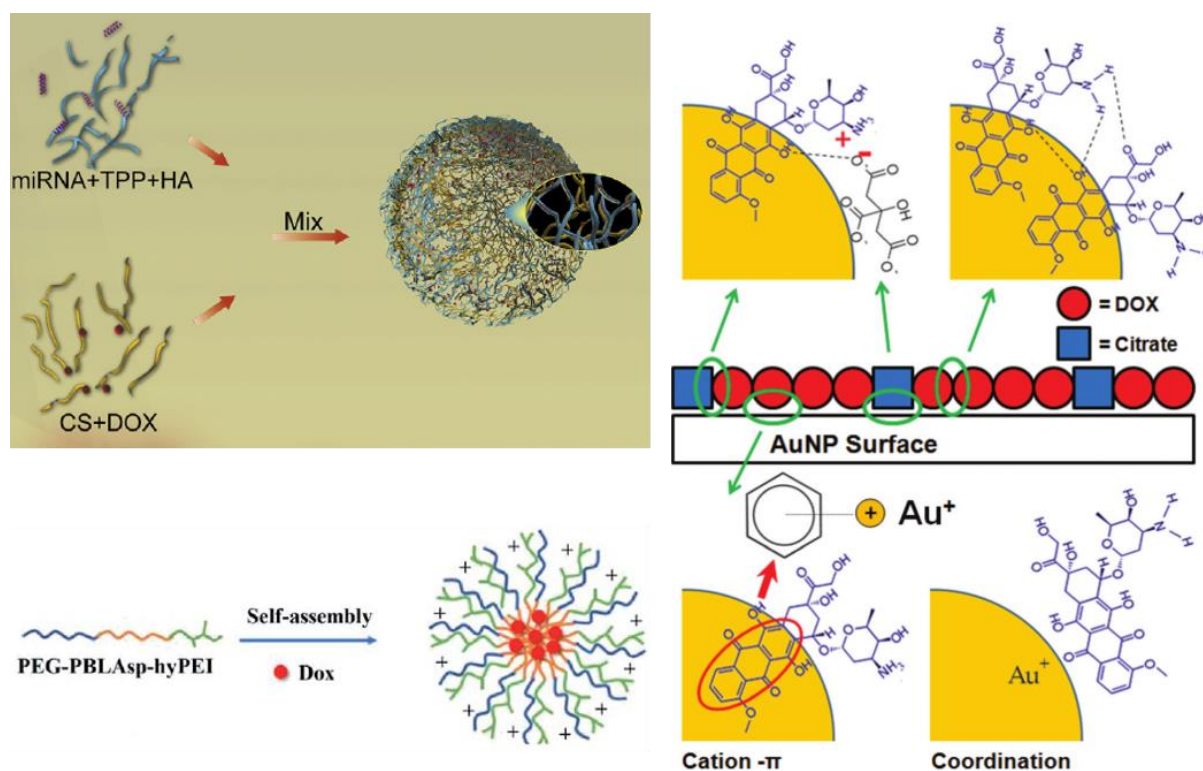


Figure 2.7 Schematic DOX loading mechanisms. Upper left: electrostatic interaction with DOX and HA as well as miRNA and chitosan, reused from [78] with copyright. Lower left: hydrophobic interaction of DOX with the hydrophobic core of polymer micelles, reused from [116] with copyright. Right: physical adsorptions of DOX to AuNPs, reused from [112] with copyright.

Another loading approach of hydrophobic DOX is the mainly hydrophobic interaction with the core space of micelles, solid lipid nanoparticles (SLNs), and nanoemulsions. Feng *et al.* prepared an amphiphilic triblock polymer of polyethylene glycol (PEG)-poly(β -benzyl L-aspartate) (PBLAsp)-PEI, where a hydrophobic block of PBLAsp interacts with the poorly water soluble DOX via self-assembling to micelles [116]. The hydrophobic DOX can be dispersed in a solid core of SLNs with a monolayer phospholipid coating [117]. Chen *et al.* produced cholesterol-PEG incorporated in pH-responsive SLNs that entrap DOX in the trilaurin-based hydrophobic core of the SLNs at pH 7.4 [118]. A nanoemulsion is an aqueous droplet consisting of two immiscible liquids to dissolve the hydrophobic DOX in an oil phase core, but its anionic surface charge is unsuitable to co-load anionic genes unless the surface is modified [119].

The avoidable pre-leakage of the physically loaded DOX from the delivery vectors encourages the covalent conjugation of DOX using chemical bonds to carriers on a polymer base or other material bases with a surface modification. Leong *et al.* prepared a PEG-protected Generation 4 polylysine dendrimer to conjugate DOX via cathepsin B-cleavable peptide linkers to enhance prolonged lung retention and good systemic circulation [120]. Ranjbar-Navazi *et al.* conjugated DOX to D-glucosamine and folate bifunctionalized InP/ZnS QDs via stable amide bond formation between the primary amine of DOX and the carboxylic surface of the QDs in the absence of amidase [121]. The functional groups of DOX used in covalent conjugation are the ketone group on a short side chain of the cyclohexane ring and the primary amine group at a daunosamine sugar linked to the cyclohexane ring (Figure 2.1). Ou *et al.* conjugated DOX to an enzyme-degradable diblock-*N*-(2-hydroxypropyl) methacrylamide (HPMA) polymer via a hydrazone bond between the ketone group of DOX and the acid-sensitive hydrazine moiety of the polymer with an excellent *in vivo* biocompatibility at a high loading capacity [122]. Zhu *et al.* produced PAMAM dendrimer-entrapped AuNPs with the covalent conjugation of DOX via acidic-sensitive cis-aconityl linkage using the primary amine group of DOX [123].

2.4.1.3 Effective gene loading

Therapeutic synergy with DOX and sub-gene drugs, such as miRNAs, siRNAs, plasmid DNAs (pDNAs) and aptamers, can be diverse, depending on the delivery efficiency of the carriers. Due to their anionic property, effective gene loading is directly associated with the intensity of positively charged moieties in the carriers, cationic polymers, cationic lipids, and surface-modified inorganics [79, 80].

Chitosan is a natural polymer-based gene delivery vector. Deng *et al.* formed natural polymer nanoparticles as a co-delivery vector via simultaneous interaction of miR-34a with chitosan and protonated DOX with anionic HA, but the chitosan-based nanoparticles demonstrated less-controlled release profiles [78]. The strongly positively charged synthetic polymers, PEI with

molecular weight of 25 kDa and PAMAM G6, demonstrate a high gene loading capacity and severe cytotoxicity, while the weakly charged polymers, low molecular weight of PEI (PEI800) and PAMAM G0, reduce both gene loading and cytotoxicity [91, 92, 124]. Our team synthesized degradable microgels from PEI800 with redox-cleavable disulfide crosslinkers to amplify the positive charge to be sufficiently strong for effective pDNA loading [88]. The degradable microgels return the charge to one weak enough for losing interaction with the genes and releasing them in a reductant cytosol condition as well as maintaining an acceptable cytotoxicity level to normal kidney cell line HEK293T. Yue *et al.* produced PEI nanoparticles using diselenide bonds as crosslinkers, thereby demonstrating better durability under physiological conditions and faster degradation in a cytosol environment than those using disulfide bonds [125].

The cationic surface of lipid vesicles is also suitable for gene interaction. Xu *et al.* produced cationic liposome, consisting of 1,2-dioleoyl-3-trimethylammonium-propane (DOTAP), cholesterol, and core-entrapped hydrophilic DOX, to co-deliver miR-101 to hepatocellular carcinoma with synergetic *in vivo* and *in vitro* antitumor effects [126]. Liu *et al.* prepared cationic DOTAP-based SLNs for the electrostatic interaction with miR-200c and the encapsulation of a hydrophobic drug in their core to treat CSCs in breast cancer [127].

Cationic modification on the surface of inorganic-based vectors allows the loading of anionic genes. Liu *et al.* modified the surface of MSNs with disulfide bond-linked PEI (1.8 kDa) to interact with miR-145 and entrap DOX in MSN pores, resulting in synergistic antitumor effects on orthotopic colorectal cancer [128]. Ren *et al.* synthesized PAMAM-modified hollow AuNPs for the interaction of miR-21i with the strong polycations and the adsorption of DOX in the hollow surface to enhance anticancer efficacy [129].

Therefore, the large molecular weight of cationic moieties can effectively load the genes via electrostatic interaction, but the remaining positive charges can result in a low delivery efficiency by RES clearance and severe cytotoxicity by non-selective charge interaction-mediated endocytosis. Furthermore, over-binding of the carriers to both DOX and genes can impede the drug release at the tumor site, creating a dilemma.

2.4.2 Blood circulation

Non-toxic material-based co-delivery carriers loaded with DOX and genes are systemically administered via intravenous (IV) injection. The carriers are expected to prolong the circulation in the bloodstream without degradation of the loaded genes by serum nucleases and clearance of the vectors by RES or the kidney until their successive extravasation via the pores of tumor vasculature.

2.4.2.1 Avoiding nuclease degradation

The supporting nucleic acid drugs, miRNAs, siRNAs, pDNAs, and Apts, are easily degraded during blood circulation by serum nucleases that hydrolyze the phosphodiester bonds of the polynucleotides. Zagorovsky *et al.* discovered the superior avoidance of the shorter oligonucleotide, such as miRNAs, from nuclease degradation compared with other nucleic acids [130].

Non-viral gene delivery vectors have been used to protect the loaded genes from degradation using protective layers. A conventional material used in the protective layer on the surface of the vectors is PEG, a polyether, consisting of long hydrophilic polymer chains that create a steric hindrance to the approach of nucleases [131]. Chemical modification with PEG, termed PEGylation, has been widely applied to the surface of diverse carrier types, e.g., polymers, micelles, SLNs, and MOFs. [71, 118, 132, 133]. However, the long polymer chain of PEG for the steric hindrance of serum adsorption also hinders the cellular uptake of the PEGylated

carriers [134]. Hama *et al.* suggested a charge-convertible liposome to overcome the PEG dilemma via surface coating with a peptide consisting of the negatively charged glutamic acid under physiological conditions and the positively protonatable histidine in the slightly acidic extracellular tumor environment [135]. The negatively charged vectors in blood circulation could avoid serum adsorption via electrostatic repulsion, while the positively converted charge at the tumor site could enhance cellular uptake of the vector via electrostatic interaction with the anionic cell membrane.

Serum protein binding to the positively charged surface of the vectors is also associated with their non-selective biodistribution due to the presence of targeting ligands in the serum proteins, such as transferrin, that can transport the bound carriers to the erythron and peripheral tissues [136]. Another newly emerging material for the protective layer on delivery vectors to avoid serum protein adsorption is HA, a glycosaminoglycan of the soft tissue extracellular matrix. An anionic surface modification using HA can permanently protect the co-delivery carriers from anionic serum protein adsorption via charge repulsion and support the selective cellular uptake via HA receptor-mediated endocytosis [137, 138].

2.4.2.2 Avoiding RES clearance

To prolong systemic circulation of co-delivery vectors, it is significantly important to evade detection and removal by the immune system, termed RES or mononuclear phagocyte system (MPS) clearance. The presence of a foreign substance in the bloodstream can stimulate antibody generation by B lymphocytes for marking as an antigen to enhance phagocytosis in the immune response [139]. Activation of the immune response is dependent on the characteristics of the vectors, such as surface charge, size, and geometric structure.

Such an antibody is a type of opsonin, anionic serum molecules in blood that bind to the cationic surface of delivery vectors via a process termed opsonization [140]. Opsonization

promotes opsonin receptor-mediated phagocytosis and the entrapment of the vectors in the RES organs, such as the spleen, liver, lung, and lymph nodes, resulting in clearance from the delivery course [141]. Therefore, surface modification using PEG or HA can confer a stealth function to the carriers for the protection from opsonization via steric hindrance or charge repulsion, thereby prolonging their systemic circulation [142, 143].

In addition to the surface charge, opsonization enlarges the carrier size, which facilitates detection by the RES and removal from delivery pathway [80]. By measuring *in vivo* blood circulation half-life, maximal limitations of particle size diameter to minimize RES clearance have been identified as 200 nm for micelles and 150 nm for spherical nanoparticles [144]. A particle size >200 nm limits the passage through spleen pores, resulting in accumulation in the spleen [145]. However, inorganic nanoparticles, such as AuNPs, silver nanoparticles, and titanium dioxide nanoparticles (TiO₂NPs), sized <100 nm have reported a high level of liver accumulation [76]. The flow of blood to the liver sinusoids occurs via fenestrated capillaries with a pore size up to 150 nm [146]. Nanoparticles smaller than the pores can extravasate and become accumulated in the liver. Kulkarni *et al.* produced anionic polystyrene nanoparticles (PSNPs) sized 20, 50, 100, 200, and 500 nm to investigate the size effect on *in vivo* distribution, resulting in an exceptionally high accumulation of the 50-nm PSNPs in the liver and spleen and 500-nm PSNPs in the spleen [147]. On the basis of RES clearance, a suitable size of delivery carriers can be narrowed to 100–200 nm.

RES clearance is also associated with the carrier geometric structures, such as spheres, hexagons, and rods, and their aspect ratio (AR) and axial length. Increasing the AR of CdTe QD-cystine composites in sphere, rod, and needle structures decreases macrophage uptake [148]. Hexagonal block copolymer nanoparticles exhibit less accumulation in the MPS organs than spherical nanoparticles at sizes >120 nm, while no difference in their behaviors are observed at sizes <70 nm [149]. In a comparison of the accumulation of rod structures in the

liver and spleen depending on axial length, shorter rods are mostly found in the liver, whereas longer ones are trapped in the spleen [146]. Therefore, a long and high AR of non-spherically shaped delivery carriers is better suited to prolonged blood circulation than spherical nanoparticles.

2.4.2.3 Avoiding renal clearance

Another factor to consider for prolonging systemic circulation of delivery vectors is the avoidance of renal clearance. Active kidney glomerular filtration strongly relies on a carrier size <6 nm in radius due to the diffusion through capillary endothelial pores, regardless of geometric features [146]. From an *in vivo* inhalation study, TiO₂NPs with a diameter < 20 nm were found in the kidney as well as the spleen, liver, and lungs [150]. Hence, delivery carrier size >20 nm can effectively avoid the renal clearance.

2.4.2.4 Effective extravasation

Tumorigenesis is accompanied by rapid angiogenesis via an exceptionally high expression of VEGF to deliver blood and nutrients to newly created neighboring tumor cells [151]. The new blood vessels are rapidly generated and contain large permeable endothelial layers [151]. Extravasation of delivery carriers into the tumor interstitium is possible via the leaky vasculature, termed by Maeda *et al.* as the enhanced permeability and retention (EPR) effect [152]. In general, carriers <500 nm can extravasate, although the pore size of the tumor vasculature varies according to tumor type [80]. However, a delivery carrier with a diameter smaller than the endothelial pore of fenestrated capillaries located in other organs can lead to non-selective distribution and reduction of delivery efficiency.

Passive targeting of delivery carriers to the tumor interstitium via the EPR effect occurs when the leaky blood vessel-induced high interstitial fluid pressure (IFP) inside tumors is compromised [144]. Larger pores generate higher IFPs that drive fluid flow away from the

tumor center and negatively influence the approach delivery vectors to tumors [153]. Chauhan *et al.* demonstrated that tumor interstitial normalization decreases the pore size of tumor vasculature and increases tumor penetration rates of particles [154].

To summarize, surface-modified delivery carriers with an appropriate size and shape enhance blood circulation via evasion of nuclease degradation, opsonization, RES, and renal clearance. However, it appears inefficient to allow the flow of delivery carriers to target cancer cells by matching the size of the carrier and the pore that is passively targeted via EPR and IFP, unless the passive targeting is supplemented by a more active targeting method.

2.4.3 Extracellular microenvironment

Following successful extravasation, delivery carriers loaded with DOX and genes and present in the extracellular tumor microenvironment are confronted with effective and selective cell internalization.

2.4.3.1 Effective cell internalization

The delivery carriers can enter cells via direct penetration or endocytosis. The cellular uptake of the carriers highly relies on their physicochemical properties, such as size, charge, solubility, and components.

2.4.3.1.1 Penetration

A direct route to the cytosol involves cellular uptake of the carriers via penetration without passage through endosomes and lysosomes, which eliminates the possible risk of lysosomal degradation by multiple enzymes in the acidic environment. Direct translocation of the carriers involves some hypothetical mechanisms, such as micelle formation, pore formation, and adaptive translocation, which is an energy and temperature-independent destabilization of the plasma membrane [155]. Conditions enabling the carriers to penetrate and cross over the

plasma membrane include a small diameter size and association with cell-penetrating peptides (CPPs) or pH-low insertion peptides (pHLIPs).

Delivery carriers with a small size can directly enter cells via an energy independent non-endocytic pathway. Mu *et al.* synthesized amorphous silica nanoparticles with a diameter of 14 nm, which enter the cytoplasm of A549 cells via direct penetration [156]. Bao *et al.* prepared positively charged-layered double hydroxide lactate nanosheets with a diameter of 30–60 nm and thickness of 0.5–2 nm, which freely penetrated into BY-2 cells [157].

The delivery carriers associated with CPPs, including human immunodeficiency virus (HIV) transactivator of transcription (Tat), arginine, and penetratin peptides, facilitate cellular uptake via energy independent membrane destabilization. Zaro and Shen discovered that Tat (YGRKKRRQRRR) and arginine YG(I-R)₉ primarily translocate into the cytosol of ovarian cells [158]. Watson *et al.* found longer penetratin (P16) more efficient for cytosol translocation than shorter penetratin (P7), due to better interaction of P16 with the fluid phase of bilayered lipid membranes than P7 [159]. However, the strong positive charge of carriers obtained by increasing the length of arginine or concentration of Tat and R₉ prefers the endocytic pathway instead of penetration [158, 160]. The large size also allows nanoparticles to preferentially enter cells via endocytosis. Arginine-conjugated MSNs with a size of 300 nm show 80% cellular uptake via endocytosis and only 20% uptake via penetration [161].

pHLIP-mediated penetration is another non-endocytic uptake pathway. pHLIPs are water soluble and remain in the extracellular environment at neutral pH, and they insert and remain in the cellular membrane by forming a stable transmembrane α -helix [155]. Cheng *et al.* delivered miR-155 inhibitor (antimiR-155) with pHLIP conjugation via disulfide bond to a mouse model of lymphoma, demonstrating direct translocation of antimiR-155 to the cytosol and inhibition of miR-155 in solid tumors (pH 6) [162].

2.4.3.1.2 Endocytosis

The most common route for cellular uptake of the carriers is endocytosis. In the endocytic pathway, the plasma membrane engulfs the carriers and subsequently pinches off to form endocytic vesicles that develop into or fuse with endosomes and transport the carriers to lysosomes [163]. Endosomal rupture releases the delivery carriers into the cytosolic environment.

Phagocytosis in the process of RES clearance is a class of endocytosis via specific ligand receptor mediation for particles with opsonization or sized 200–2000 nm [164, 165]. The major endocytic route is clathrin-mediated endocytosis, which includes receptor mediation to form membrane vesicles sized 60–120 nm for particle entry into cells [163]. Another route is caveolae-dependent endocytosis using caveolae, flask-shaped membrane invaginations with a cavity size of 50–80 nm, for transporting signals of cell growth, apoptosis, and angiogenesis as well as transcytosis of diseases, such as viruses and other pathogens [166]. As caveolae-dependent endocytosis sometimes bypasses lysosomes, it is better to avoid this route for delivery carriers that utilize lysosomal acid-responsive bonds in drug conjugation and release by controlling carrier size.

The surface charge of the delivery carrier is a critical factor for effective endocytosis. Positively charged carriers can strictly enter cells via clathrin-mediated endocytosis, whereas negatively charged carriers enter via both clathrin- and caveolae-mediated endocytosis [167]. Engineering of the surface charge of the carriers to a positive charge can enhance the electrostatic interaction with the phospholipid membrane in terms of the thermodynamic aspect and accelerate membrane engulfment [168]. Liu *et al.* demonstrated that PEI-PEG nanoparticles deliver DOX and pDNA to breast cancer cells with better transfection efficiency over a counter-carrier of liposomes [169]. Lin *et al.* prepared AuNPs with negative, neutral, and positive surface charges to compare cellular uptake and cytotoxicity [170]. As the surface charge increases from

negative to positive, cellular uptake of AuNPs is enhanced. However, strengthening the positive charge density results in direct penetration due to membrane disruption and severe cytotoxicity. Furthermore, it is highly probable that positively charged carriers will undergo opsonization followed by phagocytosis.

The hydrophobicity of delivery carriers affects their binding to the hydrophobic core of bilayered lipid membranes. The hydrophobic nanoparticles are stable in the middle of the membrane and become stuck without stimulating membrane wrapping for endocytosis, whereas semi-hydrophilic nanoparticles induce membrane engulfment [166]. However, hydrophobic nanoparticles sized 10–40 Å can become embedded in the hydrophobic core of the membrane and directly penetrate into the cytosol instead undergoing endocytosis [171].

Taken together, an effective cellular uptake of delivery carriers can be obtained by the determination of their size, surface charge, water solubility, and components, which lead to strategic delivery via penetration or endocytosis. However, cellular uptake via both routes still induces non-selective tumor delivery, potentially causing side effects.

2.4.3.2 Selective cell internalization

The cellular uptake of delivery vectors to only target cancer cells highly supports carrier-aided anticancer chemotherapy with enhanced delivery efficiency and minimized off-target-induced side effects. Targeting ligands on the surface of nanocarriers can allow interaction with specific receptors of the target cells via ligand–receptor binding. The specific receptors should be widely spread on the surface of the target cancer cells compared with normal cells. Targeting ligands can be classified as antibodies, peptides, aptamers, and HA.

Monoclonal antibodies (mAB) originating from cloned immune cells have been clinically utilized following US FDA approvals over the past three decades [172, 173]. Native forms of mABs possess their two binding sites as a merit, but their fragment crystalline (Fc) domain

interaction with Fc receptors on normal cells induces immunogenicity as a defect [174]. Fragment forms of mAB, such as antigen-binding fragment and single-chain variable fragment, can reduce the binding to normal cells and enhance specific binding to EGFR and VEGF receptors on cancer cells [173].

In the class of peptides, transferrin, a serum protein, allows carriers to arrive at the transferrin receptor-overexpressed cancer cells [80, 136]. Other targeting peptides include linear Arg-Gly-Asp (RGD) and cyclic RGD (cRGD), which interact with overexpressed $\alpha_v\beta_3$ integrin in tumor cells as well as neovascular endothelial cells and macrophages [175, 176]. The cationic peptides from lysine or arginine can induce cytotoxicity by disrupting mammalian membranes [177].

Targeting ligands with anionic properties are synthetic aptamers that bind to specific receptors, such as AS1411 to nucleolin and A10 to prostate-specific membrane antigen (PSMA). However, in practice, low satisfaction with their targeting ability requires their improvement [68]. Another negatively charged targeting agent is HA, a polysaccharide, which binds to its receptors overexpressed in invasive cancer cells. The interaction between HA and its receptors, such as CSC biomarker CD44 and receptor for HA-mediated motility, plays roles in inflammation, tumorigenesis, and metastasis [178]. Zhao *et al.* synthesized lipid nanoparticles with surface modification using HA for active cancer targeting and CPPs for direct translocation to the cytosol [179]. Additionally, HA-modified delivery carriers effectively enter the invasive cancer cells via HA receptor-mediated endocytosis [180]. Therefore, surface modification with HA holds great potential for anionic protection in blood circulation, active targeting, and receptor-mediated endocytosis into invasive cancer cells.

2.4.4 Intracellular microenvironment

Cellular internalized delivery vectors via active targeting and endocytosis should satisfy intracellular factors such as endosomal escape, spatiotemporal release, and excretion.

2.4.4.1 Effective endosomal escape

Following endocytosis, delivery carriers loaded with co-drugs are trapped in endosomes and further lysosomes with the danger of degradation by lysosomal enzymes and acidic conditions [181]. Cationic polymer-based carriers can avoid lysosomal degradation via the proton sponge effect [81]. Cationic or pH-responsive polymers in endosomes and lysosomes act as a proton sponge by adsorbing protons influxed from exterior endosomes to decrease the pH up to 4.0. Accumulation of the counter-ions supplied with the protons leads to osmotic swelling and triggers endosomal membrane rupture. The nanocarriers can escape from the endosome, termed endosomal escape.

Patil *et al.* synthesized triblock polymer nanocarriers of PAMAM-PEG-poly-L-lysine with effective endosomal escape via a tertiary amine-induced proton sponge effect [182]. Bonner *et al.* compared the endosomal escape with different types of PEIs, such as linear PEI, branched PEI (bPEI), and crosslinked linear PEI [183]. The effective performance of most of the PEIs, with the exception of low molecular weight bPEI, indicates secondary amine-dominated pH buffering. Panyam *et al.* measured the time for endosomal escape of the PLGA-based biodegradable nanoparticles as <10 min [184].

Although endocytotic pathways possess a risk of lysosomal degradation, cationic amine group-incorporated carriers can actively escape the endosome to the cytosol within a very short time.

2.4.4.2 Spatiotemporal release

Delivery carriers loaded with DOX and genes in the intracellular microenvironment are confronted with a controlled release of their cargoes by overcoming premature leakage and

incomplete release. In the case of physical loading of DOX to inside pores of MSNs, DOX can be prematurely released in the delivery course via open pores and become stuck in the deep inside of the pores. The electrostatic interaction between a slightly protonated amine group of DOX ($pK_a = 7.6$) and deprotonated silanol groups of MSN ($pK_a = 3.5$) is relatively stable at a physiological pH of 7.4, with possible leakage [51, 185]. However, the interaction in an acidic lysosomal pH of 4.5–5.0 is insufficiently stable to protonate the silanol group for the electrostatic repulsion-mediated release of the stuck DOX.

Delivery vectors should release their cargo drugs in targeted locations at an appropriate time to maximize therapeutic effects. The spatiotemporal release of DOX and gene can be triggered by extracellular or intracellular stimuli.

2.4.4.2.1 Extracellular stimuli-driven release

The use of extracellular stimuli has a key merit in the predetermination of location and timing for the release of co-drugs. Extracellular stimuli for co-drug release include high temperature, magnetic fields, ultrasound, and near infrared (NIR) light.

Thermoresponsive linkages or materials are involved in delivery systems for drug release under an external heating. Riedinger *et al.* conjugated DOX via local temperature-cleavable linkage of 2,2' azobis[*N*-(2-carboxyethyl)-2-methylpropionamidine] to IONPs [186]. The DOX release profile is directly proportional to increasing local heat. However, the effective release of DOX requires local heating up to 45 °C, higher than body temperature, which may damage normal cells and gene drugs. Rehman *et al.* produced thermoresponsive SLNs using lauric acid with oleic acid or linoleic acid, resulting in a burst release of co-entrapped drugs following heating to 39 °C due to solid-liquid phase transition [187]. However, a sustained leaking of drugs at 37 °C due to the narrow temperature range decreases delivery efficiency.

An alternating magnetic field (AMF) can generate thermal fluctuations, which drive the rotational movements of DOX. Santos *et al.* applied AMF at $H \times f = 4.9 \times 10^9 \text{ A m}^{-1}\text{s}^{-1}$ for 30 min to release the physically adsorbed DOX in β -cyclodextrin-decorated superparamagnetic nanoparticles [188]. The release of 92% of the loaded DOX with effective anticancer results on human lung cancer cell line A549 was observed. The AMF can increase heat up to 45 °C, with possible damages.

Therapeutic ultrasound is another external stimulus that triggers drug release. Rapoport *et al.* directly applied ultrasound to tumor tissue for the conversion of nanoemulsion droplets to microbubbles, which increases the volume containing the drugs and effects their release [189]. However, the instant high temperature shock from the ultrasound may damage normal cells.

NIR laser or light can be applied to release drugs from AuNPs via surface plasmon resonance. A continuous exposure to NIR light decays plasmons on the surface of AuNPs with electron relaxation, which reduces the attraction between AuNPs and drugs and releases the drugs [190]. Ren *et al.* applied NIR laser (964 nm wavelength) to PAMAM-modified hollow AuNPs to release DOX from the surface of AuNPs [129]. NIR light can also destabilize a micelle. Cao *et al.* employed NIR light (765 nm wavelength) to cleave 2-nitrobenzyl alcohol on the hydrophobic moiety in chitosan-based micelles, achieving fast, controlled release of drugs in deep tissue [191].

Although extracellular stimuli can remotely control the drug release as predetermined by the operator, the extra operation required for generating stimuli can induce possible side effects and a burden of cost and time to patients.

2.4.4.2.2 Intracellular stimuli-driven release

Intracellular environments, including acidic conditions, reductants, and enzymes, can stimulate delivery carriers to release their cargoes via hydrolyzing covalent linkers, decomposing carrier

morphologies, or reducing crosslinkers in the carrier structure (Figure 2.8). The methods of biostimuli-mediated drug release do not require any extra operation after IV injection.

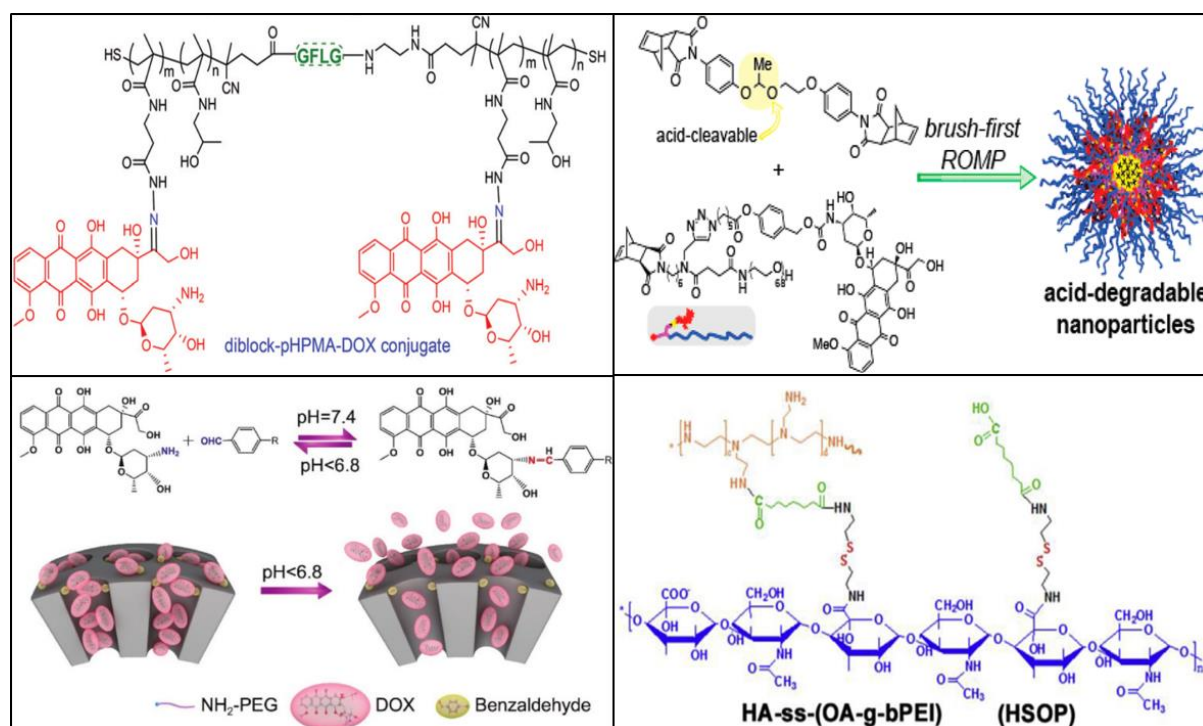


Figure 2.8 Intracellular stimuli-cleavable linkers. Upper left: acid-cleavable hydrazone bond and lysosomal enzyme cathepsin B-cleavable GFLG peptide linker, reused from [122] with copyright. Upper right: acid-cleavable acetal crosslinker, reused from [194] (<https://pubs.acs.org/doi/10.1021/mz5004097>) with copyright, further permission directed to ACS. Lower left: weak acid-cleavable benzoic imine bond used in self-gatekeeping, reused from [196] with copyright. Lower right: disulfide bond crosslinkers, reused from [200] with copyright.

The acidity of the extracellular tumor space endosome-lysosome pathway is gradually strengthened from pH 6.8 in the tumor extracellular microenvironment to pH 6.0–6.6 in early endosomes and pH 5.0 in late endosomes to pH of 4.5 in lysosomes [192, 193]. The acidic environment can hydrolyze pH-sensitive linkers, such as hydrazone bonds, acetal linkers, *cis*-aconityl linkers, and benzoic imine bonds. Ou *et al.* used a hydrazone bond to conjugate DOX to an HPMA polymer, resulting in effective leakage control at pH 7.4 and the intensive release of DOX at pH 5.4 [122]. Gao *et al.* utilized low pH-cleavable acetal crosslinkers in both brush-arm star polymer nanoparticle formation and DOX conjugation, thereby simultaneously

degrading the carriers and releasing DOX in an acidic environment [194]. Srinophakun and Boonmee conjugated DOX to glycol chitosan using *cis*-aconityl linkage that releases DOX via effective hydrolysis in the acidic environment of the lysosome [195]. The *cis*-aconityl linkage is a thermodynamically more stable conjugation in a normal environment, which can suppress the leakage of loaded DOX in the bloodstream. Zeng *et al.* also minimized the leakage problem of MSNs using a pH-sensitive benzoic imine covalent bond between DOX and benzaldehyde-functionalized MSNs as a gatekeeper [196]. In an acidic tumor extracellular microenvironment, the MSNs can open the gate via hydrolysis of the benzoic imine bond to allow the release of DOX from conjugation and encapsulation deep inside the pores.

Acidic cellular conditions can also reduce the encapsulation capability of drug carriers by decomposing the structure or altering the properties to cause drug release. Zhang *et al.* prepared ZIF-8 for the delivery of DOX using its high pore volume and a pH-stimulated release behavior [115]. The DOX release under acidic conditions of pH 5.0 is attributed to ZIF-8 decomposition via metal-oxygen bond-accelerated hydrolysis, thereby releasing approximately 40% of loaded DOX over 132 h. However, premature leakage through the pores in aqueous buffer at pH 7.4 remains less controlled, with the release of approximately 30% of loaded DOX over an equal time. Chen *et al.* produced SLNs to deliver DOX via acidic condition-facilitative release of DOX in the breast cancer cell line MCF-7/MDR, resulting in the release of 55% of the loaded DOX at pH 4.7 and 25% at pH 7.4 [118]. The protonated DOX in the acidic condition can lose interaction with hydrophobic core components of SLNs, such as hydrophobic trilaurin and protonated laurate ($pK_a = 5.34$ for the carboxyl moiety), thereby being releasing them from the core. Therefore, delivery carriers with pH-sensitive moieties can effectively control DOX release in an acidic pathway. However, lysosomal environment-based releasing strategies require an extremely active reaction to intensively release DOX over a short time because of lysosomal nuclease degradation of the co-delivered genes.

Other intracellular stimuli include enzymes that cleave amide bonds in peptide linkages. The amide bonds are normally stable under physiological conditions, whereas specific enzymes selectively hydrolyze them. Zhang *et al.* synthesized methoxy-PEGylated dendrimer with DOX conjugation via a Gly-Phe-Leu-Gly (GFLG) tetrapeptide linker that can be hydrolyzed by cathepsin B, a cysteine protease overexpressed in lysosomes of tumor endothelial cells [197]. These allow the release of drugs in a specific location: the lysosomes of tumor cells. A more specific tumor-related enzyme is prostate-specific antigen (PSA), which is secreted by prostate tumor cells. DeFeo-Jones *et al.* used *N*-glutaryl-(4-hydroxypropyl)-Ala-Ser-cyclohexaglycyl-Gln-Ser-Leu-COOH to covalently bond to the amine moiety of DOX for selective DOX delivery in prostate cancer [198]. The PSA cleaves the peptide linkers, including Gln-Ser-Leu sequences, releasing Leu-DOX in PSA-secreting prostate cancer cells but not in non-PSA secreting cells. Hence, site-specific enzymes can tightly control the target location and cells for drug release.

Endogenous thiol molecules, such as GSH, cysteine, and other cysteine-containing peptides, are highly concentrated in the tumor cytosol (14–20 mM) for the detoxification of free radicals and ROS [24, 199]. The thiol molecules play a role in disulfide exchange with redox-sensitive crosslinkers used in the formation of carrier structures, resulting in degradation of the carriers and drug release into the cytosol. Yin *et al.* synthesized a redox-sensitive micelle, (HA-SS-(octandioic acid (OA)-g-bPEI), to deliver aurora kinase A gene-specific siRNA and hydrophobic drugs to MDA-MB-231 cells [200]. In an aqueous buffer at pH 7.4 with 20 mM GSH, the micelles can cleave disulfide linkage between HA and OA, resulting in micelle disassembly and rapid release of the loaded co-drugs. Lu *et al.* synthesized disulfide-crosslinked Arg-Asp polypeptide to deliver pDNA in a bone-metastatic tumor by electrostatically forming a polypeptide-pDNA complex between the Arg moieties with the enhanced positively charged and negatively charged pDNA [201]. The complex loses the

electrostatic interactions with pDNA in the cytosol via reduction of the disulfide crosslinkers, becoming oligopeptides that release the pDNA. Therefore, the location of drug release from delivery carriers crosslinked with a disulfide bond can be controlled in the cytosol of cancer cells.

The location of DOX release influences its therapeutic effects via different apoptotic signaling pathways. Nuclear DOX directly induces DNA damage-induced apoptosis, while cytosolic DOX is highly involved in ROS-induced apoptosis. This broadens the stereotyped site of DOX release and DOX activity from only the nucleus to the cytosol. Besides, DOX released in the tumor extracellular microenvironment can reduce delivery efficiency. Therefore, it is critical to choose appropriate biostimuli-sensitive moieties for highly controlled drug release at the target location without premature leakage.

2.4.4.2.3 Sequential release

An advanced strategy to maximize therapeutic efficacy in multidrug-resistant cancers is the sequentially temporal treatment of anti-MDR gene drugs in advance of DOX treatment. The anti-MDR gene drugs, such as small interfering RNA (siRNA) and miR-21i, play a key role in reversing MDR prior to DOX administration as the major anticancer drug. The first administration of siRNA for P-gp inhibition leads to notable suppression of DOX exporters and requires a far less amount of DOX incorporation to achieve an identical therapeutic efficacy on multidrug-resistant cancer cell lines Caco-2/MDR1, MDA-MB-468/MDR1, and MCF-7/A than conventional chemotherapies [202, 203]. Ren *et al.* sequentially delivered miR-21i and then DOX, separated by a 4-h interval, to MDA-MB-231 CSCs, resulting in a >3-fold increase in anticancer efficacy than could be achieved with simultaneous delivery of the co-drugs [129]. They used an extracellular stimulus of NIR laser to control the timing of DOX release. However, we do not know the most appropriate timing of drug release in each target

cell. Such higher therapeutic efficacy with lesser DOX usage via sequential therapy of the co-drugs requires further research to obtain complete anticancer therapy with minimal side effects.

Taken together, a matching between intracellular stimuli and their sensitive moieties can equip co-drug delivery systems with the function of auto-control in their cargo release at the most suitable timing in each targeted cell, which may critically enhance delivery efficiency.

2.4.4.3 Complete excretion

The accumulation of delivery carriers after the release of loaded drugs in patient's body can induce considerable cytotoxicity and hinder further administration. Carriers are completely removed from the patient's body via urinary excretion and should be <6 nm in radius to filter through the kidneys [146]. Recent research has shown that a renal-clearable size of the delivery vectors and the use of biodegradable carriers should overcome the remaining accumulation obstacles.

Renal-clearable nanoparticles have been synthesized in the form of QDs, silica nanoparticles (SiNPs), polymer nanodots, and ultrasmall AuNPs. Choi *et al.* firstly synthesized CdSe/ZnS QDs with a hydrodynamic diameter <5.5 nm for rapid and efficient renal clearance [204]. Benezra *et al.* produced SiNPs with cRGD and optical dye incorporation in a hydrodynamic size of 7.0 nm for the detection of metastatic melanoma [205]. Shen *et al.* prepared ultrasmall coordination polymer nanodots with a renal-clearable diameter 5 nm for imaging [206]. However, the small-sized nanoparticles have been utilized for the purpose of optical imaging but not drug delivery. Ranjbar-Navazi *et al.* synthesized DOX-conjugated InP/ZnS QDs with a diameter of 11 nm by transmission electron microscopy [121]. Huo *et al.* used ultrasmall AuNPs with a size of 2.0 nm for the purpose of interfering with target gene transcription in the nucleus of cancer cells and HIV-infected cells by delivering triplex-forming oligonucleotides on the surface of the AuNPs [207].

Biodegradable nanoparticles have been developed to overcome the possible renal clearance of the ultrasmall nanoparticles in the delivery course before reaching their target cells. There are a number of biodegradable delivery vectors, e.g., biodegradable polymer nanogels and biodegradable dendrimers [94, 208]. Degradation of the biodegradable vectors into small molecular weight monomers or oligomers can be achieved via intracellular stimuli following the release of their cargo drugs. It is noteworthy that the degraded monomers and oligomers should be sufficiently small and non-toxic to the kidney for biocompatible urinary excretion.

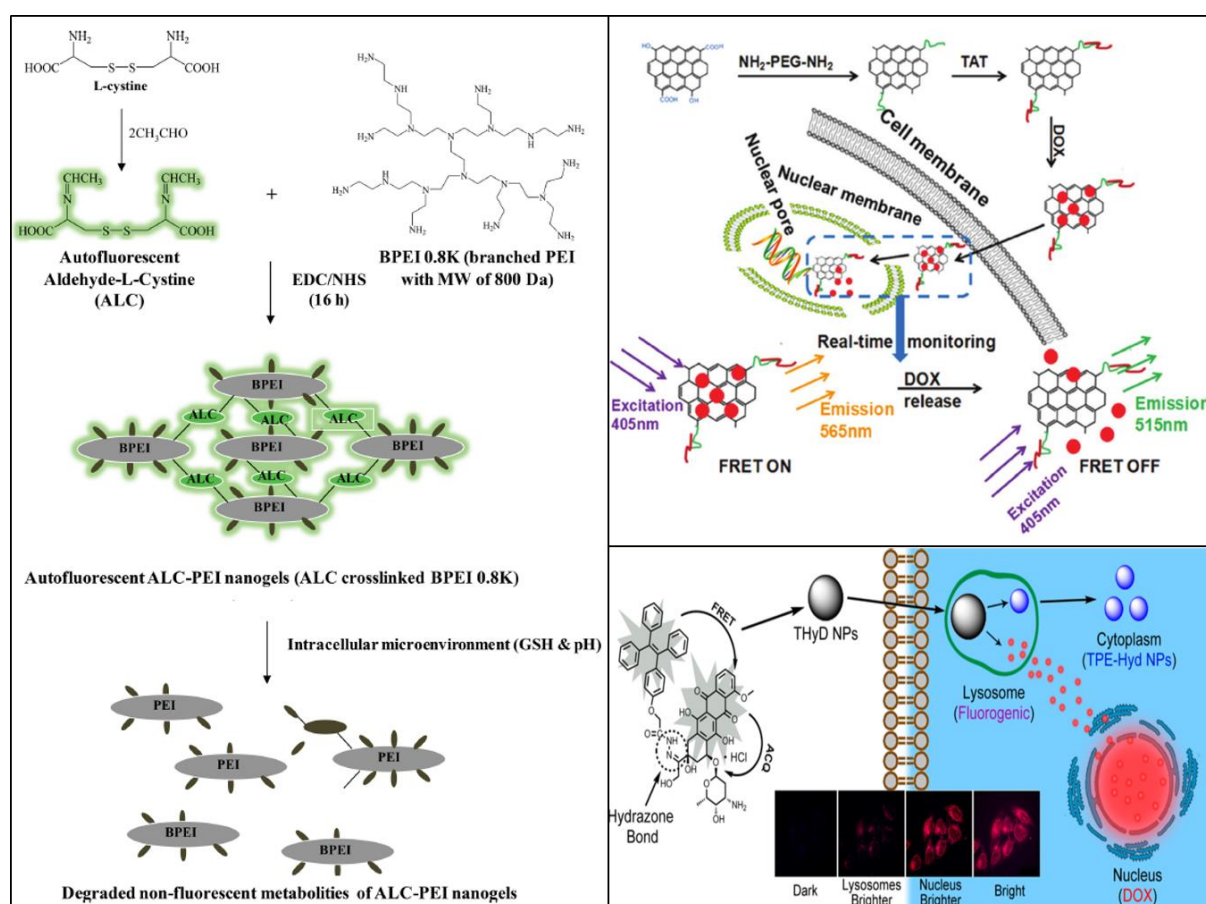


Figure 2.9 Methods to trace carriers and drug release. Left: label-free autofluorescent polymer nanogels and degradation-induced fluorescence-off, reused from [212] with copyright. Upper right: FRET-on between GQDs loaded with DOX and FRET-off when DOX is released, reused from [216] with copyright. Lower right: quenching of DOX via ACQ when conjugated to TPE and fluorescence-on of DOX after cleaving the hydrazone bond, reused from [217] with copyright.

2.4.5 Traceability over delivery course

Invisible conditions inside the body require traceability of the carriers and drugs to assess their delivery process in real-time (Figure 2.9). The association of imaging materials in delivery carriers provides information concerning their biodistribution and delivery efficiency. The optical properties of inorganic material-based carriers facilitate tracking of the delivery course. The superparamagnetism of IONPs enables MR imaging. Li *et al.* designed PEI-modified Fe₃O₄@SiO₂ nanoparticles for delivery of VEGF small hairpin RNA and MR imaging [209]. QDs are inorganic fluorophores with advanced properties of a wide wavelength range of excitation, a narrow emission bandwidth, and long-term imaging *in vitro* and *in vivo*. Wang *et al.* produced manganese-doped ZnSe QDs (d-dots) with PEI surface modification for the delivery of K-Ras siRNA and fluorescence imaging [210]. AuNPs with optical properties of light scattering and surface plasmon resonance allow computed tomography (CT) imaging and control spatiotemporal drug release. Kim *et al.* synthesized PSMA targeting aptamer-conjugated AuNPs for CT imaging and DOX delivery to prostate cancer cells [211].

Non-optical polymer-based delivery carriers also enable tracking of their pharmacokinetics. Our group proposed label-free autofluorescent nanogels for fluorescence imaging and pDNA delivery [212]. Disulfide-crosslinked bPEI contains autofluorescent aldehyde-L-cystine that emits fluorescence at 488 nm with excitation at 462 nm and releases pDNA in the cytosol. An anticancer DOX drug possesses inherent fluorescence with maximum excitation at 480–490 nm and emission at 580 nm. Delivery carriers with DOX conjugation allow monitoring of the cellular uptake of the carriers via fluorescence imaging of DOX [213]. Gene drugs obtain fluorescence via labeling with organic dyes, such as fluorescein amidite (FAM) and cyanine 5.5 (Cy5.5). Lin *et al.* utilized FAM-labeled siRNA to trace delivery carriers via siRNA binding to cationic poly(lactic acid) nanoparticles for silencing mutant *K-Ras* genes [214]. Palanca-

Wessels *et al.* synthesized polymeric micelles to deliver Cy5.5-labeled siRNA for traceable delivery and target gene suppression [215].

The detection of drug release from delivery systems provides spatiotemporal information to assess delivery quality and efficiency. To distinguish between loaded and released drug states, fluorescence from fluorophore-labeled co-drugs, such as DOX and FAM- or Cy5.5-labeled nucleic acids, should be transferred or quenched by carrier fluorophores, such as graphene quantum dots (GQDs), tetraphenylethylene (TPE), and black hole quencher. Chen *et al.* synthesized GQDs with Tat peptide and PEG surface modification for the delivery of DOX to the nuclei of HeLa cells and real-time monitoring of the DOX separation process [216]. The fluorescence emission wavelength of GQDs under excitation at 405 nm in the loaded DOX state is 565 nm due to Förster resonance energy transfer (FRET) between GQDs and DOX, while that of DOX in the released state is 515 nm due to off of the FRET. Xue *et al.* produced TPE molecules with hydrazone bond-linked DOX to monitor DOX release in MCF-7 cells [217]. In the DOX-conjugated state, TPE under excitation at 330 nm transfers the emitted energy to DOX under excitation at 477 nm, but both TPE and DOX are quenched due to energy transfer relay (ETR) from TPE to DOX as well as aggregation-caused quenching (ACQ) of DOX itself. In the DOX-released state, both TPE and DOX can emit the quenched fluorescence due to their far distance that hinders ETR and ACQ. For the effective quenching of the fluorescence emitted from a donor excitation, the emission wavelength of the donor should be the same as the excitation wavelength of an acceptor and the distance between them $<100 \text{ \AA}$ [218]. Qiu *et al.* designed a photocontrolled aptamer-based molecular beacon with a Cy3 fluorophore and a BHQ2 quencher modification to detect manganese superoxide dismutase (MnSOD) messenger RNA (mRNA) in blastoderm cells [219]. Detection of the MnSOD mRNA by the molecular beacon occurs via emission of the quenched fluorescence of Cy3 at 563 nm by BHQ2.

2.5 Summary and Future perspectives

The most active anticancer effects caused by DOX-based chemotherapy are due to the activation of two apoptotic pathways starting from the nucleus and cytosol of the target cells. Long-term DOX administration induces MDR, which encourages the incorporation of sub-drugs for therapeutic synergy. Strategies for enhancing therapeutic efficacy include co-therapy with gene drugs miR-21i and Apt and their sequential release to mitigate MDR by inhibiting anti-apoptotic signaling pathways and DOX exporters. However, non-selective distribution of the cytotoxic drugs induces severe side effects and low therapeutic efficiency. The strategy for high therapeutic efficiency and minimal side effects is the use of smart co-delivery carriers to selectively deliver the co-drugs to the target cells.

Successive design of smart co-delivery carriers should meet all the required factors in the delivery course via systemic administration. On the basis of the crucial factors, delivery carriers are expected to be biocompatible over the delivery course. Delivery systems for side-effect-free administration should satisfy all the factors, such as non-toxic materials in the carriers, no premature drug release, no clearance via systemic circulation, no normal cellular uptake, and no accumulation in the patient's body. Hence, the delivery systems should be non-toxic material-based biodegradable particles sized 100–200 nm with covalent conjugation to DOX, a negatively charged surface, and active targeting ligands. Furthermore, the delivery systems should yield degraded fragments with a radius < 6 nm that are biocompatible with kidney cells. Additionally, higher delivery efficiency requires the further functions of a high loading capacity of DOX and gene, rapid endosomal escape, spatiotemporally controlled release, and real-time monitoring. Therefore, the carriers should utilize stimuli-sensitive crosslinkers in their formation and DOX conjugation or gatekeepers on the DOX encapsulated in pores, contain strong positively charged moieties for electrostatic interaction with gene and endosomal escape, and include optical materials.

Some functional conditions, such as materials, charge, size, and loading mechanism, are still in conflict with each other for both side-effect-free and high delivery efficiency, but this must be overcome. Moreover, an exceptionally safe and effective anticancer therapy encourages designing the co-delivery systems to include a biocompatible evaluation *in vitro* and *in vivo* when delivery systems are loaded with co-drugs, which increases their feasibility in clinical applications. The use of Apt as a supplementary drug in isolating ATP to inhibit ABC transporters may be another strategy to enhance therapeutic efficacy. Advanced therapeutic strategies of multiple drug delivery and sequential delivery should involve an appropriately engineered design for the controlled release of multiple drugs by matching intracellular stimuli with the location and timing of drug release. More engineering approaches to the real-time assessment of spatiotemporal drug release should be motivated to provide crucial feedback on the design of delivery systems and contribute to the development of diverse and active therapeutic strategies.

Acknowledgement

We are grateful for the research grant of the Australian Research Council DP110102877 and DP140104062. SY would like to appreciate the APA scholarship provided by the University of Adelaide.

References

- [1] J. Greene, B. Hennessy, The role of anthracyclines in the treatment of early breast cancer, *J. Oncol. Pharm. Pract.*, 21 (2015) 201-212.
- [2] H. Zhao, X. Zhang, Enhanced apoptosis and inhibition of gastric cancer cell invasion following treatment with LDH@Au loaded Doxorubicin, *Electron. J. Biotechnol.*, 32 (2018) 13-18.
- [3] M. Li, Z. Tang, J. Lin, Y. Zhang, S. Lv, W. Song, Y. Huang, X. Chen, Synergistic antitumor effects of doxorubicin-loaded carboxymethyl cellulose nanoparticle in combination with endostar for effective treatment of non-small-cell lung cancer, *Adv. Healthc. Mater.*, 3 (2014) 1877-1888.
- [4] C. Pisano, S.C. Cecere, M. Di Napoli, C. Cavaliere, R. Tambaro, G. Facchini, C. Scaffa, S. Losito, A. Pizzolorusso, S. Pignata, Clinical trials with pegylated liposomal Doxorubicin in the treatment of ovarian cancer, *J. Drug Deliv.*, 2013 (2013) 898146.
- [5] N. Durán, W.J. Fávaro, Nanopharmaceuticals and Their Applications in Bladder Cancer Therapy: a Mini Review, *J. Braz. Chem. Soc.*, 29 (2018) 973-981.
- [6] G. Minotti, P. Menna, E. Salvatorelli, G. Cairo, L. Gianni, Anthracyclines: Molecular Advances and Pharmacologic Developments in Antitumor Activity and Cardiotoxicity, *Pharmacol. Rev.*, 56 (2004) 185-229.
- [7] J. Marinello, M. Delcuratolo, G. Capranico, Anthracyclines as Topoisomerase II Poisons: From Early Studies to New Perspectives, *Int. J. Mol. Sci.*, 19 (2018) 3480.
- [8] R.W. Lin, C.J. Ho, H.W. Chen, Y.H. Pao, L.E. Chen, M.C. Yang, S.B. Huang, S. Wang, C.H. Chen, C. Wang, P53 enhances apoptosis induced by doxorubicin only under conditions of severe DNA damage, *Cell Cycle*, 17 (2018) 2175-2186.
- [9] M. Schreiber, A. Kolbus, F. Piu, A. Szabowski, U. Möhle-Steinlein, J. Tian, M. Karin, P. Angel, E.F. Wagner, Control of cell cycle progression by c-Jun is p53 dependent, *Genes Dev.*, 13 (1999) 607-619.
- [10] M.M. Vleugel, A.E. Greijer, R. Bos, E. van der Wall, P.J. van Diest, c-Jun activation is associated with proliferation and angiogenesis in invasive breast cancer, *Hum. Pathol.*, 37 (2006) 668-674.
- [11] L. Ouyang, Z. Shi, S. Zhao, F.-T. Wang, T.-T. Zhou, B. Liu, J.-K. Bao, Programmed cell death pathways in cancer: a review of apoptosis, autophagy and programmed necrosis, *Cell Prolif.*, 45 (2012) 487-498.
- [12] R. Krishna, L.D. Mayer, Multidrug resistance (MDR) in cancer: Mechanisms, reversal using modulators of MDR and the role of MDR modulators in influencing the pharmacokinetics of anticancer drugs, *Eur. J. Pharm. Sci.*, 11 (2000) 265-283.
- [13] C. Holohan, S. Van Schaeybroeck, D.B. Longley, P.G. Johnston, Cancer drug resistance: an evolving paradigm, *Nat. Rev. Cancer*, 13 (2013) 714-726.

- [14] L. Agledal, M. Niere, M. Ziegler, The phosphate makes a difference: cellular functions of NADP, *Redox Rep*, 15 (2010) 2-10.
- [15] T. Simunek, M. Sterba, O. Popelova, M. Adamcova, R. Hrdina, V. Gersl, Anthracycline-induced cardiotoxicity: Overview of studies examining the roles of oxidative stress and free cellular iron, *Pharmacol. Rep.*, 61 (2009) 154-171.
- [16] D.W. Edwardson, R. Narendrula, S. Chewchuk, K. Mispel-Beyer, J.P.J. Mapletoft, A.M. Parissenti, Role of Drug Metabolism in the Cytotoxicity and Clinical Efficacy of Anthracyclines, *Curr. Drug Metab.*, 16 (2015) 412-426.
- [17] S.W. Ryter, H.P. Kim, A. Hoetzel, J.W. Park, K. Nakahira, X. Wang, A.M. Choi, Mechanisms of cell death in oxidative stress, *Antioxid. Redox Signal.*, 9 (2007) 49-89.
- [18] M. Redza-Dutordoir, D.A. Averill-Bates, Activation of apoptosis signalling pathways by reactive oxygen species, *Biochim. Biophys. Acta*, 1863 (2016) 2977-2992.
- [19] N. Pilco-Ferreto, G.M. Calaf, Influence of doxorubicin on apoptosis and oxidative stress in breast cancer cell lines, *Int. J. Oncol.*, 49 (2016) 753-762.
- [20] B. Tegze, Z. Szállási, I. Haltrich, Z. Pénczváltó, Z. Tóth, I. Likó, B. Györffy, Parallel Evolution under Chemotherapy Pressure in 29 Breast Cancer Cell Lines Results in Dissimilar Mechanisms of Resistance, *PLoS One*, 7 (2012) e30804.
- [21] L. Bao, S. Hazari, S. Mehra, D. Kaushal, K. Moroz, S. Dash, Increased Expression of P-Glycoprotein and Doxorubicin Chemoresistance of Metastatic Breast Cancer Is Regulated by miR-298, *Am. J. Pathol.*, 180 (2012) 2490-2503.
- [22] C. Leontiou, J.H. Lakey, C.A. Austin, Mutation E522K in Human DNA Topoisomerase II β Confers Resistance to Methyl N-(4'-(9-acridinylamino)-phenyl)carbamate hydrochloride and Methyl N-(4'-(9-acridinylamino)-3-methoxy-phenyl) methane sulfonamide but Hypersensitivity to Etoposide, *Mol. Pharmacol.*, 66 (2004) 430-439.
- [23] K.B. Tan, M.R. Mattern, W.K. Eng, F.L. McCabe, R.K. Johnson, Nonproductive rearrangement of DNA topoisomerase I and II genes: correlation with resistance to topoisomerase inhibitors, *J. Natl. Cancer Inst.*, 81 (1989) 1732-1735.
- [24] J. Deng, D. Coy, W. Zhang, M. Sunkara, A.J. Morris, C. Wang, L. Chaiswing, D. St Clair, M. Vore, P. Jungsuwadee, Elevated glutathione is not sufficient to protect against doxorubicin-induced nuclear damage in heart in multidrug resistance-associated protein 1 (Mrp1/Abcc1) null mice, *J. Pharmacol. Exp. Ther.*, 355 (2015) 272-279.
- [25] N. Verma, M. Vinayak, A low dose of doxorubicin improves antioxidant defence system and modulates anaerobic metabolism during the development of lymphoma, *Indian J. Pharmacol.*, 44 (2012) 308-313.
- [26] M. Konopleva, A. Tari, Z. Estrov, D. Harris, Z. Xie, S. Zhao, G. López-Berestein, M. Andreeff, Liposomal Bcl-2 antisense oligonucleotides enhance proliferation, sensitize acute myeloid leukemia to cytosine-arabioside, and induce apoptosis independent of other antiapoptotic proteins, *Blood*, 95 (2000) 3929-3938.

- [27] T.A. Buchholz, X. Tu, K.K. Ang, F.J. Esteva, H.M. Kuerer, L. Pusztai, M. Cristofanilli, S.E. Singletary, G.N. Hortobagyi, A.A. Sahin, Epidermal growth factor receptor expression correlates with poor survival in patients who have breast carcinoma treated with doxorubicin-based neoadjuvant chemotherapy, *Cancer*, 104 (2005) 676-681.
- [28] L. Huang, L. Fu, Mechanisms of resistance to EGFR tyrosine kinase inhibitors, *Acta Pharm. Sin. B*, 5 (2015) 390-401.
- [29] J.Á.F. Vara, E. Casado, J. de Castro, P. Cejas, C. Belda-Iniesta, M. González-Barón, PI3K/Akt signalling pathway and cancer, *Cancer Treat. Rev.*, 30 (2004) 193-204.
- [30] A.M. Abukhdeir, B.H. Park, P21 and p27: roles in carcinogenesis and drug resistance, *Expert Rev. Mol. Med.*, 10 (2008) e19-e19.
- [31] J. Karar, A. Maity, PI3K/AKT/mTOR Pathway in Angiogenesis, *Front. Mol. Neurosci.*, 4 (2011).
- [32] J.R. Molina, A.A. Adjei, The Ras/Raf/MAPK Pathway, *J. Thorac. Oncol.*, 1 (2006) 7-9.
- [33] A.M. Narasimha, M. Kaulich, G.S. Shapiro, Y.J. Choi, P. Sicinski, S.F. Dowdy, Cyclin D activates the Rb tumor suppressor by mono-phosphorylation, *eLife*, 3 (2014) e02872.
- [34] M. Navandar, A. Garding, S.K. Sahu, A. Pataskar, S. Schick, V.K. Tiwari, ERK signalling modulates epigenome to drive epithelial to mesenchymal transition, *Oncotarget*, 8 (2017) 29269-29281.
- [35] S. Shin, C.A. Dimitri, S.-O. Yoon, W. Dowdle, J. Blenis, ERK2 but not ERK1 induces epithelial-to-mesenchymal transformation via DEF motif-dependent signaling events, *Mol. Cell*, 38 (2010) 114-127.
- [36] S. Floor, W.C.G. van Staveren, D. Larsimont, J.E. Dumont, C. Maenhaut, Cancer cells in epithelial-to-mesenchymal transition and tumor-propagating-cancer stem cells: distinct, overlapping or same populations, *Oncogene*, 30 (2011) 4609.
- [37] L. Hu, F. Zou, J.R. Grandis, D.E. Johnson, Chapter 4 - The JNK Pathway in Drug Resistance, in: D.E. Johnson (Ed.) *Targeting Cell Survival Pathways to Enhance Response to Chemotherapy*, Academic Press, 2019, pp. 87-100.
- [38] N.V. Oleinik, N.I. Krupenko, S.A. Krupenko, Cooperation between JNK1 and JNK2 in activation of p53 apoptotic pathway, *Oncogene*, 26 (2007) 7222.
- [39] X. Zhan, X. Feng, Y. Kong, Y. Chen, W. Tan, JNK signaling maintains the mesenchymal properties of multi-drug resistant human epidermoid carcinoma KB cells through snail and twist1, *BMC Cancer*, 13 (2013) 180.
- [40] C.D. Andl, T. Mizushima, K. Oyama, M. Bowser, H. Nakagawa, A.K. Rustgi, EGFR-induced cell migration is mediated predominantly by the JAK-STAT pathway in primary esophageal keratinocytes, *Am. J. Physiol. Gastrointest. Liver Physiol.*, 287 (2004) G1227-1237.
- [41] I.A.W. Ho, K.Y.W. Chan, W.-H. Ng, C.M. Guo, K.M. Hui, P. Cheang, P.Y.P. Lam, Matrix metalloproteinase 1 is necessary for the migration of human bone marrow-derived mesenchymal stem cells toward human glioma, *Stem cells*, 27 (2009) 1366-1375.

- [42] H. Pan, K. Vojnits, T.T. Liu, F. Meng, L. Yang, Y. Wang, J. Huard, C.S. Cox, K.P. Lally, Y. Li, MMP1 gene expression enhances myoblast migration and engraftment following implanting into mdx/SCID mice, *Cell Adh. Migr.*, 9 (2015) 283-292.
- [43] M. Saxena, M.A. Stephens, H. Pathak, A. Rangarajan, Transcription factors that mediate epithelial-mesenchymal transition lead to multidrug resistance by upregulating ABC transporters, *Cell Death Dis.*, 2 (2011) e179.
- [44] M.M. Zhu, J.L. Tong, Q. Xu, F. Nie, X.T. Xu, S.D. Xiao, Z.H. Ran, Increased JNK1 Signaling Pathway Is Responsible for ABCG2-Mediated Multidrug Resistance in Human Colon Cancer, *PLoS One*, 7 (2012) e41763.
- [45] K.P. Locher, Review. Structure and mechanism of ATP-binding cassette transporters, *Philos. Trans. R. Soc. Lond. B Biol. Sci.*, 364 (2009) 239-245.
- [46] S.M. Swain, F.S. Whaley, M.S. Ewer, Congestive heart failure in patients treated with doxorubicin, *Cancer*, 97 (2003) 2869-2879.
- [47] G. Damodar, T. Smitha, S. Gopinath, S. Vijayakumar, Y. Rao, An evaluation of hepatotoxicity in breast cancer patients receiving injection Doxorubicin, *Ann. Med. Health Sci. Res.*, 4 (2014) 74-79.
- [48] C.-C. Peng, C.-L. Hsieh, Y.-B. Ker, H.-Y. Wang, K.-C. Chen, R.Y. Peng, Selected nutraceutic screening by therapeutic effects on doxorubicin-induced chronic kidney disease, *Mol. Nutr. Food Res.*, 56 (2012) 1541-1558.
- [49] E.C. Bredahl, K.B. Pfannenstiel, C.J. Quinn, R. Hayward, D.S. Hydock, Effects of Exercise on Doxorubicin-Induced Skeletal Muscle Dysfunction, *Med. Sci. Sports Exerc.*, 48 (2016) 1468-1473.
- [50] Z. Liu, A.C. Fan, K. Rakhra, S. Sherlock, A. Goodwin, X. Chen, Q. Yang, D.W. Felsher, H. Dai, Supramolecular Stacking of Doxorubicin on Carbon Nanotubes for In Vivo Cancer Therapy, *Angew. Chem. Int. Ed.*, 48 (2009) 7668-7672.
- [51] M. Dalmark, Characteristics of doxorubicin transport in human red blood cells, *Scand. J. Clin. Lab. Invest.*, 41 (1981) 633-639.
- [52] S. Eksborg, Extraction of Daunorubicin and Doxorubicin and Their Hydroxyl Metabolites: Self-Association in Aqueous Solution, *J. Pharm. Sci.*, 67 (1978) 782-785.
- [53] D.P. Bartel, Metazoan MicroRNAs, *Cell*, 173 (2018) 20-51.
- [54] W. Hu, C. Tan, Y. He, G. Zhang, Y. Xu, J. Tang, Functional miRNAs in breast cancer drug resistance, *Onco Targets Ther.*, 11 (2018) 1529-1541.
- [55] Z.-X. Wang, B.-B. Lu, H. Wang, Z.-X. Cheng, Y.-M. Yin, MicroRNA-21 Modulates Chemosensitivity of Breast Cancer Cells to Doxorubicin by Targeting PTEN, *Arch. Med. Res.*, 42 (2011) 281-290.
- [56] J. Niu, Y. Shi, G. Tan, C.H. Yang, M. Fan, L.M. Pfeffer, Z.-H. Wu, DNA Damage Induces NF- κ B-dependent MicroRNA-21 Up-regulation and Promotes Breast Cancer Cell Invasion, *J. Biol. Chem.*, 287 (2012) 21783-21795.

- [57] V. Grünwald, L. DeGraffenried, D. Russel, W.E. Friedrichs, R.B. Ray, M. Hidalgo, Inhibitors of mTOR Reverse Doxorubicin Resistance Conferred by PTEN Status in Prostate Cancer Cells, *Cancer Res.*, 62 (2002) 6141-6145.
- [58] C. Porta, C. Paglino, A. Mosca, Targeting PI3K/Akt/mTOR Signaling in Cancer, *Front. Oncol.*, 4 (2014) 64-64.
- [59] D.R. Gutsaeva, M. Thounaojam, S. Rajpurohit, F.L. Powell, P.M. Martin, S. Goei, M. Duncan, M. Bartoli, STAT3-mediated activation of miR-21 is involved in down-regulation of TIMP3 and neovascularization in the ischemic retina, *Oncotarget*, 8 (2017) 103568-103580.
- [60] J. Liu, R. Zhai, J. Zhao, F. Kong, J. Wang, W. Jiang, Q. Xin, X. Xue, Y. Luan, Programmed cell death 4 overexpression enhances sensitivity to cisplatin via the JNK/c-Jun signaling pathway in bladder cancer, *Int. J. Oncol.*, (2018).
- [61] Y.H. Feng, C.J. Tsao, Emerging role of microRNA-21 in cancer, *Biomed. Rep.*, 5 (2016) 395-402.
- [62] S. Zhang, L. Han, J. Wei, Z. Shi, P. Pu, J. Zhang, X. Yuan, C. Kang, Combination treatment with doxorubicin and microRNA-21 inhibitor synergistically augments anticancer activity through upregulation of tumor suppressing genes, *Int. J. Oncol.*, 46 (2015) 1589-1600.
- [63] F. Zhi, H. Dong, X. Jia, W. Guo, H. Lu, Y. Yang, H. Ju, X. Zhang, Y. Hu, Functionalized Graphene Oxide Mediated Adriamycin Delivery and miR-21 Gene Silencing to Overcome Tumor Multidrug Resistance In Vitro, *PLoS One*, 8 (2013) e60034.
- [64] Y. Naro, N. Ankenbruck, M. Thomas, Y. Tivon, C.M. Connelly, L. Gardner, A. Deiters, Small Molecule Inhibition of MicroRNA miR-21 Rescues Chemosensitivity of Renal-Cell Carcinoma to Topotecan, *J. Med. Chem.*, 61 (2018) 5900-5909.
- [65] A. Drakaki, M. Koutsoumpa, N.A. O'Brien, C. Vorvis, D. Iliopoulos, D.J. Slamon, A chemically-modified miR-21 inhibitor (ADM-21) as a novel potential therapy in bladder cancer, *J. Clin. Oncol.*, 35 (2017) 335-335.
- [66] B. Zhou, D. Wang, G. Sun, F. Mei, Y. Cui, H. Xu, Effect of miR-21 on Apoptosis in Lung Cancer Cell Through Inhibiting the PI3K/ Akt/NF- κ B Signaling Pathway In Vitro and in Vivo, *Cell. Physiol. Biochem.*, 46 (2018) 999-1008.
- [67] E. Austreid, S. Knappskog, P.E. Lonning, H.P. Eikesdal, The influence of doxorubicin on PTEN and PI3K-Akt-mTOR signaling in human breast cancer, *Cancer Res.*, 73 (2013) P5-08-05-P05-08-05.
- [68] A.V. Lakhin, V.Z. Tarantul, L.V. Gening, Aptamers: problems, solutions and prospects, *Acta Naturae*, 5 (2013) 34-43.
- [69] P. Yu, X. He, L. Zhang, L. Mao, Dual Recognition Unit Strategy Improves the Specificity of the Adenosine Triphosphate (ATP) Aptamer Biosensor for Cerebral ATP Assay, *Anal. Chem.*, 87 (2015) 1373-1380.
- [70] W.D. Pu, L. Zhang, C.Z. Huang, Graphene oxide as a nano-platform for ATP detection based on aptamer chemistry, *Analytical Methods*, 4 (2012) 1662-1666.

- [71] H. Wang, Y. Li, M. Zhang, D. Wu, Y. Shen, G. Tang, Y. Ping, Redox-Activatable ATP-Depleting Micelles with Dual Modulation Characteristics for Multidrug-Resistant Cancer Therapy, *Adv. Healthc. Mater.*, 6 (2017).
- [72] R. Mo, T. Jiang, R. DiSanto, W. Tai, Z. Gu, ATP-triggered anticancer drug delivery, *Nat. Commun.*, 5 (2014).
- [73] R. Mo, T. Jiang, W. Sun, Z. Gu, ATP-responsive DNA-graphene hybrid nanoaggregates for anticancer drug delivery, *Biomaterials*, 50 (2015) 67-74.
- [74] Y. Chen, D.-Y. Gao, L. Huang, In vivo delivery of miRNAs for cancer therapy: Challenges and strategies, *Adv. Drug Del. Rev.*, 81 (2015) 128-141.
- [75] S. Hossen, M.K. Hossain, M.K. Basher, M.N.H. Mia, M.T. Rahman, M.J. Uddin, Smart nanocarrier-based drug delivery systems for cancer therapy and toxicity studies: A review, *J. Adv. Res.*, 15 (2019) 1-18.
- [76] V. De Matteis, Exposure to Inorganic Nanoparticles: Routes of Entry, Immune Response, Biodistribution and In Vitro/In Vivo Toxicity Evaluation, *Toxics*, 5 (2017) 29.
- [77] X. Qian, L. Long, Z. Shi, C. Liu, M. Qiu, J. Sheng, P. Pu, X. Yuan, Y. Ren, C. Kang, Star-branched amphiphilic PLA-b-PDMAEMA copolymers for co-delivery of miR-21 inhibitor and doxorubicin to treat glioma, *Biomaterials*, 35 (2014) 2322-2335.
- [78] X. Deng, M. Cao, J. Zhang, K. Hu, Z. Yin, Z. Zhou, X. Xiao, Y. Yang, W. Sheng, Y. Wu, Y. Zeng, Hyaluronic acid-chitosan nanoparticles for co-delivery of MiR-34a and doxorubicin in therapy against triple negative breast cancer, *Biomaterials*, 35 (2014) 4333-4344.
- [79] H. Wang, Y. Jiang, H. Peng, Y. Chen, P. Zhu, Y. Huang, Recent progress in microRNA delivery for cancer therapy by non-viral synthetic vectors, *Adv. Drug Del. Rev.*, 81 (2015) 142-160.
- [80] S.H. Ku, K. Kim, K. Choi, S.H. Kim, I.C. Kwon, Tumor-Targeting Multifunctional Nanoparticles for siRNA Delivery: Recent Advances in Cancer Therapy, *Adv. Healthc. Mater.*, 3 (2014) 1182-1193.
- [81] S.A. Smith, L.I. Selby, A.P.R. Johnston, G.K. Such, The Endosomal Escape of Nanoparticles: Toward More Efficient Cellular Delivery, *Bioconjug. Chem.*, (2018).
- [82] C. Ding, Z. Li, A review of drug release mechanisms from nanocarrier systems, *Mater. Sci. Eng. C Mater. Biol. Appl.*, 76 (2017) 1440-1453.
- [83] M. Yu, J. Zheng, Clearance Pathways and Tumor Targeting of Imaging Nanoparticles, *ACS Nano*, 9 (2015) 6655-6674.
- [84] B. Shi, X. Du, J. Chen, L. Fu, M. Morsch, A. Lee, Y. Liu, N. Cole, R. Chung, Multifunctional Hybrid Nanoparticles for Traceable Drug Delivery and Intracellular Microenvironment-Controlled Multistage Drug-Release in Neurons, *Small*, 13 (2017) 1603966.
- [85] D. Liu, F. Yang, F. Xiong, N. Gu, The Smart Drug Delivery System and Its Clinical Potential, *Theranostics*, 6 (2016) 1306-1323.

- [86] K. Lundstrom, *Viral Vectors in Gene Therapy, Diseases*, 6 (2018) 42.
- [87] J.B. Zhang, S. Yun, J.X. Bi, S. Dai, Y.G. Du, A.C.W. Zannettino, H. Zhang, Enhanced multi-lineage differentiation of human mesenchymal stem/stromal cells within poly(N-isopropylacrylamide-acrylic acid) microgel-formed three-dimensional constructs, *J. Mater. Chem. B*, 6 (2018) 1799-1814.
- [88] B. Zhang, H. Zhang, S. Dai, J. Bi, Cell-penetrating peptide-labelled smart polymers for enhanced gene delivery, *Eng. Life Sci.*, 17 (2017) 193-203.
- [89] M.S. Hamid Akash, K. Rehman, S. Chen, Natural and Synthetic Polymers as Drug Carriers for Delivery of Therapeutic Proteins, *Polymer Reviews*, 55 (2015) 371-406.
- [90] E. Calzoni, A. Cesaretti, A. Polchi, A. Di Michele, B. Tancini, C. Emiliani, Biocompatible Polymer Nanoparticles for Drug Delivery Applications in Cancer and Neurodegenerative Disorder Therapies, *J. Funct. Biomater.*, 10 (2019).
- [91] A. Zakeri, M.A.J. Kouhbanani, N. Beheshtkhoo, V. Beigi, S.M. Mousavi, S.A.R. Hashemi, A. Karimi Zade, A.M. Amani, A. Savardashtaki, E. Mirzaei, S. Jahandideh, A. Movahedpour, Polyethylenimine-based nanocarriers in co-delivery of drug and gene: a developing horizon, *Nano Rev. Exp.*, 9 (2018) 1488497.
- [92] R.V. Araujo, S.D.S. Santos, E. Igne Ferreira, J. Giarolla, New Advances in General Biomedical Applications of PAMAM Dendrimers, *Molecules*, 23 (2018) 2849.
- [93] B.D. Monnery, M. Wright, R. Cavill, R. Hoogenboom, S. Shaunak, J.H.G. Steinke, M. Thanou, Cytotoxicity of polycations: Relationship of molecular weight and the hydrolytic theory of the mechanism of toxicity, *Int. J. Pharm.*, 521 (2017) 249-258.
- [94] D. Huang, D. Wu, Biodegradable dendrimers for drug delivery, *Mater. Sci. Eng. C Mater. Biol. Appl.*, 90 (2018) 713-727.
- [95] M.W. Kim, S.-H. Kwon, J.H. Choi, A. Lee, A Promising Biocompatible Platform: Lipid-Based and Bio-Inspired Smart Drug Delivery Systems for Cancer Therapy, *Int. J. Mol. Sci.*, 19 (2018) 3859.
- [96] P. Yingchoncharoen, D.S. Kalinowski, D.R. Richardson, Lipid-Based Drug Delivery Systems in Cancer Therapy: What Is Available and What Is Yet to Come, *Pharmacol. Rev.*, 68 (2016) 701-787.
- [97] M.L. Miller, A.J. Di Pasqua, Biocompatibility of Mesoporous Silica Nanoparticles? AU - Shi, Yi, *Comments Inorg. Chem.*, 36 (2016) 61-80.
- [98] C.L. Villiers, H. Freitas, R. Couderc, M.-B. Villiers, P.N. Marche, Analysis of the toxicity of gold nano particles on the immune system: effect on dendritic cell functions, *J. Nanopart. Res.*, 12 (2010) 55-60.
- [99] A.M. Alkilany, C.J. Murphy, Toxicity and cellular uptake of gold nanoparticles: what we have learned so far?, *J. Nanopart. Res.*, 12 (2010) 2313-2333.
- [100] Y.-P. Jia, B.-Y. Ma, X.-W. Wei, Z.-Y. Qian, The in vitro and in vivo toxicity of gold nanoparticles, *Chin. Chem. Lett.*, 28 (2017) 691-702.

- [101] M. Hatami, Toxicity assessment of multi-walled carbon nanotubes on *Cucurbita pepo* L. under well-watered and water-stressed conditions, *Ecotoxicol. Environ. Saf.*, 142 (2017) 274-283.
- [102] K. Fujita, M. Fukuda, S. Endoh, J. Maru, H. Kato, A. Nakamura, N. Shinohara, K. Uchino, K. Honda, Size effects of single-walled carbon nanotubes on in vivo and in vitro pulmonary toxicity, *Inhal. Toxicol.*, 27 (2015) 207-223.
- [103] B.B. Manshian, A.M. Abdelmonem, K. Kantner, B. Pelaz, M. Klapper, C. Nardi Tironi, W.J. Parak, U. Himmelreich, S.J. Soenen, Evaluation of quantum dot cytotoxicity: interpretation of nanoparticle concentrations versus intracellular nanoparticle numbers, *Nanotoxicology*, 10 (2016) 1318-1328.
- [104] X. Wang, J. Tian, K.T. Yong, X. Zhu, M.C. Lin, W. Jiang, J. Li, Q. Huang, G. Lin, Immunotoxicity assessment of CdSe/ZnS quantum dots in macrophages, lymphocytes and BALB/c mice, *J. Nanobiotechnology*, 14 (2016) 10.
- [105] A. Nel, T. Xia, L. Mädler, N. Li, Toxic Potential of Materials at the Nanolevel, *Science*, 311 (2006) 622-627.
- [106] E.B. Ehlerding, F. Chen, W. Cai, Biodegradable and Renal Clearable Inorganic Nanoparticles, *Adv. Sci. (Weinh)*, 3 (2016) 1500223.
- [107] D. Edge, C.M. Shortt, O.L. Gobbo, S. Teughels, A. Prina-Mello, Y. Volkov, P. MacEaney, M.W. Radomski, F. Markos, Pharmacokinetics and bio-distribution of novel super paramagnetic iron oxide nanoparticles (SPIONs) in the anaesthetized pig, *Clin. Exp. Pharmacol. Physiol.*, 43 (2016) 319-326.
- [108] S. Naqvi, M. Samim, M. Abdin, F.J. Ahmed, A. Maitra, C. Prashant, A.K. Dinda, Concentration-dependent toxicity of iron oxide nanoparticles mediated by increased oxidative stress, *Int. J. Nanomedicine*, 5 (2010) 983-989.
- [109] G. Jarockyte, E. Daugelaite, M. Stasys, U. Statkute, V. Poderys, T.C. Tseng, S.H. Hsu, V. Karabanovas, R. Rotomskis, Accumulation and Toxicity of Superparamagnetic Iron Oxide Nanoparticles in Cells and Experimental Animals, *Int. J. Mol. Sci.*, 17 (2016) 1193.
- [110] U. Bulbake, S. Doppalapudi, N. Kommineni, W. Khan, Liposomal Formulations in Clinical Use: An Updated Review, *Pharmaceutics*, 9 (2017).
- [111] A.D. Trofimov, A.A. Ivanova, M.V. Zyuzin, A.S. Timin, Porous Inorganic Carriers Based on Silica, Calcium Carbonate and Calcium Phosphate for Controlled/Modulated Drug Delivery: Fresh Outlook and Future Perspectives, *Pharmaceutics*, 10 (2018) 167.
- [112] D. Curry, A. Cameron, B. MacDonald, C. Nganou, H. Scheller, J. Marsh, S. Beale, M. Lu, Z. Shan, R. Kaliaperumal, H. Xu, M. Servos, C. Bennett, S. MacQuarrie, K.D. Oakes, M. Mkandawire, X. Zhang, Adsorption of doxorubicin on citrate-capped gold nanoparticles: insights into engineering potent chemotherapeutic delivery systems, *Nanoscale*, 7 (2015) 19611-19619.
- [113] C. Rungnim, T. Rungrotmongkol, R.P. Poo-Arporn, pH-controlled doxorubicin anticancer loading and release from carbon nanotube noncovalently modified by chitosan: MD simulations, *J. Mol. Graph. Model.*, 70 (2016) 70-76.

- [114] S. Shen, Y. Wu, Y. Liu, D. Wu, High drug-loading nanomedicines: progress, current status, and prospects, *Int. J. Nanomedicine*, 12 (2017) 4085-4109.
- [115] H. Zhang, W. Jiang, R. Liu, J. Zhang, D. Zhang, Z. Li, Y. Luan, Rational Design of Metal Organic Framework Nanocarrier-Based Codelivery System of Doxorubicin Hydrochloride/Verapamil Hydrochloride for Overcoming Multidrug Resistance with Efficient Targeted Cancer Therapy, *ACS Appl. Mater. Interfaces*, 9 (2017) 19687-19697.
- [116] H. Feng, D. Chu, Z. Li, Z. Guo, L. Jin, B. Fan, J. Zhang, J. Li, A DOX-loaded polymer micelle for effectively inhibiting cancer cells, *RSC Advances*, 8 (2018) 25949-25954.
- [117] V. Mishra, K.K. Bansal, A. Verma, N. Yadav, S. Thakur, K. Sudhakar, J.M. Rosenholm, Solid Lipid Nanoparticles: Emerging Colloidal Nano Drug Delivery Systems, *Pharmaceutics*, 10 (2018).
- [118] H.H. Chen, W.C. Huang, W.H. Chiang, T.I. Liu, M.Y. Shen, Y.H. Hsu, S.C. Lin, H.C. Chiu, pH-Responsive therapeutic solid lipid nanoparticles for reducing P-glycoprotein-mediated drug efflux of multidrug resistant cancer cells, *Int. J. Nanomedicine*, 10 (2015) 5035-5048.
- [119] M.H. Alkhatib, W.S. Alshehri, F.B. Abdu, In Vivo Evaluation of the Anticancer Activity of the Gemcitabine and Doxorubicin Combined in a Nanoemulsion, *J. Pharm. Bioallied Sci.*, 10 (2018) 35-42.
- [120] N.J. Leong, D. Mehta, V.M. McLeod, B.D. Kelly, R. Pathak, D.J. Owen, C.J.H. Porter, L.M. Kaminskas, Doxorubicin Conjugation and Drug Linker Chemistry Alter the Intravenous and Pulmonary Pharmacokinetics of a PEGylated Generation 4 Polylysine Dendrimer in Rats, *J. Pharm. Sci.*, 107 (2018) 2509-2513.
- [121] Z. Ranjbar-Navazi, M. Eskandani, M. Johari-Ahar, A. Nemati, H. Akbari, S. Davaran, Y. Omid, Doxorubicin-conjugated D-glucosamine- and folate- bi-functionalised InP/ZnS quantum dots for cancer cells imaging and therapy, *J. Drug Target.*, 26 (2018) 267-277.
- [122] Y. Ou, K. Chen, H. Cai, H. Zhang, Q. Gong, J. Wang, W. Chen, K. Luo, Enzyme/pH-sensitive polyHPMA-DOX conjugate as a biocompatible and efficient anticancer agent, *Biomater. Sci.*, 6 (2018) 1177-1188.
- [123] J. Zhu, G. Wang, C.S. Alves, H. Tomas, Z. Xiong, M. Shen, J. Rodrigues, X. Shi, Multifunctional Dendrimer-Entrapped Gold Nanoparticles Conjugated with Doxorubicin for pH-Responsive Drug Delivery and Targeted Computed Tomography Imaging, *Langmuir*, 34 (2018) 12428-12435.
- [124] E. Frohlich, The role of surface charge in cellular uptake and cytotoxicity of medical nanoparticles, *Int. J. Nanomedicine*, 7 (2012) 5577-5591.
- [125] D. Yue, G. Cheng, Y. He, Y. Nie, Q. Jiang, X. Cai, Z. Gu, Influence of reduction-sensitive diselenide bonds and disulfide bonds on oligoethylenimine conjugates for gene delivery, *J. Mater. Chem. B*, 2 (2014) 7210-7221.
- [126] F. Xu, J.Z. Liao, G.Y. Xiang, P.X. Zhao, F. Ye, Q. Zhao, X.X. He, MiR-101 and doxorubicin codelivered by liposomes suppressing malignant properties of hepatocellular carcinoma, *Cancer Med.*, 6 (2017) 651-661.

- [127] J. Liu, T. Meng, M. Yuan, L. Wen, B. Cheng, N. Liu, X. Huang, Y. Hong, H. Yuan, F. Hu, MicroRNA-200c delivered by solid lipid nanoparticles enhances the effect of paclitaxel on breast cancer stem cell, *Int. J. Nanomedicine*, 11 (2016) 6713-6725.
- [128] H.-J. Liu, X. Luan, H.-Y. Feng, X. Dong, S.-C. Yang, Z.-J. Chen, Q.-Y. Cai, Q. Lu, Y. Zhang, P. Sun, M. Zhao, H.-Z. Chen, J.F. Lovell, C. Fang, Integrated Combination Treatment Using a “Smart” Chemotherapy and MicroRNA Delivery System Improves Outcomes in an Orthotopic Colorectal Cancer Model, *Adv. Funct. Mater.*, 28 (2018).
- [129] Y. Ren, R. Wang, L. Gao, K. Li, X. Zhou, H. Guo, C. Liu, D. Han, J. Tian, Q. Ye, Y.T. Hu, D. Sun, X. Yuan, N. Zhang, Sequential co-delivery of miR-21 inhibitor followed by burst release doxorubicin using NIR-responsive hollow gold nanoparticle to enhance anticancer efficacy, *J. Control. Release*, 228 (2016) 74-86.
- [130] K. Zagorovsky, L.Y.T. Chou, W.C.W. Chan, Controlling DNA-nanoparticle serum interactions, *Proc. Natl. Acad. Sci. U. S. A.*, 113 (2016) 13600-13605.
- [131] P. Mishra, B. Nayak, R.K. Dey, PEGylation in anti-cancer therapy: An overview, *Asian J. Pharm. Sci.*, 11 (2016) 337-348.
- [132] J. Qian, M. Xu, A. Suo, W. Xu, T. Liu, X. Liu, Y. Yao, H. Wang, Folate-decorated hydrophilic three-arm star-block terpolymer as a novel nanovehicle for targeted co-delivery of doxorubicin and Bcl-2 siRNA in breast cancer therapy, *Acta Biomater.*, 15 (2015) 102-116.
- [133] I. Abanades Lazaro, S. Haddad, J.M. Rodrigo-Munoz, R.J. Marshall, B. Sastre, V. Del Pozo, D. Fairen-Jimenez, R.S. Forgan, Surface-Functionalization of Zr-Fumarate MOF for Selective Cytotoxicity and Immune System Compatibility in Nanoscale Drug Delivery, *ACS Appl. Mater. Interfaces*, 10 (2018) 31146-31157.
- [134] T. Wang, J.R. Upponi, V.P. Torchilin, Design of multifunctional non-viral gene vectors to overcome physiological barriers: Dilemmas and strategies, *Int. J. Pharm.*, 427 (2012) 3-20.
- [135] S. Hama, S. Itakura, M. Nakai, K. Nakayama, S. Morimoto, S. Suzuki, K. Kogure, Overcoming the polyethylene glycol dilemma via pathological environment-sensitive change of the surface property of nanoparticles for cellular entry, *J. Control. Release*, 206 (2015) 67-74.
- [136] E. Tolosano, Increasing serum transferrin to reduce tissue iron overload due to ineffective erythropoiesis, *Haematologica*, 100 (2015) 565-566.
- [137] X. Du, P.L. Dubin, D.A. Hoagland, L. Sun, Protein-selective coacervation with hyaluronic acid, *Biomacromolecules*, 15 (2014) 726-734.
- [138] H. Yin, F. Zhao, D. Zhang, J. Li, Hyaluronic acid conjugated β -cyclodextrin-oligoethylenimine star polymer for CD44-targeted gene delivery, *Int. J. Pharm.*, 483 (2015) 169-179.
- [139] A.O. Kordon, H. Abdelhamed, H. Ahmed, J.Y. Park, A. Karsi, L.M. Pinchuk, Phagocytic and Bactericidal Properties of Channel Catfish Peritoneal Macrophages Exposed to *Edwardsiella ictaluri* Live Attenuated Vaccine and Wild-Type Strains, *Front. Microbiol.*, 8 (2017) 2638.

- [140] G.L. Szeto, E.B. Lavik, Materials design at the interface of nanoparticles and innate immunity, *J. Mater. Chem. B*, 4 (2016) 1610-1618.
- [141] I.V. Zelepukin, A.V. Yaremenko, E.V. Petersen, S.M. Deyev, V.R. Cherkasov, P.I. Nikitin, M.P. Nikitin, Magnetometry based method for investigation of nanoparticle clearance from circulation in a liver perfusion model, *Nanotechnology*, 30 (2019) 105101.
- [142] J.H. Park, G. von Maltzahn, L. Zhang, M.P. Schwartz, E. Ruoslahti, S.N. Bhatia, M.J. Sailor, Magnetic Iron Oxide Nanoworms for Tumor Targeting and Imaging, *Adv. Mater.*, 20 (2008) 1630-1635.
- [143] L. Zhong, L. Xu, Y. Liu, Q. Li, D. Zhao, Z. Li, H. Zhang, H. Zhang, Q. Kan, Y. Wang, J. Sun, Z. He, Transformative hyaluronic acid-based active targeting supramolecular nanoplatform improves long circulation and enhances cellular uptake in cancer therapy, *Acta Pharm. Sin. B*, 9 (2019) 397-409.
- [144] N. Hoshyar, S. Gray, H. Han, G. Bao, The effect of nanoparticle size on in vivo pharmacokinetics and cellular interaction, *Nanomedicine (Lond)*, 11 (2016) 673-692.
- [145] S.M. Moghimi, Mechanisms of splenic clearance of blood cells and particles: towards development of new splenotropic agents, *Adv. Drug Del. Rev.*, 17 (1995) 103-115.
- [146] M.B. Fish, A.J. Thompson, C.A. Fromen, O. Eniola-Adefeso, Emergence and Utility of Nonspherical Particles in Biomedicine, *Ind. Eng. Chem. Res.*, 54 (2015) 4043-4059.
- [147] S.A. Kulkarni, S.-S. Feng, Effects of Particle Size and Surface Modification on Cellular Uptake and Biodistribution of Polymeric Nanoparticles for Drug Delivery, *Pharm. Res.*, 30 (2013) 2512-2522.
- [148] Z. Lu, Y. Qiao, X.T. Zheng, M.B. Chan-Park, C.M. Li, Effect of particle shape on phagocytosis of CdTe quantum dot–cystine composites, *MedChemComm*, 1 (2010) 84.
- [149] S.-Y. Lin, W.-H. Hsu, J.-M. Lo, H.-C. Tsai, G.-H. Hsiue, Novel geometry type of nanocarriers mitigated the phagocytosis for drug delivery, *J. Control. Release*, 154 (2011) 84-92.
- [150] I. Pujalte, D. Dieme, S. Haddad, A.M. Serventi, M. Bouchard, Toxicokinetics of titanium dioxide (TiO₂) nanoparticles after inhalation in rats, *Toxicol. Lett.*, 265 (2017) 77-85.
- [151] P. Carmeliet, R.K. Jain, Molecular mechanisms and clinical applications of angiogenesis, *Nature*, 473 (2011) 298.
- [152] H. Maeda, J. Wu, T. Sawa, Y. Matsumura, K. Hori, Tumor vascular permeability and the EPR effect in macromolecular therapeutics: a review, *J. Control. Release*, 65 (2000) 271-284.
- [153] C.H. Heldin, K. Rubin, K. Pietras, A. Ostman, High interstitial fluid pressure - an obstacle in cancer therapy, *Nat. Rev. Cancer*, 4 (2004) 806-813.
- [154] V.P. Chauhan, T. Stylianopoulos, J.D. Martin, Z. Popovic, O. Chen, W.S. Kamoun, M.G. Bawendi, D. Fukumura, R.K. Jain, Normalization of tumour blood vessels improves the delivery of nanomedicines in a size-dependent manner, *Nat. Nanotechnol.*, 7 (2012) 383-388.

- [155] Z. Li, Y. Zhang, D. Zhu, S. Li, X. Yu, Y. Zhao, X. Ouyang, Z. Xie, L. Li, Transporting carriers for intracellular targeting delivery via non-endocytic uptake pathways, *Drug Deliv.*, 24 (2017) 45-55.
- [156] Q. Mu, N.S. Hondow, L. Krzeminski, A.P. Brown, L.J. Jeuken, M.N. Routledge, Mechanism of cellular uptake of genotoxic silica nanoparticles, *Part. Fibre Toxicol.*, 9 (2012) 29.
- [157] W. Bao, J. Wang, Q. Wang, D. O'Hare, Y. Wan, Layered Double Hydroxide Nanotransporter for Molecule Delivery to Intact Plant Cells, *Sci. Rep.*, 6 (2016) 26738.
- [158] J.L. Zaro, W.-C. Shen, Quantitative comparison of membrane transduction and endocytosis of oligopeptides, *Biochem. Biophys. Res. Commun.*, 307 (2003) 241-247.
- [159] G.M. Watson, K. Kulkarni, R. Brandt, M.P. Del Borgo, M.-I. Aguilar, J.A. Wilce, Shortened Penetratin Cell-Penetrating Peptide Is Insufficient for Cytosolic Delivery of a Grb7 Targeting Peptide, *ACS omega*, 2 (2017) 670-677.
- [160] C.Y. Jiao, D. Delaroche, F. Burlina, I.D. Alves, G. Chassaing, S. Sagan, Translocation and endocytosis for cell-penetrating peptide internalization, *J. Biol. Chem.*, 284 (2009) 33957-33965.
- [161] C.H. Wu, Y.P. Chen, S.H. Wu, Y. Hung, C.Y. Mou, R.P. Cheng, Enhanced non-endocytotic uptake of mesoporous silica nanoparticles by shortening the peptide transporter arginine side chain, *ACS Appl. Mater. Interfaces*, 5 (2013) 12244-12248.
- [162] C.J. Cheng, R. Bahal, I.A. Babar, Z. Pincus, F. Barrera, C. Liu, A. Svoronos, D.T. Braddock, P.M. Glazer, D.M. Engelman, W.M. Saltzman, F.J. Slack, MicroRNA silencing for cancer therapy targeted to the tumour microenvironment, *Nature*, 518 (2015) 107-110.
- [163] M. Kaksonen, A. Roux, Mechanisms of clathrin-mediated endocytosis, *Nat. Rev. Mol. Cell Biol.*, 19 (2018) 313-326.
- [164] V. Schäfer, H. von Briesen, R. Andreesen, A.-M. Steffan, C. Royer, S. Tröster, J. Kreuter, H. Rübsamen-Waigmann, Phagocytosis of Nanoparticles by Human Immunodeficiency Virus (HIV)-Infected Macrophages: A Possibility for Antiviral Drug Targeting, *Pharm. Res.*, 9 (1992) 541-546.
- [165] Y. Liu, A. Ibricevic, J.A. Cohen, J.L. Cohen, S.P. Gunsten, J.M.J. Fréchet, M.J. Walter, M.J. Welch, S.L. Brody, Impact of hydrogel nanoparticle size and functionalization on in vivo behavior for lung imaging and therapeutics, *Mol. Pharm.*, 6 (2009) 1891-1902.
- [166] S. Behzadi, V. Serpooshan, W. Tao, M.A. Hamaly, M.Y. Alkawareek, E.C. Dreaden, D. Brown, A.M. Alkilany, O.C. Farokhzad, M. Mahmoudi, Cellular uptake of nanoparticles: journey inside the cell, *Chem. Soc. Rev.*, 46 (2017) 4218-4244.
- [167] O. Harush-Frenkel, N. Debotton, S. Benita, Y. Altschuler, Targeting of nanoparticles to the clathrin-mediated endocytic pathway, *Biochem. Biophys. Res. Commun.*, 353 (2007) 26-32.
- [168] Y. Li, N. Gu, Thermodynamics of charged nanoparticle adsorption on charge-neutral membranes: a simulation study, *J. Phys. Chem. B*, 114 (2010) 2749-2754.

- [169] C. Liu, F. Liu, L. Feng, M. Li, J. Zhang, N. Zhang, The targeted co-delivery of DNA and doxorubicin to tumor cells via multifunctional PEI-PEG based nanoparticles, *Biomaterials*, 34 (2013) 2547-2564.
- [170] J. Lin, H. Zhang, Z. Chen, Y. Zheng, Penetration of Lipid Membranes by Gold Nanoparticles: Insights into Cellular Uptake, Cytotoxicity, and Their Relationship, *ACS Nano*, 4 (2010) 5421-5429.
- [171] E.M. Curtis, A.H. Bahrami, T.R. Weikl, C.K. Hall, Modeling nanoparticle wrapping or translocation in bilayer membranes, *Nanoscale*, 7 (2015) 14505-14514.
- [172] D. Peer, J.M. Karp, S. Hong, O.C. Farokhzad, R. Margalit, R. Langer, Nanocarriers as an emerging platform for cancer therapy, *Nat. Nanotechnol.*, 2 (2007) 751-760.
- [173] M.v. Mehren, G.P. Adams, L.M. Weiner, Monoclonal Antibody Therapy for Cancer, *Annu. Rev. Med.*, 54 (2003) 343-369.
- [174] E. Ball, J. McDermott, J. Griffin, F. Davey, R. Davis, C. Bloomfield, Expression of the three myeloid cell-associated immunoglobulin G Fc receptors defined by murine monoclonal antibodies on normal bone marrow and acute leukemia cells, *Blood*, 73 (1989) 1951-1956.
- [175] J.S. Desgrosellier, D.A. Cheresh, Integrins in cancer: biological implications and therapeutic opportunities, *Nat. Rev. Cancer*, 10 (2010) 9-22.
- [176] H. Yamaguchi, J. Takagi, T. Miyamae, S. Yokota, T. Fujimoto, S. Nakamura, S. Ohshima, T. Naka, S. Nagata, Milk fat globule EGF factor 8 in the serum of human patients of systemic lupus erythematosus, *J. Leukoc. Biol.*, 83 (2008) 1300-1307.
- [177] L. Otvos, Jr., J.D. Wade, Current challenges in peptide-based drug discovery, *Front. Chem.*, 2 (2014) 62.
- [178] S. Misra, V.C. Hascall, R.R. Markwald, S. Ghatak, Interactions between Hyaluronan and Its Receptors (CD44, RHAMM) Regulate the Activities of Inflammation and Cancer, *Front. Immunol.*, 6 (2015) 201.
- [179] H. Zhao, M. Wu, L. Zhu, Y. Tian, M. Wu, Y. Li, L. Deng, W. Jiang, W. Shen, Z. Wang, Z. Mei, P. Li, H. Ran, Z. Zhou, J. Ren, Cell-penetrating Peptide-modified Targeted Drug-loaded Phase-transformation Lipid Nanoparticles Combined with Low-intensity Focused Ultrasound for Precision Theranostics against Hepatocellular Carcinoma, *Theranostics*, 8 (2018) 1892-1910.
- [180] Y. He, G. Cheng, L. Xie, Y. Nie, B. He, Z. Gu, Polyethyleneimine/DNA polyplexes with reduction-sensitive hyaluronic acid derivatives shielding for targeted gene delivery, *Biomaterials*, 34 (2013) 1235-1245.
- [181] D. Ma, Enhancing endosomal escape for nanoparticle mediated siRNA delivery, *Nanoscale*, 6 (2014) 6415-6425.
- [182] M.L. Patil, M. Zhang, T. Minko, Multifunctional Triblock Nanocarrier (PAMAM-PEG-PLL) for the Efficient Intracellular siRNA Delivery and Gene Silencing, *ACS Nano*, 5 (2011) 1877-1887.

- [183] D.K. Bonner, X. Zhao, H. Buss, R. Langer, P.T. Hammond, Crosslinked linear polyethylenimine enhances delivery of DNA to the cytoplasm, *J. Control. Release*, 167 (2013) 101-107.
- [184] J. Panyam, W.Z. Zhou, S. Prabha, S.K. Sahoo, V. Labhasetwar, Rapid endo-lysosomal escape of poly(DL-lactide-co-glycolide) nanoparticles: implications for drug and gene delivery, *FASEB J.*, 16 (2002) 1217-1226.
- [185] M. Gisbert-Garzarán, M. Manzano, M. Vallet-Regí, pH-Responsive Mesoporous Silica and Carbon Nanoparticles for Drug Delivery, *Bioengineering (Basel)*, 4 (2017) 3.
- [186] A. Riedinger, P. Guardia, A. Curcio, M.A. Garcia, R. Cingolani, L. Manna, T. Pellegrino, Subnanometer Local Temperature Probing and Remotely Controlled Drug Release Based on Azo-Functionalized Iron Oxide Nanoparticles, *Nano Lett.*, 13 (2013) 2399-2406.
- [187] M. Rehman, A. Ihsan, A. Madni, S.Z. Bajwa, D. Shi, T.J. Webster, W.S. Khan, Solid lipid nanoparticles for thermoresponsive targeting: evidence from spectrophotometry, electrochemical, and cytotoxicity studies, *Int. J. Nanomedicine*, 12 (2017) 8325-8336.
- [188] E.C.d.S. Santos, A. Watanabe, M.D. Vargas, M.N. Tanaka, F. Garcia, C.M. Ronconi, AMF-responsive doxorubicin loaded β -cyclodextrin-decorated superparamagnetic nanoparticles, *New J. Chem.*, 42 (2018) 671-680.
- [189] N.Y. Rapoport, A.M. Kennedy, J.E. Shea, C.L. Scaife, K.H. Nam, Controlled and targeted tumor chemotherapy by ultrasound-activated nanoemulsions/microbubbles, *J. Control. Release*, 138 (2009) 268-276.
- [190] F. Wang, Y. Shen, W. Zhang, M. Li, Y. Wang, D. Zhou, S. Guo, Efficient, dual-stimuli responsive cytosolic gene delivery using a RGD modified disulfide-linked polyethylenimine functionalized gold nanorod, *J. Control. Release*, 196 (2014) 37-51.
- [191] J. Cao, S. Huang, Y. Chen, S. Li, X. Li, D. Deng, Z. Qian, L. Tang, Y. Gu, Near-infrared light-triggered micelles for fast controlled drug release in deep tissue, *Biomaterials*, 34 (2013) 6272-6283.
- [192] S. Piao, R.K. Amaravadi, Targeting the lysosome in cancer, *Ann. N. Y. Acad. Sci.*, 1371 (2016) 45-54.
- [193] X. Zhang, Y. Lin, R.J. Gillies, Tumor pH and its measurement, *J. Nucl. Med.*, 51 (2010) 1167-1170.
- [194] A.X. Gao, L. Liao, J.A. Johnson, Synthesis of Acid-Labile PEG and PEG-Doxorubicin-Conjugate Nanoparticles via Brush-First ROMP, *ACS Macro Lett.*, 3 (2014) 854-857.
- [195] T. Srinophakun, J. Boonmee, Preliminary study of conformation and drug release mechanism of doxorubicin-conjugated glycol chitosan, via cis-aconityl linkage, by molecular modeling, *Int. J. Mol. Sci.*, 12 (2011) 1672-1683.
- [196] X.W. Zeng, G. Liu, W. Tao, Y. Ma, X.D. Zhang, F. He, J.M. Pan, L. Mei, G.Q. Pan, A Drug-Self-Gated Mesoporous Antitumor Nanoplatform Based on pH-Sensitive Dynamic Covalent Bond, *Adv. Funct. Mater.*, 27 (2017) 1605985.

- [197] C. Zhang, D. Pan, K. Luo, N. Li, C. Guo, X. Zheng, Z. Gu, Dendrimer-doxorubicin conjugate as enzyme-sensitive and polymeric nanoscale drug delivery vehicle for ovarian cancer therapy, *Polym. Chem.*, 5 (2014) 5227-5235.
- [198] D. DeFeo-Jones, V.M. Garsky, B.K. Wong, D.M. Feng, T. Bolyar, K. Haskell, D.M. Kiefer, K. Leander, E. McAvoy, P. Lumma, J. Wai, E.T. Senderak, S.L. Motzel, K. Keenan, M. Van Zwieten, J.H. Lin, R. Freidinger, J. Huff, A. Oliff, R.E. Jones, A peptide-doxorubicin 'prodrug' activated by prostate-specific antigen selectively kills prostate tumor cells positive for prostate-specific antigen in vivo, *Nat. Med.*, 6 (2000) 1248-1252.
- [199] P.T. Wong, S.K. Choi, Mechanisms of Drug Release in Nanotherapeutic Delivery Systems, *Chem. Rev.*, 115 (2015) 3388-3432.
- [200] T. Yin, L. Wang, L. Yin, J. Zhou, M. Huo, Co-delivery of hydrophobic paclitaxel and hydrophilic AURKA specific siRNA by redox-sensitive micelles for effective treatment of breast cancer, *Biomaterials*, 61 (2015) 10-25.
- [201] Y. Lu, W. Jiang, X. Wu, S. Huang, Z. Huang, Y. Shi, Q. Dai, J. Chen, F. Ren, S. Gao, Peptide T7-modified polypeptide with disulfide bonds for targeted delivery of plasmid DNA for gene therapy of prostate cancer, *Int. J. Nanomedicine*, 13 (2018) 6913-6927.
- [202] J.A. MacDiarmid, N.B. Amaro-Mugridge, J. Madrid-Weiss, I. Sedliarou, S. Wetzel, K. Kochar, V.N. Brahmabhatt, L. Phillips, S.T. Pattison, C. Petti, B. Stillman, R.M. Graham, H. Brahmabhatt, Sequential treatment of drug-resistant tumors with targeted minicells containing siRNA or a cytotoxic drug, *Nat. Biotech.*, 27 (2009) 643-651.
- [203] J. Jiang, S.-j. Yang, J.-c. Wang, L.-j. Yang, Z.-z. Xu, T. Yang, X.-y. Liu, Q. Zhang, Sequential treatment of drug-resistant tumors with RGD-modified liposomes containing siRNA or doxorubicin, *Eur. J. Pharm. Biopharm.*, 76 (2010) 170-178.
- [204] H.S. Choi, W. Liu, P. Misra, E. Tanaka, J.P. Zimmer, B. Itty Ipe, M.G. Bawendi, J.V. Frangioni, Renal clearance of quantum dots, *Nat. Biotechnol.*, 25 (2007) 1165-1170.
- [205] M. Benezra, O. Penate-Medina, P.B. Zanzonico, D. Schaer, H. Ow, A. Burns, E. DeStanchina, V. Longo, E. Herz, S. Iyer, J. Wolchok, S.M. Larson, U. Wiesner, M.S. Bradbury, Multimodal silica nanoparticles are effective cancer-targeted probes in a model of human melanoma, *J. Clin. Invest.*, 121 (2011) 2768-2780.
- [206] S. Shen, D. Jiang, L. Cheng, Y. Chao, K. Nie, Z. Dong, C.J. Kutyreff, J.W. Engle, P. Huang, W. Cai, Z. Liu, Renal-Clearable Ultrasmall Coordination Polymer Nanodots for Chelator-Free ^{64}Cu -Labeling and Imaging-Guided Enhanced Radiotherapy of Cancer, *ACS Nano*, 11 (2017) 9103-9111.
- [207] S. Huo, S. Jin, X. Ma, X. Xue, K. Yang, A. Kumar, P.C. Wang, J. Zhang, Z. Hu, X.J. Liang, Ultrasmall gold nanoparticles as carriers for nucleus-based gene therapy due to size-dependent nuclear entry, *ACS Nano*, 8 (2014) 5852-5862.
- [208] Y. Li, D. Maciel, J. Rodrigues, X. Shi, H. Tomas, Biodegradable Polymer Nanogels for Drug/Nucleic Acid Delivery, *Chem. Rev.*, 115 (2015) 8564-8608.
- [209] T. Li, X. Shen, Y. Chen, C. Zhang, J. Yan, H. Yang, C. Wu, H. Zeng, Y. Liu, Polyetherimide-grafted $\text{Fe}(3)\text{O}(4)@\text{SiO}_2(2)$ nanoparticles as theranostic agents for

simultaneous VEGF siRNA delivery and magnetic resonance cell imaging, *Int. J. Nanomedicine*, 10 (2015) 4279-4291.

[210] Y. Wang, C. Yang, R. Hu, H.T. Toh, X. Liu, G. Lin, F. Yin, H.S. Yoon, K.T. Yong, Assembling Mn:ZnSe quantum dots-siRNA nanoplexes for gene silencing in tumor cells, *Biomater. Sci.*, 3 (2015) 192-202.

[211] D. Kim, Y.Y. Jeong, S. Jon, A drug-loaded aptamer-gold nanoparticle bioconjugate for combined CT imaging and therapy of prostate cancer, *ACS Nano*, 4 (2010) 3689-3696.

[212] B. Shi, H. Zhang, S.Z. Qiao, J. Bi, S. Dai, Intracellular microenvironment-responsive label-free autofluorescent nanogels for traceable gene delivery, *Adv. Healthc. Mater.*, 3 (2014) 1839-1848.

[213] J.D. Wallat, J.K. Harrison, J.K. Pokorski, pH Responsive Doxorubicin Delivery by Fluorous Polymers for Cancer Treatment, *Mol. Pharm.*, 15 (2018) 2954-2962.

[214] G. Lin, R. Hu, W.C. Law, C.K. Chen, Y. Wang, H. Li Chin, Q.T. Nguyen, C.K. Lai, H.S. Yoon, X. Wang, G. Xu, L. Ye, C. Cheng, K.T. Yong, Biodegradable nanocapsules as siRNA carriers for mutant K-Ras gene silencing of human pancreatic carcinoma cells, *Small*, 9 (2013) 2757-2763.

[215] M.C. Palanca-Wessels, G.C. Booth, A.J. Convertine, B.B. Lundy, G.Y. Berguig, M.F. Press, P.S. Stayton, O.W. Press, Antibody targeting facilitates effective intratumoral siRNA nanoparticle delivery to HER2-overexpressing cancer cells, *Oncotarget*, 7 (2016) 9561-9575.

[216] H. Chen, Z. Wang, S. Zong, P. Chen, D. Zhu, L. Wu, Y. Cui, A graphene quantum dot-based FRET system for nuclear-targeted and real-time monitoring of drug delivery, *Nanoscale*, 7 (2015) 15477-15486.

[217] X. Xue, S. Jin, C. Zhang, K. Yang, S. Huo, F. Chen, G. Zou, X.-J. Liang, Probe-Inspired Nano-Prodrug with Dual-Color Fluorogenic Property Reveals Spatiotemporal Drug Release in Living Cells, *ACS Nano*, 9 (2015) 2729-2739.

[218] S.A.E. Marras, F.R. Kramer, S. Tyagi, Efficiencies of fluorescence resonance energy transfer and contact-mediated quenching in oligonucleotide probes, *Nucleic Acids Res.*, 30 (2002) e122-e122.

[219] L. Qiu, C. Wu, M. You, D. Han, T. Chen, G. Zhu, J. Jiang, R. Yu, W. Tan, A targeted, self-delivered, and photocontrolled molecular beacon for mRNA detection in living cells, *J. Am. Chem. Soc.*, 135 (2013) 12952-12955.

Chapter 3. Microenvironment-degradable multifunctional microgels for selective co-delivery of DOX and miRNA-21 inhibitor for enhanced anticancer therapy

*Seonho Yun, Jiabin Zhang, Hesamoddin Rabiee, Hu Zhang, Jingxiu Bi, Sheng Dai**

School of Chemical Engineering, University of Adelaide, Adelaide, SA 5005, Australia

Prof. H. Zhang

Amgen Bioprocessing Centre, Keck Graduate Institute, 535 Watson Drive, Claremont, CA
91711

Prof. S. Dai

Department of Chemical Engineering, Brunel University London, Uxbridge, UB8 3PH, United
Kingdom

sheng.dai@brunel.ac.uk

Statement of Authorship

Title of Paper	Microenvironment-degradable multifunctional microgels for selective co-delivery of DOX and miRNA-21 inhibitor for enhanced anticancer therapy
Publication Status	<input type="checkbox"/> Published <input type="checkbox"/> Accepted for Publication <input type="checkbox"/> Submitted for Publication <input checked="" type="checkbox"/> Unpublished and Unsubmitted work written in manuscript style
Publication Details	In preparation for Journal of Controlled Release

Principal Author

Name of Principal Author (Candidate)	Seonho Yun		
Contribution to the Paper	Mainly designed the experiment, material synthesis, evaluation, and manuscript writing		
Overall percentage (%)	80 %		
Certification:	This paper reports on the original research I conducted during the period of my Higher Degree by Research candidature and is not subject to any obligations or contractual agreements with a third party that would constrain its inclusion in this thesis. I am the primary author of this paper.		
Signature		Date	20/05/2019

Co-Author Contributions

By signing the Statement of Authorship, each author certifies that:

- i. the candidate's stated contribution to the publication is accurate (as detailed above);
- ii. permission is granted for the candidate to include the publication in the thesis; and
- iii. the sum of all co-author contributions is equal to 100% less the candidate's stated contribution.

Name of Co-Author	Jiabin Zhang		
Contribution to the Paper	Helped to operate evaluation part of the experiment		
Signature		Date	21/02/2019

Name of Co-Author	Hesamoddin Rabiee		
Contribution to the Paper	Helped to operate material synthesis of the experiment		
Signature		Date	27 Feb. 2019

Name of Co-Author	Hu Zhang		
Contribution to the Paper	Supervised the experiment design, data interpretation, manuscript correction		
Signature		Date	24/02/2019

Name of Co-Author	Jingxiu Bi		
Contribution to the Paper	Proof read the manuscript and evaluation		
Signature		Date	25/02/2019

Name of Co-Author	Sheng Dai		
Contribution to the Paper	Supervised the experiment design, data interpretation, manuscript correction, and corresponding author		
Signature		Date	20/05/2019

Abstract

Chemotherapy using most active anticancer drugs, such as doxorubicin (DOX), is devalued due to the dose-dependent side-effects by their unselective cell intakes and the therapeutic pathway interruption in the presence of miRNA-21. Herein, a co-delivery system of DOX and miRNA-21 inhibitor (miR-21i) based on multifunctional microgels is developed to maximize therapeutic synergies and minimize side effects. The microgels were prepared by cationic low molecular weight polyethyleneimine and glutathione-responsive diselenide crosslinkers, where DOX was loaded to microgels via acidic-cleavable hydrazone bonds and miR-21i was interacted with microgels electrostatically. Further negative charged hyaluronic acid (HA) surface coating inhibits protein adsorption during circulation and promotes active target on metastatic cancer cells through HA receptor-mediated endocytosis. The loaded DOX and miR-21i can be rapidly released to endosome/lysosome and cytosol of target cancer cells, rather than health cells, due to the effective cleavage of hydrazone and diselenide bonds in cancer cell microenvironment. Its anticancer efficiency to breast cancer MDA-MB-231 cells is 4.4-fold higher than free DOX, but its cytotoxicity to health cells is impressively low. While the delivery system is stable before endocytosis, it can be fully biodegradable in the cytosol environment for safe excretion from body. Therefore, the reported multifunctional microgels enable effective co-delivery of DOX and miR-21i to target cells with high anticancer therapeutic performance but minimal side effects.

Keywords: biodegradable, microgel, hydrazone, diselenide, co-delivery, PEI, DOX, miR-21 inhibitor

3.1 Introduction

Doxorubicin (DOX), a most active anticancer drug, is able to mitigate a wide range of cancers via regulating B-cell lymphoma-2 (Bcl-2) family proteins and activating an apoptotic pathway afterwards [1-6]. However, DOX also causes significant side effects, e.g. cardiotoxicity, hepatotoxicity and nephrotoxicity, which outweigh its anticancer therapy when increasing DOX dosage [7-11]. The severer side effects from DOX are due to higher uptake by normal cells than cancer cells when DOX is administrated systemically without a delivery agent [10, 12, 13]. Additionally, the presence of miRNA-21 (miR-21) as the oncogenic RNA in cancer cells reduces chemo-sensitivity by down-regulating programmed cell death 4 (PDCD4) and thus suppressing the apoptotic pathway [14, 15]. The co-drug therapy with DOX and miR-21 inhibitor (miR-21i) has exhibited synergistic effect on improving anticancer efficacy of DOX by inhibiting miR-21, resulting in recovery of chemo-sensitivity and activation of apoptosis [16-18]. However, miRNA therapy without a suitable delivery carrier is often associated with rapid blood clearance and metabolic alteration by the off-target effect [19, 20]. These transport issues have drawn scientific attentions to the development of a co-delivery system although a range of delivery vectors have been explored for delivering DOX or miRNA separately.

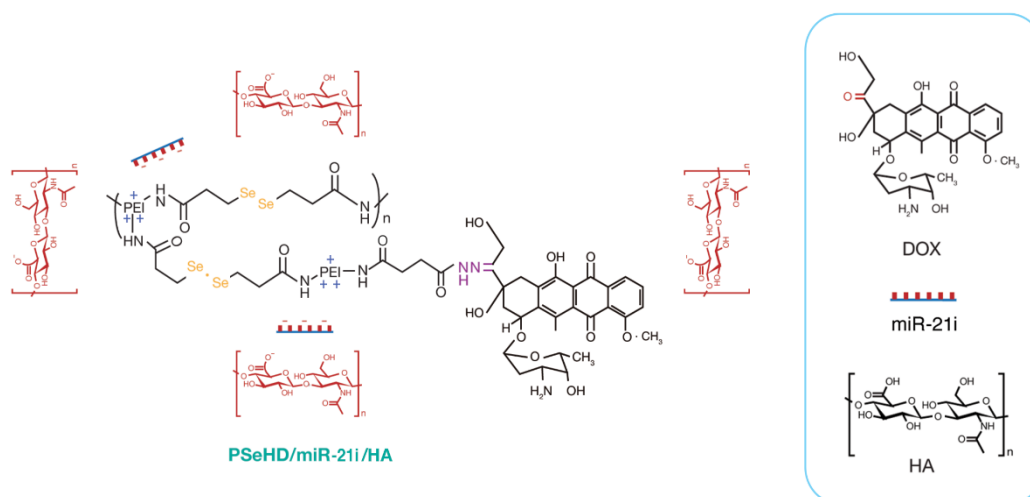
DOX delivery systems have been developed with effective loading mechanisms, such as solid lipid nanoparticles with solvent diffusion, DNA duplex with intercalation, polysaccharide with charge interaction, carbon nanotube with physical adsorption and micelle with hydrophobic interaction [21-25]. However, these loading mechanisms cannot allow DOX release in a controlled manner. To better control release, limited study has been reported on the conjugation of DOX and carriers via cleavable moieties, disulfide bonds and hydrazone bonds [26-28]. Among them, DOX conjugation by a hydrazone bond can minimize premature release at physiological circumstance (pH 7.4), enhance DOX accumulation in tumor site and release

DOX in the cancerous extracellular matrix (pH 6.0-7.0) and endosomes-lysosomes (pH 4.0-6.0) [29].

Vectors for miR-21i are confronted with dilemmatic issues in the delivery courses of gene loading, systemic circulation, extravasation, endocytosis, endosomal escape, gene release and excretion from patients' body [30, 31]. Cationic lipid-based delivery vectors, liposomes and solid lipid nanoparticles have been used to form lipoplexes with anionic genes by electrostatic interaction [32-36]. Polymer-based carriers forming polyplexes with genes have been used for aiding endosomal escape to cytosol through the proton sponge effect [32-36]. Polyethyleneimine with a molecular weight of 25k Da (PEI25k) as a gold standard of gene vectors demonstrates its high gene transfection efficiency but high cytotoxicity, whereas PEI with a low molecular weight of 800 Da (PEI800) possesses a weak gene loading ability but more biocompatibility [37]. In order to achieve high transfection and low cytotoxicity of PEI, our team reported the synthesis of biodegradable PEI microgels by crosslinking low molecular weight PEI800 by a redox cleavable disulfide linker [38-40]. Similarly, diselenide has also been reported to be redox cleavable, but with better stability in extracellular environments and faster cleavage in intracellular GSH environment [41].

Besides, high molecular weight cationic polymeric vectors can enhance gene loading, increase blood circulation time without renal clearance (> 20 nm), and improve electrostatic interaction-mediated endocytosis [31, 42]. On the other hand, these cationic carriers may interact with anionic serum to yield complexes with a large size, resulting in reticuloendothelial clearance for a size greater than 200 nm, inhibition of their extravasation through tumor derived vascular pores for a size greater than 500 nm, and their cytotoxic accumulation in patient body [30, 43]. Although polyethylene glycol (PEG) modification has been developed to overcome protein adsorption, steric hindrance derived from long PEG chains suppresses cellular uptake [44]. Hyaluronic acid (HA), a natural glycosaminoglycan as an extracellular matrix component, is

an alternative to protect cationic carriers from elimination by the immune system because of its anionic property. HA not only can avoid serum opsonization and prolong blood circulation, but also facilitate active targeting and subsequent receptor-mediated endocytosis into metastatic breast cancer cells (MDA-MB-231) due to the overexpress of a cluster of differentiation 44 (CD44) on cell surface as the HA receptor [45, 46].



Scheme 3.1 Schematic representation of the developed microenvironment-degradable multifunctional PSeHD/miR-21i/HA for selective delivery of DOX and miR-21i.

In this study, we developed a co-delivery system of DOX and miR-21i aiming for enhancing their synergistic effect on the treatment of invasive breast cancer (Scheme 3.1). This multifunctional microgel-based carrier system was prepared by crosslinking PEI800 using bio-cleavable diselenide crosslinkers. DOX was chemically conjugated by hydrazone bonds and miR-21i was introduced via electrostatic interaction. Such a system revealed high loading capability for DOX and miR-21i, but low cytotoxicity to health cells. HA surface coating was applied electrostatically to minimize serum adsorption and enhance target cell delivery through the HA receptor-mediated endocytosis. The HA coated polyplexes maintained their morphologies with a size of 160 nm during stable circulation and passive targeting. Co-loaded DOX and miR-21i could be selectively released to target cells via acidic cancer environment-

induced cleavage of hydrazone bonds and cytosol GSH-induced cleavage of diselenide bonds. The small-sized microgel fragments (< 10 nm) after the reduction of diselenide crosslinkers of microgels could be easily excreted. As a result, the reported multi-functionalized microgels have the great potential as effective carriers for anticancer drugs and miRNA co-delivery in therapeutic applications.

3.2 Methods

3.2.1 Materials

Branched polyethyleneimine MW 800 Da (PEI800), branched polyethyleneimine MW 25k Da (PEI25K), selenium, 3-chloropropionic acid, 1-ethyl-3-(3-dimethyl-laminopropyl) carbodiimide (EDC), N-hydroxysulfosuccinimide (NHS), sodium borohydride (NaBH₄), succinic anhydride, tert-butyl carbazate, trifluoroacetic acid (TFA), agarose, 1M DL-dithiothreitol solution (DTT), L-Glutathione reduced (GSH) and cell counting Kit-8 (CCK-8) were purchased from Sigma-Aldrich. Doxorubicin hydrochloride (DOX·HCl) was purchased from Wuhan Wang Lianshang Biotechnology. MicroRNA-21 inhibitor (sequence 5'-GUCCACUCUUGUCCUCA AUG-3') (miR-21i) and FAM-labelled miRNA inhibitor single stranded negative control (sequence 5'-CAGUACUUUUGUGUAGUACAA-3') (FAM-miR) were purchased from Shanghai Gene Pharma Co., Ltd. Sodium hyaluronate 60k Da (HA) was obtained from Lifecore Biomedical, LLC. Dulbecco modified eagle medium (DMEM), fetal bovine serum (FBS), penicillin-streptomycin (PS), phosphate buffered saline (PBS), Trypsin-EDTA (0.25 %) and CellMask™ Deep Red Plasma membrane Stain were purchased from Life Technologies Australia Pty Ltd. Deionised water was from a Milli-Q water system with resistance of 18.2 MΩ·cm. Spectra/Por® molecularporus membrane tubing 3.5 kDa MWCO was purchased from Spectrum Laboratories, Inc. HEK293T cell line was kindly gifted by

Professor Andrew Zannettino from South Australia Health and Medical Research Institute (SAHMRI). MDA-MB-231 cell lines were appreciably given by Dr. Qian Tang from School of Pharmacy at University of South Australia. All chemicals with analytical grade were used without further purification.

3.2.2 Synthesis of PSeH microgels

3.2.2.1 Synthesis of diselenide crosslinker (-SeSe-)

3,3'-diselanediyldipropanoic acid (-SeSe-) was synthesized following previous research with slight modification [47]. 5 mL water was added to selenium powder (1.18 g, 15 mmol) in a three-necked flask under nitrogen protection. NaBH₄ (1.13 g, 30 mmol) in 12.5 mL water was added dropwise to the flask in an ice bath over a period of 10 min under stirring. After the mixture turned colorless, another 1.18 g selenium powders were added under N₂ protection. The mixture was heated up to 105 °C for about 20 min and a reddish brown color mixture was obtained. After cooling the mixture to room temperature, 3-chloropropionic acid (3.26 g, 30 mmol) in 7.5 mL water and pH 8 (adjusting using sodium carbonate) was added. The mixture was stirred overnight at room temperature under N₂ protection, and then exposed to atmosphere for 12 h to oxidize unreacted selenium, following by filtration using a 0.45 μm syringe filter. pH was adjusted to 3 with HCl, and the coagulant was extracted twice with ethyl acetate and washed twice with water. The organic part in ethyl acetate was dried with magnesium sulphate. After ethyl acetate evaporation, crystallized pale yellow color diselenide crosslinker (-SeSe-) was produced and confirmed by Raman spectroscopy and Fourier-transform infrared spectroscopy (FTIR).

3.2.2.2 Synthesis of diselenide crosslinked PEI800 (PSeSe)

-SeSe- (304 mg, 1 mmol), NHS (460.4 mg, 4 mmol) and EDC (1150.2 mg, 6 mmol) were dissolved in 2.1 mL DMSO under N₂ protection with magnetic stirring for 45 min. PEI800 (800 mg, 1 mmol), pH 7.4 being adjusted using 3M HCl and lyophilized, was dissolved in 1.6

mL of DMSO and injected into the EDC activated solution. The mixture was magnetically stirred at room temperature for 2 days under nitrogen, and then dialyzed against water using dialysis tubes (3.5 kDa MWCO) for 5 days with daily change of water. After lyophilisation, PSeSe was obtained and checked by FTIR. The quantity of amine groups in PSeSe was detected through conductivity and pH titration. 2.4 mg of PSeSe in 48 mL of deionized water was titrated dropwise by 0.1 M sodium hydroxide solution with continuous magnetic stirring. The pH and conductivity (μS) data from a pH-conductivity meter (AQUA conductivity/pH) were recorded to quantify amine groups of PSeSe.

3.2.2.3 Synthesis of hydrazine bond conjugated PEI microgels (PSeH)

PSeSe (100 mg, 496 μmol of amine group) was re-dissolved in 10 mL DMSO in a two-necked flask under nitrogen protection. Succinic anhydride (4.96 mg, 49.6 μmol , 10 % molar ratio to amine in PSeSe) in 2 mL DMSO was injected to the suspension of PSeSe. After overnight magnetic stirring at room temperature under N_2 , the mixture turned into transparent grey color. After dialysis against deionized water using a 3.5kDa MWCO tube and freeze drying, PSeCOOH10%, carboxylic group conjugated microgels, was obtained. Besides, the feed molar ratio of succinic anhydride to amine in PSeSe were also varied from 5 to 20 % to produce the PSeCOOH5% and PSeCOOH20%.

PSeCOOH10% (61.1 mg, 28.6 μmol of COOH group) was re-dissolved in 10 mL of DMSO under nitrogen gas flow. NHS (13.17 mg, 114.4 μmol) and EDC (32.9 mg, 171.6 μmol) dissolved in 2 mL DMSO were added into the suspension with magnetic stirring for 45 min. Tert-butyl carbazate (5.67 mg, 42.9 μmol) dissolved in 1 mL of DMSO was then injected into the mixture and stirred at room temperature for 16 h. Dialysis against deionized water was carried out to purify the microgels for 5 days. After being lyophilized, microgels with BOC-protected hydrazine bond conjugates (PSeBOC10%) was produced. Similarly, PSeBOC5% and PSeBOC20% were also synthesized from PSeCOOH5% and PSeCOOH20%.

Finally, TFA (2 ml, 26 mmol) was injected into the suspension of PSeBOC10% (55.3 mg, 23.7 μmol of BOC group) in 10 mL DMSO under nitrogen environment. The mixture was magnetically stirred at room temperature for 24 h. After dialysis and freeze dry, hydrazine bond conjugated microgels of PSeH10% (PSeH) was obtained. Similar approach was used to prepare the microgels of PSeH5% and PSeH20% as well.

The hydrodynamic size distributions of PSeH microgels in 25 mM DTT aqueous solution was detected at 37 °C for 5 days via dynamic light scattering (DLS) measurement in a Malvern Zetasizer Nano ZS (ZEN 3600).

3.2.3 Co-drug loading and release

3.2.3.1 DOX loading (PSeHD) and release

PSeH (30 mg, 13.4 μmol of hydrazine group) was dissolved in 5 mL pH 7.4 PBS buffer solution, and DOX·HCl (7.8 mg, 13.4 μmol) dissolved in 5 mL pH 7.4 PBS with 2 μL of acetic acid. The mixture was magnetically stirred at room temperature under dark and nitrogen atmosphere for overnight. Dark dialysis of the mixture against deionized water was carried out in a cold room at 4 °C with vigorous stirring, and 31.2 mg of DOX loaded microgels (PSeHD) was obtained after lyophilisation.

Since the quantity of unloaded DOX was measured from the UV-vis absorbance of DOX at 479.5 nm (DOX calibration curve in [Figure 3.S5](#)), DOX loading could be calculated using the equation:

$$\text{DOX Loading (\%)} = \frac{(\text{feed DOX} - \text{unloaded DOX})}{\text{DOX loaded microgels}} \times 100 \quad (1)$$

PSeH5% and PSeH20% were also utilized to load DOX and quantify DOX loadings.

For the *ex vivo* DOX release assay, each 5 ml of PSeHD (1mg mL⁻¹) placed in a dialysis bag (MWCO 3.5kDa) was immersed in 95 mL of PBS pH7.4, PBS pH6.5 and acetate buffered

saline (ABS, 0.2 M) pH5.0, and then incubated in a horizontal shaker at 37 °C with 100 rpm. 1 mL of buffer saline was taken to measure the absorbance of the released DOX from the dialysis bags using a UV-vis spectrophotometer at pre-determined time intervals.

3.2.3.2 MicroRNA-21 inhibitor (miR-21i) loading (PSeHD/miR-21i) and release

1 μL miRNA-21 inhibitor (miR-21i, $0.42 \text{ nmol } \mu\text{L}^{-1}$) in RNase-free water (DEPC water) was mixed with pre-determined N/P ratios of PSeHD dissolved in DEPC water, and incubated at room temperature for 20 min. For the N/P ratios, amine contents in PSeHD were determined by conductivity and pH titration (Figure 3.S7). Agarose gel (0.8%) electrophoresis was run at 100 V for 60 min, and then the fluorescent images of RNA migration patterns under UV irradiation were photographed using a G-BOX (SYNGENE, A Division of Synoptics Ltd). For comparison, PSeH20%D complex was also employed to determine the fully retarded N/P ratio in electrophoresis.

For *ex vivo* releasing of loaded miR-21i, PSeHD/miR-21i polyplexes with a 4.0 N/P ratio were incubated in 20 mM GSH at 37 °C for 24 h. Gel electrophoresis was carried out in 0.8 % agarose gel at 100 V for 60 min. The RNA migration image of PSeHD/miR-21i treated with 20 mM GSH for 24 h was captured by a G-BOX and compared with the one without GSH treatment.

3.2.4 *Ex vivo* multi-function assays

3.2.4.1 Hyaluronic acid surface coating (PSeHD/miR-21i/HA)

PSeHD/miR-21i (at a 10.0 N/P ratio) suspended in DEPC water was mixed with hyaluronic acid (HA) at 5.0 w/w ratio of HA to miR-21i at room temperature for 20 min to obtain the designated PSeHD/miR-21i/HA.

3.2.4.2 Surface charge conversion and *ex vivo* serum protein adsorption

Zeta-potentials of PSeHD, PSeHD/miR-21i and PSeHD/miR-21i/HA in 10 mM NaCl solution were measured via a Malvern Zetasizer Nano ZS (ZEN 3600) at 25 °C to confirm the electrostatic interaction.

100 µL of PSeHD/miR-21i/HA polyplex (1 mg mL⁻¹) and 100 µL of bovine serum albumin (BSA) solution (2 mg mL⁻¹) were incubated with gentle shaking at 37 °C for 30 min and centrifuged. 100 µL of supernatant was diluted in 1 mL serum-free deionized water to determine the concentration of BSA in the supernatant via a UV-vis measurement at 280 nm. The BSA adsorption rate (%) was calculated using following equation:

$$\text{BSA adsorption rate (w/w \%)} = \frac{\text{feed BSA} - \text{supernatant BSA}}{\text{feed BSA}} \times 100 \quad (2)$$

PEI800 and Lipofectamine2000 were utilized as controls with a UV-vis calibration curve shown in [Figure 3.S9](#).

3.2.4.3 Degradation of PSeHD/miR-21i/HA polyplexes

The hydrodynamic particle sizes of PSeHD/miR-21i/HA was detected at 37 °C via dynamic light scattering using a Malvern Zetasizer Nano ZS (ZEN 3600). PSeHD/miR-21i/HA, consisting 20 µL of miR-21i (0.42 nmol µL⁻¹) at a 10 N/P ratio of PSeHD and five times HA to miR-21i (w/w), were diluted in deionized water for particle size measurements.

Degradation of PSeHD/miR-21i/HA polyplexes was evaluated by measuring their particle sizes under three mimicking environments at PBS buffer pH7.4: 0 M GSH for physiological condition, 10 µM GSH for extracellular microenvironment, and 20 mM GSH for cytosols. An aliquot from the microgel solutions was collected at the pre-designed time during continuous shaking at 100 rpm under 37 °C with their size being detected using dynamic light scattering at 37 °C.

3.2.5 Cell culture

Breast cancer cell line (MDA-MB-231) and kidney cell line (HEK 293T) were incubated with Dulbecco Modified Eagle Medium (DMEM) supplemented with 10% (vol/vol) fetal bovine serum (FBS) and 1% (vol/vol) penicillin-streptomycin (PS) in an incubator (Contherm Scientific Ltd.) under a humidified atmosphere at 37 °C with 5 % CO₂. Trypsin-EDTA (0.25 %) was used to recover cells after culture.

3.2.6 Cellular uptake assays

Cellular uptake into cells was monitored qualitatively by an Olympus FV3000 confocal laser scanning microscope (CLSM). MDA-MB 231 cells with a seeding density of 0.1×10^6 cells per well were cultured on a glass cover slip at the bottom of a 12 well plate with their culture medium for 24 h in an incubator. 50 μ L sample was prepared with 12.5 μ g PSeHD/FAM-miR/HA at 4.0 % DOX, 10.0 N/P of FAM-labelled miRNA inhibitor single stranded negative control (FAM-miR) and 5.0 folds weight of HA to FAM-miR. The sample was applied to the cells after replacing the old medium with 950 μ L of fresh one, and further incubated at 37 °C for 4 h. After being washed by PBS, cells were stained by the CellMask™ Deep Red Plasma Membrane Stain for 10 min, and then fixed in 4 % formaldehyde for 10 min. After 3 washes with PBS, the cellular uptake of carriers was observed by fluorescent images of DOX (blue), FAM-miR (green) and cells (red) via the CLSM. The uptake images of carriers were compared to those of cells without carriers and those of cells after HA pre-treatment (10 mg HA/mL culture medium for 24 h).

Quantitative cellular uptake was determined by a flow cytometer (BD FACSCalibur™). MDA-MB 231 cells with a density of 0.05×10^6 cells per well were grown in a 24 well plate with 500 μ L culture medium for 24 h. The culture medium was replaced with 450 μ L of fresh medium and 50 μ L of solution containing 5 μ g PSeHD/FAM-miR/HA at 10.0 N/P and 5.0 wt HA/wt FAM-miR. Control cells without PSeHD/FAM-miR/HA and HA pre-treated cells with

PSeHD/FAM-miR/HA were prepared. The 24 well plate were incubated for another 4 h. After rinsing 3 times by PBS, cells were collected by trypsin-EDTA treatment to quantify the fluorescent intensities of DOX and FAM-miR for cellular uptake. The intensity of FL-1 (ex. 488, em. 530 nm) and FL-2 (ex. 488, em. 585 nm) represents FAM-miR and DOX.

3.2.7 *In vitro* biocompatibility assays of microgels without co-drugs

Biocompatibility of PSeH microgels was evaluated via *in vitro* HEK293T viability assays using the Cell Counting Kit-8 (CCK-8). Cell survival rates were compared to these from PEI25k as a negative control and from PEI800 and lipofectamine2000 as positive controls. HEK293T cells (5000 cells per well) were cultured in a 96 well plate with 100 μ L of culture medium in an incubator for 24 h. 10 μ L of three different concentrations (1.0, 10.0, 50.0 μ g mL⁻¹) of microgels were added to the well plate, followed by another 48 h incubation. After another 4 h incubation with CCK-8 solution, the well plate were inserted in a microplate reader (ELx808 BioTek) to measure the absorbance at 450 nm with cell survival rates being determined from the following equation:

$$\text{Cell survival rate (\%)} = \frac{A-B}{C-B} \times 100 \quad (3)$$

where A is the absorbance of microgel samples; B is the absorbance of blank (no cells); and C is the absorbance of control (only cells without samples).

Biocompatibility of biodegraded microgels was evaluated against HEK 293T cells. Various concentrations (1.0, 10.0, 50.0 μ g mL⁻¹) of PSeH solutions with 20 mM GSH were incubated at the same condition for cell culture for 24 h. These biodegraded microgels were applied to pre-cultured HEK 293T cells in a 96 well plate for another 48 h incubation. After CCK-8 treatment, the survival rates of kidney cells in each well were determined via the microplate reader and Equation 3.

3.2.8 *In vitro* cell viability assays for the efficacy of PSeHD/miR-21i/HA

The therapeutic efficacy of PSeHD/miR-21i/HA was evaluated via the cell viability assays using both MDA-MB-231 and HEK 293T cells. Each type of cells was incubated in a 96 well plate for 24 h, and then incubated for another 48 h in the presence of PSeHD/miR-21i/HA (DOX loaded concentration varies from 0.1, 0.25, 0.5, 1.0 to 2.5 $\mu\text{g mL}^{-1}$). After subsequent 4 h CCK-8 treatment, cell survival rates were obtained from microplate reader. Cell viabilities against PSeHD/miR-21i/HA were compared with those against PSeHD/miR-21i, PSeHD and DOX·HCl for both cell lines.

3.3 Results and Discussion

3.3.1 Synthesis of PSeH microgels

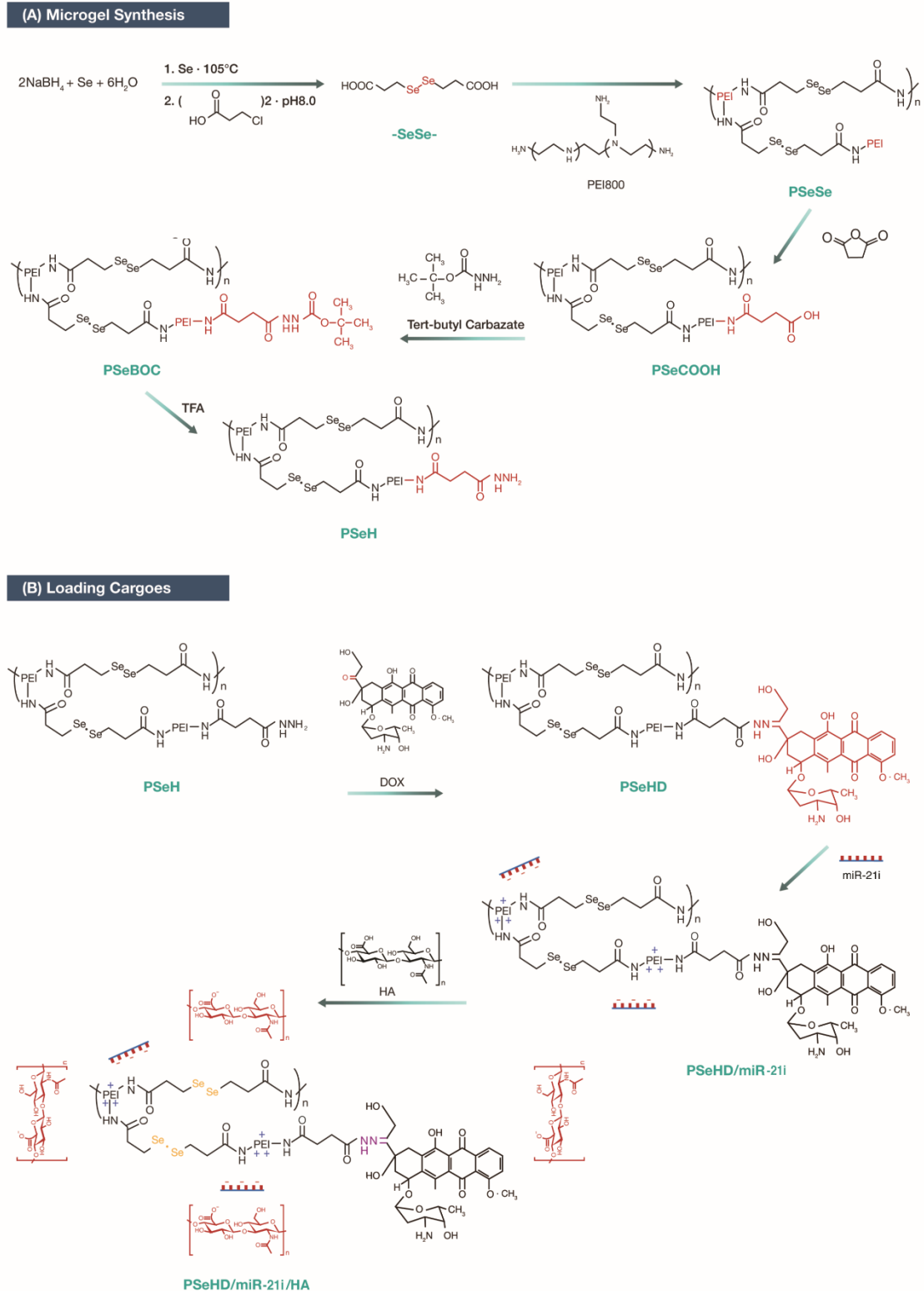
Positively charged polymers are oftentimes chosen as the non-virus vectors to load and deliver nucleic acids. PEI with its molecular weight of 25 KDa is a gold standard for gene delivery but has significant cytotoxicity. Our previous studies have shown that chemical-crosslinked PEI800 microgels had minor cytotoxicity and excellent gene delivery capability [39]. In this study, low toxic and multifunctional PSeH microgels were synthesized by crosslinking low molecular weight branched-PEI800 with diselenide bonds (Scheme 3.2A) and then conjugating anticancer drug of DOX by hydrazine bonds as new co-delivery carriers of DOX and microRNA-21 inhibitor (miR-21i) (Scheme 3.2B).

The smart crosslinker of 3,3'-diselanediyldipropanoic acid (-SeSe-) containing a redox-cleavable diselenide bond was synthesized with a yield of 57 %. The Raman peaks of the selenium-selenium bond (-Se-Se-) and selenium-carbon bond (-Se-C-) are evident at the Raman shifts of 291 and 517 cm^{-1} (Figure 3.S1) [48, 49]. In addition, the new peak at 520 cm^{-1} can be observed from the FTIR spectrum (Figure 3.S2) of (-SeSe-), which is related to the

new selenium-carbon bond. 1690 cm^{-1} is the vibration band of $-\text{COOH}$, which is consistent with the 3-chloroproionic acid precursor.

PEI800 was crosslinked by 3,3'-diselanediyldipropanoic acid (**-SeSe-**) to form PEI microgel (**PSeSe**) with a yield of 73 %. FTIR spectra (Figure 3.S2) confirm successful synthesis of microgels. Distinct PEI800 peaks at 3351 , 1547 , and 1042 cm^{-1} correspond to the N-H stretching, N-H bending and C-N stretching, and the peak at 520 cm^{-1} is related to for Se-C stretching. The shift of C=O stretching from 1690 to 1630 cm^{-1} indicates the formation of amide bonds between PEI800 and the crosslinker (**-SeSe-**). The amount of amine groups of **PSeSe** was measured by pH and conductometric titrations (Figure 3.S3B), where $4.96\text{ }\mu\text{mol amine mg}^{-1}\text{ PSeSe}$ is obtained and this crosslinking reaction consumes 35 % of amine of PEI800 (Figure 3.S3A).

pH-responsive hydrazine bond was then introduced to **PSeSe** to produce smart co-delivery carrier PSeH10% (**PSeH**) microgels with a yield of 48 %. Besides, PSeH5% and PSeH20% microgels with 5% and 20% feed molar ratios of hydrazine to amine in **PSeSe** microgels were also synthesized. Successful synthesis of these redox-sensitive **PSeH** microgels is confirmed via measuring the hydrodynamic sizes and relevant particle size distributions in 25 mM DL-dithiothreitol solution (DTT) over time in Figure 3.S4. There is only one narrow single peak of the microgel at 217 nm before exposure to DTT, and the size distribution after 0.5 h DTT interaction centered at 198 nm. After 2 h, two peaks are observed in the distribution with the small size at 10 nm and the large one at 190 nm. Increasing time from 8 to 24 h, the amount of 10 nm particles increases and the peak of large particles keep on dropping. Associated with the cleavage of diselenide crosslinkers of microgels, more and more PEI fractures are detached. After 5 days, only 10 nm small particles can be observed, indicating the fully degradation of the **PSeH** microgels in the presence of DTT.



Scheme 3.2 (A) Synthesis of PSeH microgels as co-delivery carriers, (B) loading of DOX (PSeHD), miR-21i (PSeHD/miR-21i) and HA (PSeHD/miR-21i/HA) to PSeH microgels.

3.3.2 Controlled loading and releasing of DOX and miR-21i

3.3.2.1 DOX loading (PSeHD) and releasing

To effectively eliminate leakage and uncontrolled release during the delivery course, DOX as a model anticancer drug was loaded to PSeH microgels through a hydrazone bond. The ketone group of DOX in the presence of acetic acid was covalently conjugated to the hydrazine amine group in PSeH [50]. DOX loading to the microgels via various molar hydrazine groups produced PSeH5%D, PSeH10%D, and PSeH20%D. DOX loading was determined by the difference between DOX feed and residual using the Equation 1. The amount of feed and unloaded DOX was obtained via spectroscopic measurements (Figure 3.S6) with a UV-vis calibration curve at a wavelength of 479.5 nm (Figure 3.S5). DOX loading for PSeH5%D, PSeH10%D, and PSeH20%D are 1.0, 4.0 and 18.7 wt %, indicating DOX loading increases with the substituted hydrazine in microgels.

The selective *ex vivo* DOX release profiles of PSeH10%D (**PSeHD**) complexes were conducted using a dialysis method against different pH buffer solutions mimicking intracellular environments: pH 5.0 for endo-lysosomes, pH 6.5 for extracellular environment of cancer cells, and pH 7.4 for the extracellular environment of normal cells. In Figure 3.1A, 92 ± 4.6 % of loaded DOX is released from PSeHD at pH 5.0 over 48 h, while 52 ± 4.2 % and 28 ± 2.2 % of DOX at pH 6.5 and pH 7.4 during the same duration. These controlled releasing patterns of DOX outweigh those from non-conjugative DOX loading methods [21-25]. The formed hydrazone bonds can be cleaved at the pH of intracellular late endosomes or lysosomes and the extracellular environment of cancer cells, but are rather stable at the physiological pH of the extracellular environment of normal cells. The pH responsive release of chemically loaded DOX in PSeHD microgels confirms its potential for controlled release of anticancer drugs to target cells.

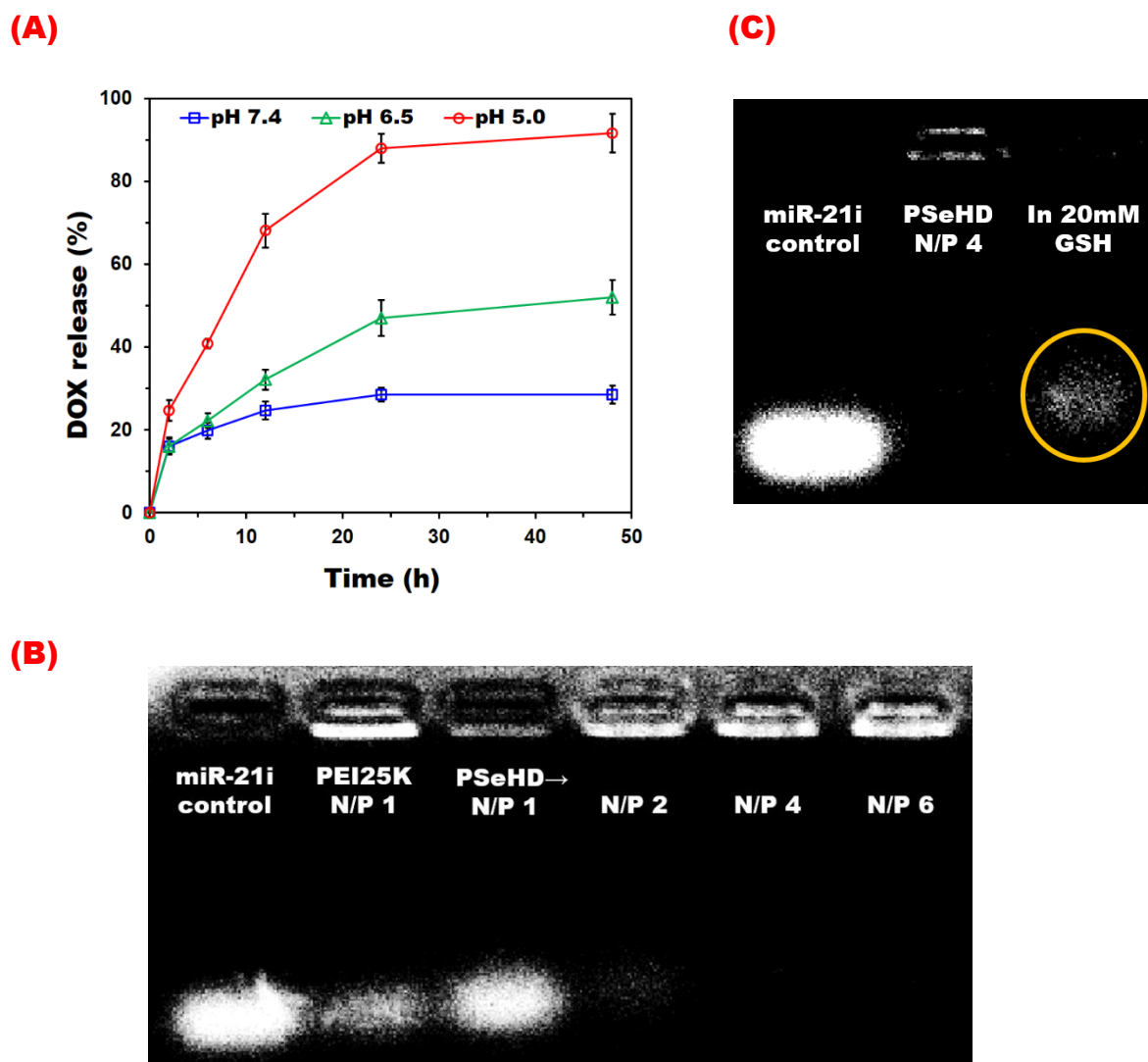


Figure 3.1 (A) Hydrazone bond cleavage to determine DOX release from PSeHD microgels at pH 5.0, 6.5 and 7.4 buffer solutions after 48 h. ($P < 0.05$, $n = 3$), (B) Loading of miR-21i to PSeHD at different N/P ratios (1, 2, 4 and 6), PEI25K as the reference, (C) Comparison of miR-21i release after incubation in 20 mM GSH for 24 h.

3.3.2.2 MicroRNA-21 inhibitor loading (PSeHD/miR-21i) and releasing

The anticancer efficiency of DOX in metastatic cancer cells is undermined due to the presence of miRNA-21 (miR-21), which requires a co-delivery carrier for miR-21 inhibitor (miR-21i) and DOX to enhance the therapeutic effect of DOX by inhibiting miR-21 and activating apoptosis [14, 18]. PSeHD complexes loaded miR-21i by electrostatic interaction, forming PSeHD/miR-21i polyplexes. Anionic phosphate (P) in miR-21i binds to cationic nitrogen (N)

in PSeHD complex in aqueous solution. The miR-21i loading capacity was evaluated via a 0.8 % agarose gel retardation assay. In [Figure 3.1B](#), full retardation of PSeHD is achieved at an N/P ratio (PSeHD to miR-21i) of 4. Comparing with the PEI25K as a positive control, miR-21i migration from the polyplexes with PEI25K is slightly less than PSeHD at an equivalent N/P ratio of 1, but far more than PSeHD at the N/P ratio of 2. Therefore, PSeHD shows miR-21i loading capability as good as PEI25K. miR-21i loading to PSeH20%D was also evaluated ([Figure 3.S8](#)), and full retardation occurred at 10 N/P. PSeH20%D complexes have a high DOX loading but a low miR-21i loading capacity since DOX conjugation consumes some amine groups of microgels and thus sacrifices positive charge density for miR-21i loading. In addition, the amine groups in hydrazine and DOX are inefficient to load miR-21i since their pK_a values (7.20 and 7.55) are closed to physiological pH 7.4 [51, 52]. Moreover, the presence of large and hydrophobic DOX in microgels further contributes to a decrease in electrostatic interaction between nucleic acid and PEI. That can be further confirmed with a high miR-21i loading affinity and a low DOX loading by PSeH5%D. Taken together, miR-21i loading capacity of the complexes is inversely proportional to their DOX loading ability, and PSeH10%D (**PSeHD**) shows a balanced DOX and miR-21i loading ([Table 3.S1](#)).

The *ex vivo* miR-21i releasing profiles were evaluated via agarose gel electrophoresis after incubating PSeHD/miR-21i (4 N/P) microgels for 24 h at 37 °C with and without the presence of 20 mM GSH ([Figure 3.1C](#)). miR-21i is migrated out of the PSeHD/miR-21i polyplexes with GSH, while miR-21i is full-retarded by PSeHD/miR-21i polyplexes without GSH. The diselenide bonds in complexes can be reduced in the presence of 20 mM GSH similar to the reductive microenvironment in cytosol [53]. PSeHD is degraded into small fragments after cleavage of crosslinkers. Low molecular PEI has weak interaction with miR-21i, and thereby the previously loaded miR-21is are released. This result strongly supports the polyplexes release miR-21i in the cytosol of cancer cells due to the presence of reducing enzymes.

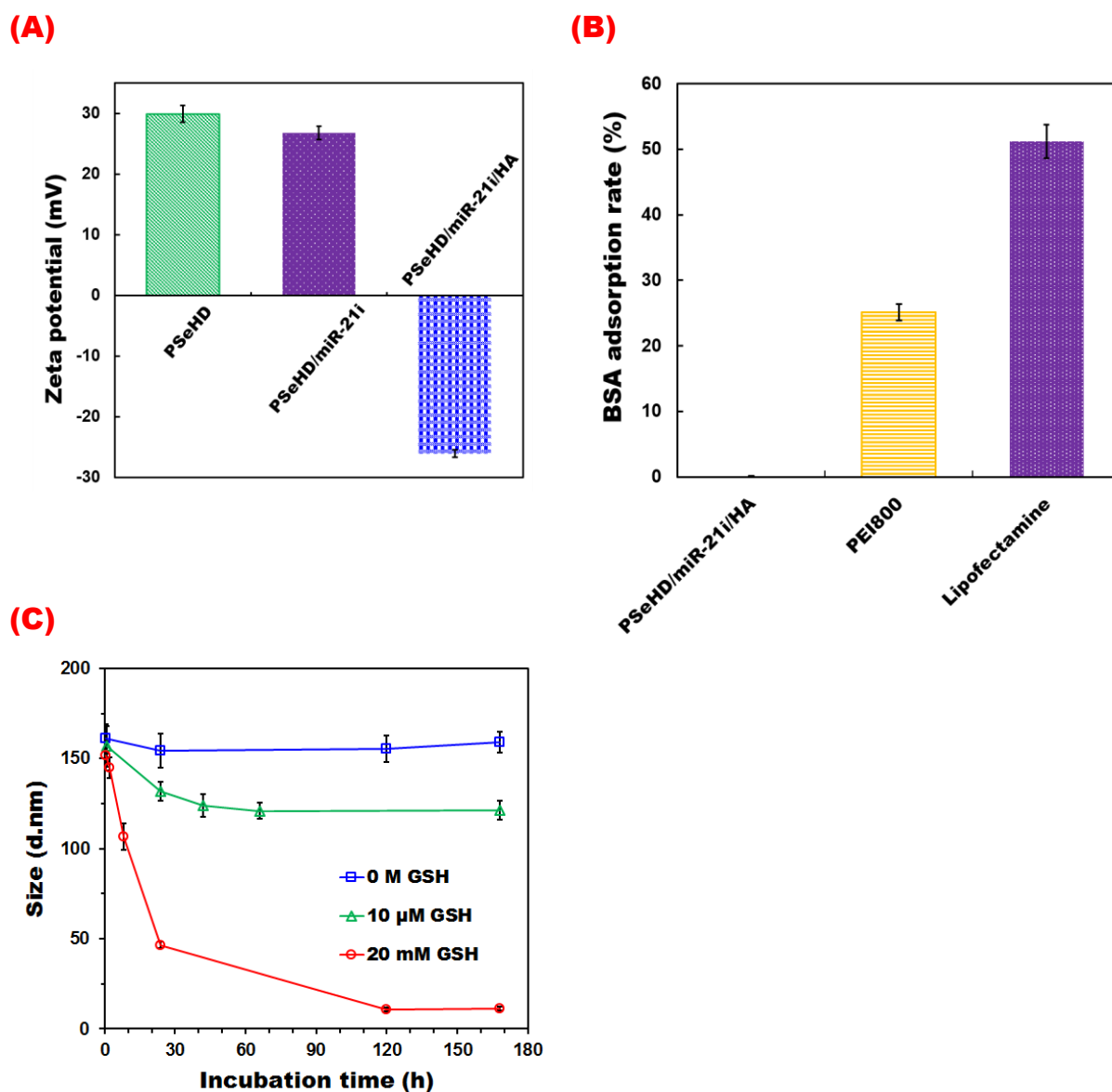


Figure 3.2. (A) Zeta potentials of PSeHD, PSeHD/miR-21i at 10 N/P and PSeHD/miR-21i/HA at 5 w/w ratio of HA to miR-21i ($P < 0.05$, $n = 3$). (B) Protein adsorption by PSeHD/miR-21i/HA (5 w/w ratio of HA to miR-21i) against BSA with PEI800 and Lipofectamine2000 as controls ($n = 3$), (C) *ex vivo* biodegradability of PSeHD/miR-21i/HA by measuring hydrodynamic sizes in PBS 7.4 with 0 M, 10 μ M and 20 mM GSH over 168 h. ($n = 3$)

3.3.3 *Ex vivo* multi-function assays

3.3.3.1 Hyaluronic acid surface coating (PSeHD/miR-21i/HA)

Cationic polymer gene delivery carriers may interact with anionic serum during blood circulation, leading to capture by reticuloendothelial system (RES), such as liver and spleen, before reaching their destination [30, 54]. The carriers may be endocytosed by electrostatic interaction with any cell membrane unselectively, resulting in a low delivery selectivity and strong side effects [55, 56]. To protect the delivery systems from serum adsorption and enable selective endocytosis, hyaluronic acid (HA) was coated to PSeHD/miR-21i polyplexes (at a 10 N/P) by electrostatic interaction with a HA to miR-21i feed weight ratio of 5, producing the PSeHD/miR-21i/HA.

3.3.3.2 Surface charge conversion and *ex vivo* serum protein adsorption

Positive charged PSeHD complexes facilitates miR-21i and HA loading through electrostatic interaction, and endosome/lysosome escaping via the proton sponge effect [57]. After loading miR-21i to PSeHD, HA is introduced to generate a surface negative charged PSeHD/miR-21i/HA. Zeta-potentials of PSeHD, PSeHD/miR-21i and PSeHD/miR-21i/HA were measured at 25 °C (Figure 3.2A). A positive zeta-potential of PSeHD at $+30.0 \pm 1.4$ mV slightly decreases to $+28.0 \pm 1.1$ mV after loading miR-21i at the 10 N/P, and further reduces to -26.1 ± 0.9 mV after HA surface coating. The results indicate successful HA coating to the PSeHD/miR-21i polyplexes via electrostatic interaction.

Negative-charged co-delivery system of PSeHD/miR-21i/HA is able to minimize protein adsorption and maintain its structural integrity during the blood circulation. The stability of delivery carriers during blood circulation was evaluated by *ex vivo* BSA adsorption assays. In Figure 3.2B, BSA adsorption onto the PSeHD/miR-21i/HA is almost negligible, as low as 0.15 ± 0.01 % of total BSA, in comparison with 25.2 ± 1.3 % and 51.2 ± 2.6 % for PEI800 and

Lipofectamine2000. Negatively charged surfaces of PSeHD/miR-21i/HA induce electrostatic repulsion against negatively-charged serum proteins. As a result, PSeHD/miR-21i/HA is able to escape from rapid RES removal and prolong blood circulation time, and thus maintain its high stability during systemic circulation.

3.3.3.3 Controlled degradation of PSeHD/miR-21i/HA delivery systems

PSeHD/miR-21i/HA polyplexes are designed to ensure their sizes between 20 and 200 nm, which promotes passive targeting of the polyplexes to cancer cells by the EPR effects [58]. The polyplexes maintain their morphology during systemic circulation to minimize miR-21i loss before cellular uptake. On the other hand, the PSeHD/miR-21i/HA delivery system is biodegradable under the intracellular cytoplasm microenvironment to release miR-21i and the degraded fragments are excreted from the patient body [31]. Diselenide crosslinkers are stable under a physiological condition to maintain the polyplex structures of PSeHD/miR-21i/HA, but can be cleaved in the presence of reductive enzymes at a high concentration. The responsiveness of PSeHD/miR-21i/HA polyplexes to the reductive environment was evaluated in pH 7.4 PBS buffer with different *ex vivo* mimicking environments: 0 M GSH for a normal physiological condition, 10 μ M GSH for an extracellular tumor environment, and 20 mM GSH for a cytosol condition [53]. Degradation experiments were monitored with the hydrodynamic size change of PSeHD/miR-21i/HA polyplexes at these conditions and 37 °C.

In pH 7.4 PBS with 0 M of GSH, PSeHD/miR-21i/HA polyplexes have good stability by retaining their initial size of 161 ± 8.1 nm over 7 days (Figure 3.2C). At the GSH level of 10 μ M and pH 7.4, the polyplex size slightly drops to 121 ± 5.5 nm over 7days. These results confirm PSeHD/miR-21i/HA possesses a stable size under the mimicking environments of blood circulation and the extracellular environment of healthy cells so that its accumulation in cancer tissue can be enhanced by passive cancer targeting due to the enhanced permeability and retention (EPR) effect and minimal premature leakage of miR-21i [59].

On the other hand, a high concentration of GSH in cancer cytosol condition induces a reduction in particle size associated with the degradation of polyplexes by cleavage of the diselenide bonds of crosslinkers. 20 mM GSH was chosen to mimic the cytosol condition. From [Figure 3.2C](#), the initial size of PSeHD/miR-21i/HA rapidly reduces to 46 ± 1.7 nm within 24 h, and further decreases to 10 ± 1.1 nm after 5 days. This result strongly supports PSeHD/miR-21i/HA polyplexes are fully biodegradable in the mimicking cytosol condition. After releasing cargoes into cytosol, the microgel carrier will be fully degraded into small-sized particles and excreted from body [31, 42, 60].

3.3.4 Cellular uptake assays

Delivery systems with surface HA coating can be endocytosed via HA receptors, such as CD44 and RHAMM, which are widely spread on the surface of invasive MDA-MB-231 cells, but are rarely distributed on the surface of normal cells or non-invasive breast cancer cells (e.g., MCF7) [61]. To monitor cellular uptake of PSeHD/miR-21i/HA to MDA-MB-231 cells via HA receptors mediated endocytosis, PSeHD/FAM-miR/HA was prepared using fluorescent dye labelled miRNA (FAM-miR) replacing miR-21i with evaluation being qualitatively and quantitatively measured by CLSM and flow cytometer.

Cellular uptake of PSeHD/FAM-miR/HA were imaged under a CLSM. FAM-miR and DOX were excited at 488 nm and emitted at 530 and 580 nm, and cells were stained by the CellMask™ Deep Red plasma membrane stain (ex: 640 nm, em: 666 nm). [Figure 3.3A](#) shows cells without any loading as a control with red color for the stained membranes. For the system in the presence of PSeHD/FAM-miR/HA, the red color (cells) overlaps with green (FAM-miR) and blue (DOX) colors to emit a purple color ([Figure 3.3B](#)), indicating uptake of the PSeHD/FAM-miR/HA to cells. While incubating PSeHD/FAM-miR/HA with the HA pretreated cells, [Figure 3.3C](#) shows a limited amount of green and blue colors, indicating cell uptake of PSeHD/FAM-miR/HA is impaired due to block of the HA receptors by pretreated

HA. The CLSM results suggest that the PSeHD/miR-21i/HA is endocytosed to metastatic cancer cells via surface HA receptors, while it has a limited capacity of entering cells without HA receptors.

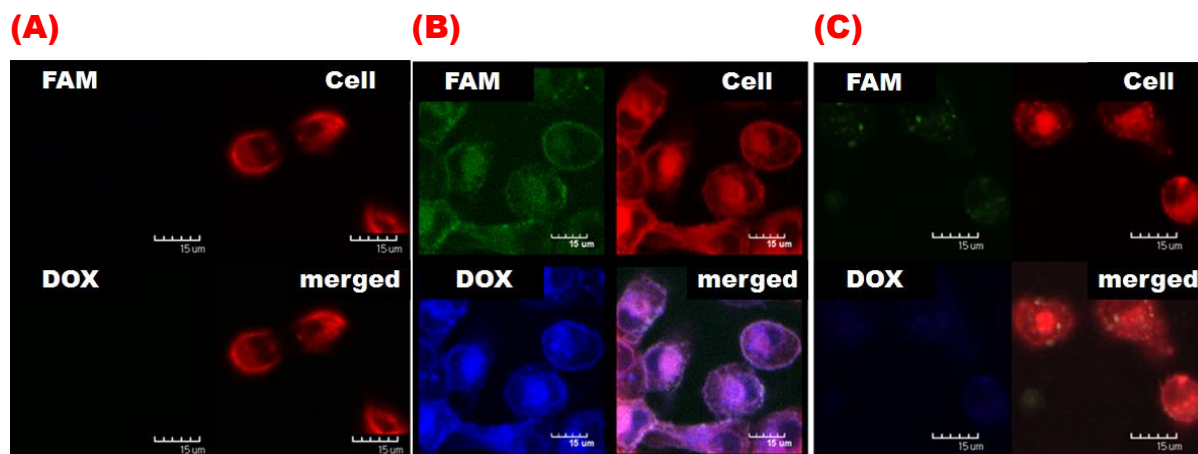


Figure 3.3 Qualitative cellular uptake under a confocal laser scanning microscope (CLSM): (A) MDA-MB-231 cells without delivery carriers, (B) MDA-MB-231 cells with delivery carriers loaded with FAM-miR and DOX (PSeHD/FAM-miR/HA), (C) HA pre-treated MDA-MB-231 cells with the delivery carriers loaded with FAM-miR and DOX (PSeHD/FAM-miR/HA), scale bar 15 μ m.

Cellular uptake of PSeHD/FAM-miR/HA into MDA-MB 231 was further quantitatively evaluated via flow cytometry. For the control of cells without PSeHD/FAM-miR/HA (Figure 3.S10A), 97 % cells in left-down section exhibit no fluorescence at the wavelengths of FAM and DOX. In the presence of PSeHD/FAM-miR/HA, 98 % cells are positioned at the right-upper side in Figure 3.S10B with strong fluorescent signals of FAM and DOX, indicating a high efficiency of cellular uptake of PSeHD/FAM-miR/HA. For the HA pre-treated cells, less than 4 % FAM and DOX signals are depicted in Figure 3.S10C. Quantitative analysis results agree well with those from CLSM that PSeHD/FAM-miR/HA selectively enters MDA-MB-231 cells via HA receptor-mediated endocytosis. Since HA pre-treated MDA-MB 231 cells have no free surface receptors for PSeHD/FAM-miR/HA, these cells behave as normal cells or non-invasive breast cancer cells. It may conclude that the PSeHD/miR-21i/HA polyplexes

actively target invasive breast cancer cells of MDA-MB-231, while they may not be uptaken by normal cells or non-invasive breast cancer cells.

3.3.5 Biocompatibility evaluation

If anticancer chemotherapy is conducted with a delivery carrier, it is mandatory to demonstrate its minimal side effects to healthy cells throughout delivery process. Healthy cell viability assays were operated to evaluate biocompatibility of the delivery system under conditions of before co-drug loading, after co-drug loading and after co-drug release.

3.3.5.1 Microgels before DOX and miR-21i loading

The biocompatibility of PSeH microgels before DOX and miR-21i loading were *in vitro* evaluated via cell viability assays on the kidney cell line (HEK293T) after 48 h incubation. In [Figure 3.4A](#), the PSeH microgels exhibit 85 ± 7.1 % cell survival at a concentration of $50 \mu\text{g mL}^{-1}$, which is comparable to the 86 ± 5.0 % for PEI800 and 82 ± 3.9 % for Lipofectamine2000 as positive controls. In contrast, PEI25k shows high cytotoxicity with 49 ± 4.1 % HEK293T cell survival rate at $50 \mu\text{g mL}^{-1}$. The PSeH microgels as delivery carriers prepared by crosslinking low molecular weight PEI800 retain competent biocompatibility of PEI800, which is similar to our previously reported disulfide crosslinked PEI800 [39].

3.3.5.2 Microgels after DOX and miR-21i loading

Biocompatibility of delivery carriers with therapeutic loading was examined via HEK293T cell viability assays after 48 h incubation against free DOX, DOX loaded microgels (PSeHD), and miR-21i inhibitor (10 N/P) loaded PSeHD with HA coating (PSeHD/miR-21i/HA). Diverse DOX loading concentrations of PSeH microgels from 0.1 to $2.5 \mu\text{g mL}^{-1}$ were employed to evaluate their side effect to normal cells. PSeHD and PSeHD/miR-21i/HA show remarkably high cell survival (96.2 ± 2.0 % and 93.6 ± 4.5 %) as a DOX concentration below $1 \mu\text{g mL}^{-1}$ ([Figure 3.4B](#)), and the cell survival rate decreases to 75 % at the highest DOX concentration

of $2.5 \mu\text{g mL}^{-1}$. As a negative control, free DOX displays significant cytotoxicity to healthy cells with a sharp drop of the cell survival rate to $45.9 \pm 10.7 \%$ at a DOX concentration of $0.5 \mu\text{g mL}^{-1}$, and further down to $35.4 \pm 4.7 \%$ at a DOX concentration of $2.5 \mu\text{g mL}^{-1}$. The most cytotoxic sample to HEK293T cells is free DOX due to its highest cellular uptake via diffusion and hydrophobic interaction with the lipid cellular membrane [52]. However, for the developed smart delivery systems, DOX being conjugated to microgels to form hydrazone bonds are stable in physiological condition (pH 7.4), and thus effectively minimizing DOX release. The stability of the hydrazone bond in PSeHD may be maintained after endocytosis, even in the acidic endosomes-lysosomes. Time for highly positive charged polymer nanoparticles to escape from endosomes-lysosomes is less than 10 minutes, too short to effectively cleave the hydrazone bond and intensively release DOX, supported in [Figure 3.1A](#) and Panyam et al. [62, 63]. On the other hand, PSeHD/miR-21i/HA maintains good biocompatibility as that of PSeHD, whereas PSeHD/miR-21i without HA is less biocompatible ([Figure 3.4E](#)). DOX release profiles from PSeHD and PSeHD/miR-21i in pH 7.4 PBS are compared in [Figure 3.S11](#). An increase in DOX release might be attributed to a decrease in the buffering capability of PSeHD after miR-21i loading. Additionally, cell apoptosis may be provoked by PDCD4 due to loss of suppression by miR-21 after miR-21i is released from PSeHD/miR-21i, while the miR-21 activity of 3 relative inhibiting folds (RIFs) and the miR-21 expression level of near 0.005 ($2^{\Delta\text{Ct}}$) in HEK293T cells are lower than those in many tumor-derived cell lines [64, 65]. The better biocompatibility of PSeHD/miR-21i/HA than PSeHD/miR-21i to normal cells is associated with HA coating. Endocytosis of negatively-charged PSeHD/miR-21i/HA into HEK293T cells is limited as HA receptors of CD44 and RHAMM are rarely expressed [61]. Due to the specific cancer-targeting function of PSeHD/miR-21i/HA, toxicity of this cancer chemotherapy system to healthy cells can be significantly reduced. The cell survival rate against PSeHD/miR-21i/HA at a DOX concentration of $2.5 \mu\text{g mL}^{-1}$ is 75 %, but this DOX concentration is far above the

recommended treatment dosage of around $0.1 \mu\text{g mL}^{-1}$ [66]. Therefore, the PSeHD/miR-21i/HA system may be safely considered for cancer chemotherapy with minimal side effects.

3.3.5.3 Microgel fragments after DOX and miR-21i release

The HEK293T cell viabilities against biodegraded PSeH microgel fragments were evaluated. From previous *ex vivo* study, PSeH microgels is biodegraded into 10 nm fragments in the mimicking intracellular environment of 20 mM GSH. Although these small sized fragments can be readily excreted from a patient body via kidney, their *in vitro* cytotoxicity remains unknown [31, 67]. The fragments of biodegraded PSeH microgels under the mimicking cytosol environment (20 mM GSH 24 h) show $97.2 \pm 3.7\%$ survival rate of HEK293T cells at a DOX concentration of $50 \mu\text{g mL}^{-1}$ (Figure 3.4C). The result is better than 86 % of cell survival against PSeH microgels and PEI800 respectively, which may be due to its smaller size than PSeH microgels and a lower charge density than PEI800. Therefore, it is expected that the biodegraded microgels can be excreted without damage to the patient's kidney.

As a result, the smart PSeH microgel delivery carriers before cargo loading, after cargo (DOX and miR-21i) loading and after cargo release have shown great biocompatibility, rendering a great potential for chemotherapy with minimal side-effects.

3.3.6 Synergistic therapeutic effect on metastatic breast cancer cells

The therapeutic efficacy of doxorubicin (DOX) and miRNA-21 inhibitor (miR-21i) delivered by PSeH microgels on metastatic breast cancer cells (MDA-MB-231) was evaluated via *in vitro* viability assays. The survival rates of the invasive breast cancer cell were studied after 48 h incubation with DOX·HCl (free DOX), PSeHD, PSeHD/miR-21i and PSeHD/miR-21i/HA over an equivalent DOX concentration range from 0.1 to $2.5 \mu\text{g mL}^{-1}$. The anticancer

therapeutic effect of DOX has been significantly enhanced for PSeHD, and further improved for the PSeHD/miR-21i after miR-21i loading (Figure 3.4D).

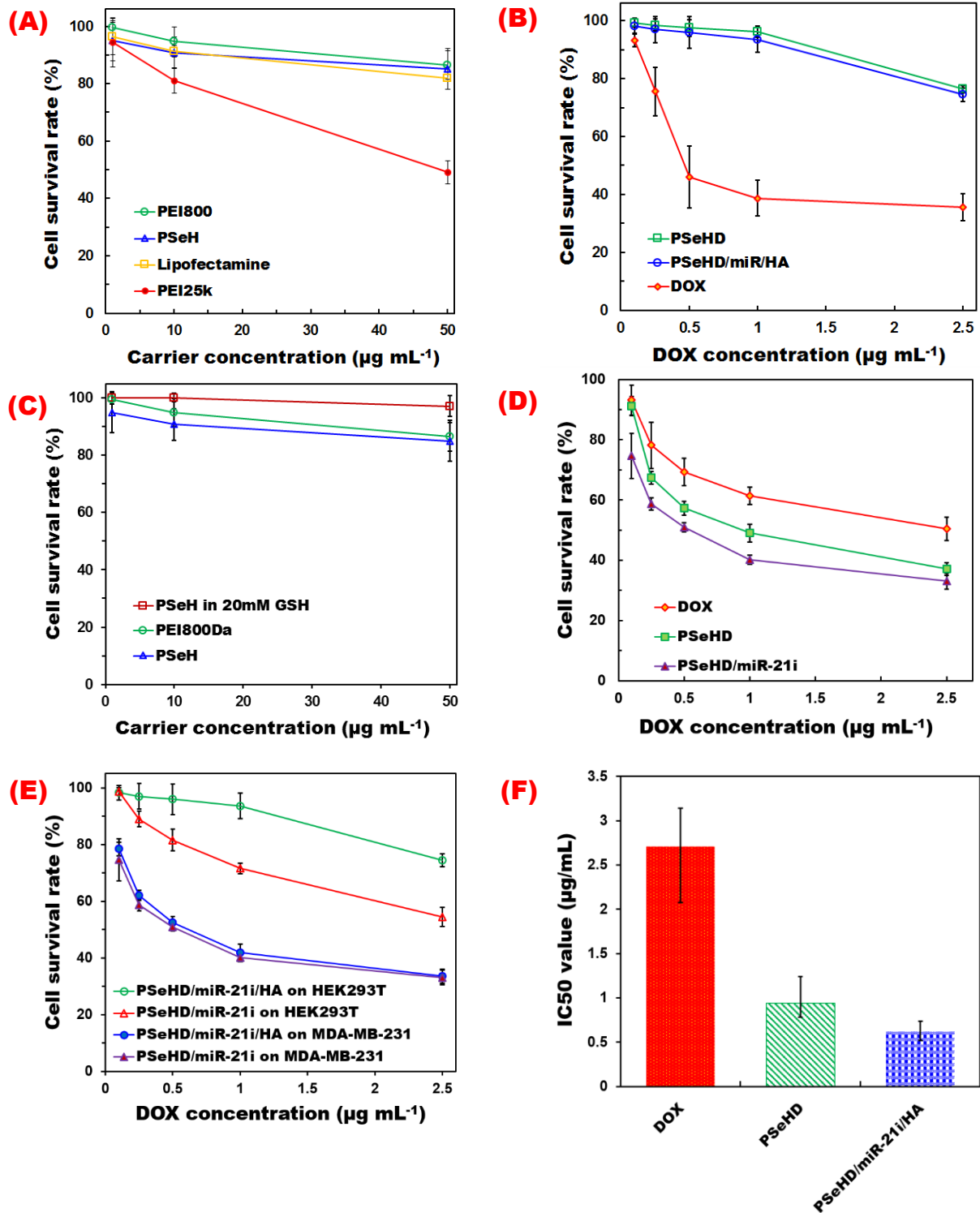


Figure 3.4 Cell viability, (A) HEK293T survival rate against various carriers (PEI800, PSeH, lipofectamine2000 and PEI25k) before loading DOX (n = 4), (B) HEK293T survival rates against free DOX and DOX loaded PSeHD and PSeHD/miR-21i (10 N/P) (n = 4), (C) HEK293T survival rates against PEI800, PSeH and degraded fragments of PSeH after incubation in 20 mM GSH for 24 h ($P < 0.05$, n = 4), (D) MDA-MB-231 survival rate against free DOX, PSeHD and PSeHD/miR-21i (10 N/P) (n = 4), (E) Comparison of cell survival rates of HEK293T cells and MDA-MB-231 cells against PSeHD/miR-21i and PSeHD/miR-21i/HA (n = 3) (10 N/P and 5 w/w ratio of HA to miR-21i), and (F) IC_{50} values ($\mu\text{g mL}^{-1}$) of free DOX, PSeHD and PSeHD/miR-21i/HA. ($P < 0.0001$, n = 4)

With increasing DOX concentration, cancer cell survival rates decrease for all samples. Treatment with free DOX leads to one half of cells survived at a DOX concentration of $2.5 \mu\text{g mL}^{-1}$. In the PSeHD group, a lower survival rate ($37 \pm 2.2 \%$) than free DOX at $2.5 \mu\text{g DOX mL}^{-1}$ is shown. The improved therapeutic efficacy of PSeHD is due to its higher cellular uptake, which aligns well with a similar result with a breast cancer cell line MCF-7 by Misra et al. [68]. Cancer cellular uptake of free DOX is lower than that of normal cells [10]. At a slightly acidic extracellular environment of cancer cells ($\sim \text{pH } 6.5$), free DOX is protonated (pKa 7.55 of amine in DOX), which inhibits its interaction with hydrophobic tails of phospholipid cellular membrane and leads to a lower permeability than un-protonated DOX [52, 69]. Additionally, the Eksborg's partition experiment also supports reduced diffusion of free DOX from a slightly acidic aqueous environment to an intracellular organic phase due to the formation of DOX dimer and tetramer with protonated DOX [70]. Therefore, less cytotoxicity of free DOX is found for cancer cells than normal cells, as shown in [Figures 3.4B and 3.4D](#) and previous reports [11, 12].

In contrast to free DOX, PSeHD enters cancer cells via endocytosis by electrostatic interaction with cell membrane [71]. Conjugation of DOX with PSeHD via a pH responsive hydrazone bond is partially cleaved or weakened in a slightly acidic cancer extracellular environment ([Figure 3.1A](#)). The released DOX in the extracellular fluid or loosely bound DOX to the carriers might be engulfed into cells by micropinocytosis and transported to acidic endosomes-

lysosomes for intensive release of DOX [72]. Therefore, delivery of DOX by PSeHD results in a higher therapeutic efficacy than free DOX to cancer cells.

After loading miR-21i onto PSeHD microgels (PSeHD/miR-21i), the cell survival rate of MDA-MB-231 cells against PSeHD/miR-21i is down to $33.1 \pm 2.6 \%$ at a DOX concentration of $2.5 \mu\text{g mL}^{-1}$. PSeHD/miR-21i delivery systems can release miR-21i into cytosol of the cells in the presence of 10 to 20 mM glutathione (GSH), which induces cleavage of diselenide bonds of the polyplex carriers [53]. The biodegraded fragments have weak electrostatic interaction with miR-21i and release them to cytosol. Comparing with the therapeutic performance of free DOX and PSeHD, PSeHD/miR-21i demonstrates a synergistic effect from both DOX and miR-21i on invasive breast cancer treatment. The miR-21i inhibits the activity of miR-21 in the cancer cells, thus inducing cell apoptosis by increasing PDCD4 and re-sensitizing to DOX by expression of phosphatase and tensin homolog (PTEN) [14, 17].

In order to understand the contribution of HA, MDA-MB-231 cell viabilities for the PSeHD/miR-21i with or without HA were evaluated (Figure 3.4E). The MDA-MB-231 cell survival rate (%) of PSeHD/miR-21i/HA is 33.5 ± 2.5 at a DOX concentrations of $2.5 \mu\text{g mL}^{-1}$ with a difference of 0.45% in comparison with that of PSeHD/miR-21i. Endocytosis of PSeHD/miR-21i/HA is mainly through the receptor-mediated endocytosis pathway via CD44, while PSeHD/miR-21i endocytosis via electrostatic interaction with negatively charged phospholipids of cell membrane [73, 74]. These demonstrate HA-receptor and electrostatic interaction mediated endocytosis of the delivery system lead to identical therapeutic results to MDA-MB-231 cells with overexpressed HA receptors. However, significant difference is observed for HEK 293T cells (Figure 3.4E). The HEK293T survival rate against the HA coated delivery system, PSeHD/miR-21i/HA, is far higher than that against PSeHD/miR-21i without HA by 20 % at a DOX concentration of $2.5 \mu\text{g mL}^{-1}$. Due to lack of HA receptors on the surface of HEK293T cells and negatively charged HA coating, PSeHD/miR-21i/HA cannot enter

HEK293T cells through HA-receptors or electrostatic interactions, whereas positively charged PSeHD/miR-21i without HA can enter the healthy cells via electrostatic interaction [61, 71]. It is clear that the HA coated delivery system, PSeHD/miR-21i/HA, can selectively target cancer cells with an improved therapeutic efficiency and reduced off-target induced side effects.

The DOX concentration for 50 % cell death is classified as the IC_{50} as shown in [Figure 3.4F](#). The IC_{50} values of PSeHD/miR-21i/HA, PSeHD and free DOX are 0.610, 0.942 and 2.706 $\mu\text{g mL}^{-1}$, respectively. The IC_{50} value difference for three samples is attributed to the synergistic effect of co-drug therapy using DOX and miR-21i. The quantitative therapeutic efficacy of PSeHD/miR-21i/HA to MDA-MB-231 cells is 4.4 times higher than free DOX, indicating the PSeHD/miR-21i/HA co-delivery system has outstanding advantages over traditional therapeutic systems, summarized in [Table 3.S2](#).

3.4 Conclusion

Multifunctional microgels of PSeH with HA surface coating were synthesized for controlled delivery of DOX and miR-21i to target cancer cells for outstanding synergistic anticancer effects and minimal side effects. The delivery polyplexes, PSeHD/miR-21i/HA, consist of diselenide bond-crosslinked PEI800 to load miR-21i, functional hydrazine bonds for DOX conjugation loading and HA for protection and cell targeting. DOX conjugation to PSeH minimizes its pre-mature release and promotes controlled release at acidic cancer microenvironments. Diselenide-crosslinked PEI800 allows effective electrostatic interaction with miR-21i and its stability during blood circulation enables enhanced accumulation at the cancer sites before endocytosis. GSH in cytosol facilitates microgel degradation to renal clearable sized fragments and controlled release of miR-21i. HA surface coating inhibits protein adsorption and promotes active cancer targeting by the HA receptor-mediated

endocytosis. *In vitro* cell viability assays of metastatic breast cancer cell line (MDA-MB-231) demonstrate a great antitumor efficacy of PSeHD/miR-21i/HA over free DOX. On the other hand, PSeH microgels (before co-drug loading, after co-drug loading and after co-drug release) exhibit minimal toxicity to healthy cells. Therefore, this fully microenvironment-degradable smart microgels possess a great promise as a co-delivery carrier of DOX and miR-21i for high efficient antitumor chemotherapy with notable biocompatibility.

Acknowledgement

We are grateful for the research grant of the Australian Research Council DP110102877 and DP140104062. SY would like to appreciate the APA scholarship provided by the University of Adelaide. We also thank Wookyeong Lee for assisting scheme design.

References

- [1] N. Pilco-Ferreto, G.M. Calaf, Influence of doxorubicin on apoptosis and oxidative stress in breast cancer cell lines, *Int. J. Oncol.*, 49 (2016) 753-762.
- [2] C. Pisano, S.C. Cecere, M. Di Napoli, C. Cavaliere, R. Tambaro, G. Facchini, C. Scaffa, S. Losito, A. Pizzolorusso, S. Pignata, Clinical trials with pegylated liposomal Doxorubicin in the treatment of ovarian cancer, *J Drug Deliv*, 2013 (2013) 898146.
- [3] N. Durán, W.J. Fávaro, Nanopharmaceuticals and Their Applications in Bladder Cancer Therapy: a Mini Review, *J. Braz. Chem. Soc.*, 29 (2018) 973-981.
- [4] M. Li, Z. Tang, J. Lin, Y. Zhang, S. Lv, W. Song, Y. Huang, X. Chen, Synergistic antitumor effects of doxorubicin-loaded carboxymethyl cellulose nanoparticle in combination with endostar for effective treatment of non-small-cell lung cancer, *Adv Healthc Mater*, 3 (2014) 1877-1888.
- [5] X. Meng, Q. Zhang, G. Zheng, R. Pang, T. Hua, S. Yang, J.I.E. Li, Doxorubicin combined with celecoxib inhibits tumor growth of medullary thyroid carcinoma in xenografted mice, *Oncol. Lett.*, 7 (2014) 2053-2058.
- [6] H. Zhao, X. Zhang, Enhanced apoptosis and inhibition of gastric cancer cell invasion following treatment with LDH@Au loaded Doxorubicin, *Electron. J. Biotechnol.*, 32 (2018) 13-18.
- [7] K. Chandran, D. Aggarwal, R.Q. Migrino, J. Joseph, D. McAllister, E.A. Konorev, W.E. Antholine, J. Zielonka, S. Srinivasan, N.G. Avadhani, B. Kalyanaraman, Doxorubicin Inactivates Myocardial Cytochrome c Oxidase in Rats: Cardioprotection by Mito-Q, *Biophys. J.*, 96 (2009) 1388-1398.
- [8] S. Singla, N.R. Kumar, J. Kaur, In vivo Studies on the Protective Effect of Propolis on Doxorubicin-Induced Toxicity in Liver of Male Rats, *Toxicol. Int.*, 21 (2014) 191-195.
- [9] N.M. Elsherbiny, M. El-Sherbiny, Thymoquinone attenuates Doxorubicin-induced nephrotoxicity in rats: Role of Nrf2 and NOX4, *Chem. Biol. Interact.*, 223 (2014) 102-108.
- [10] S. Wang, E.A. Konorev, S. Kotamraju, J. Joseph, S. Kalivendi, B. Kalyanaraman, Doxorubicin induces apoptosis in normal and tumor cells via distinctly different mechanisms. intermediacy of H(2)O(2)- and p53-dependent pathways, *J. Biol. Chem.*, 279 (2004) 25535-25543.
- [11] U. Tiddefelt, B. Sundman-Engberg, C. Paul, Intracellular uptake and cytotoxic effect in vitro of doxorubicin and epirubicin in human leukemic and normal hematopoietic cells, *Cancer Chemother. Pharmacol.*, 29 (1991) 7-12.
- [12] R. Biabanikhankahdani, K.L. Ho, N.B. Alitheen, W.S. Tan, A Dual Bioconjugated Virus-Like Nanoparticle as a Drug Delivery System and Comparison with a pH-Responsive Delivery System, *Nanomaterials (Basel)*, 8 (2018) 236.

- [13] Z. Liu, A.C. Fan, K. Rakhra, S. Sherlock, A. Goodwin, X. Chen, Q. Yang, D.W. Felsher, H. Dai, Supramolecular Stacking of Doxorubicin on Carbon Nanotubes for In Vivo Cancer Therapy, *Angew. Chem. Int. Ed.*, 48 (2009) 7668-7672.
- [14] X. Pan, Z.-X. Wang, R. Wang, MicroRNA-21: A novel therapeutic target in human cancer, *Cancer Biol. Ther.*, 10 (2010) 1224-1232.
- [15] L.Y.W. Bourguignon, C.C. Spevak, G. Wong, W. Xia, E. Gilad, Hyaluronan-CD44 Interaction with Protein Kinase C ϵ Promotes Oncogenic Signaling by the Stem Cell Marker Nanog and the Production of MicroRNA-21, Leading to Down-regulation of the Tumor Suppressor Protein PDCD4, Anti-apoptosis, and Chemotherapy Resistance in Breast Tumor Cells, *J. Biol. Chem.*, 284 (2009) 26533-26546.
- [16] N.S. Wickramasinghe, T.T. Manavalan, S.M. Dougherty, K.A. Riggs, Y. Li, C.M. Klinge, Estradiol downregulates miR-21 expression and increases miR-21 target gene expression in MCF-7 breast cancer cells, *Nucleic Acids Res.*, 37 (2009) 2584-2595.
- [17] Z.-X. Wang, B.-B. Lu, H. Wang, Z.-X. Cheng, Y.-M. Yin, MicroRNA-21 Modulates Chemosensitivity of Breast Cancer Cells to Doxorubicin by Targeting PTEN, *Arch. Med. Res.*, 42 (2011) 281-290.
- [18] F. Zhi, H. Dong, X. Jia, W. Guo, H. Lu, Y. Yang, H. Ju, X. Zhang, Y. Hu, Functionalized Graphene Oxide Mediated Adriamycin Delivery and miR-21 Gene Silencing to Overcome Tumor Multidrug Resistance In Vitro, *PLoS One*, 8 (2013) e60034.
- [19] R.L. Juliano, S. Alahari, H. Yoo, R. Kole, M. Cho, Antisense Pharmacodynamics: Critical Issues in the Transport and Delivery of Antisense Oligonucleotides, *Pharm. Res.*, 16 (1999) 494-502.
- [20] Y. Chen, D.-Y. Gao, L. Huang, In vivo delivery of miRNAs for cancer therapy: Challenges and strategies, *Adv. Drug Del. Rev.*, 81 (2015) 128-141.
- [21] R.K. Subedi, K.W. Kang, H.-K. Choi, Preparation and characterization of solid lipid nanoparticles loaded with doxorubicin, *Eur. J. Pharm. Sci.*, 37 (2009) 508-513.
- [22] R. Mo, T. Jiang, R. DiSanto, W. Tai, Z. Gu, ATP-triggered anticancer drug delivery, *Nat Commun*, 5 (2014).
- [23] X. Deng, M. Cao, J. Zhang, K. Hu, Z. Yin, Z. Zhou, X. Xiao, Y. Yang, W. Sheng, Y. Wu, Y. Zeng, Hyaluronic acid-chitosan nanoparticles for co-delivery of MiR-34a and doxorubicin in therapy against triple negative breast cancer, *Biomaterials*, 35 (2014) 4333-4344.
- [24] X. Zhang, L. Meng, Q. Lu, Z. Fei, P.J. Dyson, Targeted delivery and controlled release of doxorubicin to cancer cells using modified single wall carbon nanotubes, *Biomaterials*, 30 (2009) 6041-6047.
- [25] H.Y. Feng, D.D. Chu, Z.R. Li, Z.H. Guo, L. Jin, B.B. Fan, J.J. Zhang, J.G. Li, A DOX-loaded polymer micelle for effectively inhibiting cancer cells, *Rsc Advances*, 8 (2018) 25949-25954.

- [26] N. Li, C. Guo, Z. Duan, L. Yu, K. Luo, J. Lu, Z. Gu, A stimuli-responsive Janus peptide dendron–drug conjugate as a safe and nanoscale drug delivery vehicle for breast cancer therapy, *J Mater Chem B*, 4 (2016) 3760-3769.
- [27] Y. Su, Y. Hu, Y. Du, X. Huang, J. He, J. You, H. Yuan, F. Hu, Redox-Responsive Polymer–Drug Conjugates Based on Doxorubicin and Chitosan Oligosaccharide-g-stearic Acid for Cancer Therapy, *Mol. Pharm.*, 12 (2015) 1193-1202.
- [28] J.D. Wallat, J.K. Harrison, J.K. Pokorski, pH Responsive Doxorubicin Delivery by Fluorous Polymers for Cancer Treatment, *Mol. Pharm.*, 15 (2018) 2954-2962.
- [29] D.-W. Dong, B. Xiang, W. Gao, Z.-Z. Yang, J.-Q. Li, X.-R. Qi, pH-responsive complexes using prefunctionalized polymers for synchronous delivery of doxorubicin and siRNA to cancer cells, *Biomaterials*, 34 (2013) 4849-4859.
- [30] T. Wang, J.R. Upponi, V.P. Torchilin, Design of multifunctional non-viral gene vectors to overcome physiological barriers: Dilemmas and strategies, *Int. J. Pharm.*, 427 (2012) 3-20.
- [31] S.H. Ku, K. Kim, K. Choi, S.H. Kim, I.C. Kwon, Tumor-Targeting Multifunctional Nanoparticles for siRNA Delivery: Recent Advances in Cancer Therapy, *Adv. Healthc. Mater.*, 3 (2014) 1182-1193.
- [32] K.F. Pirollo, G. Zon, A. Rait, Q. Zhou, W. Yu, R. Hogrefe, D.E.H. Chang, Tumor-Targeting Nanoimmunoliposome Complex for Short Interfering RNA Delivery, *Hum. Gene Ther.*, 17 (2006) 117-124.
- [33] H.R. Kim, I.K. Kim, K.H. Bae, S.H. Lee, Y. Lee, T.G. Park, Cationic Solid Lipid Nanoparticles Reconstituted from Low Density Lipoprotein Components for Delivery of siRNA, *Mol. Pharm.*, 5 (2008) 622-631.
- [34] C.G. Zhang, W.J. Zhu, Y. Liu, Z.Q. Yuan, S.D. Yang, W.L. Chen, J.Z. Li, X.F. Zhou, C. Liu, X.N. Zhang, Novel polymer micelle mediated co-delivery of doxorubicin and P-glycoprotein siRNA for reversal of multidrug resistance and synergistic tumor therapy, *Sci. Rep.*, 6 (2016) 23859.
- [35] Y. Ren, R. Wang, L. Gao, K. Li, X. Zhou, H. Guo, C. Liu, D. Han, J. Tian, Q. Ye, Y.T. Hu, D. Sun, X. Yuan, N. Zhang, Sequential co-delivery of miR-21 inhibitor followed by burst release doxorubicin using NIR-responsive hollow gold nanoparticle to enhance anticancer efficacy, *J. Control. Release*, 228 (2016) 74-86.
- [36] D. Ma, Enhancing endosomal escape for nanoparticle mediated siRNA delivery, *Nanoscale*, 6 (2014) 6415-6425.
- [37] H. Yin, F. Zhao, D. Zhang, J. Li, Hyaluronic acid conjugated β -cyclodextrin-oligoethylenimine star polymer for CD44-targeted gene delivery, *Int. J. Pharm.*, 483 (2015) 169-179.
- [38] X. Du, B. Shi, Y. Tang, S. Dai, S.Z. Qiao, Label-free dendrimer-like silica nanohybrids for traceable and controlled gene delivery, *Biomaterials*, 35 (2014) 5580-5590.
- [39] B. Zhang, H. Zhang, S. Dai, J. Bi, Cell-penetrating peptide–labelled smart polymers for enhanced gene delivery, *Eng. Life Sci.*, 17 (2017) 193-203.

- [40] B. Shi, H. Zhang, S.Z. Qiao, J. Bi, S. Dai, Intracellular microenvironment-responsive label-free autofluorescent nanogels for traceable gene delivery, *Adv Healthc Mater*, 3 (2014) 1839-1848.
- [41] D. Yue, G. Cheng, Y. He, Y. Nie, Q. Jiang, X. Cai, Z. Gu, Influence of reduction-sensitive diselenide bonds and disulfide bonds on oligoethylenimine conjugates for gene delivery, *J. Mater. Chem. B*, 2 (2014) 7210-7221.
- [42] S. Shen, D. Jiang, L. Cheng, Y. Chao, K. Nie, Z. Dong, C.J. Kuttyreff, J.W. Engle, P. Huang, W. Cai, Z. Liu, Renal-Clearable Ultrasmall Coordination Polymer Nanodots for Chelator-Free ⁶⁴Cu-Labeling and Imaging-Guided Enhanced Radiotherapy of Cancer, *ACS Nano*, 11 (2017) 9103-9111.
- [43] A. Schroeder, D.A. Heller, M.M. Winslow, J.E. Dahlman, G.W. Pratt, R. Langer, T. Jacks, D.G. Anderson, Treating metastatic cancer with nanotechnology, *Nat. Rev. Cancer*, 12 (2011) 39-50.
- [44] S. Hama, S. Itakura, M. Nakai, K. Nakayama, S. Morimoto, S. Suzuki, K. Kogure, Overcoming the polyethylene glycol dilemma via pathological environment-sensitive change of the surface property of nanoparticles for cellular entry, *J. Control. Release*, 206 (2015) 67-74.
- [45] S. Mizrahy, S.R. Raz, M. Hasgaard, H. Liu, N. Soffer-Tsur, K. Cohen, R. Dvash, D. Landsman-Milo, M.G.E.G. Bremer, S.M. Moghimi, D. Peer, Hyaluronan-coated nanoparticles: The influence of the molecular weight on CD44-hyaluronan interactions and on the immune response, *J. Control. Release*, 156 (2011) 231-238.
- [46] H.S.S. Qhattal, X. Liu, Characterization of CD44-Mediated Cancer Cell Uptake and Intracellular Distribution of Hyaluronan-Grafted Liposomes, *Mol. Pharm.*, 8 (2011) 1233-1246.
- [47] G. Cheng, Y. He, L. Xie, Y. Nie, B. He, Z. Zhang, Z. Gu, Development of a reduction-sensitive diselenide-conjugated oligoethylenimine nanoparticulate system as a gene carrier, *Int. J. Nanomedicine*, 7 (2012) 3991-4006.
- [48] K. Helios, A. Pietraszko, W. Zierkiewicz, H. Wójtowicz, D. Michalska, The crystal structure, infrared, Raman and density functional studies of bis(2-aminophenyl) diselenide, *Polyhedron*, 30 (2011) 2466-2472.
- [49] D. Lin-Vien, N.B. Colthup, W.G. Fateley, J.G. Grasselli, *The handbook of infrared and Raman characteristic frequencies of organic molecules*, Elsevier, 1991.
- [50] A.B. Thomas, P.N. Tupe, R.V. Badhe, R.K. Nanda, L.P. Kothapalli, O.D. Paradkar, P.A. Sharma, A.D. Deshpande, Green route synthesis of Schiff's bases of isonicotinic acid hydrazide, *Green Chem. Lett. Rev.*, 2 (2009) 23-27.
- [51] A.L. Green, Studies on the mechanism of inhibition of monoamine-oxidase by hydrazine derivatives, *Biochem. Pharmacol.*, 13 (1964) 249-261.
- [52] M. Dalmark, Characteristics of doxorubicin transport in human red blood cells, *Scand. J. Clin. Lab. Invest.*, 41 (1981) 633-639.

- [53] F.Q. Schafer, G.R. Buettner, Redox environment of the cell as viewed through the redox state of the glutathione disulfide/glutathione couple, *Free Radic. Biol. Med.*, 30 (2001) 1191-1212.
- [54] H. Yin, R.L. Kanasty, A.A. Eltoukhy, A.J. Vegas, J.R. Dorkin, D.G. Anderson, Non-viral vectors for gene-based therapy, *Nat. Rev. Genet.*, 15 (2014) 541-555.
- [55] F. Xu, W. Lu, H. Wu, L. Fan, X. Gao, X. Jiang, Brain delivery and systemic effect of cationic albumin conjugated PLGA nanoparticles, *J. Drug Target.*, 17 (2009) 423-434.
- [56] X. Dai, C. Tan, Combination of microRNA therapeutics with small-molecule anticancer drugs: Mechanism of action and co-delivery nanocarriers, *Adv. Drug Del. Rev.*, 81 (2015) 184-197.
- [57] M. Wang, T. Liu, L. Han, W. Gao, S. Yang, N. Zhang, Functionalized O-carboxymethyl-chitosan/polyethylenimine based novel dual pH-responsive nanocarriers for controlled co-delivery of DOX and genes, *Polym. Chem.*, 6 (2015) 3324-3335.
- [58] S. Liang, X.-Z. Yang, X.-J. Du, H.-X. Wang, H.-J. Li, W.-W. Liu, Y.-D. Yao, Y.-H. Zhu, Y.-C. Ma, J. Wang, E.-W. Song, Optimizing the Size of Micellar Nanoparticles for Efficient siRNA Delivery, *Adv. Funct. Mater.*, 25 (2015) 4778-4787.
- [59] Y. Nakamura, A. Mochida, P.L. Choyke, H. Kobayashi, Nanodrug Delivery: Is the Enhanced Permeability and Retention Effect Sufficient for Curing Cancer?, *Bioconjug. Chem.*, 27 (2016) 2225-2238.
- [60] E.B. Ehlerding, F. Chen, W. Cai, Biodegradable and Renal Clearable Inorganic Nanoparticles, *Adv Sci (Weinh)*, 3 (2016) 1500223.
- [61] S.R. Hamilton, S.F. Fard, F.F. Paiwand, C. Tolg, M. Veiseh, C. Wang, J.B. McCarthy, M.J. Bissell, J. Koropatnick, E.A. Turley, The hyaluronan receptors CD44 and Rhamm (CD168) form complexes with ERK1,2 that sustain high basal motility in breast cancer cells, *J. Biol. Chem.*, 282 (2007) 16667-16680.
- [62] J. Panyam, W.Z. Zhou, S. Prabha, S.K. Sahoo, V. Labhasetwar, Rapid endo-lysosomal escape of poly(DL-lactide-co-glycolide) nanoparticles: implications for drug and gene delivery, *FASEB J.*, 16 (2002) 1217-1226.
- [63] J. Panyam, V. Labhasetwar, Biodegradable nanoparticles for drug and gene delivery to cells and tissue, *Adv. Drug Del. Rev.*, 64 (2012) 61-71.
- [64] W. Tian, X. Dong, X. Liu, G. Wang, Z. Dong, W. Shen, G. Zheng, J. Lu, J. Chen, Y. Wang, Z. Wu, X. Wu, High-Throughput Functional MicroRNAs Profiling by Recombinant AAV-Based MicroRNA Sensor Arrays, *PLoS One*, 7 (2012) e29551.
- [65] Y. Naro, N. Ankenbruck, M. Thomas, Y. Tivon, C.M. Connelly, L. Gardner, A. Deiters, Small Molecule Inhibition of MicroRNA miR-21 Rescues Chemosensitivity of Renal-Cell Carcinoma to Topotecan, *J. Med. Chem.*, 61 (2018) 5900-5909.
- [66] B.J. Cusack, S.P. Young, J. Driskell, R.D. Olson, Doxorubicin and doxorubicinol pharmacokinetics and tissue concentrations following bolus injection and continuous infusion of doxorubicin in the rabbit, *Cancer Chemother. Pharmacol.*, 32 (1993) 53-58.

- [67] H. Wang, Y. Jiang, H. Peng, Y. Chen, P. Zhu, Y. Huang, Recent progress in microRNA delivery for cancer therapy by non-viral synthetic vectors, *Adv. Drug Del. Rev.*, 81 (2015) 142-160.
- [68] R. Misra, S.K. Sahoo, Intracellular trafficking of nuclear localization signal conjugated nanoparticles for cancer therapy, *Eur. J. Pharm. Sci.*, 39 (2010) 152-163.
- [69] A. Parsegian, Energy of an Ion crossing a Low Dielectric Membrane: Solutions to Four Relevant Electrostatic Problems, *Nature*, 221 (1969) 844.
- [70] S. Eksborg, Extraction of Daunorubicin and Doxorubicin and Their Hydroxyl Metabolites: Self-Association in Aqueous Solution, *J. Pharm. Sci.*, 67 (1978) 782-785.
- [71] L.F. Kou, J. Sun, Y.L. Zhai, Z.G. He, The endocytosis and intracellular fate of nanomedicines: Implication for rational design, *Asian J. Pharm. Sci.*, 8 (2013) 1-10.
- [72] S. Falcone, E. Cocucci, P. Podini, T. Kirchhausen, E. Clementi, J. Meldolesi, Macropinocytosis: regulated coordination of endocytic and exocytic membrane traffic events, *J. Cell Sci.*, 119 (2006) 4758-4769.
- [73] I. Noh, H.-O. Kim, J. Choi, Y. Choi, D.K. Lee, Y.-M. Huh, S. Haam, Co-delivery of paclitaxel and gemcitabine via CD44-targeting nanocarriers as a prodrug with synergistic antitumor activity against human biliary cancer, *Biomaterials*, 53 (2015) 763-774.
- [74] G. Sahay, D.Y. Alakhova, A.V. Kabanov, Endocytosis of nanomedicines, *J. Control. Release*, 145 (2010) 182-195.

Supporting Information

Microenvironment-degradable multifunctional microgels for selective co-delivery of DOX and miRNA-21 inhibitor for enhanced anticancer therapy

*Seonho Yun, Jiabin Zhang, Hesamoddin Rabiee, Hu Zhang, Jingxiu Bi, Sheng Dai**

Table 3.S1 Comparison on the DOX and miR-21i loading capability of various complexes, PSeH5%D, PSeH10%D (PSeHD), PSeH20%D (P < 0.05)

Type of complexes	Hydrazine contents mol% (hydrazine/amine)	DOX loading wt% (DOX/complexes)	miRNA full loading (N/P ratio)
PSeH5%D	5	1.1	N/A
PSeHD	10	4.0	4
PSeH20%D	20	18.7	10

Table 3.S2 Comparison on the anticancer therapeutic performance of various DOX systems from their relative IC₅₀ values on MDA-MB-231 cells.

Therapeutic systems	Relative IC ₅₀ (free DOX / therapeutic systems)	Citation
Free DOX	1.0	
PSeHD/miR-21i/HA	4.4	Here
PGA-PTX-DOX	1.6	[1]
¹⁹ F-DOX	1.5	[2]
DOX loaded vesicles	1.0	[3]
DOX/NG	1.3	[4]
DOX@MSNs-PPFA/Bcl-2	1.3	[5]

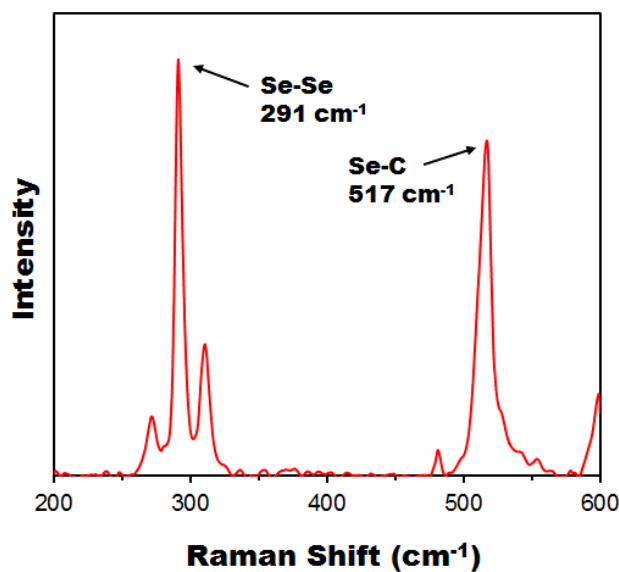


Figure 3.S1 Raman spectrum of the synthesized diselenide crosslinker (-SeSe-).

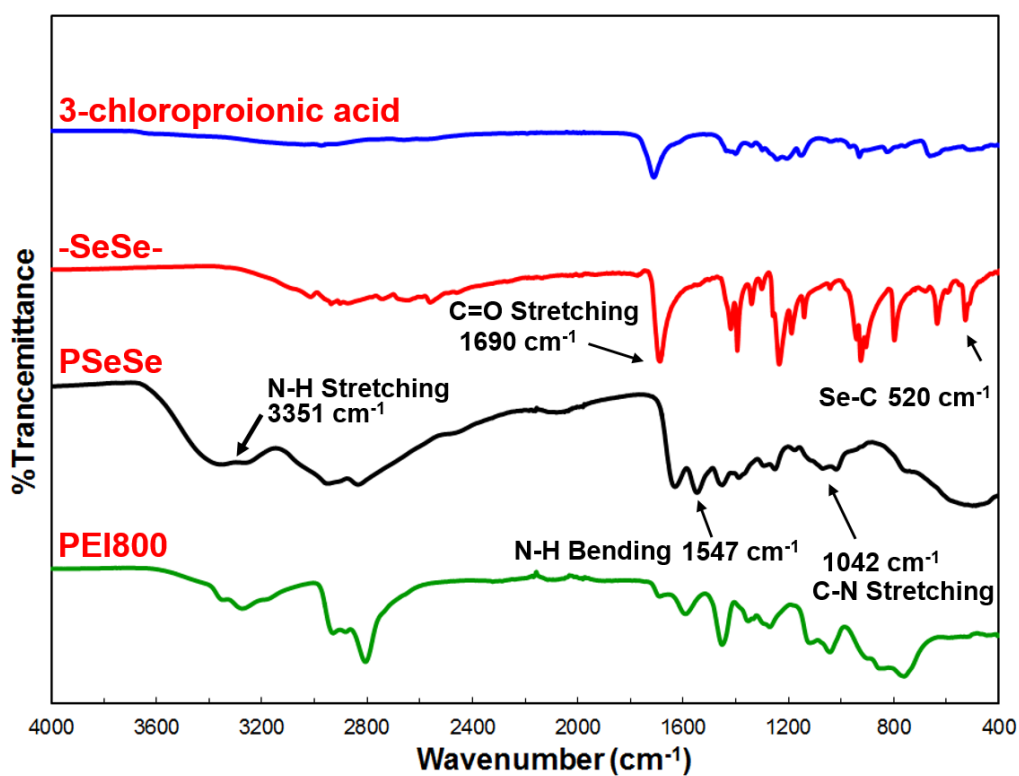


Figure 3.S2 FTIR spectra of 3-chloropropionic acid, diselenide crosslinker of (-SeSe-), branched PEI800 and diselenide crosslinked PEI800 microgels (PSeSe).

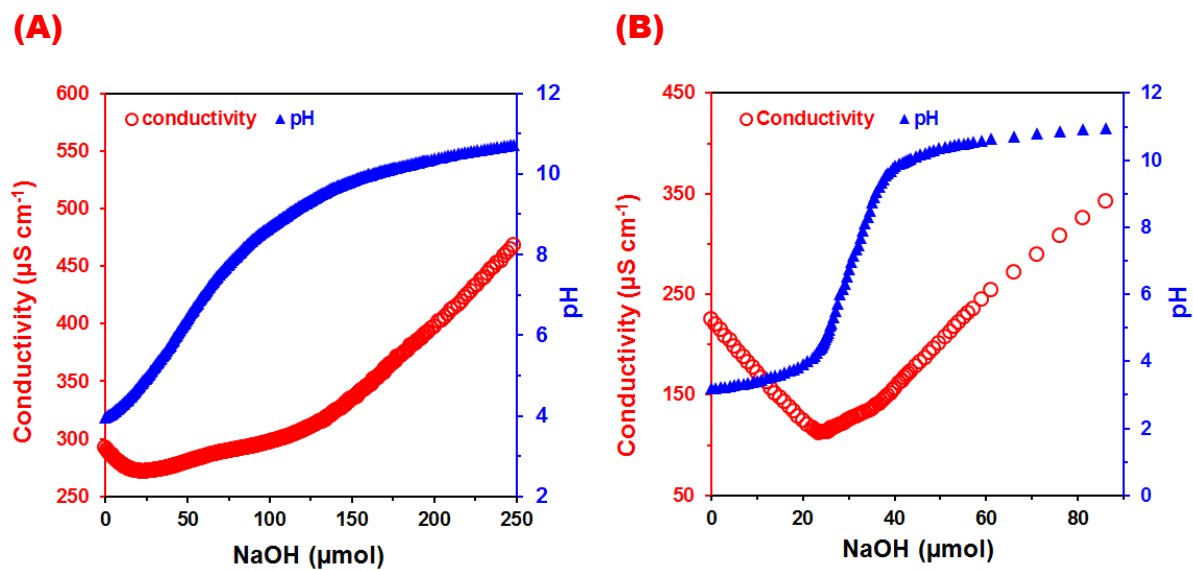


Figure 3.S3 Conductivity and pH titrations for (A) PEI800 (10 mg) and (B) PSeSe (2.4 mg) at room temperature.

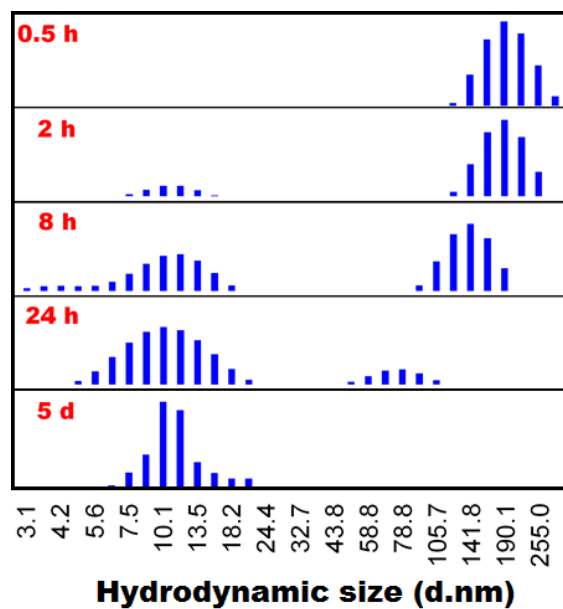


Figure 3.S4 Time dependent size distributions of PSeH microgels in 25 mM DTT aqueous solution at room temperature ($n = 3$)

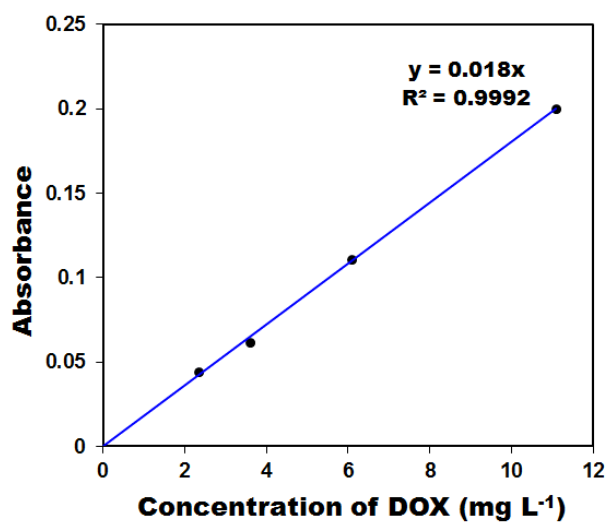


Figure 3.S5 UV-vis calibration curve of DOX aqueous solutions at the wavelength of 479.5 nm and room temperature.

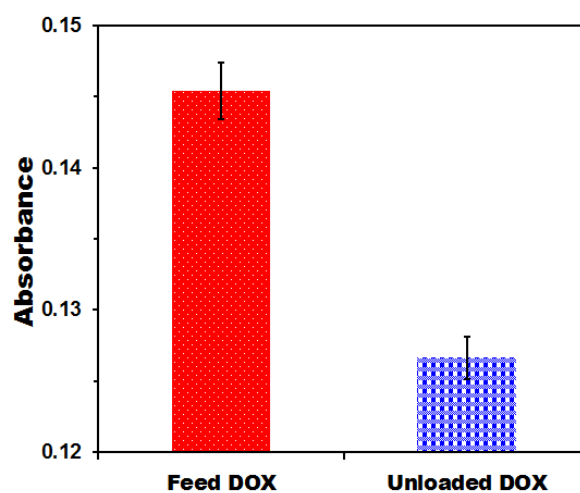


Figure 3.S6 UV-vis absorbance at 479.5 nm of feed DOX and unloaded DOX after conjugation to PSeH microgels.

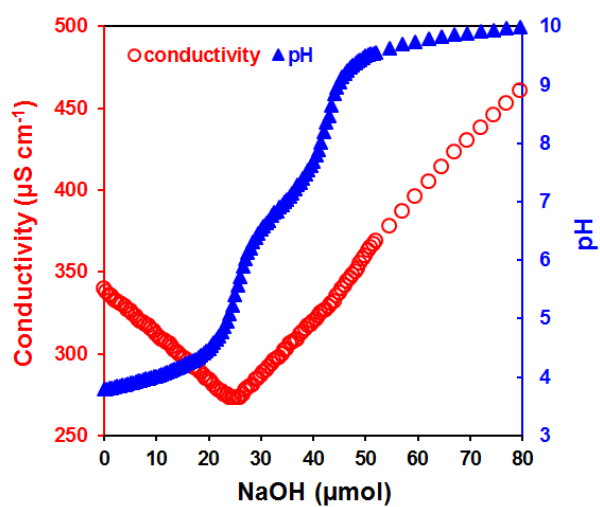


Figure 3.S7 Conductivity and pH titration of PSeHD microgels (1.4 mg) at room temperature.

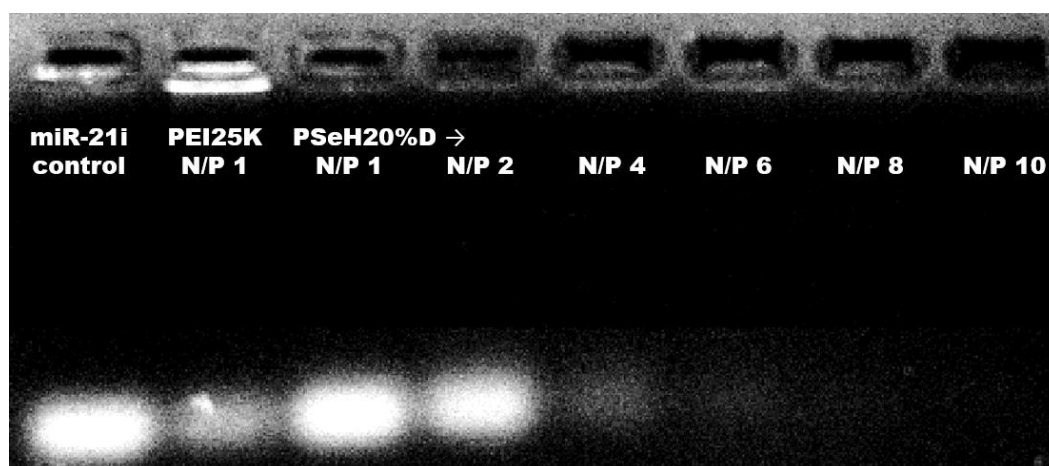


Figure 3.S8 Loading assays of miR-21i to PSeH20%D at different N/P ratios from 1 to 10, PEI25K at the N/P of 1 as the reference, images from agarose gel electrophoresis.

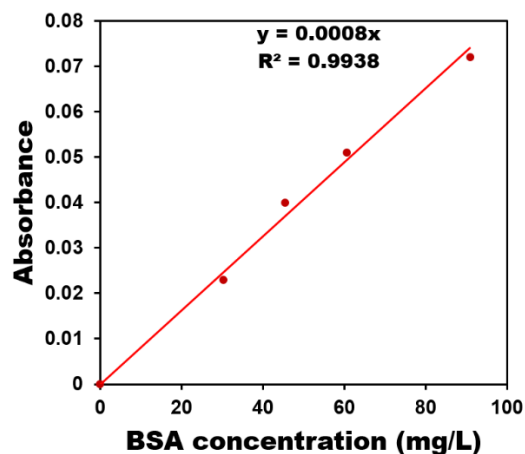


Figure 3.S9 UV-vis calibration curve for bovine serum albumin (BSA) absorbance at 280 nm and room temperature.

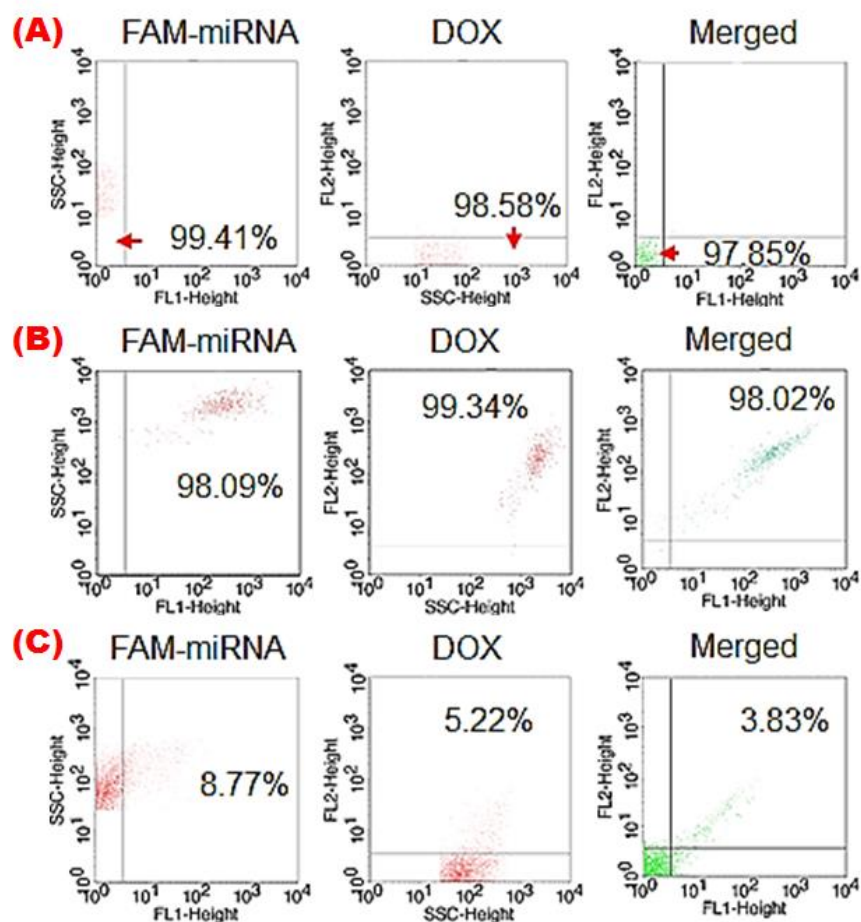


Figure 3.S10 Flow cytometry for quantitative cellular uptake of PSeHD/FAM-miR/HA, (A) MDA-MB-231 cells without PSeHD/FAM-miR/HA as a control, (B) MDA-MB-231 cells with PSeHD/FAM-miR/HA, and (C) HA pre-treated MDA-MB-231 cells with PSeHD/FAM-miR/HA, FL1 and FL2 indicate FAM and DOX respectively.

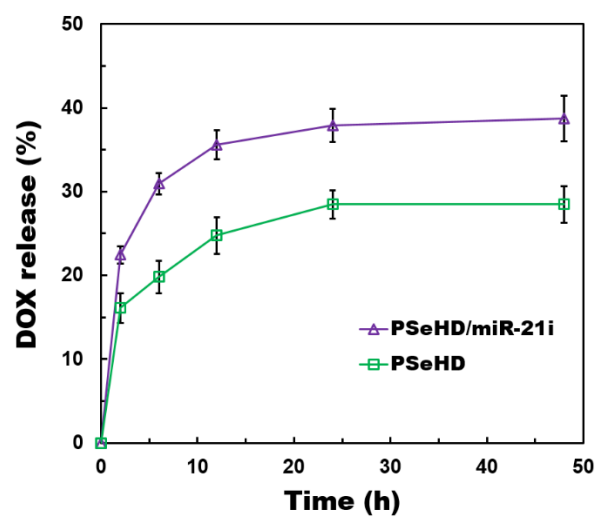


Figure 3.S11 *Ex vivo* DOX release in pH 7.4 PBS from PSeHD and PSeHD/miR-21i. (n = 3)

References

- [1] E. Markovsky, H. Baabur-Cohen, R. Satchi-Fainaro, Anticancer polymeric nanomedicine bearing synergistic drug combination is superior to a mixture of individually-conjugated drugs, *J. Control. Release*, 187 (2014) 145-157.
- [2] J.D. Wallat, J.K. Harrison, J.K. Pokorski, pH Responsive Doxorubicin Delivery by Fluorous Polymers for Cancer Treatment, *Mol. Pharm.*, 15 (2018) 2954-2962.
- [3] C. Yang, S.Q. Liu, S. Venkataraman, S.J. Gao, X. Ke, X.T. Chia, J.L. Hedrick, Y.Y. Yang, Structure-directing star-shaped block copolymers: Supramolecular vesicles for the delivery of anticancer drugs, *J. Control. Release*, 208 (2015) 93-105.
- [4] R. Mo, T. Jiang, R. DiSanto, W. Tai, Z. Gu, ATP-triggered anticancer drug delivery, *Nat Commun*, 5 (2014).
- [5] X. Zhou, L. Chen, W. Nie, W. Wang, M. Qin, X. Mo, H. Wang, C. He, Dual-Responsive Mesoporous Silica Nanoparticles Mediated Codelivery of Doxorubicin and Bcl-2 siRNA for Targeted Treatment of Breast Cancer, *J. Phys. Chem. C*, 120 (2016) 22375-22387.

Chapter 4 Design of dual-locked smart microgels for effective co-delivery of DOX and miRNA-21 inhibitor to multidrug resistant cancer cells

*Seonho Yun, Jiabin Zhang, Hesamoddin Rabiee, Hu Zhang, Jingxiu Bi, Sheng Dai**

S. Yun, J. Zhang, H. Rabiee, Prof. H. Zhang, Prof. J. Bi, Prof. S. Dai

School of Chemical Engineering, the University of Adelaide, Adelaide, SA 5005, Australia

Prof. H. Zhang

Amgen Bioprocessing Centre, Keck Graduate Institute, 535 Watson Drive, Claremont, CA
91711

Prof. S. Dai

Department of Chemical Engineering, Brunel University London, Uxbridge, UB8 3PH, United
Kingdom

sheng.dai@brunel.ac.uk

Statement of Authorship

Title of Paper	Design of dual-locked smart microgels for effective co-delivery of DOX and miRNA-21 inhibitor to multidrug resistant cancer cells
Publication Status	<input type="checkbox"/> Published <input type="checkbox"/> Accepted for Publication <input type="checkbox"/> Submitted for Publication <input checked="" type="checkbox"/> Unpublished and Unsubmitted work written in manuscript style
Publication Details	In preparation for submission

Principal Author

Name of Principal Author (Candidate)	Seonho Yun		
Contribution to the Paper	Mainly designed the experiment, material synthesis, evaluation, and manuscript writing		
Overall percentage (%)	80 %		
Certification:	This paper reports on the original research I conducted during the period of my Higher Degree by Research candidature and is not subject to any obligations or contractual agreements with a third party that would constrain its inclusion in this thesis. I am the primary author of this paper.		
Signature		Date	20/05/2019

Co-Author Contributions

By signing the Statement of Authorship, each author certifies that:

- i. the candidate's stated contribution to the publication is accurate (as detailed above);
- ii. permission is granted for the candidate to include the publication in the thesis; and
- iii. the sum of all co-author contributions is equal to 100% less the candidate's stated contribution.

Name of Co-Author	Jiabin Zhang		
Contribution to the Paper	Helped to operate evaluation part of the experiment		
Signature		Date	21/02/2019

Name of Co-Author	Hesamoddin Rabiee		
Contribution to the Paper	Helped to operate material synthesis of the experiment		
Signature		Date	21 Feb. 2019

Name of Co-Author	Hu Zhang		
Contribution to the Paper	Supervised the experiment design, data interpretation, manuscript correction		
Signature		Date	24/02/2019

Name of Co-Author	Jingxiu Bi		
Contribution to the Paper	Proof read the manuscript and evaluation		
Signature		Date	25/02/2019

Name of Co-Author	Sheng Dai		
Contribution to the Paper	Supervised the experiment design, data interpretation, manuscript correction, and corresponding author		
Signature		Date	20/05/2019

Abstract

Multidrug resistance (MDR) of cancers with chronic administration of chemotherapy increases dosage and side effects. In this study, we develop novel functional microgels to deliver doxorubicin (DOX) and miRNA-21 inhibitor (miR-21i) to MDR cancer cells aiming of synergistic anticancer treatment and minimal side effects. To achieve this, our fully biodegradable microgels are prepared via crosslinking biocompatible low molecular weight of PEI800 with a redox-cleavable diselenide crosslinker. Double-locks of hydrazone and diselenide bonds are used for DOX conjugation, and cationic amines of PEI800 for loading miR-21i through electrostatic interaction. After drug and microRNA inhibitor loading, the complexes are coated by hyaluronic acid (HA) for charge convert and cancer cell targeting via HA receptor-mediated endocytosis. Stable systemic circulation of the designed co-delivery systems at physiological condition is evident associated with the structural advantages of anionic surface charges and dual-lock design to eliminate protein adsorption and drug premature leakage. On the other hand, selective cancer targeting of the system is strongly supported via cellular uptake assays owing to HA mediated endocytosis. Moreover, minimal side effect is proved from HEK293T cell survival rate of 95.1 % at a DOX concentration of 2.5 $\mu\text{g mL}^{-1}$. In targeting cancer cells, cancer intracellular environment are able to cleave hydrazone and diselenide bond to release loaded DOX and miR-21i in cytosol. Consequently, 3.2 times higher anticancer effect than naked DOX on MDR cancer cell lines of MDA-MB-231-R12w can appeal a great potential for its further high-efficient therapeutic applications.

Keywords: multidrug resistance, hydrazone bond, diselenide bond, DOX, miR-21 inhibitor, dual conjugation, PEI800, biocompatible, biodegradable

4.1 Introduction

Doxorubicin (DOX) is considered to a representative anthracycline drug for broad ranges of cancers, including triple-negative breast cancers with ineffective endocrine therapy via hormone receptors [1, 2]. DOX can effectively damage DNA by inhibition of topoisomerase II α and support apoptosis activation by inhibition of B-cell lymphoma-2 protein [3, 4]. However, DOX also induces serious side effects to the organs of liver, spleen, lung, heart and kidney, caused by remarkable drug accumulation in organs during systemic administration [5-7]. With chronic administration of DOX, the anticancer efficiency drops down with emerging multidrug resistance (MDR), such as DOX efflux-pump of ATP-binding cassette (ABC) transporter with overexpressing P-glycoprotein and chemo-resistance by targeting phosphatase and tensin homolog (PTEN) and programmed cell death 4 (PDCD4) with overexpressing miRNA-21 [8, 9]. With the aid of miRNA-21 inhibitor (miR-21i) to block the miRNA-21 activity, DOX shows improving prognosis on cancer cells with MDR [10, 11]. For safe and systemic administration, co-delivery carriers of DOX and miR-21i should be developed to target MDR cancer cells and avoid side effects from off-target cells as well as eliminating drug pre-leakage.

Practically, various delivery systems have been developed to load DOX by physical interactions, such as solvent diffusion, physical encapsulation and electrostatic interaction, but always expressing unmanageable premature release of loaded DOX at mimicking physiological condition [12-14]. The other method of DOX loading is to conjugate drug to carriers via a cleavable linker, such as esters, amides, hydrazones, acetal-core crosslinkers or disulfides, to controllably release under a certain internal/external stimuli such as pH and/or redox. Although this method reduced premature release, their averaged anticancer efficiency was lower than that of free DOX [15-17].

For miR-21i delivery, cationic polymer-based non-viral vectors have been widely developed recently to electrostatically load anionic gene drugs, such as plasmid DNA, siRNA and miRNA, to facilitate their endosomal escape through the proton sponge effects [18-22]. However, high positive charge densities of polymer vectors of polyethyleneimine (PEI) with a molecular weight of 25 kDa (PEI25k) or poly(L-lysine) (PLL) always induce cell membrane damage via the hydrolysis of lipid phosphoester bonds [23]. From our recent studies, high cytotoxicity of these polycations could be avoided by the introduction of biodegradable microgels via crosslinking biocompatible and weak-charged polymers using various cleavable crosslinkers to achieve effective gene loading but minimal cell toxicity [24, 25].

On the other hand, stable systemic circulation is another essential factor in co-delivery system design. Although carriers with their sizes less than 10 nm or over 200 nm can be cleared by renal or reticuloendothelial system (RES), cationic carriers interact with anionic serum in blood circulation to increase size and easier clearance [26, 27]. Surface protection with polyethylene glycol (PEG) has been an option to avoid drug-protein adsorption/interaction, but block endocytosis by steric hindrance from long chains of PEG [28]. However, carrier surface with hyaluronic acid (HA), as an anionic polysaccharide of extracellular component, can overcome PEG dilemma with surface charge convert and HA receptor mediated endocytosis via cluster of differentiation 44 (CD44) or receptor for hyaluronan-mediated motility (RHAMM), which are overexpressed on the surface of metastatic cancer cells [29].

We here present an advanced design for the co-delivery of DOX and miR-21i to achieve outstanding anti-MDR cancer performance but minimal side effects. In detail, biodegradable cationic microgel carriers are synthesized by conjugating biocompatible PEI800 with diselenide crosslinkers for miR-21i loading. Besides, DOX are conjugated to the microgels via double-locks of pH sensitive hydrazone bonds and redox cleavable diselenide bonds to effectively suppress DOX premature leakage in systemic circulation. Finally, HA surface

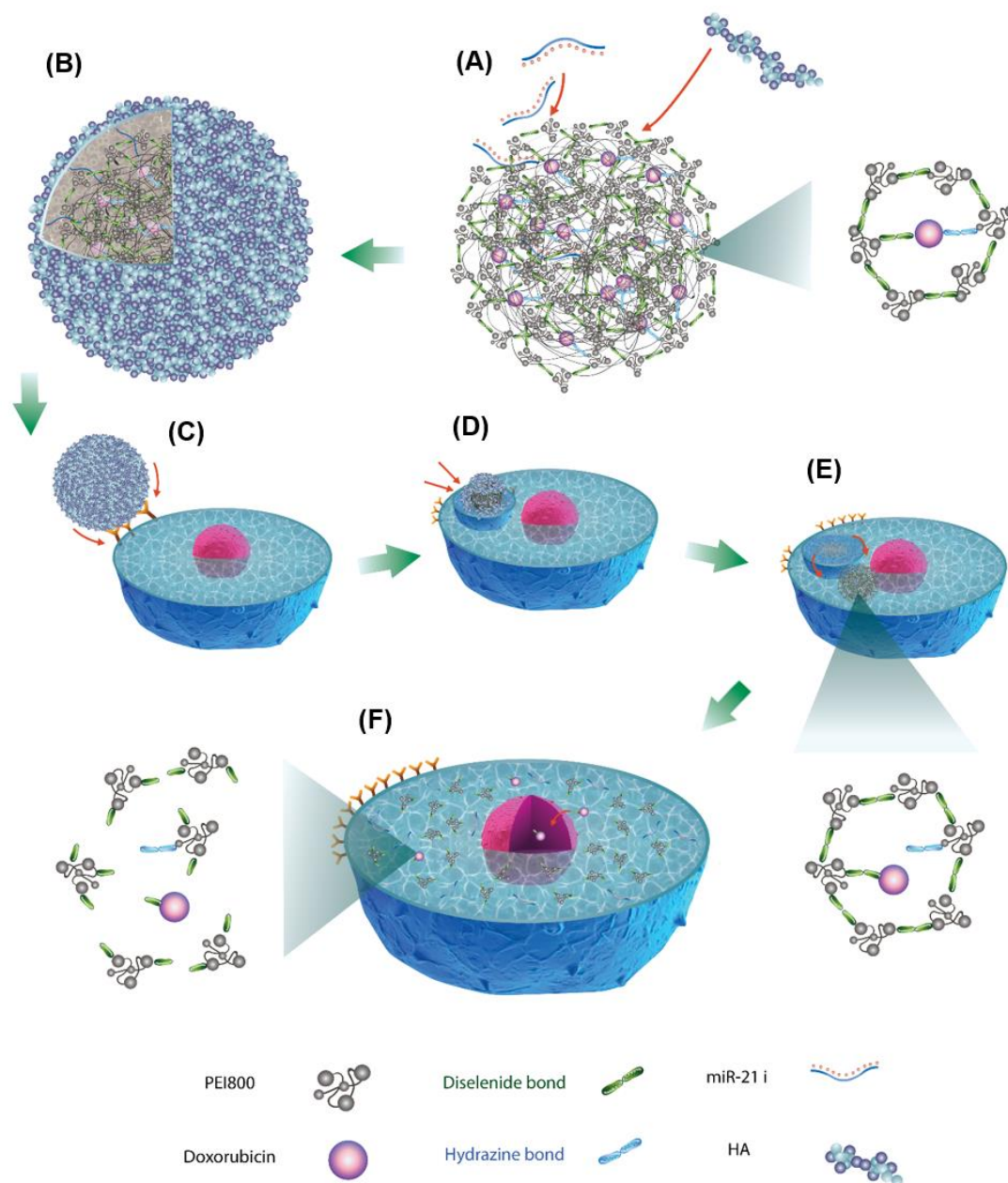
coating to the DOX and miR-21i co-loaded polyplexes allows charge convert and selective endocytosis to metastatic cancer via HA receptor mediation. The delivery system with a hydrodynamic size of 150 nm at physiological condition can be full degraded after exposing to intracellular microenvironment of MDR cancer cells, allowing release of DOX and miR-21i in cancer cytosol (Scheme 4.1) together with easier excretion of carrier fractures from patient body. Resultantly, the co-delivery system with remarkable anti-MDR cancer synergies and minimal side effects can contribute to further therapeutic applications and provide optimistic future to patients who are suffering from MDR cancers.

4.2 Material and methods

4.2.1 Materials

Selenium, 3-chloropropionic acid, sodium borohydride (NaBH₄), branched-polyethyleneimine MW. 800Da (PEI800), 1-ethyl-3-(3-dimethyl-laminopropyl) carbodiimide (EDC), N-hydroxysulfosuccinimide (NHS), succinic anhydride, tert-butyl carbazate, trifluoroacetic acid (TFA), and L-Glutathione reduced (GSH) were purchased from Sigma-Aldrich. Doxorubicin hydrochloride (DOX·HCl) was obtained from Wuhan Wang Lianshang Biotechnology Co., Ltd. FAM-labelled miRNA inhibitor single stranded negative control with a random sequence (sequence 5'-CAGUACUUUUGUGUAGUACAA) and miRNA-21 inhibitor (sequence 5'-GUCCACUCUUGUCCUCAUG-3') were manufactured by Shanghai GenePharma Co.,Ltd. Sodium Hyaluronate MW. 66kDa-99kDa (HA) was purchased from Lifecore Biomedical, LLC. Dulbecco Modified Eagle Medium (DMEM), fetal bovine serum (FBS), penicillin-streptomycin (PS), and phosphate buffered saline (PBS) from Life Technologies Australia Pty Ltd., and Leibovitz's Medium (L-15) and Cell Counting Kit-8 (CCK-8) from Sigma-Aldrich were utilized in in vitro evaluation. MDA-MB-231 and HEK293T cell lines were kindly gifted from Dr Qian Tang from School of Pharmacy at University of South Australia and Professor

Andrew Zannettino from South Australia Health and Medical Research Institute (SAHMRI), respectively. Deionised water was supplied from Milli-Q water purification system (Spectrum Laboratories, Inc.).



Scheme 4.1 Scheme description for the DOX and miR-21i co-loading and co-delivery to cancer cells: (A) DOX-conjugated PEI microgel via diselenide and hydrazone bonds (PSeHD-SeSeP) and miR-21i loading and HA surface coating to the PSeHD-SeSeP, (B) co-delivery system of PSeHD-SeSeP/miR-21i/HA, (C) HA receptor-mediated endocytosis, (D) PSeHD-SeSeP/miR-21i/HA in endosome/lysosome, (E) hydrazone bond cleaved in acidic lysosome and endosomal escape, and (F) diselenide bond cleaved in glutathione-concentrated cancer cytosol and release of DOX and miR-21i.

4.2.2 Synthesis of DOX loaded microgels (PSeHD-SeSeP)

4.2.2.1 Diselenide-bond crosslinker (-SeSe-)

Diselenide crosslinker (-SeSe-) of 3,3'-diselanediyldipropanoic acid was synthesized with a slightly modified method from previous study [30]. Selenium powder (1.18 g, 15 mmol) suspension in water (5 mL) in a flask under nitrogen protection was stirred with dropwise adding sodium borohydride (1.13 g, 30 mmol) aqueous solution (12.5 mL, 4 °C) in an ice bath for 10 min. The same amount of selenium powder (1.18 g, 15 mmol) was subsequently added into the colorless solution under N₂ protection. The mixed solution was heated and stirred at 105 °C for about 20 min to become reddish-brown color. 3-chloropropionic acid (3.26 g, 30 mmol) aqueous solution of 7.5 mL with pH adjusting to 8.0 by sodium carbonate was added to the reactor flask after cooling down to room temperature. The mixture was stirred under nitrogen protection for overnight and then open to atmosphere for another 12 h for unreacted selenium oxidization. The mixture pH after being filtered (0.45 µm syringe filter) was adjusted to 3.0 with 3 M HCl, and resultant coagulant was extracted with ethyl acetate. After water wash, magnesium sulphate dry and filtering, diselenide bond crosslinker (-SeSe-) was crystalized from ethyl acetate. To confirm successful synthesis of -SeSe-, Rama spectroscopy and Fourier-transform infrared spectroscopy (FTIR) were employed.

4.2.2.2 Diselenide bond crosslinked PEI800 microgels (PSeSe)

Diselenide bond crosslinked PEI800 microgels (PSeSe) were synthesized with same methods in our previous study (Chapter 3). Mixture of -SeSe- (304 mg, 1 mmol), EDC (1150.2 mg, 6 mmol), and NHS (460.4 mg, 4 mmol) in DMSO (2.1 mL) under nitrogen protection were magnetically stirred at room temperature for 45 min. Freeze-dried PEI800 (800 mg, 1 mmol, pH 7.4) after pH 7.4 adjustment with 3 M HCl, was dissolved in DMSO (1.6 mL) and added to the mixture for another 2 days stirring under N₂ protection. PSeSe was produced after dialysis against deionized water using a 3.5 kDa MWCO tube for 5 days with daily water

change and freeze-dry. PSeSe was characterized with FTIR, conductivity and pH titration (AQUA conductivity/pH), and the zeta potential of PSeSe was measured in phosphate buffered saline (PBS) at pH 7.4 and 25 °C (Malvern zetasizer ZEN3600).

Redox cleavable PSeSe was tested to confirm the successful microgel synthesis with measuring the size decreasing patterns through dynamic light scattering (DLS) using a zetasizer. Hydrodynamic sizes of PSeSe microgels at pH 7.4 of PBS with 20 mM of glutathione (GSH), 10 μ M GSH, and without GSH were measured at predetermined time.

4.2.2.3 Hydrazine bond introduction to PSeSe microgels (PSeH)

PSeH microgels were synthesized with slight modification of feed hydrazine mole ratio to amine in PSeSe microgels from our previous study. PSeSe (500 mg, 2.48 mmol of amine group, [Figure 4.S4A](#)) was re-suspended in DMSO (40 mL) in a flask under nitrogen environment. After injection of succinic anhydride (120 mg, 1.2 mmol) dissolved in DMSO (5 mL) to the flask, the mixture was stirred at room temperature for overnight, and the transparent grey color mixture was dialyzed with a MWCO 3.5 kDa tube. After freeze-dry of the mixture, carboxylic group conjugated PEI microgel (PSeCOOH) was obtained.

PSeCOOH (337.5 mg, 0.65 mmol of carboxylic group) in DMSO (20 mL) was mixed with EDC (751.54 mg, 3.92 mmol) and NHS (300.8 mg, 2.61 mmol) in DMSO (10 mL) under N₂ protection, and stirred at room temperature for 45 min. Tert-butyl carbazate (129.53 mg, 0.98 mmol) in DMSO (2 mL) was added to the mixture with further 16 h stirring. After dialysis and freeze-dry of mixture, microgels with BOC protected hydrazine group (PSeBOC) was synthesized.

PSeBOC (304 mg, 0.482 mmol of BOC group) in DMSO (30 mL) was mixed with TFA (10 ml, 130 mmol) under nitrogen circumstance, and stirred at room temperature for 24 h. PEI

microgels with hydrazine bond conjugation (PSeH) were produced after dialysis and lyophilization.

4.2.2.4 DOX conjugation to PSeH microgels via hydrazone bond (PSeHD)

PSeH (30.4 mg, 0.056 mmol of hydrazine group) was dissolved in PBS buffer solution (10 mL) of increased pH to 8.5 with 1 M NaOH. DOX·HCl (32.5 mg, 0.056 mmol) was suspended in the mixture of PBS (7 mL, pH 7.4) and acetic acid (5 μ L). PSeH and DOX·HCl solutions were mixed and stirred under dark and nitrogen protection at room temperature for overnight. The mixture was dialyzed against deionized water in the cold room at 4 °C and light protection for 24 h with frequent water change. After lyophilization, DOX conjugated microgels via hydrazone bond (PSeHD) were obtained, and the hydrodynamic size of PSeHD was measured with DLS from a zetasizer. DOX loading (wt. %) to PSeHD complexes were calculated using following Equation:

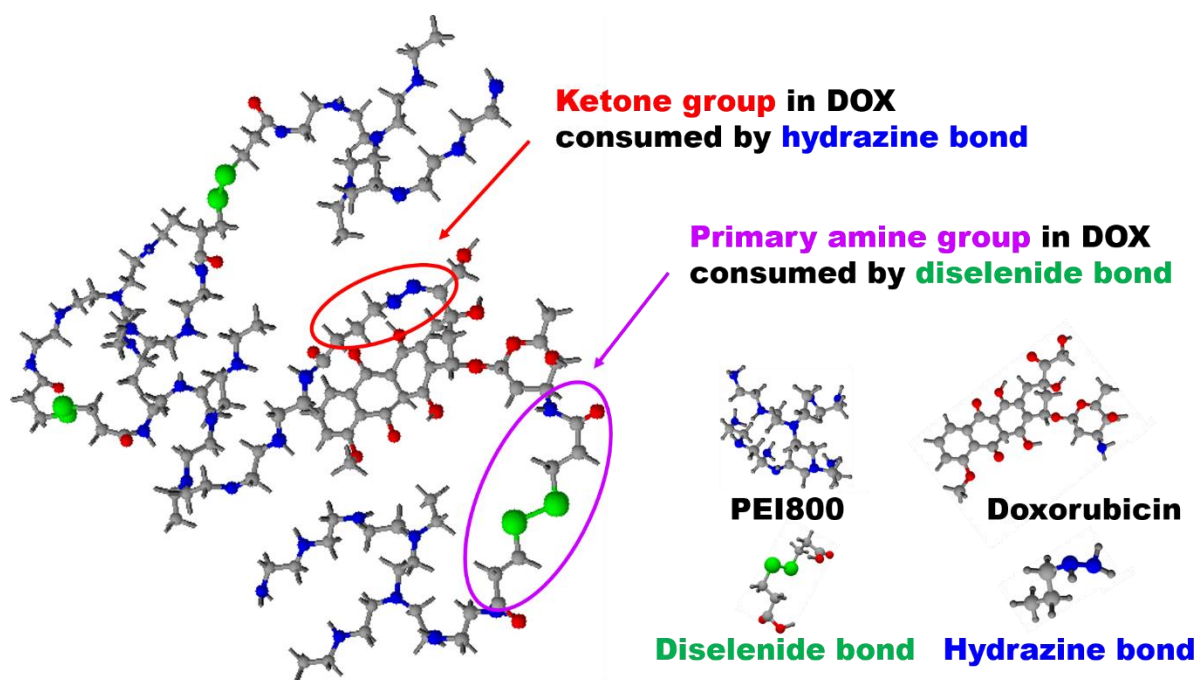
$$DOX \text{ loading } (\%) = \frac{(total \ DOX - unloaded \ DOX)}{DOX \ loaded \ microgels} \times 100 \quad (1)$$

Quantification of unloaded DOX was obtained from the absorbance measurement of free DOX residual at 479.5 nm using a UV-vis spectrophotometer through a pre-established DOX calibration curve (Figure 4.S5).

4.2.2.5 Diselenide crosslinking loaded DOX and PEI800 (PSeHD-SeSeP)

-SeSe- (15.21 mg, 0.05 mmol), EDC (57.5 mg, 0.3 mmol) and NHS (23 mg, 0.2 mmol) were dissolved in DMSO (2 mL), and magnetically stirred at ambient temperature for 45 min under nitrogen protection. PSeHD (40mg, 0.021 mmol of amine group in DOX) in DMSO (5 mL) was injected into the mixture, followed by another 45 min stirring under light protection. After injecting PEI800 (40 mg, 0.05 mmol) in DMSO (1 mL) into the mixture, magnetic stirring was continued for further 2 days. Dialysis against deionized water was carried out using dialysis tube (MWCO 7 kDa) at 4 °C for 7 days with daily water change. After lyophilization, PEI

microgels with dual-locker conjugated DOX (PSeHD-SeSeP) was produced (Scheme 4.2). Zeta potential and hydrodynamic size of PSeHD-SeSeP were measured with zetasizer (ZEN 3600), and the amine content in PSeHD-SeSeP was obtained from conductivity and pH titration. DOX loading (wt. %) to PSeHD-SeSeP was determined from same methods as PSeHD.



Scheme 4.2 Scheme of diselenide crosslinked PEI800 microgels with DOX loading via dual-locks of hydrazone and diselenide bonds.

4.2.3 *Ex vivo* DOX releasing assays

PSeHD-SeSeP complexes dissolved in deionized water (5 mL, 1 mg mL⁻¹) were transferred to a dialysis tube (MWCO 3.5kDa) for dialysis against various conditions of buffer solutions (95 mL) in a horizontal shaker at 37 °C with 100 rpm for 48 h. The various conditions of buffer solutions are: 0 M GSH at pH 7.4; 10 μM GSH at pH 7.4; 20 mM GSH at pH 7.4; 0 M GSH at pH 6.5; 0 M GSH at pH 5.0; and 0 M GSH at pH 5.0 for the first 6 h and 20 mM GSH at pH 7.4 for further 42 h. Phosphate buffered saline (PBS) was used for pH 7.4 and pH 6.5 and acetate buffered saline (ABS, 0.2 M) was prepared for pH 5.0. The absorbance of an aliquot

from the buffer solution was measured at the wavelength of 479.5 nm by UV-Vis spectrophotometer at pre-determined time intervals. The amount of DOX released was determined according to the DOX calibration curve (Figure 4.S5). For comparison, the quantity of *ex vivo* DOX releasing from PSeHD was evaluated with the buffer conditions of 0 M GSH at pH 7.4, pH 6.5, and pH 5.0.

4.2.4 miR-21i loading and *ex vivo* releasing assay

miR-21i in DEPC water (1 μL , 0.42 nmol μL^{-1}) was incubated with the PSeHD-SeSeP complexes at predetermined mole ratios of nitrogen (N) in the microgels (Figure 4.S4B) to phosphate (P) in miR21i (N/P ratio) from 1.0 to 6.0 at ambient temperature for 20 min. 1 N/P ratio complex of PEI25k and miR-21i and naked miR-21i were used as positive control and negative control separately. Agarose gel (0.8%) electrophoresis was executed at 100 volts for 60 min. The miR-21i migration patterns in the gel were fluorescently imaged under UV irradiation and captured by a G-BOX (SYNGENE).

Ex vivo releasing assay of loaded miR-21i from PSeHD-SeSeP (10 N/P ratio) was evaluated with agarose gel electrophoresis after incubation in 20 mM GSH at 37 °C for 48 h and 72 h. Agarose gel electrophoresis was run at 100 volts for 60 min, and the miR-21i migration images were photographed with a G-BOX.

4.2.5 Characterization of PSeHD-SeSeP/miR-21i/HA delivery systems

4.2.5.1 HA surface coating (PSeHD-SeSeP/miR-21i/HA)

PSeHD-SeSeP after miR-21i (20 μL , 0.42 nmol μL^{-1}) loading at a 10 N/P ratio in DEPC water was mixed with 5-folds weight of hyaluronic acid (HA) to miR-21i. The mixture was incubated at ambient temperature for 20 min, and the PSeHD-SeSeP/miR-21i/HA delivery systems were produced.

4.2.5.2 Surface charge measurements

Zeta potential of PSeHD-SeSeP/miR-21i/HA in pH 7.4 PBS buffer was detected at 25 °C from a Malvern Zetasizer (ZEN 3600), and compared with that of PSeHD-SeSeP and PSeHD-SeSeP/miR-21i.

4.2.5.3 *Ex vivo* stability and degradability of co-delivery systems

PSeHD-SeSeP/miR-21i/HA delivery systems were suspended in buffered solutions with four-different conditions, 0 M of GSH at pH 7.4, 10 μ M of GSH at pH 7.4, 20 mM of GSH at pH 7.4, and 0 M of GSH at pH 5.0 for initial 4 h and subsequent 20 mM of GSH at pH 7.4 (PBS for pH 7.4 and ABS for pH 5.0). The solutions were continuously shaken at 37 °C with 100 rpm. Hydrodynamic sizes of PSeHD-SeSeP/miR-21i/HA in various buffered salines were detected at 37 °C via DLS measurements at pre-determined time over 7 days.

4.2.6 Culture of cell lines (HEK293T, MDA-MB-231-S, MDA-MB-231-R)

Cell lines of human embryonic kidney cell line (HEK293T), DOX sensitive breast cancer cell lines (MDA-MB-231-S), and DOX resistant breast cancer cell lines (MDA-MB-231-R) were cultured in a humidified incubator (Contherm Scientific Limited) with 5 % CO₂ at 37 °C. Culture medium for HEK293T was prepared with mixture of Dulbecco Modified Eagle Medium (DMEM), fetal bovine serum (FBS) (10 % (vol.)), and penicillin-streptomycin 10,000 U/mL (PS) (1% (vol.)) Breast cancer cell lines with DOX sensitivity (MDA-MB-231-S) were cultured with the mixture of Leibovitz's Medium (L-15), FBS (10 %), and PS (1 %). DOX resistant breast cancer cell lines (MDA-MB-231-R) were incubated with L-15, FBS (10 %), PS (1%) and DOX incorporation of 0.01 μ g mL⁻¹ until 8th weeks and then 0.02 μ g mL⁻¹ from 9th to 12th weeks. Culture mediums were refreshed every 48 h and Trypsin-EDTA (0.25%) was used to recover all three types of cells.

Resistance of MDA-MB-231-R to DOX was determined with cell viability assay at pre-determined time of cell culturing period with DOX, such as 0th, 4th, 8th and 12th week, indicating to MDA-MB-231-S, -R4w, -R8w, and -R12w. MDA-MB-231-R cells were incubated in a 96-well plate for 24 h, and were further incubated with various DOX concentrations in fresh medium, 0.1, 0.5, 1, and 2.5 $\mu\text{g mL}^{-1}$ for 48 h. After changing medium to DMEM based medium and Cell Counting Kit-8 (CCK-8) treatment for 4 h, absorbance of surviving cell is measured by wavelength 450 nm in a microplate reader (ELx808 BioTek) to determine the MDA-MB-231-R cell survival rates using following Equation:

$$\text{Cell survival rate (\%)} = \frac{(S-B)}{(C-B)} \times 100 \quad (2)$$

where S is the absorbance of DOX samples, B is that of blank without cells, and C is that of control with only cells but not DOX.

4.2.7 Cellular uptake assays

Cellular uptake of PSeHD-SeSeP/miR-21i/HA delivery systems was qualitatively assayed with a confocal laser scanning microscope (CLSM) (Olympus FV3000). Breast cancer cells (MDA-MB-231-S) (0.1×10^6 cells per well) were seeded onto a glass cover slip in a 12-well plate, and cultured with L-15 based mixture medium for 24 h. PSeHD-SeSeP/FAM-miR/HA, insisting of PSeHD-SeSeP complexes (12.5 μg with 8.2 wt % of loaded DOX), FAM-labeled miRNA negative control with a random sequence (FAM-miR) at 10 N/P, and 5-folds HA to FAM-miR of weight ratio, were prepared for CLSM imaging analysis. PSeHD-SeSeP/FAM-miR/HA (50 μL) were applied on the cells with fresh medium (950 μL), and incubated for further 4 h. After staining cell membrane with CellMaskTM Deep Red Plasma membrane Stain and fixing with formaldehyde (4%), fluorescent images from DOX, FAM-miR, and cells were monitored by CLSM, giving the color of blue, green and red. To block HA receptors on the surface of cells, MDA-MB-231-S cells were incubated with HA (10 mg mL^{-1}) in the medium for 24 h,

producing the HA pretreated cells. For comparison, the fluorescent images of control cells without PSeHD-SeSeP/FAM-miR/HA and HA-pretreated cells with PSeHD-SeSeP/FAM-miR/HA were obtained via CLSM.

Cellular uptake of the delivery carriers was quantified with flow cytometer (BD FACSCalibur™). MDA-MB-231-S cells (0.05×10^6 cells per well) were seeded in a 24-well plate and cultured by the same method for the CLSM. PSeHD-SeSeP/FAM-miR/HA delivery carriers (5 μg , at 10.0 N/P, 5-folds HA to FAM-miR, 50 μL per well) were added to the cells with fresh culture medium (450 μL per well). After incubation for 4 h, cells were washed 3 times with PBS and collected with trypsin-EDTA to measure the intensities of fluorescence from DOX and FAM-miR, displaying as FL-2 (585 nm) and FL-1 (530 nm) with excitation at 488 nm wavelength. Control cells without PSeHD-SeSeP/FAM-miR/HA and HA-pretreated cells with PSeHD-SeSeP/FAM-miR/HA were also prepared to compare the quantity of cellular uptake of PSeHD-SeSeP/FAM-miR/HA.

4.2.8 Biocompatibility evaluation

In vitro viability assays of human embryonic kidney cells (HEK293T) against PSeSe, PSeH microgels and the biodegraded PSeHat 20 mM GSH for 48 h were evaluated to confirm biocompatibility of synthesized microgels. HEK293T cells (10,000 cells per well) were seeded in a 96-well plate, and incubated with DMEM based culture medium (100 μL per well) in a moisturized incubator at 37 °C and 5 % CO_2 for 24 h. The microgels (10 μL , 50 $\mu\text{g mL}^{-1}$) were inoculated to the cells with a fresh medium for further 48 h. After 4 h CCK-8 treatment, absorbance of surviving cells was measured, and cell survival rate (%) was calculated with Equation (2). For comparison purpose, PEI800 and Lipofectamine2000 as positive controls and PEI25k as a negative control were assayed with identical methods.

In vitro viability of the HEK293T cells against the co-delivery systems with DOX and miR-21i, PSeHD-SeSeP/miR-21i/HA, was evaluated to check the side-effect of the co-drug delivery system. HEK293T cells (10,000 cells per well) were incubated in a 96-well plate with DMEM medium for 24 h. The delivery systems (10 μ L) at increasing DOX loaded concentrations, 0.1, 0.25, 0.5, 1, and 2.5 (μ g mL⁻¹), and 10 N/P miR-21i with 5-folds HA (wt/wt), were applied to the cells with fresh medium for another 48 h incubation. With CCK-8 treatment for further 4 h, cell survival rates were determined. The cell viability assays against PSeHD-SeSeP, PSeHD-SeSeP/miR-21i and free DOX were executed for comparison.

4.2.9 Viability assays on DOX sensitive or resistant cancer cells

Therapeutic efficacy of combined DOX and miR-21i delivery system, PSeHD-SeSeP/miR-21i/HA, was evaluated through the cell viability assays to one DOX-sensitive breast cancer cell line of MDA-MB-231-S and two DOX-resistant breast cancer cell lines of MDA-MB-231-R4w and MDA-MB-231-R12w. Each cancer cell line (10,000 per well) was seeded into every single 96-well plate with their culture media, and incubated for 24 h. PSeHD-SeSeP/miR-21i/HA of 10 μ L per well, consisting of various DOX loaded concentrations, 0.1, 0.5, 1, and 2.5 (μ g mL⁻¹), and 10 N/P ratio of miR-21i and 5-fold weight ratio of HA to miR-21i, was added to the top of fresh L-15 based medium (100 μ L per well), and was incubated for 48 h. After changing L-15 based medium to DMEM based medium and CCK-8 treatment for further 4 h, the survival rate (%) of each type of cells against the co-drug delivery systems was obtained. *In vitro* cell viability assays against PSeHD-SeSeP/HA and free DOX were also evaluated to these three types of cells as comparison of therapeutic efficacy.

4.3 Results and Discussion

4.3.1 Synthesis of DOX loaded microgels (PSeHD-SeSeP)

4.3.1.1 Synthesis of biodegradable microgels (PSeSe)

Polymer based vectors for advanced gene-delivery have contradictory conditions, i.e., effective anionic gene loading from strong positive charged (e.g., PEI25k) polymers and minor cytotoxicity from weak positive charged (e.g., PEI800) polymers. In this study, biodegradable microgels are synthesized to achieve both high charge density and outstanding biocompatibility by crosslinking low molecular weight PEI800 using a redox-sensitive diselenide crosslinker (-SeSe-).

3,3'-diselanyldipropionic acid of diselenide crosslinker -SeSe- was produced with a yield of 56.5 %. Raman shifts at 291 and 517 cm^{-1} (Figure 4.S1) confirm the successful synthesis of -SeSe-, indicating selenium-selenium and selenium-carbon bonds, [31, 32]. PSeSe microgels were prepared by crosslinking PEI800 via the -SeSe- with a yield of 72.4 %. FTIR spectra are evident for successful microgel synthesis (Figure 4.S2). Peaks for primary amine N-H stretching, N-H bending, and C-N stretching of PEI800 are observed at 3351, 3273, 1547, and 1070 cm^{-1} from PSeSe, as well as Se-C stretching of -SeSe- at 520 cm^{-1} . In microgel spectrum, the formation of amide bond between PEI800 and -SeSe- are observed at 1630 cm^{-1} as amide C=O stretching, which is shifted from ketone C=O stretching of -SeSe- at 1690 cm^{-1} . The molar amount of amine in 1 mg of PSeSe microgels was measured with conductivity and pH titration (Figure 4.S4A), displaying 4.96 $\mu\text{mol mg}^{-1}$.

To satisfy high gene loading capacity and biocompatibility, PSeSe microgels should be highly positive on surface and be biodegradable into small fractures after entering cells to avoid cytotoxicity coming from high charge density and their accumulation in patient body. For the surface charge density, zeta potential of the PSeSe microgels (38.1 ± 2.1 mV) was measured,

and compared with that of PEI25k (38.7 ± 2.9 mV) and PEI800 (8.2 ± 3.7 mV) as a positive and a negative control (Figure 4.S3A). Zeta-potential of the PSeSe microgels is similar to that of PEI25k for promising gene loading. To confirm biodegradability, hydrodynamic sizes of PSeSe were monitored over 72 h with DLS measurement at pH 7.4 of PBS buffer at various conditions, 0 M, 10 μ M, and 20 mM of reductive enzyme glutathione (GSH) (Figure 4.S3B). Initial hydrodynamic size of PSeSe is 228.0 ± 9.3 nm, which slightly decreases to 186.2 ± 6.0 nm at 4 h and maintains until 72 h in the condition of 0 M GSH. The slight size decrease for the first 4 h might be attributed to nucleophilic attack on diselenide bonds in the PBS buffer with full of phosphate ions [33]. In 10 μ M GSH, a moderate size decreasing pattern is observed with 176.4 ± 2.1 nm at 4 h and 163.1 ± 10.8 nm at 72 h. Opposed to stable microgels in 0 or 10 μ M GSH, PSeSe in 20 mM GSH shows steep size-drop to 11.1 ± 9.7 nm at 48 h and further decrease to 3.7 ± 1.9 nm at 72 h. These confirm the bio-degradation of the microgels via cleavage of diselenide crosslinker is highly dependent on the concentration of GSH. Yue et al. support two distinct cleavage patterns of the diselenide bonds at gradient GSH levels as an evidence of the controlled biodegradation [25].

4.3.1.2 DOX loading to microgels with hydrazone and diselenide bonds (PSeHD-SeSeP)

Doxorubicin possesses outstanding anticancer efficiency and also severe side effects induced by its cytotoxicity, which promotes us to develop delivery systems with highly controlled releasing function to eliminate premature leakage before reaching target cancer cells. In this study, two intracellular stimuli-cleavable linkers of hydrazone and diselenide bonds are utilized in DOX conjugation to the PSeSe microgels.

For DOX loading, hydrazine bond was first conjugated to PSeSe to consume 48.4% (mol) of amine in PSeSe, producing PSeH microgels with a yield of 45.5%. Subsequently, DOX was conjugated to PSeSe through Schiff base formation between ketone group in DOX and primary

amine in PSeSe, achieving PSeHD complexes with DOX loading via a pH sensitive hydrazone bond. To prevent hydrazone bond cleavage during its formation process, PBS buffer at pH 8.5 was used to dissolve PSeH before mixing with acidic mixture of DOX·HCl and acetic acid. DOX loading in PSeHD can be calculated using Equation (1), where the amount of unloaded DOX can be obtained from its absorbance at 479.5 nm from UV-vis spectroscopic measurement with DOX calibration curve of light absorbance to DOX concentration (Figure 4.S5), resulting in 29 wt. % of DOX loading.

Another PEI800 was supplemented to further conjugate the loaded DOX to PSeHD complexes via diselenide crosslinkers. Activated carboxylic groups in both side of -SeSe- are covalently bonded to primary amine groups in DOX and PEI800 (Scheme 4.2). In addition to the crosslinking between DOX and PEI800, the added PEI800 can be crosslinked to amine groups in the surface of the complexes by -SeSe-, which produces PSeHD-SeSeP complexes (Scheme 4.1A).

With successful addition of PEI800 to PSeHD, some properties of PSeHD-SeSeP are shifted from PSeHD. First, hydrodynamic size increases from PSeHD of 176.5 ± 26.5 nm to PSeHD-SeSeP of 213.1 ± 45.8 nm. Moreover, the added weight of PEI800 to PSeHD decreases DOX loading ratio from PSeHD of 29 wt. % to PSeHD-SeSeP of 8.2 wt. %. Furthermore, the sacrificed amine groups in PSeHD for the hydrazine introduction to PSeSe is found to be supplemented in PSeHD-SeSeP. The recovery of amine groups results in the amine content ratio of 4 μ mol in 1 mg of PSeHD-SeSeP (Figure 4.S4B) and the increase of zeta potential from PSeHD of 7.7 ± 3.1 mV to PSeHD-SeSeP of 37.2 ± 1.5 mV.

4.3.2 Exceptional control of DOX release

Advanced suppression of side effects and high therapeutic efficiency require an exceptionally controlled DOX release from delivery carriers to suppress pre-mature release in systemic

circulation and accelerate target release in cancer cells. PSeHD-SeSeP with dual linkers for DOX conjugation is designed for the purpose of the exceptional control of DOX release. DOX release from PSeHD-SeSeP by dual-linker was compared with that from PSeHD by single-linker via *ex vivo* releasing assays. In [Figure 4.1A](#), DOX being released from the PSeHD are $93.5 \pm 4.8 \%$ and $53.1 \pm 4.8 \%$ at pH 5.0 and 6.5 over 48 h due to the rapid cleavage of pH sensitive hydrazone bond. However, $29.0 \pm 2.6 \%$ of DOX release is observed at pH 7.4 over the same time intervals. Although hydrolysis of hydrazone is rapid at acidic pH, the hydrazone bearing two electron-withdrawing groups is also found being labile even at neutral pH and undergoes hydrolysis [34]. This supports the hydrazone bond for only conjugation route of DOX in PSeHD is not enough to suppress DOX pre-leakage at neutral pH during systemic circulation.

Comparing to the single-linker, PSeHD-SeSeP with dual-linker for DOX conjugation via pH responsive hydrazone and redox sensitive diselenide bond displays outstanding controllability of DOX releasing. PSeHD-SeSeP can effectively control the premature leakage of DOX in the mimicking physiological condition of 0 M GSH at pH 7.4. DOX releasing from PSeHD-SeSeP is $5.8 \pm 1.6 \%$, which is far low to that from PSeHD over 48 h. Although the pH value of buffer is decreased to 6.5 and 5.0 to cleave the hydrazone bond, the dual-DOX conjugation system releases 8.1 ± 1.4 and $8.7 \pm 1.6 \%$ over 48 h ([Figure 4.1B](#)), indicating DOX is still conjugated to the carriers by diselenide bond. In addition, the increasing concentration of GSH from 10 μ M to 20 mM at pH 7.4 to reduce the diselenide bond limitedly affects DOX releasing from 8.7 ± 1.7 to $19.0 \pm 2.8 \%$ over 48 h ([Figure 4.1C](#)), which approves hydrazone bond in the systems is still conjugated with DOX. On the other hand, PSeHD-SeSeP can release DOX with $90.8 \pm 3.7 \%$ over 48 h in the sequential condition of buffer, pH 5.0 in the first 6 h and then 20 mM GSH at pH 7.4 for further 42 h ([Figure 4.1D](#)). These indicate the delivery system can release DOX due to two different linkers, hydrazone and diselenide bonds, are cleaved after

passing through mimicking acidic endo/lysosome and then reaching to the mimicking target cellular cytosol with 20 mM of reductive GSH. Therefore, with this dual-Dox conjugation system, PSeHD-SeSeP is likely to selectively release cytotoxic drugs in cancer cytosol, but not in systemic circulation.

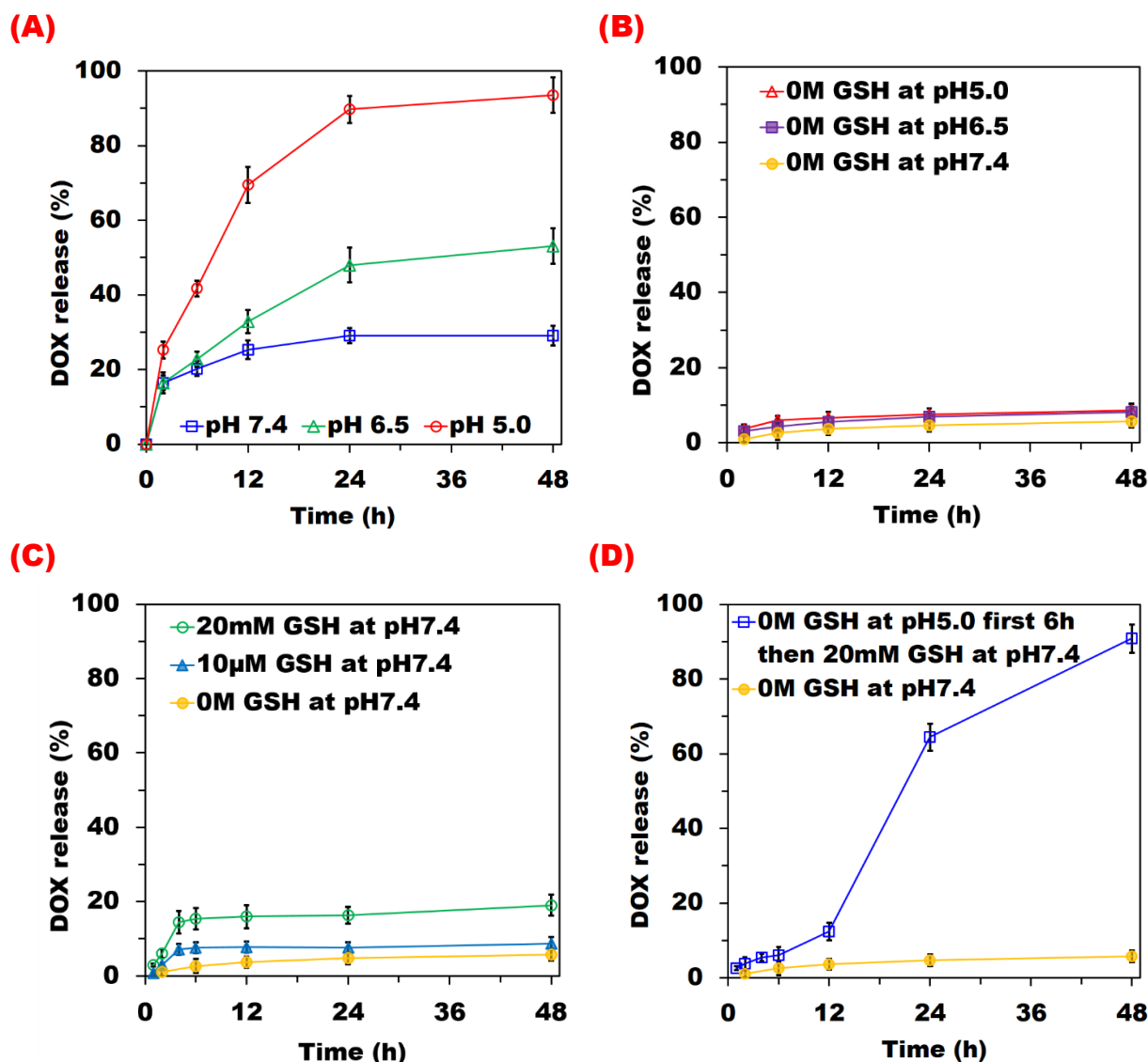


Figure 4.1 *ex vivo* DOX releasing assays, DOX releasing from (A) PSeHD at pH 7.4, 6.5, and 5.0 with 0 M GSH over 48 h, (B) PSeHD-SeSeP at pH 7.4, 6.5, and 5.0 with 0 M GSH, (C) PSeHD-SeSeP at pH 7.4 with 0 M GSH, 10 μ M GSH, and 20 mM GSH over 48 h, and (D) PSeHD-SeSeP at pH 7.4 with 0 M GSH and at sequential condition of 0 M GSH at pH 5.0 for 6 h then 20 mM GSH at pH 7.4, ($P < 0.05$, $n = 3$).

4.3.3 miR-21i loading and *ex vivo* releasing assay

Presence of miRNA-21 reduces the anticancer efficacy of DOX in metastatic cancer cells, and increases expression of miR-21 in DOX-resistant cancer cells, thus inhibiting the overall therapeutic effect [9, 11]. In this study, miRNA-21 inhibitor (miR-21i) is delivered to metastatic cancer cells and drug resistant metastatic cancer cells via the co-delivery system of PSeHD-SeSeP/miR-21i polyplexes. miR-21i loading capacity to the PSeHD-SeSeP was evaluated using 0.8 % agarose gel electrophoresis at various N/P (PSeHD-SeSeP to miR-21i) molar ratios of 1, 2, 4, 5, and 6. Full retardation of miR-21i from PSeHD-SeSeP is observed at the N/P of 5 (Figure 4.2A). Compared with PSeHD, it is obvious that the surface amines promote miR-21i loading because PSeHD cannot fully load miR-21i at an N/P ratio of 30 (Figure 4.S6).

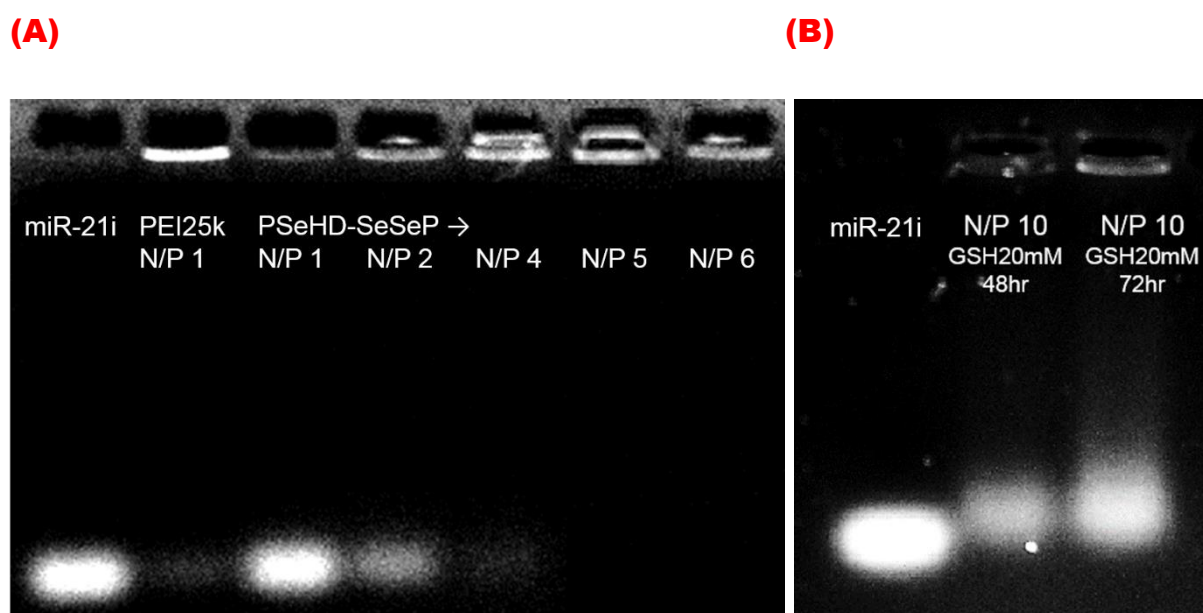


Figure 4.2 Agarose gel retardation assays for (A) miR-21i loading to PSeHD-SeSeP at N/P ratios from 1 to 6, where naked miR-21i and its polyplexes with PEI25k at the N/P ratio 1 are used as negative control and positive control. (B) miR-21i releasing profiles from the PSeHD-SeSeP/miR-21i at a N/P ratio 10 after incubation with 20 mM GSH for 48 h and 72 h.

The *ex vivo* miR-21i releasing was evaluated by agarose gel retardation assay after incubating PSeHD-SeSeP/miR-21i at a N/P ratio of 10 with mimicking cytosol of presence 20 mM GSH

at 37 °C for 48 h and 72 h. miR-21i migrations from the polyplexes in the presence of reductive enzyme GSH are enhanced with increasing incubation time from 48 to 72 h (Figure 4.2B). The diselenide crosslinker in PSeHD-SeSeP can be cleaved by GSH, and the PSeHD-SeSeP can be degraded to small fractures (Figure 4.S3B). Similar as PEI800, these low molecular PEI fractures will lose interaction with miR-21i (Figure 4.S3A) and resultantly release the loaded miR-21i. *Ex vivo* evaluation supports the PSeHD-SeSeP can release miR-21i to the cytosol of target cells by response of reducing enzyme.

4.3.4 Characterization of PSeHD-SeSeP/miR-21i/HA delivery system

Positive charges of synthesized microgel carriers promote miR-21i loading, but become obstacles during the delivery course due to possible serum protein adsorption and off-target endocytosis via electrostatic interaction, resulting in reticuloendothelial system (RES) clearance and cytotoxic to normal cells [26]. Here, PSeHD-SeSeP/miR-21i polyplexes are subject to further surface coating with hyaluronic acid (HA) to convert positive to negative surfaces in order eliminate serum adsorption and facilitate cancer cell uptake through HA receptor mediated endocytosis for selective delivery. HA was electrostatically coated to PSeHD-SeSeP/miR-21i (at a 10 N/P) with 5-fold weight ratio to miR-21i, producing the PSeHD-SeSeP/miR-21i/HA complex. Successful HA coating was confirmed from zeta potential measurements, where zeta potentials are 37.2 ± 1.5 , 28.7 ± 1.5 and -33.2 ± 1.8 mV for PSeHD-SeSeP, PSeHD-SeSeP/miR-21i and PSeHD-SeSeP/miR-21i/HA (Figure 4.3A). Our previous study shows HA coated polyplexes rarely adsorb bovine serum albumin, 0.15 % feed compared with 25.2% for PEI800 and 51.2 % for Lipofectamine2000 (Chapter 3). Therefore, the PSeHD-SeSeP/miR-21i/HA system can be stable during systemic circulation by avoiding RES clearance. To confirm the stability in circulation, hydrodynamic sizes of PSeHD-SeSeP/miR-21i/HA in mimicking physiological environment (pH 7.4; GSH 0 M) and extracellular microenvironment (pH 7.4; GSH 10 μ M) were *ex vivo* evaluated over 1 week

(Figure 4.3B). Initial size of PSeHD-SeSeP/miR-21i/HA at 192.2 ± 24.6 nm, is well maintained and reaches to 173.7 ± 4.9 nm over 7 days in mimicking physiological environment. On the other hand, in the mimicker extracellular environment, the size of PSeHD-SeSeP/miR-21i/HA decreases to 162.4 ± 11.9 nm after 48 h and to 158.7 ± 20.1 nm over 1 week. This means diselenide bonds in PSeHD-SeSeP are inefficiently cleaved in the low concentration of GSH. As polarizability volume of selenium (3.8 \AA) is larger than that of sulfur (2.9 \AA), a rate constant for nucleophilic attack of thiol from GSH can be lower than that for stability of diselenide bond [33]. Those results support the stable circulation of PSeHD-SeSeP/miR-21i/HA in delivery course.

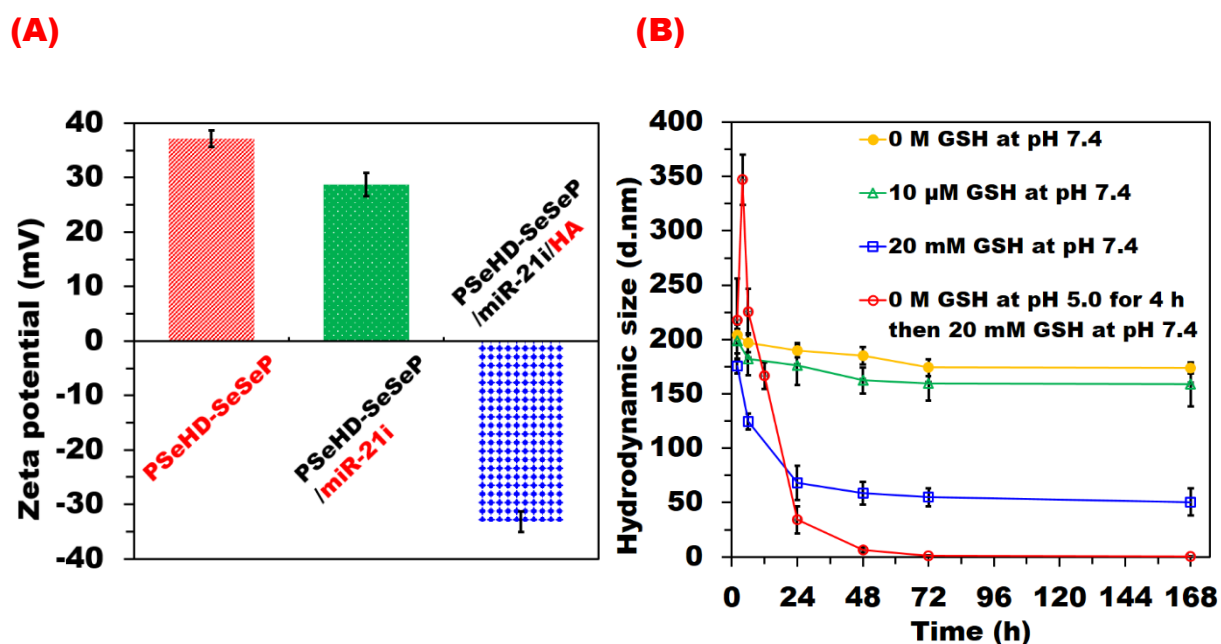


Figure 4.3 (A) Comparison on the zeta potentials of PSeHD-SeSeP, PSeHD-SeSeP/miR-21i and PSeHD-SeSeP/miR-21i/HA, (n=4), (B) Hydrodynamic sizes of PSeHD-SeSeP/miR-21i/HA at pH 7.4 with different GSH concentrations of 0, 10, and 20 mM, and the sequential condition of pH 5.0 and 0 M GSH for 4 h then pH 7.4, 20 mM GSH, (n=4).

Biodegradability of PSeHD-SeSeP/miR-21i/HA is crucial for releasing loaded DOX and miR-21i to target cancer cells by cleavage of hydrazone bonds and diselenide bonds. Hydrodynamic

sizes of PSeHD-SeSeP/miR-21i/HA were *ex vivo* evaluated in mimicking intracellular cytosol (20 mM GSH in pH 7.4 PBS buffer) and sequential intracellular delivery course from endo/lysosome to cytosol (0 M GSH in pH 5.0 ABS buffer for first 4 h then 20 mM GSH in pH 7.4 PBS buffer) over 7 days (Figure 4.3B). In the medium of 20 mM of GSH and pH 7.4, particle size drops to 68.2 ± 15.8 nm over 1 day and then maintains at 50.5 ± 12.3 nm for 1 week. Such results are opposed to the full degradation of PSeSe in 20 mM of GSH over 3 days (Figure 4.S3B). These indicate diselenide bonds in PSeHD-SeSeP/miR-21i/HA are reduced by the high concentration of reductive enzyme of GSH, but hydrazone bonds are still stable at pH 7.4. On the other hand, in the mimicking delivery course from endo/lysosome to cytosol, initial size of the PSeHD-SeSeP/miR-21i/HA increases to 347.1 ± 23.2 nm at pH 5.0 over 4 h due to microgel electro-repulsive stretching after hydrazone bond cleavage. However, after subsequently exposing to 20 mM GSH in pH 7.4 PBS, particle size significantly drops to 34.0 ± 12.4 nm over 24 h and further decreases to 1-2 nm over 7 days. Under this mimicking condition, both hydrazone and diselenide bonds of PSeHD-SeSeP/miR-21i/HA can be sequentially destroyed by acidic pH and GSH and release loaded drugs to target cell cytosol. In addition, debris of the microgel carriers can be easily excreted from patient body as degraded fractures is smaller than 10 nm [35].

4.3.5 DOX resistance of MDA-MB-231-R

To evaluate *in vitro* anticancer synergistic effect of DOX and miR-21i to DOX resistant metastatic breast cancer cells, MDA-MB-231-R, were cultured in L-15 based culture medium with replenishing DOX for 12 weeks. At every 4 weeks after culturing the cells, the resistance of MDA-MB-231-R to DOX was evaluated by monitoring cell viabilities under DOX concentrations from 0.1 to $2.5 \mu\text{g mL}^{-1}$. Cell survival rate (%) against DOX shows increasing patterns as prolonging culture period with DOX over all DOX concentration ranges (Figure 4.S7). In detail, cell survival rate with $2.5 \mu\text{g mL}^{-1}$ DOX in 0 week is 50.4 ± 3.8 % and becomes

58.4 ± 8.9 %, 66.4 ± 5.1 % and 70.7 ± 7.9 % for 4 weeks, 8 weeks and 12 weeks, clearly indicating the DOX resistance of the MDA-MB-231-R cells.

4.3.6 Cellular uptake assays

Surface HA coating is able to enhance selective endocytosis through HA receptors of CD44 and/or RHAMM on the surface of metastatic cancer cells MDA-MB-231 [29]. To confirm the HA receptor mediated endocytosis of the PSeHD-SeSeP/miR-21i/HA delivery system, FAM labelled miRNA with a random sequence (FAM-miR) was loaded to the co-delivery system with DOX instead of miR-21i with their emission at 530 and 580 nm under the excitation at 488 nm from CLSM. MDA-MB-231 cell membrane was also stained by CellMask™ Deep Red to emit 666 nm under excitation at 640 nm. CLSM images those emission to evaluate cellular uptake of PSeHD-SeSeP/FAM-miR/HA. As a control, [Figure 4.4A](#) shows red colors for the cell membranes without other colors for load. In [Figure 4.4B and 4.4C](#), the green from FAM-miR and the blue from DOX overlap with the red from the stained cells to give off purple color, indicating cell intake of PSeHD-SeSeP/FAM-miR/HA. To confirm ineffective endocytosis of the HA coated delivery systems to cells without HA receptors, HA pre-treated cells were prepared to block HA receptors. [Figure 4.4D](#) indicates that the PSeHD-SeSeP/FAM-miR/HA systems are difficultly endocytosed in lieu of HA-receptor mediations as evident from few green and blue colors being observed on the red color for HA pre-treated cells. The qualitative results from the CLSM prove PSeHD-SeSeP/FAM-miR/HA HA can selectively enter metastatic cancer cells with HA receptors rather than cells without the receptors.

The receptor-mediated endocytosis of PSeHD-SeSeP/FAM-miR/HA delivery systems was further quantitatively examined by flow cytometry. More than 97 % of control cells without the PSeHD-SeSeP/FAM-miR/HA are located on the down-left section of [Figure 4.S8A](#). For the cells after administration of PSeHD-SeSeP/FAM-miR/HA, 92.7 % FAM and DOX fluorescent signals are located on the upper-right section of [Figure 4.S8B](#), indicating highly

efficient cellular uptake of the delivery systems. However, after blocking HA receptors on cell surface, only 3.8 % FAM and DOX signals are positioned on the upper-right section of [Figure 4.S8C](#). The quantitative results from flow cytometric analysis also support HA receptor-mediated endocytosis of PSeHD-SeSeP/FAM-miR/HA to MDA-MB-231.

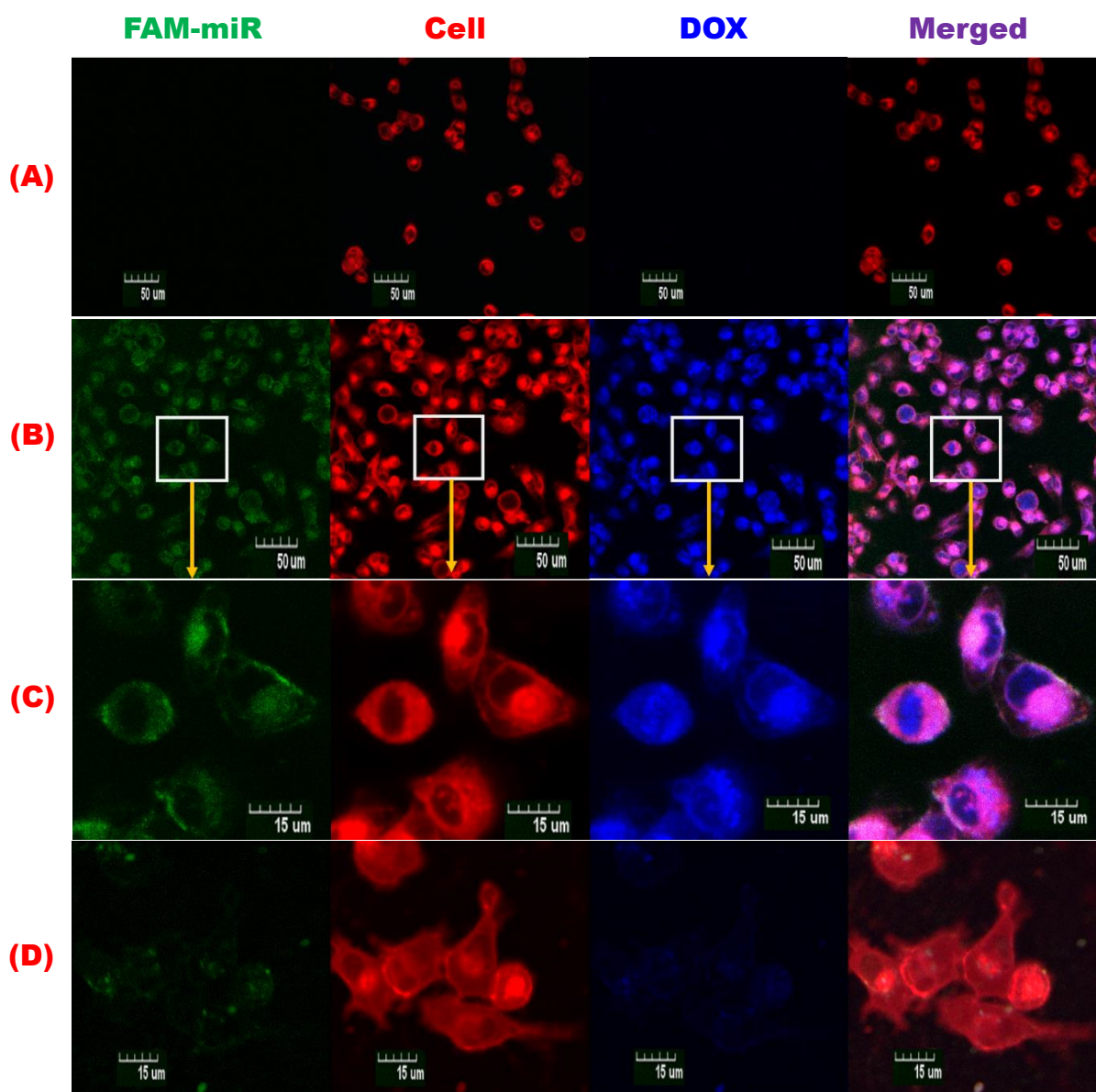


Figure 4.4 MDA-MB-231 cellular uptake assays of PSeHD-SeSeP/FAM-miR/HA system by confocal laser scanning microscopy (CLSM), (A) Cells only without the PSeHD-SeSeP/FAM-miR/HA, (B) Cells with PSeHD-SeSeP/FAM-miR/HA system in low magnification and (C) in high magnification, and (D) HA pre-treated cells with the PSeHD-SeSeP/FAM-miR/HA.

Besides, HA receptors are not widely spread on the surface of healthy cells [29]. As HA receptors on the surface of HA pre-treated cells are blocked, HA pre-treated cells behave as healthy cells in the course of cell uptake. Therefore, it may conclude that PSeHD-SeSeP/miR-21i/HA can be selectively endocytosed to metastatic cancer cells but not to healthy cells via HA receptor mediation.

4.3.7 Evaluation on side effect of co-delivery system

One of the targets of designing current delivery system is to minimize the side effects of anticancer chemotherapy. Biocompatibility of delivery carriers without DOX loading and with DOX loading was evaluated against human embryonic kidney cell line (HEK293T). For the delivery carriers without DOX loading, cell survival rates of 50 $\mu\text{g mL}^{-1}$ PSeH, PSeSe, and microgel debris being treated by 20 mM of GSH for 48 h are 85.0 ± 2.4 , 95.0 ± 1.4 and 97.2 ± 0.92 % respectively (Figure 4.5A). These survival rates are similar to that of PEI800 (86.4 ± 1.7) and Lipofectamine2000 (82.0 ± 1.3 %), and far higher than the 49.1 ± 1.4 % for PEI25k as a negative control. The high biocompatibility of the microgel carriers is introduced by the application of biocompatible PEI800 and consumption of primary amine groups during crosslinking. As the primary amine content of the microgels decreases, the decomposed fragments of the microgels are more biocompatible than PEI800 and provide the possibility of safe excretion.

To further confirm minimal side-effect of our delivery system after loading DOX and miR-21i, HEK 293T cell survival rates against PSeHD-SeSeP/miR-21i/HA (10 N/P and 5-folds wt. of HA to miR-21i) with loaded DOX concentrations from 0.1 to 2.5 $\mu\text{g mL}^{-1}$, were evaluated and compared with free DOX, PSeHD-SeSeP, and PSeHD-SeSeP/miR-21i at same concentrations after 48 h incubation (Figure 4.5B). The survival rate (%) of free DOX is 45.9 ± 10.7 at a concentration of 0.5 $\mu\text{g mL}^{-1}$ and further drops to 35.5 ± 4.7 . After DOX being loaded to PSeH microgel by hydrazone and diselenide bonds, PSeHD-SeSeP displays outstanding high cell

survival rate (%) of 94.0 ± 0.64 at the highest DOX concentration of $2.5 \mu\text{g mL}^{-1}$. This remarkable biocompatibility of PSeHD-SeSeP is due to the dual-linkers for DOX conjugation. In Chapter 3, a delivery system with DOX loading through a single-linker of hydrazone bond (PSeHD) shows HEK293T survival rate of 75 % at a DOX concentration of $2.5 \mu\text{g mL}^{-1}$. The addition of the diselenide bond for DOX conjugation can suppress the release of DOX to HEK293T. Suppression of DOX release from PSeHD-SeSeP can be observed in either hydrazone or diselenide bond being conjugating DOX, as seen in Figure 4.1. First, the physiological pH of 7.4 in the extracellular environment of normal cells and the rapid endosomal escape by proton sponge effect of less than 10 min may in part cleave the hydrazone bond [22]. In addition, the 2.8 fold lower level of GSH in normal cells than in cancer cells may partially cleave GSH concentration-dependent diselenide bond [36]. Partial cleavage of hydrazone and diselenide bonds can maintain DOX load and inhibit DOX release to HEK293T cells.

Although miR-21i loaded PSeHD-SeSeP shows slightly lower survive rate of 81.1 ± 2.3 % at the DOX concentration of $2.5 \mu\text{g mL}^{-1}$, HA coated system of PSeHD-SeSeP/miR-21i/HA exhibits outstanding HEK293T survival rate of 95.1 ± 1.3 %. After miR-21i loading, inhibition of a few of miR-21 in HEK293T cells by miR-21i may upregulate programmed cell death 4 (PDCD4), and activate apoptosis [37]. However, surface HA coating makes PSeHD-SeSeP/miR-21i/HA difficult to enter HEK293T cells via HA receptor mediation due to the lack of HA receptors on the surface of normal cells [29]. The high HEK293T cell viability of PSeHD-SeSeP/miR-21i/HA caused by dual-linker DOX binding and surface HA coating minimizes side-effects on normal cells associated with cancer therapeutic delivery.

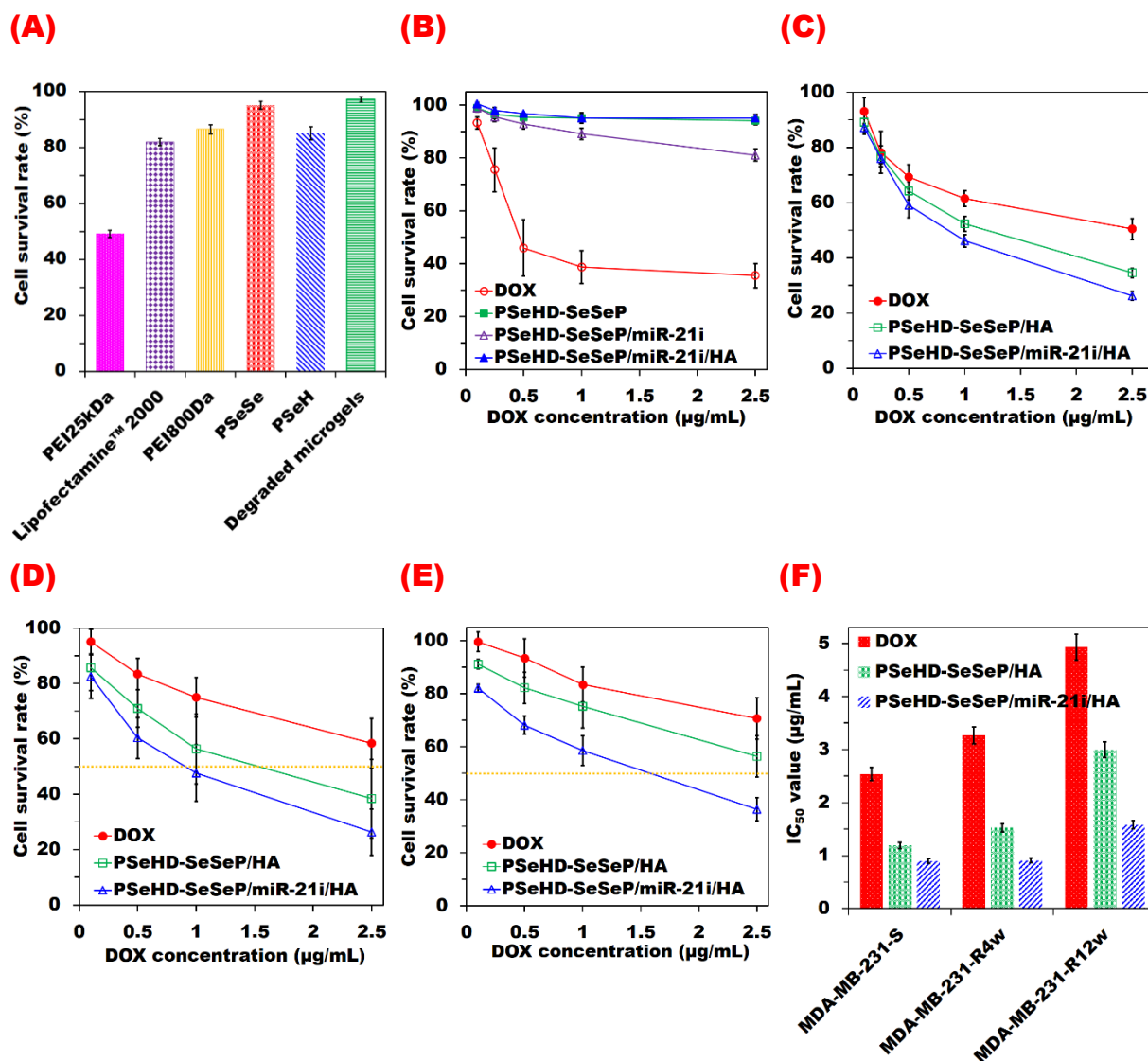


Figure 4.5 Cell viability, (A) HEK293T survival rate against microgel carriers without loading DOX (PSeSe, PSeH and degraded microgel fracture products), PEI25k as a negative control and Lipofectamine2000/PEI800 as positive controls, (n = 4), (B) HEK293T survival rate against delivery carriers with DOX loading (PSeHD-SeSeP, PSeHD-SeSeP/miR-21i and PSeHD-SeSeP/miR-21i/HA) and free DOX as a negative control, (n = 12), (C) MDA-MB-231-S survival rate against free DOX, PSeHD-SeSeP/HA and PSeHD-SeSeP/miR-21i/HA, (n = 12), (D) MDA-MB-231-R4w survival rate against free DOX, PSeHD-SeSeP/HA and PSeHD-SeSeP/miR-21i/HA, (n = 4), (E) MDA-MB-231-R12w survival rate against free DOX, PSeHD-SeSeP/HA and PSeHD-SeSeP/miR-21i/HA, (n = 8), and (F) IC₅₀ value, DOX concentration for half cell death, of free DOX, PSeHD-SeSeP/HA and PSeHD-SeSeP/miR-21i/HA against MDA-MB-231-S, MDA-MB-231-R4w, and MDA-MB-231-R12w cells, (n = 4).

4.3.8 Comparison on viability of PSeHD-SeSeP/miR-21i/HA on DOX sensitive and resistant cancer cells

Anticancer therapeutic synergy effects of DOX and miR-21i using the PSeHD-SeSeP/miR-21i/HA on DOX sensitive and resistant metastatic breast cancer cells were examined in this study. The survival rates of DOX sensitive metastatic breast cancer cells (MDA-MB-231-S) and the cells with ascending level of DOX resistance (MDA-MB-231-R4w and MDA-MB-231-R12w) were assayed after 48h incubation with free DOX, PSeHD-SeSeP/HA, and PSeHD-SeSeP/miR-21i/HA over a range of DOX concentrations from 0.1 to 2.5 $\mu\text{g mL}^{-1}$. Two distinct patterns are observed in the analysis. First, the survival rate of all cells decreases with increasing DOX concentrations. Secondly, the anticancer effect of free DOX is enhanced using the delivery system of PSeHD-SeSeP/HA, and integrates with the miR-21i of PSeHD-SeSeP/miR-21i/HA to create a more synergistic effect.

In [Figure 4.5C](#), DOX sensitive MDA-MB-231-S cell survival rate for DOX is $50.5 \pm 3.8 \%$ at a DOX concentration of 2.5 $\mu\text{g mL}^{-1}$. The MDA-MB-231-S survival rate falls to $34.5 \pm 2.5 \%$ for PSeHD-SeSeP/HA and to $26.1 \pm 1.6 \%$ for PSeHD-SeSeP/miR-21i/HA at the same concentration of DOX. The pattern of decreasing MDA-MB-231-S cell survival rate after using delivery system and delivering miR-21i is the same for DOX-resistant MDA-MB-231-R4w and MDA-MB-231-R12w. In [Figure 4.5D](#), the survival rate (%) of MDA-MB-231-R4w cells against free DOX, PSeHD-SeSeP/HA and PSeHD-SeSeP/miR-21i/HA is 58.4 ± 8.9 , 38.4 ± 14.2 and 26.3 ± 8.4 at a DOX concentration of 2.5 $\mu\text{g mL}^{-1}$. Although there is more DOX resistance to MDA-MB-231-R4w, MDA-MB-231-R12w in [Figure 4.5E](#) shows the identical pattern of cell survival rate against free DOX ($70.7 \pm 7.9 \%$), PSeHD-SeSeP/HA ($56.3 \pm 7.9 \%$) and PSeHD-SeSeP/miR-21i/HA ($36.3 \pm 4.4 \%$) at a DOX concentration of 2.5 $\mu\text{g mL}^{-1}$.

The higher anticancer performance of PSeHD-SeSeP/HA than free DOX can be due to its higher cellular uptake than DOX. Although PSeHD-SeSeP/HA enters the metastatic cancer

cells through HA receptor-mediated endocytosis, free DOX (amine pKa of 7.55) penetrates across hydrophobic core of phospholipid cell membrane after being protonated at a weak acid (pH 6.5) of cancer extracellular environment [38-40]. As the binding of positively charged DOX to the hydrophobic membrane are unworkable, the permeation of the DOX to the cells can be limited. Unlike the HEK293T viability assay (Figure 4.5B), the high anticancer efficacy of PSeHD-SeSeP compared to free DOX is due to the complete cleavage of dual-linkers, hydrazone and diselenide bonds, for DOX conjugation. Hydrazone bonds can be completely hydrolyzed in the delivery course from weak acids in the cancer extracellular environment to strong acids in endosome/lysosome. In the following delivery course to cytosol, it is possible to reduce the diselenide bonds at the cancer cytosol levels of GSH to intensively release DOX and make the difference in survival rate between normal and cancer cells for PSeHD-SeSeP.

Meanwhile, delivering miR-21i with DOX using PSeHD-SeSeP/miR-21i/HA produces a good anticancer synergy effect. Strengthening DOX resistance increases the cancer cell survival rate for free DOX and PSeHD-SeSeP/HA, but that for PSeHD-SeSeP/miR-21i/HA remains the lowest, and expands the difference between whether the presence of miR-21i. The involvement of miR-21i inhibit activity of miR-21 to upregulate PTEN and PDCD4, thereby restoring DOX sensitivity to multidrug resistant cancer cells and activating apoptosis [9, 11, 41].

DOX concentration for 50 % of cell death, as referred to IC₅₀, were calculated and shown in Figure 4.5F. The IC₅₀ values for free DOX are 2.54, 3.27, and 4.93 $\mu\text{g mL}^{-1}$ for MDA-MB-231-S, MDA-MB-231-R4w and MDA-MB-231-R12w cells. The anticancer therapy of PSeHD-SeSeP/HA shows 2-folds higher effective than that of DOX, presenting IC₅₀ values of 1.19, 1.53, and 2.99 $\mu\text{g mL}^{-1}$ on MDA-MB-231-S, MDA-MB-231-R4w, and MDA-MB-231-R12w cells. The increasing dosage requirement for free DOX and PSeHD-SeSeP/HA on MDA-MB-231-R4w and MDA-MB-231-R12w cells could be explained by the overexpression of ATP binding cassette (ABC) transporters to expel the intracellular localized DOX to

extracellular environment, reducing anticancer effects [42]. However, PSeHD-SeSeP/miR-21i/HA systems prove anticancer synergy effects with a fixed IC_{50} value of 0.9 for MDA-MB-231-S and MDA-MB-231-R4w cells. In addition, the IC_{50} value of PSeHD-SeSeP/miR-21i/HA for MDA-MD-231-R12w is 3.2 times lower than that of free DOX, indicating 3.2 times more effective for cancer.

The synergistic anticancer effects on the above cell lines suggest that PSeHD-SeSeP/miR-21i/HA can deliver DOX and miR-21i selectively and effectively to metastatic cancer cells and their multidrug resistant cells but not to normal cells. The proposed dual-lock co-delivery system of PSeHD-SeSeP/miR-21i/HA has the potential to overcome multidrug resistance in cancer treatment.

4.4 Conclusion

HA coated cationic microgels with a double-lock for anticancer drugs are synthesized for selective co-delivery of DOX and miR-21i to multidrug resistant cancer cells with exceptional anticancer synergetic effects and minimal side effects. The delivery systems of PSeHD-SeSeP/miR-21i/HA are designed on the basis of diselenide crosslinked PEI800 for miR-21i loading and double-lock linkers of hydrazone and diselenide bonds for DOX conjugation, and finally HA surface coating for charge convert and cancer cell targeting. The microgel system is well maintained in structure and size without DOX leakage, allowing stable circulation during the delivery process. HA allows the system to selectively enter cancer cells through HA receptor mediation. Only under the situation of sequentially passing through the cancer extracellular environment and endo/lysosome with acidic pH and the cytosol with reductase enzyme GSH, hydrazone and diselenide bonds can be cleaved to release loaded DOX and miR-21i. At the same time, microgel carriers are degraded into 1-2 nm fractures after releasing DOX

and miR-21i to target cells. 3.2 times higher therapeutic performance than free DOX on multidrug-resistant cells and minimal side effects on HEK293T cells prove this dual-lock cationic co-delivery system can contribute to future complex therapeutic applications.

Acknowledgement

We are grateful for the research grants of the Australian Research Council DP110102877 and DP140104062. SY would like to appreciate the APA scholarship provided by the University of Adelaide. We also thank Wookyeong Lee for assisting scheme design.

References

- [1] G. Minotti, P. Menna, E. Salvatorelli, G. Cairo, L. Gianni, Anthracyclines: Molecular Advances and Pharmacologic Developments in Antitumor Activity and Cardiotoxicity, *Pharmacol. Rev.*, 56 (2004) 185-229.
- [2] J. Greene, B. Hennessy, The role of anthracyclines in the treatment of early breast cancer, *J. Oncol. Pharm. Pract.*, 21 (2015) 201-212.
- [3] D. Carlisi, A. De Blasio, R. Drago-Ferrante, R. Di Fiore, G. Buttitta, M. Morreale, C. Scerri, R. Vento, G. Tesoriere, Parthenolide prevents resistance of MDA-MB231 cells to doxorubicin and mitoxantrone: the role of Nrf2, *Cell Death Discov.*, 3 (2017) 17078.
- [4] N. Pilco-Ferreto, G.M. Calaf, Influence of doxorubicin on apoptosis and oxidative stress in breast cancer cell lines, *Int. J. Oncol.*, 49 (2016) 753-762.
- [5] B.J. Cusack, S.P. Young, J. Driskell, R.D. Olson, Doxorubicin and doxorubicinol pharmacokinetics and tissue concentrations following bolus injection and continuous infusion of doxorubicin in the rabbit, *Cancer Chemother. Pharmacol.*, 32 (1993) 53-58.
- [6] N.M. Elsherbiny, M. El-Sherbiny, Thymoquinone attenuates Doxorubicin-induced nephrotoxicity in rats: Role of Nrf2 and NOX4, *Chem. Biol. Interact.*, 223 (2014) 102-108.
- [7] Z. Liu, A.C. Fan, K. Rakhra, S. Sherlock, A. Goodwin, X. Chen, Q. Yang, D.W. Felsher, H. Dai, Supramolecular Stacking of Doxorubicin on Carbon Nanotubes for In Vivo Cancer Therapy, *Angew. Chem. Int. Ed.*, 48 (2009) 7668-7672.
- [8] G. Kibria, H. Hatakeyama, K. Akiyama, K. Hida, H. Harashima, Comparative Study of the Sensitivities of Cancer Cells to Doxorubicin, and Relationships between the Effect of the Drug-Efflux Pump P-gp, *Biol. Pharm. Bull.*, 37 (2014) 1926-1935.
- [9] W. Hu, C. Tan, Y. He, G. Zhang, Y. Xu, J. Tang, Functional miRNAs in breast cancer drug resistance, *Onco Targets Ther.*, 11 (2018) 1529-1541.
- [10] M. Rui, Y. Qu, T. Gao, Y. Ge, C. Feng, X. Xu, Simultaneous delivery of anti-miR21 with doxorubicin prodrug by mimetic lipoprotein nanoparticles for synergistic effect against drug resistance in cancer cells, *Int. J. Nanomedicine*, 12 (2017) 217-237.
- [11] Z.-X. Wang, B.-B. Lu, H. Wang, Z.-X. Cheng, Y.-M. Yin, MicroRNA-21 Modulates Chemosensitivity of Breast Cancer Cells to Doxorubicin by Targeting PTEN, *Arch. Med. Res.*, 42 (2011) 281-290.
- [12] S.P. Jiang, S.N. He, Y.L. Li, D.L. Feng, X.Y. Lu, Y.Z. Du, H.Y. Yu, F.Q. Hu, H. Yuan, Preparation and characteristics of lipid nanoemulsion formulations loaded with doxorubicin, *Int. J. Nanomedicine*, 8 (2013) 3141-3150.
- [13] C. Yang, S.Q. Liu, S. Venkataraman, S.J. Gao, X. Ke, X.T. Chia, J.L. Hedrick, Y.Y. Yang, Structure-directing star-shaped block copolymers: Supramolecular vesicles for the delivery of anticancer drugs, *J. Control. Release*, 208 (2015) 93-105.

- [14] X. Deng, M. Cao, J. Zhang, K. Hu, Z. Yin, Z. Zhou, X. Xiao, Y. Yang, W. Sheng, Y. Wu, Y. Zeng, Hyaluronic acid-chitosan nanoparticles for co-delivery of MiR-34a and doxorubicin in therapy against triple negative breast cancer, *Biomaterials*, 35 (2014) 4333-4344.
- [15] M. Wang, T. Liu, L. Han, W. Gao, S. Yang, N. Zhang, Functionalized O-carboxymethyl-chitosan/polyethylenimine based novel dual pH-responsive nanocarriers for controlled co-delivery of DOX and genes, *Polym. Chem.*, 6 (2015) 3324-3335.
- [16] A.X. Gao, L. Liao, J.A. Johnson, Synthesis of Acid-Labile PEG and PEG-Doxorubicin-Conjugate Nanoparticles via Brush-First ROMP, *ACS Macro Lett*, 3 (2014) 854-857.
- [17] Y. Su, Y. Hu, Y. Du, X. Huang, J. He, J. You, H. Yuan, F. Hu, Redox-Responsive Polymer-Drug Conjugates Based on Doxorubicin and Chitosan Oligosaccharide-g-stearic Acid for Cancer Therapy, *Mol. Pharm.*, 12 (2015) 1193-1202.
- [18] B. Zhang, H. Zhang, S. Dai, J. Bi, Cell-penetrating peptide-labelled smart polymers for enhanced gene delivery, *Eng. Life Sci.*, 17 (2017) 193-203.
- [19] H. Ragelle, S. Colombo, V. Pourcelle, K. Vanvarenberg, G. Vandermeulen, C. Bouzin, J. Marchand-Brynaert, O. Feron, C. Foged, V. Preat, Intracellular siRNA delivery dynamics of integrin-targeted, PEGylated chitosan-poly(ethylene imine) hybrid nanoparticles: A mechanistic insight, *J. Control. Release*, 211 (2015) 1-9.
- [20] Z.-H. Peng, Y. Xie, Y. Wang, J. Li, D. Oupický, Dual-Function Polymeric HPMA Prodrugs for the Delivery of miRNA, *Mol. Pharm.*, 14 (2017) 1395-1404.
- [21] D.K. Bonner, X. Zhao, H. Buss, R. Langer, P.T. Hammond, Crosslinked linear polyethylenimine enhances delivery of DNA to the cytoplasm, *J. Control. Release*, 167 (2013) 101-107.
- [22] J. Panyam, W.Z. Zhou, S. Prabha, S.K. Sahoo, V. Labhasetwar, Rapid endo-lysosomal escape of poly(DL-lactide-co-glycolide) nanoparticles: implications for drug and gene delivery, *FASEB J.*, 16 (2002) 1217-1226.
- [23] B.D. Monnery, M. Wright, R. Cavill, R. Hoogenboom, S. Shaunak, J.H.G. Steinke, M. Thanou, Cytotoxicity of polycations: Relationship of molecular weight and the hydrolytic theory of the mechanism of toxicity, *Int. J. Pharm.*, 521 (2017) 249-258.
- [24] B. Shi, H. Zhang, S. Dai, X. Du, J. Bi, S.Z. Qiao, Intracellular Microenvironment Responsive Polymers: A Multiple-stage Transport Platform for High-Performance Gene Delivery, *Small*, 10 (2014) 871-877.
- [25] D. Yue, G. Cheng, Y. He, Y. Nie, Q. Jiang, X. Cai, Z. Gu, Influence of reduction-sensitive diselenide bonds and disulfide bonds on oligoethylenimine conjugates for gene delivery, *J. Mater. Chem. B*, 2 (2014) 7210-7221.
- [26] T. Wang, J.R. Upponi, V.P. Torchilin, Design of multifunctional non-viral gene vectors to overcome physiological barriers: Dilemmas and strategies, *Int. J. Pharm.*, 427 (2012) 3-20.
- [27] M.M. Schmidt, K.D. Wittrup, A modeling analysis of the effects of molecular size and binding affinity on tumor targeting, *Mol. Cancer Ther.*, 8 (2009) 2861-2871.

- [28] H. Hatakeyama, H. Akita, H. Harashima, A multifunctional envelope type nano device (MEND) for gene delivery to tumours based on the EPR effect: A strategy for overcoming the PEG dilemma, *Adv. Drug Del. Rev.*, 63 (2011) 152-160.
- [29] S.R. Hamilton, S.F. Fard, F.F. Paiwand, C. Tolg, M. Veiseh, C. Wang, J.B. McCarthy, M.J. Bissell, J. Koropatnick, E.A. Turley, The hyaluronan receptors CD44 and Rhamm (CD168) form complexes with ERK1,2 that sustain high basal motility in breast cancer cells, *J. Biol. Chem.*, 282 (2007) 16667-16680.
- [30] G. Cheng, Y. He, L. Xie, Y. Nie, B. He, Z. Zhang, Z. Gu, Development of a reduction-sensitive diselenide-conjugated oligoethylenimine nanoparticulate system as a gene carrier, *Int. J. Nanomedicine*, 7 (2012) 3991-4006.
- [31] K. Helios, A. Pietraszko, W. Zierkiewicz, H. Wójtowicz, D. Michalska, The crystal structure, infrared, Raman and density functional studies of bis(2-aminophenyl) diselenide, *Polyhedron*, 30 (2011) 2466-2472.
- [32] D. Lin-Vien, N.B. Colthup, W.G. Fateley, J.G. Grasselli, *The handbook of infrared and Raman characteristic frequencies of organic molecules*, Elsevier, 1991.
- [33] R.J. Hondal, S.M. Marino, V.N. Gladyshev, Selenocysteine in thiol/disulfide-like exchange reactions, *Antioxid. Redox Signal.*, 18 (2013) 1675-1689.
- [34] D.K. Kolmel, E.T. Kool, *Oximes and Hydrazones in Bioconjugation: Mechanism and Catalysis*, *Chem. Rev.*, 117 (2017) 10358-10376.
- [35] S. Shen, D. Jiang, L. Cheng, Y. Chao, K. Nie, Z. Dong, C.J. Kuttyreff, J.W. Engle, P. Huang, W. Cai, Z. Liu, Renal-Clearable Ultrasmall Coordination Polymer Nanodots for Chelator-Free ⁶⁴Cu-Labeling and Imaging-Guided Enhanced Radiotherapy of Cancer, *ACS Nano*, 11 (2017) 9103-9111.
- [36] L. Lusini, S.A. Tripodi, R. Rossi, F. Giannerini, D. Giustarini, M.T. del Vecchio, G. Barbanti, M. Cintonino, P. Tosi, P. Di Simplicio, Altered glutathione anti-oxidant metabolism during tumor progression in human renal-cell carcinoma, *Int. J. Cancer*, 91 (2001) 55-59.
- [37] W. Tian, X. Dong, X. Liu, G. Wang, Z. Dong, W. Shen, G. Zheng, J. Lu, J. Chen, Y. Wang, Z. Wu, X. Wu, High-Throughput Functional MicroRNAs Profiling by Recombinant AAV-Based MicroRNA Sensor Arrays, *PLoS One*, 7 (2012) e29551.
- [38] R. Misra, S.K. Sahoo, Intracellular trafficking of nuclear localization signal conjugated nanoparticles for cancer therapy, *Eur. J. Pharm. Sci.*, 39 (2010) 152-163.
- [39] S. Misra, V.C. Hascall, R.R. Markwald, S. Ghatak, Interactions between Hyaluronan and Its Receptors (CD44, RHAMM) Regulate the Activities of Inflammation and Cancer, *Front. Immunol.*, 6 (2015) 201.
- [40] M. Dalmark, Characteristics of doxorubicin transport in human red blood cells, *Scand. J. Clin. Lab. Invest.*, 41 (1981) 633-639.
- [41] L. Frankel, N. Christoffersen, A. Jacobsen, M. Lindow, A. Krogh, A. Lund, Programmed cell death 4 (PDCD4) is an important functional target of the microRNA miR-21 in breast cancer cells, *J. Biol. Chem.*, 283 (2008) 1026 - 1033.

[42] L. Bao, S. Hazari, S. Mehra, D. Kaushal, K. Moroz, S. Dash, Increased Expression of P-Glycoprotein and Doxorubicin Chemoresistance of Metastatic Breast Cancer Is Regulated by miR-298, *Am. J. Pathol.*, 180 (2012) 2490-2503.

Supporting information

Design of dual-locked smart microgels for effective co-delivery of DOX and miRNA-21 inhibitor to multidrug resistant cancer cells

*Seonho Yun, Jiabin Zhang, Hesamoddin Rabiee, Hu Zhang, Jingxiu Bi, Sheng Dai**

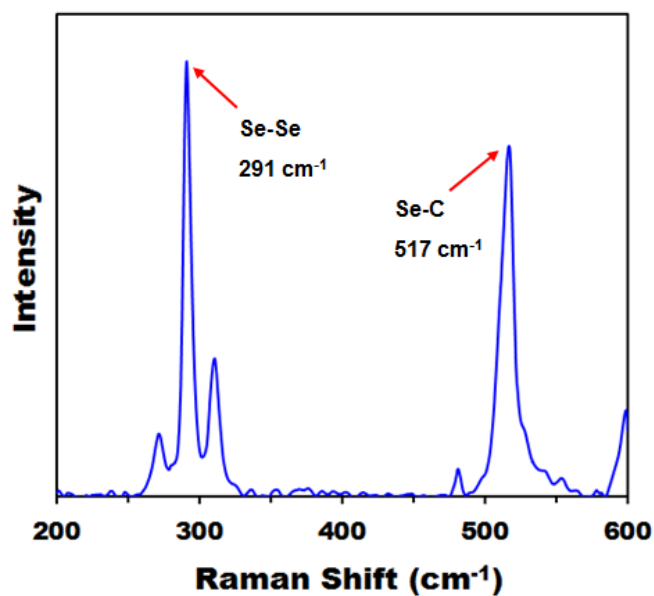


Figure 4.S1 Raman spectrum of the diselenide bond crosslinker (-SeSe-).

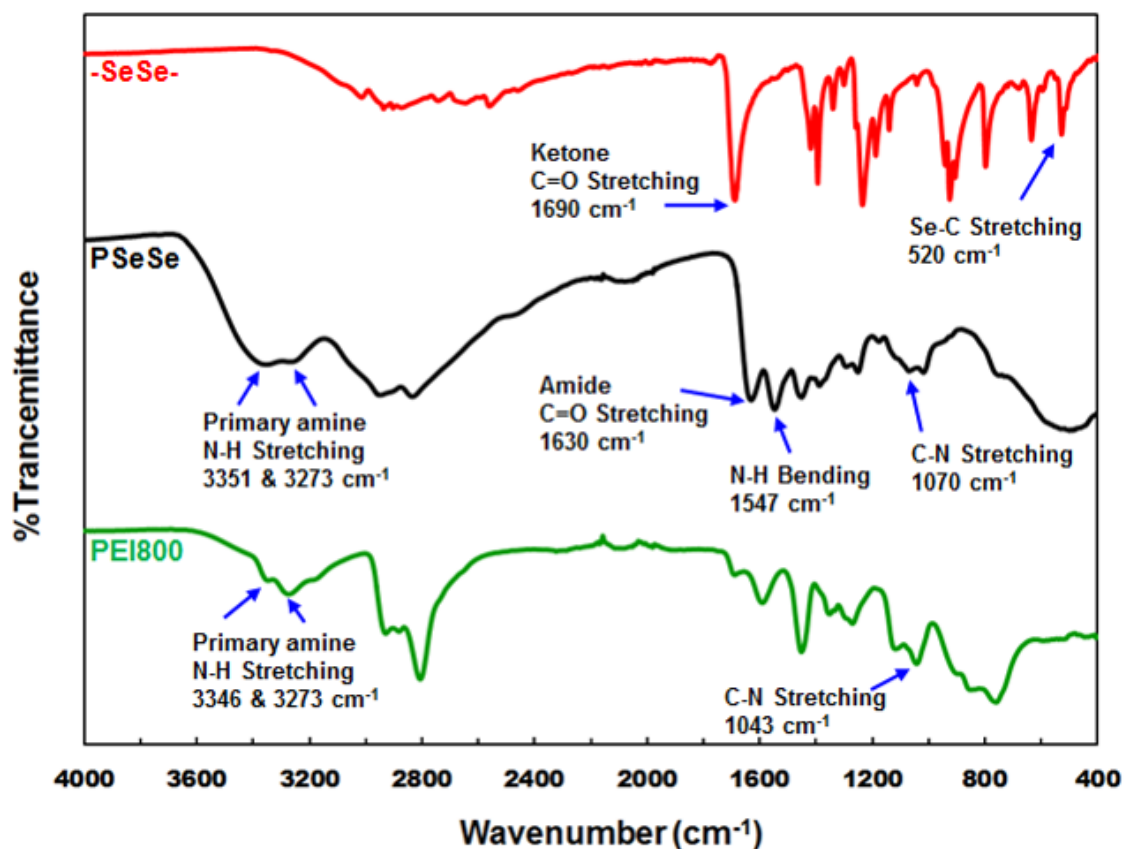


Figure 4.S2 FTIR spectra of diselenide crosslinker (-SeSe-), PEI800, and PEI800 microgels via crosslinking PEI800 with -SeSe-.

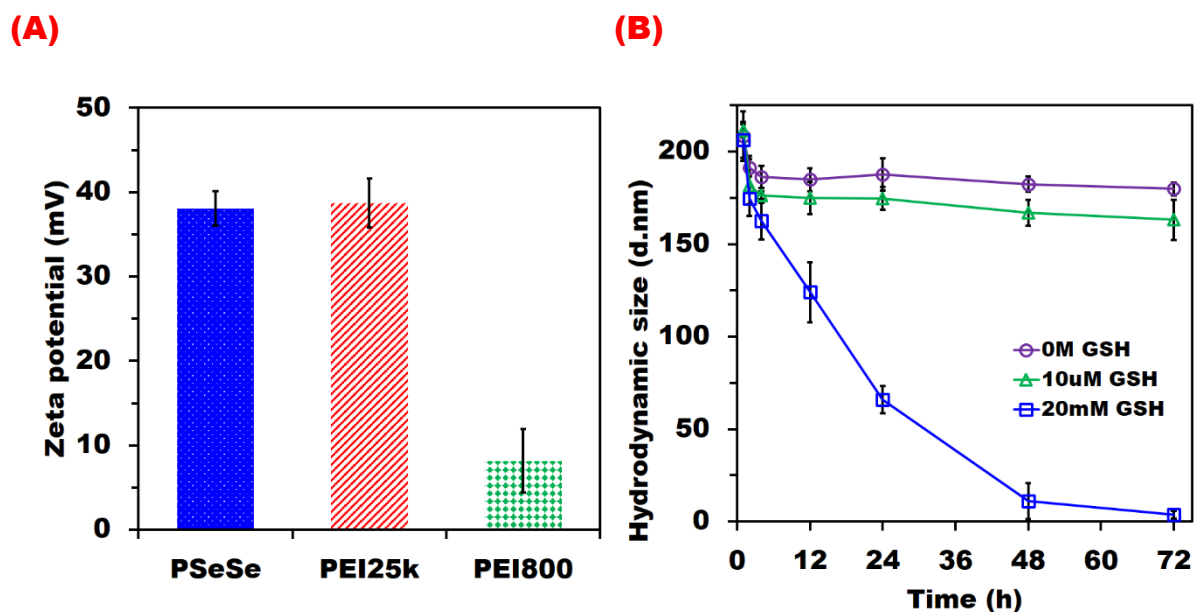


Figure 4.S3 Characterizations of diselenide bond (-SeSe-) crosslinked PEI800 microgels (PSeSe), (A) zeta potential to compare with that of PEI25k and PEI800 as a positive control and a negative control, and (B) size to confirm diselenide bond cleavage under various glutathione (GSH) concentrations of 0 M, 10 μ M, and 20 mM.

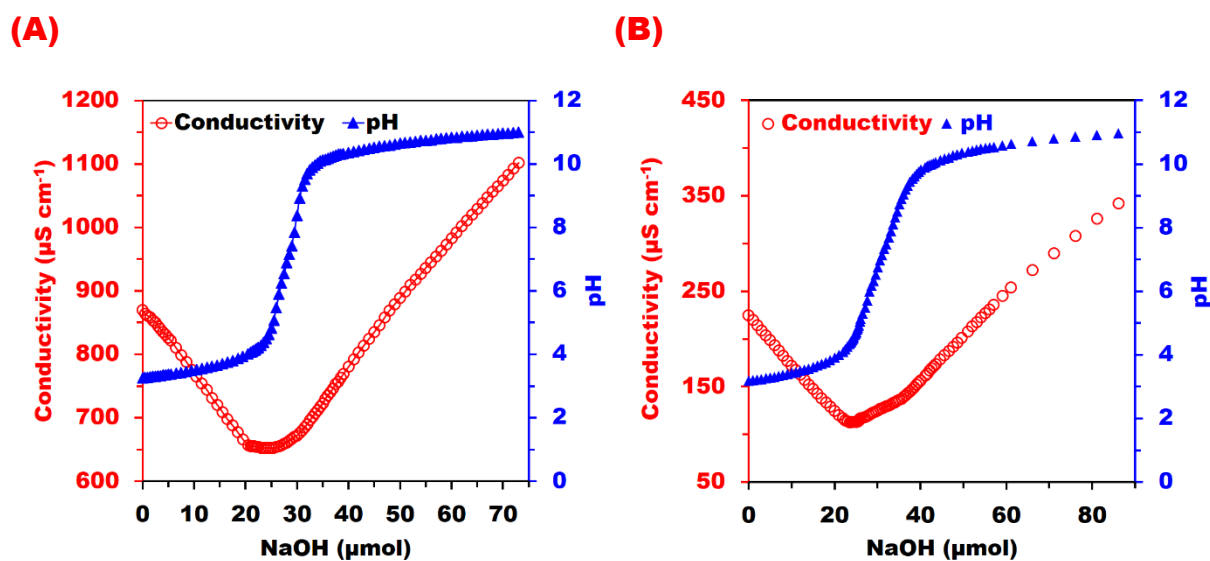


Figure 4.S4 Conductivity and pH titrations for (A) PSeSe (2.4 mg) and (B) PSeHD-SeSeP (2.65mg), measured at room temperature.

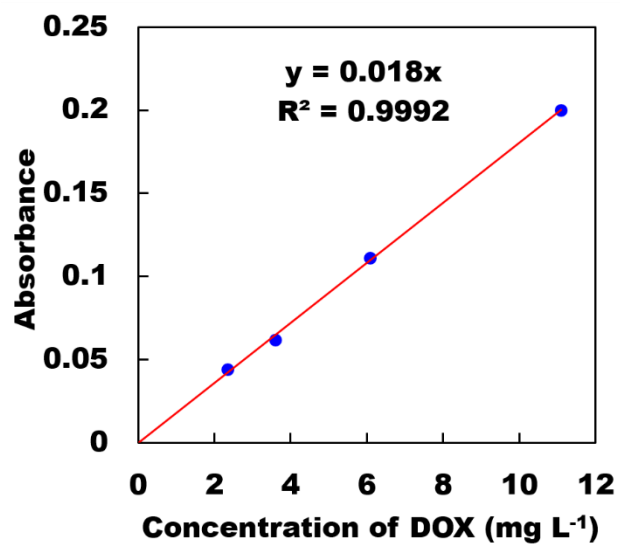


Figure 4.S5 DOX calibration curve for 479.5 absorbance at various DOX concentrations.



Figure 4.S6 Agarose gel retardation assay for miR-21i loading to PSeHD.

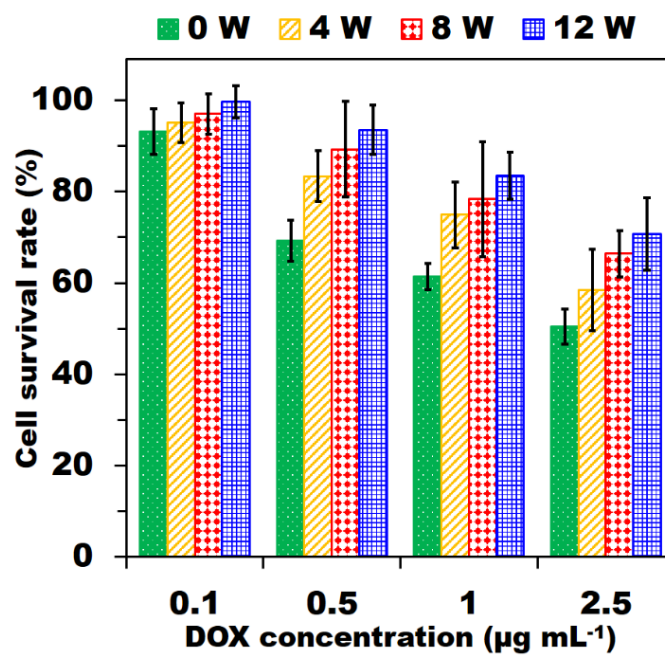


Figure 4.S7 Survival rate against DOX concentrations from 0.1 to 2.5 $\mu\text{g mL}^{-1}$ for DOX sensitive breast cancer cell, MDA-MB-231-S (0W), and DOX resistant metastatic breast cancer cells, MDA-MB-231-R4w (4W), MDA-MB-231-R8w (8W) and MDA-MB-231-R12w (12W), 4W, 8W and 12W indicate 4th, 8th and 12th weeks of the cell culture.

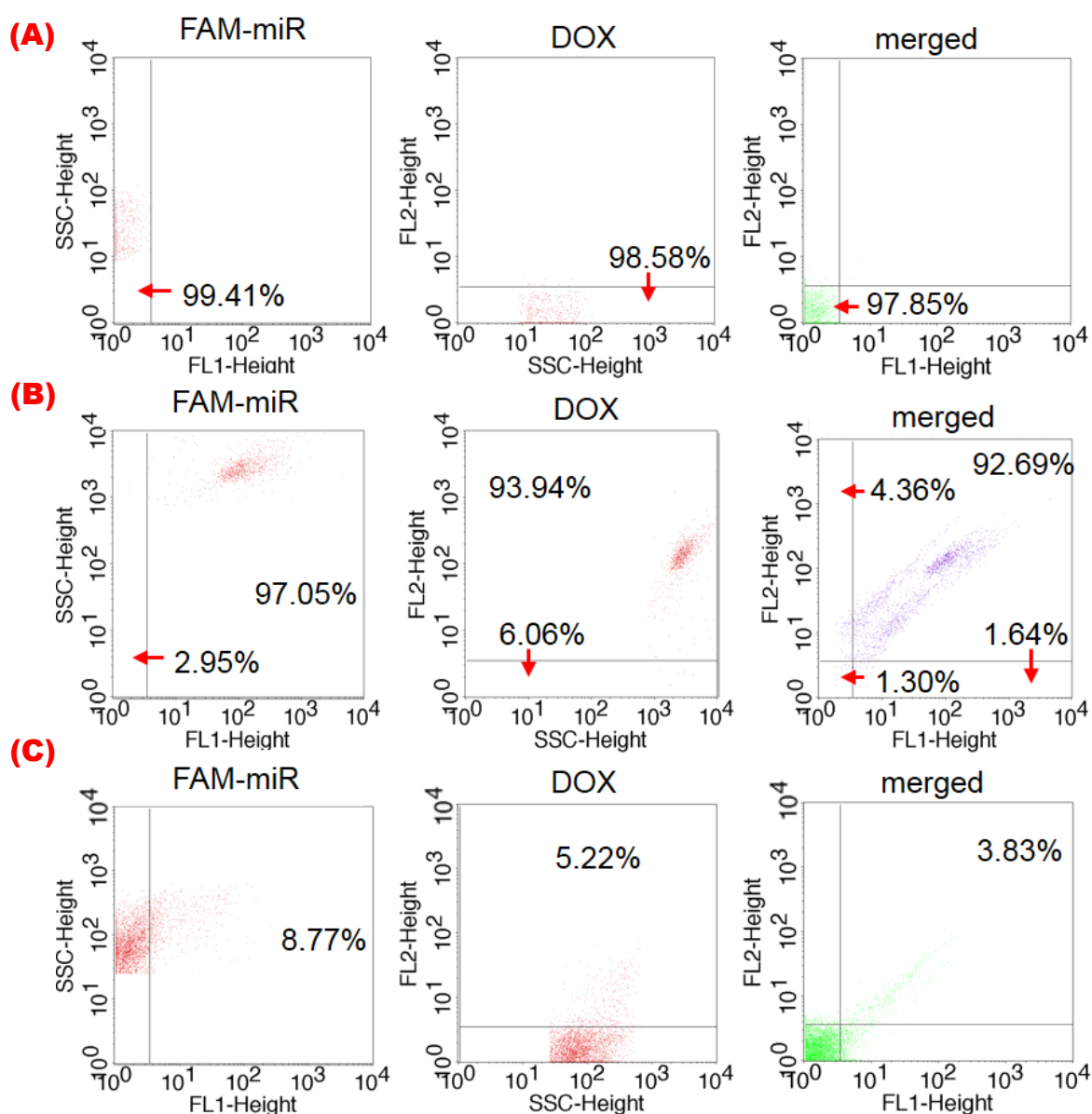


Figure 4.S8 Quantitative MDA-MB-231 cellular uptake assays of PSeHD-SeSeP/FAM-miR/HA system by flow cytometer, (A) cells only without PSeHD-SeSeP/FAM-miR/HA as a control, (B) cells with PSeHD-SeSeP/FAM-miR/HA, and (C) HA-pretreated cells with PSeHD-SeSeP/FAM-miR/HA, FL1 and FL2 represent FAM and DOX.

Chapter 5 Developing traceable nanomedicines of doxorubicin, miR-21 inhibitor and ATP aptamer for enhanced therapeutic treatment on multidrug resistant cancers

*Seonho Yun, Mahdhir Bin Amat Tugiman, Jiabin Zhang, Hu Zhang, Jingxiu Bi, Sheng Dai**

S. Yun, M.B.A. Tugiman, J. Zhang, Prof. H. Zhang, Prof. J. Bi, Prof. S. Dai

School of Chemical Engineering, the University of Adelaide, Adelaide, SA 5005, Australia

H. Zhang

Amgen Bioprocessing Centre, Keck Graduate Institute, 535 Watson Drive, Claremont, CA
91711

Prof. S. Dai

Department of Chemical Engineering, Brunel University London, Uxbridge, UB8 3PH, United
Kingdom

sheng.dai@brunel.ac.uk

Statement of Authorship

Title of Paper	Developing traceable nanomedicines of doxorubicin, miR-21 inhibitor and ATP aptamer for enhanced therapeutic treatment on multidrug resistant cancers
Publication Status	<input type="checkbox"/> Published <input type="checkbox"/> Accepted for Publication <input type="checkbox"/> Submitted for Publication <input checked="" type="checkbox"/> Unpublished and Unsubmitted work written in manuscript style
Publication Details	In preparation for submission

Principal Author

Name of Principal Author (Candidate)	Seonho Yun		
Contribution to the Paper	Mainly designed the experiment, material synthesis, evaluation, and manuscript writing		
Overall percentage (%)	80 %		
Certification:	This paper reports on the original research I conducted during the period of my Higher Degree by Research candidature and is not subject to any obligations or contractual agreements with a third party that would constrain its inclusion in this thesis. I am the primary author of this paper.		
Signature		Date	20/05/2019

Co-Author Contributions

By signing the Statement of Authorship, each author certifies that:

- i. the candidate's stated contribution to the publication is accurate (as detailed above);
- ii. permission is granted for the candidate to include the publication in the thesis; and
- iii. the sum of all co-author contributions is equal to 100% less the candidate's stated contribution.

Name of Co-Author	Jiabin Zhang		
Contribution to the Paper	Helped to operate evaluation part of the experiment		
Signature		Date	21/02/2019

Name of Co-Author	Mahdhir Bin Amat Tugiman		
Contribution to the Paper	Helped to operate the experiment		
Signature		Date	21 Feb 2019

Name of Co-Author	Hu Zhang		
Contribution to the Paper	Supervised the experiment design, data interpretation, manuscript correction		
Signature		Date	24/02/2019

Name of Co-Author	Jingxiu Bi		
Contribution to the Paper	Proof read the manuscript and evaluation		
Signature		Date	25/02/2019

Name of Co-Author	Sheng Dai		
Contribution to the Paper	Supervised the experiment design, data interpretation, manuscript correction, and corresponding author		
Signature		Date	20/05/2019

Abstract

Multidrug resistance (MDR) in invasive cancer with chronic chemotherapy leads to poor prognosis, high dosages and resultant severe side effects to patients. To exert effective therapeutic effect on multidrug-resistant cancers and minimize side effects of chemotherapeutic agents, biocompatible and fully-biodegradable microgels were prepared by crosslinking low molecular weight polyethyleneimine (PEI800) and doxorubicin (DOX) with diselenide-crosslinkers in a one-step process, and a microRNA-21 inhibitor (miR-21i) and an ATP aptamer (Apt) were complexed with the microgels to construct novel nanomedicines able to release DOX intracellularly and mitigate MDR by inhibiting oncogenic microRNA-21 and ATP-binding cassette (ABC) transporters in cancer cells. Hyaluronic acid (HA) was finally introduced to nanomedicine surface for facilitating HA receptor-mediated endocytosis and eliminating serum protein adsorption. The nanomedicine is benign to normal cells with 99.2 % viable HEK293T cells after treatment. Biodegradation and drug release of this nanomedicine simultaneously occur in response to specific tumor microenvironment with a high concentration of GSH to cleave diselenide crosslinkers. This nanomedicine displays an enhanced and synergistic therapeutic efficacy: 29.1 ± 4.7 % of metastatic breast cancer cell survival and remarkably 8.9 % of multidrug-resistant cancer cells survive after treatment with this nanomedicine at a DOX concentration of $2.5 \mu\text{g mL}^{-1}$. This nanomedicine has demonstrated great potential in combating multidrug resistant cancer cells by tri-delivery of functional therapeutic agents (DOX, miR-21i inhibitor and Apt) into cells.

Keywords: tri-delivery, nanomedicine, multidrug resistance, diselenide crosslinker, DOX, miR-21 inhibitor, ATP aptamer, hyaluronic acid, microgels

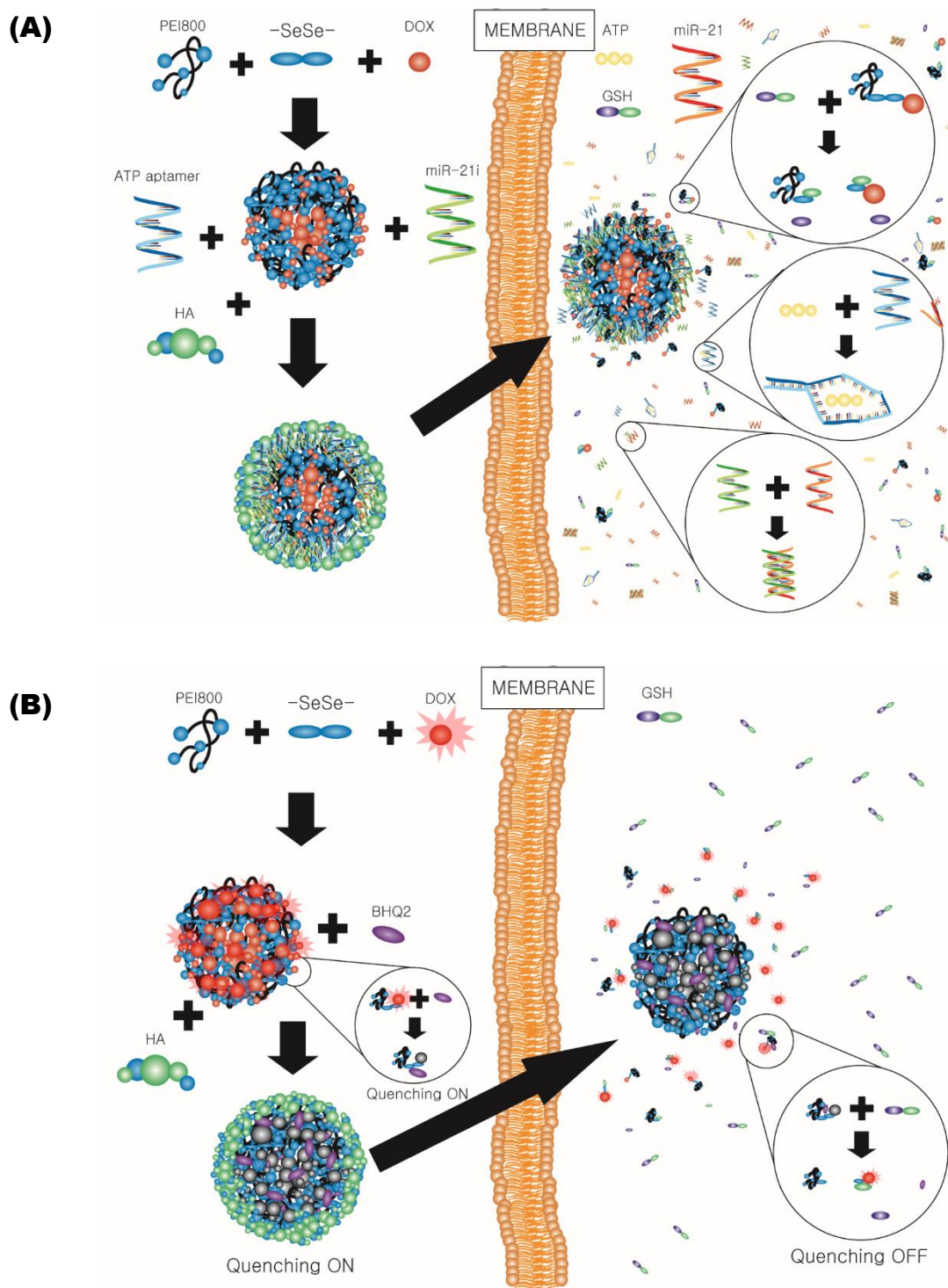
5.1 Introduction

Multidrug resistance (MDR) has posed a significant challenge in completely eradicating cancer cells since these cells have gradually gained tolerance to chemotherapeutic agents. The cancer cells possess inherent drug resistance via phosphatidylinositol-3-kinase (PI3K)/Akt and mammalian target of rapamycin (mTOR) signaling pathways to enhance cancer cell growth and survival, and expression of microRNA-21 (miR-21) to downregulate phosphatase and tensin homolog (PTEN), an inhibitor of PI3K, and programmed cell death 4 (PDCD4), a protector of tumor suppressor protein p53 [1-4]. Practically, doxorubicin (DOX), an anthracycline drug, is initially progressive in exerting its anticancer effect via intercalating adenosine triphosphate (ATP)-driven topoisomerase II and damaging DNA to activate p53, and downregulating B-cell lymphoma-2 (bcl-2) to induce apoptosis of cancer cells [5, 6]. However, chronic administration of DOX promotes MDR in cancer cells via detoxification with an increasing level in glutathione (GSH), mutation of topoisomerase II for reduced DOX intercalation, and inhibition of PTEN and PDCD4 with increasing expression of miR-21 after activation of nuclear factor kB (NF-kB) and signal transducer activator of transcription 3 (STAT3) [7-10]. In addition, overexpression of ATP-binding cassette transporters (ABC transporters) in cancer cells after chronic chemotherapy reduces intracellular accumulation of DOX [11, 12]. Meanwhile, an increased dosage of DOX and cellular uptake of DOX by normal cells result in detrimental side-effects, such as heart failure, skeletal muscle dysfunction, chronic kidney function loss, and liver injury [13-17]. Introduction of a miR-21 inhibitor (miR-21i) to multidrug-resistant cancer cells augments their sensitivity to administrated DOX [18, 19]. In addition, ATP aptamers (Apt), short single-stranded oligonucleotides to bind ATP have been used for ATP depletion in drug resistant cells by preventing efflux of anticancer drugs [20-23]. Therefore, tri-delivery of DOX, miR-21i and Apt into cancer cells may mitigate MDR and maximize the anticancer efficacy of DOX.

To date, many drug delivery carriers have been developed to physically/chemically load chemotherapeutic or gene drugs, while these carriers may not be able to meet ideal criteria for delivery of drugs: minimized side effects due to systemic toxicity, great biocompatibility with no/low inherent toxicity, controlled release of drugs, prolonged circulation, selective endocytosis, traceable delivery and enhanced anticancer efficiency. In our recent studies, strong cations with effective gene condensation ability but high cytotoxicity (e.g., PEI25k, polyamidoamine dendrimers and poly-L-lysine) are replaced by low-toxic biodegradable vesicles of crosslinked biocompatible weak cations (e.g., PEI800) using redox cleavable disulfide or diselenide molecules to achieve high transfection efficiency and biocompatibility [24-27] (Chapter 3). On the other hand, premature leakage of physically loaded DOX from a delivery vesicle, including liposome, micelle, and inorganic nanoparticles, can be improved by chemical conjugation of drug to vesicles via cleavable linkers of hydrazone or/and diselenide moieties which are specifically responsive to the acidic pH and strongly expressed GSH in tumor microenvironment [28-30] (Chapters 3 and 4). To prolong the circulation time of drug-loaded delivery systems, the hydrodynamic sizes of the systems is often controlled to be between 10 and 200 nm to improve the enhanced permeation and retention (EPR) effect and avoid renal and reticuloendothelial system (RES) clearance [31-33]. Surface modification with poly(ethylene glycol) (PEG) contributes to prolonged circulation by preventing serum protein adsorption, but increased PEGylated nanomedicines experience low efficiency in endocytosis [31-33]. Although active cancer targeting of a delivery system is realizable by surface modification with ligands for specific receptors on cancer cells, such as antibodies, peptides and aptamers, these ligands have challenging issues, such as immunogenicity from interaction between antibodies and Fc receptors on normal cells, cytotoxicity from positively charged peptides, and less efficient targeting of aptamers in practice [20, 34-36]. Anionic hyaluronic acid (HA) is suggested to prevent delivery system from serum adsorption by electrostatic

repulsion and to be selectively endocytosed to cancer cells via overexpressing HA receptors, CD44 and RHAMM [37]. Moreover, inorganic molecules can be introduced to delivery systems for imaging technologies, including UV-vis absorbance, magnetic resonance (MR) imaging and photoluminescence, to track bio-distribution in diverse clinical applications although the inorganics exhibit potential toxicity due to their high accumulation in patient body [38-41]. Quenching effect on fluorophore (e.g., quantum dot and DOX) by a quencher within 100 Å of distance can also be useful to image their intracellular localization in real-time when they are far apart from each other [42, 43].

Herein, we prepared a multi-functional tri-delivery vesicle for DOX, miR-21i and Apt in order to enhance the therapeutic effect of DOX on invasive cancers with MDR and minimizing the side-effect from both DOX and vesicle itself. Biocompatible PEI800 and DOX were simply crosslinked with intracellular cytosol GSH-cleavable diselenide crosslinkers to yield biodegradable DOX-conjugated microgels, which then electrostatically bound to miR-21i and Apt. After HA coating on the surface of the formed polyplexes, a biodegradable nanomedicine was produced with an anionic surface and a hydrodynamic size of 100 - 200 nm for prolonged systemic circulation and HA receptor-mediated endocytosis. Fluorescence from DOX allowed monitoring cellular uptake of the nanomedicine (Scheme 5.1A), and the black hole quencher (BHQ) labeling of the nanomedicine confirmed intracellular release of DOX (Scheme 5.1B). Anticancer effect of DOX was significantly enhanced via mitigating MDR by inhibiting miR-21 and DOX exporters with ATP depletion because of spontaneously release of miR-21i and Apt of the nanomedicine.



Scheme 5.1 (A) Scheme for entire process of the traceable tri-delivery system, PSeSeD/miR-21i/Apt/HA: synthesis, HA receptor-mediated endocytosis, GSH-triggered nanomedicine degradation in cytosol to release loaded DOX, miR-21i and Apt, isolating ATP by Apt, and inhibiting miR-21 by miR-21i. (B) Scheme for tracing intracellular DOX localization by quenching the fluorescence in PSeSeDBHQ but emitting fluorescence in GSH-rich cytosol.

5.2 Experimental

5.2.1 Materials

Doxorubicin hydrochloride was purchased from Wuhan Wang Lianshang Biotechnology (China). MicroRNA-21 inhibitor (sequence 5'-GUCCACUCUUGUCCUCA AUG-3') (miR-21i) and FAM-labelled miRNA inhibitor with a single strand as a negative control (sequence 5'-CAGUACUUUUGUGUAGUACAA-3') (FAM-miR) were obtained from Shanghai Gene Pharma Co., Ltd. BHQ®-2 succinimidyl ester was obtained from LGC Biosearch Technologies. Adenosine 5'-triphosphate (ATP) aptamer (sequence 5'-ACCTGGGGGAGTATTGCGGAGGAAGGT-3') was supplied from Invitrogen™. Sodium hyaluronate 60 kDa (HA) was obtained from Lifecore Biomedical, LLC. Branched polyethyleneimine 800 (PEI800), selenium, sodium borohydride (NaBH₄), 3-chloropropionic acid, 1-ethyl-3-(3-dimethyl-laminopropyl) carbodiimide (EDC), N-hydroxysulfosuccinimide (NHS), L-glutathione reduced (GSH), Leibovitz's Medium (L-15), cell counting Kit-8 (CCK-8), bis-benzimide H 33258, and ATP bioluminescent somatic cell assay kit were purchased from Sigma-Aldrich. Dulbecco modified eagle medium (DMEM), fetal bovine serum (FBS), penicillin-streptomycin (PS), Trypsin-EDTA (0.25%), and CellMask™ Deep Red Plasma Membrane Stain were supplied from Life Technologies Australia Pty Ltd. HEK293T and MDA-MB-231 cell lines were from Australia Health and Medical Research Institute and School of Pharmacy at University of South Australia. Deionised water was produced from a Spectra/Por® Milli-Q water system (18.2 MΩ·cm, Spectrum Laboratories, Inc.).

5.2.2 Synthesis of DOX loaded microgels (PSeSeD)

5.2.2.1 Diselenide crosslinker (-SeSe-)

3,3'-diselenediylidipropanoic acid, a diselenide crosslinker (-SeSe-), was synthesized from the same method being reported in our previous paper ([Chapter 3](#)). Briefly, selenium powder (1.18 g, 15 mmol) was suspended in water (5 mL) in a flask with nitrogen protection and magnetic

stirring. Sodium borohydride (1.13 g, 30 mmol) dissolved in cold water (12.5 mL) was dropwise added to the flask in an ice bath for 10 min until the solution became colorless. 1.18 g of selenium powder was then added to the solution and stirred at 105 °C under nitrogen environment for 20 min to turn the color into reddish-brown. 3-chloropropionic acid (3.26 g, 30 mmol) in water (7.5 mL, pH 8.0 being adjusted with sodium carbonate) was injected to the flask at room temperature for overnight stirring with N₂ gas protection. The mixture was further stirred under an open air environment to oxidize unreacted selenium for 12 h. After filtering with a 0.45 µm membrane filter, pH of the mixture was adjusted to 3.0 using 3 M hydrochloride. Coagulants were collected through extraction with ethyl acetate and subsequent water wash for 3 times. After drying the product in ethyl acetate using magnesium sulphate and filtering, -SeSe- with a pale yellow color was crystalized. Successful synthesis of diselenide crosslinker was confirmed by Raman spectroscopy.

5.2.2.2 DOX conjugated PEI microgels of PSeSeD and PSeSeD2X

For the synthesis of DOX conjugated PEI microgels (**PSeSeD**), mixture of -SeSe- (42.8 mg, 140.9 µmol), EDC (162.1 mg, 845.7 µmol) and NHS (64.9 mg, 563.8 µmol) in DMSO (400 µL) was magnetically stirred under nitrogen protection at ambient temperature for 45 min. DOX·HCl (16.35 mg, 28.2 µmol) in DMSO (200 µL) was injected to the mixture under light protection, and branched PEI800 (pH 8.0 being adjusted by 3M HCl, 90.2 mg, 112.7 µmol) in 200 µL DMSO was injected after an interval of 5 min. The mixture was stirred for another 2 days under dark and dialyzed with a tube of 7 kDa MWCO against deionized water at 4 °C under light protection for 32 h with water change at every 8 h. After lyophilization, PSeSeD was produced. The zeta potential and hydrodynamic size of PSeSeD in 10 mM NaCl solution at pH 7.4 were characterized with dynamic light scattering (DLS) measurement from a zeta sizer (Malvern Zetasizer Nano ZS ZEN 3600). FTIR was used to confirm the synthesis of

PSeSeD. The amine content in PSeSeD ($\mu\text{mol mg}^{-1}$) was quantified with conductivity and pH titration. DOX loading (wt. %) was calculated from following Equation:

$$\text{DOX loading (\%)} = \frac{(\text{total DOX} - \text{unloaded DOX})}{\text{DOX loaded microgels}} \times 100 \quad (1)$$

The amount of unloaded DOX was determined from a UV-vis spectroscopy (Figure 5.S3) at a wavelength of 479.5 nm.

At the same time, PEI microgels with double DOX feed (**PSeSeD2X**) was synthesized using a similar method but with the feed of DOX (32.7 mg, 56.4 μmol), PEI800 (90.2 mg, 112.7 μmol) and -SeSe- (51.4 mg, 169.1 μmol).

5.2.2.3 Black hole quencher conjugation (PSeSeDBHQ)

Black hole quencher-2 (BHQ) was conjugated to PSeSeD (**PSeSeDBHQ**) by chemical bonding of succinimidyl ester and primary amine. PSeSeD (12.6 mg, 2.17 μmol of loaded DOX) and BHQ®-2 succinimidyl ester (1.6 mg, 2.65 μmol) were dissolved in DMSO (4 mL), and the mixture was magnetically stirred at room temperature under nitrogen and light protection for overnight. After 3-day dialysis in darkness at 4 °C with frequent water change and freeze drying, PSeSeDBHQ was produced. Successful interaction of BHQ and PSeSeD was confirmed from the absorbance spectrum of a UV-vis spectrophotometer and the color change in solution.

5.2.2.4 Microgels without DOX (PSeSe) and degraded-PSeSe (Degrade-P)

PEI microgel without DOX loading (**PSeSe**) was synthesized by the same method as PSeSeD but without DOX feed. -SeSe- (34.2 mg, 112.7 μmol) was used to crosslink PEI800 (90.2 mg, 112.7 μmol) to produce PSeSe as being confirmed from FTIR.

PSeSe degradation was handled in a mimicking cytosol condition: 20 mM glutathione (GSH), pH 7.4, and 4-(2-hydroxyethyl)-1-piperazineethanesulfonic acid (HEPES) buffered glucose solution containing 20 mM HEPES and 5% glucose (HEPES buffer), producing **Degrade-P**.

The degradation process was monitored via the hydrodynamic size measurements in HEPES buffer (pH 7.4) with 20 mM GSH and without GSH at 37 °C and predetermined time intervals for 72 h.

5.2.3 *Ex vivo* DOX release and biodegradation

5.2.3.1 DOX release

PSeSeD in pH 7.4 HEPES buffer (5 mL, 1 mg mL⁻¹) was dialyzed using a tube (MWCO 3.5 kDa) against HEPES buffer (95 mL) with various GSH concentrations of 0 M, 10 μM, and 20 mM in a horizontal shaker (100 rpm) at 37 °C over 144 h. An aliquot outside the dialysis tube was withdrawn with its absorbance read at 479.5 nm via a UV-vis spectrophotometer at pre-designed time intervals. Quantification of released DOX from PSeSeD was determined from the DOX calibration curve (Figure 5.S3).

5.2.3.2 Biodegradability of PSeSeD

Bio-stability and bio-degradability of PSeSeD complexes were evaluated via hydrodynamic size measurements in HEPES buffer (pH 7.4) at different mimicking conditions: 0 M GSH for a physiological condition, 10 μM GSH for an extracellular microenvironment, and 20 mM GSH for an intracellular cytosol environment. The hydrodynamic sizes of the PSeSeD in above solutions under shaking at 100 rpm at 37 °C were measured at a predetermined time for a duration of 120 h.

5.2.4 miR-21i and Apt loading (PSeSeD/miR-21i/Apt) and release

A mixture of miR-21i (0.5 μL, 0.42 nmol μL⁻¹) and Apt (0.5 μL, 0.54 nmol μL⁻¹) was incubated with PSeSeD at room temperature for 20 min at various mixing mole ratios of nitrogen (N) in PSeSeD (Figure S6) to phosphate (P) in the mixture of miR-21i and Apt (N/P), ranging from 1 to 8. The mixture of miR-21i and Apt only without PSeSeD was employed as a control. Agarose gel (0.8 %) retardation assay was conducted at 100 volts for 1 h. The mixture migrated in the

gel was fluorescent under UV irradiation and photographed by a G-BOX. PEI25k and PEI800 as a positive and a negative control were polyplexed with the mixture of miR-21i and Apt at a predetermined N/P ratio of 0.5, 1.0, 2.0, and 3.0 for PEI25k and 4.0, 6.0, 8.0, and 10.0 for PEI800, while PSeSeD2X and PSeSe were polyplexed with miR-21i and Apt at a N/P of 1.0 to 10.0. The N/P ratio for full loading of these polyplexes was determined with agarose gel electrophoresis and G-BOX.

Release of miR-21i and Apt from PSeSeD/miR-21i/Apt polyplexes at an N/P of 10.0 was *ex vivo* assayed via agarose gel electrophoresis. The polyplexes were incubated in HEPES buffer solution with 20 mM GSH at pH 7.4 at 37 °C for 72 h, and assayed in agarose gel at 100 volts for 1 h with subsequent photographing by a G-BOX.

5.2.5 HA coating (PSeSeD/miR-21i/Apt/HA) and characterization

5.2.5.1 HA coating

Hyaluronic acid (HA) was coated to PSeSeD/miR-21i/Apt polyplexes in RNase free water (DEPC water). PSeSeD was incubated with a mixture of miR-21i and Apt at an N/P ratio of 10.0 at room temperature for 20 min and then incubated with HA at a weight ratio of HA to PSeSeD of 1.5 for 20 min to yield the PSeSeD/miR-21i/Apt/HA.

5.2.5.2 Zeta potential and particle size

Zeta-potential and hydrodynamic size of PSeSeD/miR-21i/Apt/HA were measured in 10 mM NaCl solution at pH 7.4 using a zetasizer (ZEN 3600) and compared to that of PSeSeD and PSeSeD/miR-21i/Apt.

5.2.6 Cell culture

Human embryonic kidney cell line (HEK293T), human metastatic breast cancer cell line (MDA-MB-231), and DOX resistant breast cancer cell line (MDA-MB-231-R) were cultured in a humidified incubator (Contherm Scientific Limited) at 5 % CO₂ and 37 °C. HEK293T was

cultured with Dulbecco Modified Eagle Medium (DMEM), 10 vol. % of fetal bovine serum (FBS), and 1 vol. % of penicillin-streptomycin (PS). The culture medium including Leibovitz's Medium (L-15), 10 % FBS, and 1 % PS was employed to culture MDA-MB-231. For MDA-MB-231-R culture, a low concentration of DOX (0.01 μg for 8 weeks and 0.02 $\mu\text{g mL}^{-1}$ from 9th to 12th week) was included in the L-15 based medium.

The viability assay for MDA-MB-231-R cells was executed via Cell Counting Kit-8 (CCK-8) at every 4 weeks while culturing over 12 weeks. MDA-MB-231-R was incubated in a 96-well plate with L-15 based medium without DOX for 24 h, and then further incubated with DOX·HCl (free-DOX) at an increasing concentration from 0.1 to 2.5 $\mu\text{g mL}^{-1}$ for 48 h. The well plate with CCK-8 treatment for another 4 h in the incubator was inserted in a microplate reader (ELx808 BioTek) to read absorbance at 450 nm wavelength to determine the cell survival rate (%) using the following equation:

$$\text{Cell survival rate (\%)} = \frac{(S-B)}{(C-B)} \times 100 \quad (2)$$

where S, C, and B represent the absorbance with DOX, without DOX, and a blank without cells.

5.2.7 Intracellular uptake of PSeSeD/FAM-miR/Apt/HA and localization of DOX

5.2.7.1 Tracing cellular uptake of PSeSeD/FAM-miR/Apt/HA

Intracellular uptake of PSeSeD/FAM-miR/Apt/HA was qualitatively monitored via a confocal laser scanning microscopy (CLSM) (Olympus FV3000) with replicates. MDA-MB-231 cells were incubated on glass cover slips in 3 wells of a 12-well plate with L-15 based media, and HA (10 mg mL^{-1}) was included in one well to block HA receptors to obtain HA pretreated cells. After 24 h incubation, PSeSeD/FAM-miR/HA (10.0 N/P of PSeSeD to FAM-labeled miRNA negative control with a random sequence (FAM-miR) and 1.5 weights of HA to PSeSeD) was applied to two wells of the plate: one well containing cells without HA pretreatment and the

other well with HA pretreated cell, while the third well with cells without HA pretreatment and PSeSeD/FAM-miR/HA was used as a control. After further 4 h incubation, cells in the 3 wells were treated with CellMask™ Deep Red Plasma Membrane Stain for 5 min, and fixed with formaldehyde (4 %) for 10 min. Subsequently after washing with PBS 3 times, fluorescent images were obtained with blue for DOX, green for FAM-miR, and red for cells via a CLSM.

Quantification of intracellular uptake of PSeSeD/FAM-miR/HA was determined via detecting the fluorescent intensity from DOX and FAM-miR using filters, FL-2 (ex. 488, em. 585 nm) and FL-1 (ex. 488, em. 530 nm), of a flow cytometer (BD FACSCalibur™) with replicates. MDA-MB-231 cells were cultured in two wells of a 24-well plate for 24 h. One well with PSeSeD/FAM-miR/HA and the other well without PSeSeD/FAM-miR/HA as a control were further incubated for another 4 h, and cells were then collected by trypsin-EDTA treatment and washed by PBS.

5.2.7.2 Intracellular localization of DOX and FAM-miR

Intracellular localization of DOX and FAM-miR was traced via a flow cytometer. DOX and FAM-miR loaded complexes with a quencher (BHQ), PSeSeDBHQ/FAM-miR/HA, were prepared in the same condition as PSeSeD/FAM-miR/HA, and applied to MDA-MB-231-R cells after 24 h incubation on a 24-well plate. The cells were further incubated for 4 h and 12 h, and cells without PSeSeDBHQ/FAM-miR/HA were used as a control. After treatment with trypsin-EDTA and washing with PBS, the collected cells were excited at 488 nm wavelength with a flow cytometer to detect fluorescent intensity of DOX and FAM-miR using FL-2 and FL-1 filters.

5.2.8 Biocompatibility of PSeSe microgels and PSeSeD/miR-21i/Apt/HA

Biocompatibilities of PSeSe microgels and Degrade-P fragments were evaluated via HEK293T cell viability assay. HEK293T cells were incubated in a 96-well plate for 24 h, and then exposed

to PSeSe or Degrade-P at a concentration of 1.0, 10.0, and 50.0 $\mu\text{g mL}^{-1}$, followed by further 48 h incubation. After CCK-8 treatment for 4 h, cell survival rates were determined from Equation 2 with the absorbance reading at 450 nm from the well plate using a microplate reader. The cell survival rates for PEI25k and PEI800 were compared as controls.

HEK293T viability assay against PSeSeD/miR-21i/Apt/HA (10 N/P and 1.5 wt. ratio of HA to PSeSeD) was carried out to confirm biosafety of PSeSeD/miR-21i/Apt/HA after systemic administration. HEK293T cells were incubated in a 96-well plate for 24 h. The cells were treated by PSeSeD/miR-21i/Apt/HA with an increase in DOX concentration from 0.1 to 2.5 $\mu\text{g mL}^{-1}$, and incubated for another 48 h. After CCK-8 treatment for 4 h and absorbance reading at 450 nm in a microplate reader, the cell survival rate against PSeSeD/miR-21i/Apt/HA was calculated using Equation 2. The cell viability was also measured after cells were treated by free-DOX, PSeSeD, and PSeSeD/HA as controls.

5.2.9 Anticancer efficacy PSeSeD/miR-21i/Apt/HA against MDA-MB-231 cell lines

The anticancer efficacy of PSeSeD/miR-21i/Apt/HA (10.0 N/P, 1.5 wt. ratio HA) against MDA-MB-231 cells was evaluated by counting viable cells after treatment. MDA-MB-231 cells were incubated in a 96-well plate for 24 h, and incubated for further 48 h in the presence of PSeSeD/miR-21i/Apt/HA with loaded DOX concentrations from 0.1 to 2.5 $\mu\text{g mL}^{-1}$. MDA-MB-231 cell survival ratio after exposure to PSeSeD/miR-21i/Apt/HA was obtained after 4 h CCK-8 treatment and absorbance reading in a microplate reader. For comparison, free-DOX, PSeSeD/HA (2.0 wt. ratio HA), PSeSeD/Apt/HA (20.0 N/P, 1.8 wt. ratio HA), and PSeSeD/miR-21i/HA (20.0 N/P, 1.8 wt. ratio HA) were also applied to MDA-MB-231 cells for measuring their viabilities.

5.2.10 ATP aptamer efficacy

5.2.10.1 ATP quantification

ATP contents in MDA-MB-231 and MDA-MB-231-R cells before and after treatment with Apt were determined via an ATP bioluminescent somatic cell assay kit and a fluorophotometer (Shimadzu, RF-5301PC) with replicates. MDA-MB-231 (231-S) and MDA-MB-231-R (231-R) cells (300,000 cells per well) were seeded in a 6-well plate (2 wells for 231-S and 2 wells for 231-R) and incubated for 24 h. PSeSe (54.5 μL , 0.1 mg mL^{-1}) was incubated with Apt (7.8 μL , 0.54 $\text{nmol } \mu\text{L}^{-1}$) for 20 min at room temperature, and coated by HA (8.2 μL , 1 mg mL^{-1}) to produce PSeSe/Apt/HA. An equal amount of PSeSe was coated by HA (10.9 μL , 1 mg mL^{-1}) to produce PSeSe/HA without Apt. PSeSe/Apt/HA and PSeSe/HA without Apt were added into two types of cells for another 48 h incubation. Cells were collected by trypsin-EDTA treatment and counted in a hemocytometer. 1×10^4 cells in each well were suspended in the ATP assay dilution buffer at pH 7.8 (50 μL) and mixed with the somatic cell ATP releasing agent (100 μL) and deionized water (50 μL). The mixture (100 μL) was transferred to a fluorimeter cuvette in the presence of 25-folds diluted ATP assay working solution (including luciferin and luciferase) (100 μL) and additional ATP assay dilution buffer (2 mL). The signal of luciferin fluorescence was detected at a wavelength of 530 nm via a fluorophotometer (ex. 350 nm) and ATP (pmol per cell) was quantified using a calibration curve of the fluorescence intensity to a range of ATP concentrations (nmol) (Figure 5.S9).

5.2.10.2 Qualitative therapeutic effect induced by Apt on MDA-MB-231-R

The therapeutic effect induced by Apt on multi-drug resistant MDA-MB-231-R cells was qualitatively evaluated via monitoring DOX intracellular localization after release from PSeSeDBHQ/Apt/HA and PSeSeDBHQ/HA under a CLSM. DOX and Apt loaded PSeSe with BHQ (PSeSeDBHQ/Apt/HA) was prepared. PSeSeDBHQ (60 μL , 0.1 mg mL^{-1}) was mixed with Apt (7.8 μL , 0.54 $\text{nmol } \mu\text{L}^{-1}$) for 20 min incubation at room temperature, and coated by

HA (6 μL , 1 mg mL^{-1}). PSeSeDBHQ/HA without Apt was prepared by directly coating HA (9 μL , 1 mg mL^{-1}) to PSeSeDBHQ (60 μL , 0.1 mg mL^{-1}). MDA-MB-231-R cells were incubated on glass slips of 4 wells in a 12-well plate for 24 h. Because tracing DOX intracellular localization was dependent on incubation time and the presence of Apt, two wells was incubated with PSeSeDBHQ/Apt/HA for 24 and 48 h, while the other two wells was treated with PSeSeDBHQ/HA for 24 and 48 h. Subsequently, membrane and nucleus of the cells were stained with CellMaskTM Deep Red for 5 min and bisBenzimide H 33258 for another 5 min, and fixed by formaldehyde (4%) for 10 min. After washing with PBS3 times, fluorescent images from DOX (blue), membrane (red), and nucleus (cyan) were captured via CLSM.

5.2.11 Anticancer synergy of PSeSeD/miR-21i/Apt/HA on cancer cells with MDR

The synergistic therapeutic efficacy of PSeSeD/miR-21i/Apt/HA on multi-drug resistant cell lines, MDA-MB-231-R, was quantified via the cell viability assay using CCK-8. The procedure was similar to that for MDA-MB-231 cells. Therapeutic effects induced by free-DOX, PSeSeD/HA, PSeSeD/Apt/HA, and PSeSeD/miR-21i/Apt/HA on MDA-MB-231-R were also evaluated.

5.3 Results and Discussion

5.3.1 Synthesis of PSeSeD microgels

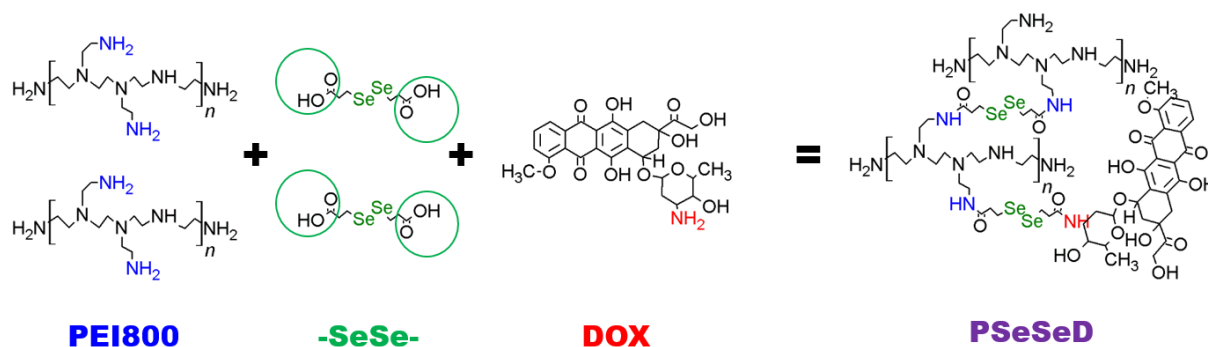
5.3.1.1 DOX conjugated biodegradable microgels (PSeSeD)

Conjugation of doxorubicin (DOX) to a delivery carrier with cleavable linkers may protect DOX from pre-leakage before reaching tumor site, while DOX release is realized by cleaving the linker in response to specific tumor microenvironment. For delivery of miR-21i and Apt, strong positive charged polymers with a large molecular weight intrinsically show a high loading efficiency due to electrostatic interaction between anionic genes/Apt and cationic

polymers, but severe cytotoxicity and accumulation in a patient's body are often associated with cationic polymers. In this study, biodegradable microgels with DOX conjugation were prepared by crosslinking low molecular weight PEI800 with DOX in the presence of -SeSe- in one reactor and miR-21i and Apt were complexed with DOX conjugated microgels by electrostatic interaction.

The redox-sensitive diselenide crosslinker, 3,3'-diselanediyldipropanoic acid (-SeSe-), was prepared with a yield of 56.5 %, in which the Se-Se bond and the Se-C bond are observed in Raman shifts at 291 and 517 cm^{-1} (Figure 5.S1). DOX conjugated microgels (PSeSeD) were formed by crosslinking DOX and PEI800 at a feed mole ratio of 0.25:1 with -SeSe- in a reactor (Scheme 5.2) with a yield of 48 %. PSeSeD has a zeta potential of 58.3 ± 1.4 mV and a hydrodynamic size of 218.7 ± 13.4 nm from a Malvern zetasizer measurement. Successful synthesis of PSeSeD is confirmed from FTIR spectra of PEI800, PEI800 microgels without DOX (PSeSe) and PSeSeD (Figure 5.S2). Distinct PEI800 peaks at 3356, 3251 and 1541 cm^{-1} for N-H stretching of primary amine and N-H bending are detected in the PSeSeD spectrum and peaks from crosslinking by -SeSe- at 1630 and 527 cm^{-1} for C=O stretching and Se-C stretching. Conjugated DOX is evident at 3078, 1408 and 985 cm^{-1} of the FTIR spectrum for aromatic C-H stretching and O-H bending from DOX. Conductivity and pH titration reveals the amine group of 4.2 $\mu\text{mol mg}^{-1}$ in PSeSeD (Figure 5.S6A). DOX loading in PSeSeD determined by Equation 1 is found to be 9.35 wt. %.

By doubling the feed molar ratio of DOX to PEI800 (0.5:1) in comparison with 0.25:1 for PSeSeD, **PSeSeD2X** was produced by crosslinking DOX and PEI800 with -SeSe- with a yield of 56 %. The zeta potential and the hydrodynamic size of PSeSeD2X reduce to 31.5 ± 4.5 mV and 136.8 ± 24.3 nm respectively, while DOX loading increases by 1.8 times (16.5 wt. %) in comparison with that in PSeSeD (9.35 wt.%) (Table 5.S1). The results indicate DOX loading in the microgels can be controlled by adjusting the feed ratio of DOX to PEI800.



Scheme 5.2 Synthesis of PSeSeD by crosslinking PEI800 and DOX with –SeSe–

5.3.1.2 Preparation of PSeSeDBHQ, PSeSe, and Degrade-P

To trace intracellular localization of DOX and FAM-labelled miRNA with a random sequence (FAM-miR), black hole quencher-2 (BHQ) was conjugated to PSeSeD by covalently bonding succinimidyl ester in BHQ to the primary amine group in PSeSeD, producing **PSeSeDBHQ**. Emissions from DOX at a wavelength of 580 nm and FAM at 530 nm can be quenched by BHQ in the integrated structure of PSeSeDBHQ, while the emissions from DOX and FAM can be switched on for fluorescence detection after they are release from PSeSeDBHQ with a quenching distance more than 10 nm between BHQ and DOX or FAM [42]. Successful synthesis of PSeSeDBHQ is confirmed by a UV-vis absorbance peak at 541.5 nm and a dark purple color of the product, comparing to an absorbance peak at 488 nm and a red color of PSeSeD (Figure 5.S4).

To deliver Apt alone without DOX for the ATP assay, PEI800 was crosslinked by –SeSe– to produce **PSeSe** microgels with a zeta potential and a particle size of 68.3 ± 0.68 mV and 260.0 ± 22.9 nm (Table 5.S1). The amine content in PSeSe is determined via conductivity and pH titration to be $4.96 \mu\text{mol mg}^{-1}$ (Figure 5.S6B).

To evaluate *in vitro* biocompatibility of degraded microgels with normal kidney cell lines (HEK293T), PSeSe microgels were incubated with 20 mM glutathione (GSH) at pH 7.4 for 72 h, producing **Degrade-P** with a zeta potential and a size of 0.96 ± 3.9 mV and 3.7 ± 1.9 nm. [Figure 5.S5](#) shows the size of PSeSe decreases in 20 mM GSH to mimic the cytosol reductase with extension of the incubation time up to 72 h, while the size of PSeSe is maintained in 0 M GSH during the entire experimental time, supporting the microgels are only biodegradable under a redox condition by cleaving the diselenide crosslinker, -SeSe-.

5.3.2 Cytosol responsive DOX release and biodegradation of PSeSeD

The drug delivery carrier is ideally designed to release drugs selectively in intracellular target sites to enhance therapeutic efficacy and to reduce pre-leakage during blood circulation for reducing side effects. DOX and PEI800 were crosslinked by a diselenide crosslinker (-SeSe-) to form cationic PSeSeD which can interact with miR-21i and Apt by electrostatic interaction, and cleavage of redox-sensitive -SeSe- is able to release DOX and miR-21i/Apt. PSeSeD was incubated in a mimicking cellular microenvironment at pH 7.4 with 0 M, 10 μ M, and 20 mM GSH, representing a physiological condition, an extracellular microenvironment, and a cytosol environment. [Figure 5.1A](#) displays a significant amount of loaded DOX is controllably released from PSeSeD at 20 mM GSH with 28.6 ± 1.3 % over 12 h and 55.7 ± 1.8 % over 144 h, whereas only 18% of DOX release at both 0 and 10 μ M of GSH over 144 h. These data strongly support the release profiles are regulated by GSH, i.e., intensive cleavage of -SeSe- at cytosol condition but much less cleavage at a physiological or extracellular environment.

Cytosol GSH-responsive cleavage of -SeSe- is also demonstrated in the biodegradability experiments ([Figure 5.1B](#)). The PSeSeD hydrodynamic size of 218.7 ± 13.4 nm reduces to 150.3 ± 7.1 nm over 6 h exposing to 20 mM GSH, and further down to 2.08 ± 0.08 nm over 5 days, whereas exposing to 0 μ M GSH or 10 μ M GSH, PSeSeD slightly decreases in size over first 6 h and then remains at 180.1 ± 7.4 nm and 131.7 ± 5.4 nm over 5 days. Therefore, PSeSeD

keeps its integral structure during the delivery course in a physiological condition and an extracellular environment but degrades into small fragments in the cytosol environment.

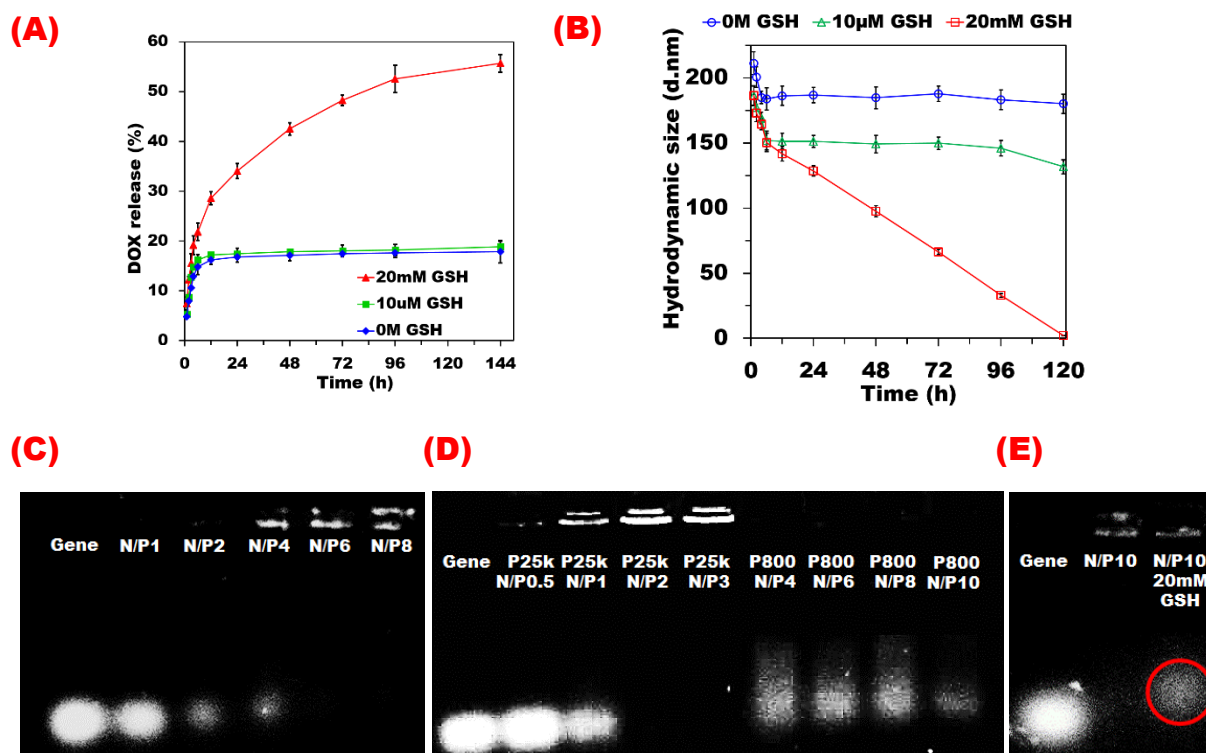


Figure 5.1 (A) DOX releasing profiles from PSeSeD at pH 7.4 and different concentrations of GSH over 144 h (n = 4). (B) Hydrodynamic size distributions of PSeSeD at pH 7.4 and various GSH concentrations (n = 4). Gene of miR-21i and Apt loading assay via agarose gel electrophoresis for (C) PSeSeD at N/P ratios of 1, 2, 4, 6 and 8 with naked gene as a control, and (D) PEI25kDa (P25k) at N/P ratios (0.5, 1, 2 and 3) and PEI800Da (P800) at N/P ratios (4, 6, 8 and 10) as the references. (E) Gene of miR-21i and Apt releasing profiles of the PSeSeD/miR-21i/Apt (N/P 10) after incubation with 20 mM GSH at pH 7.4 for 72 h.

5.3.3 miR-21i and Apt loading (PSeSeD/miR-21i/Apt) and release

PSeSeD with a zeta potential of 58.3 ± 1.4 mV and its stability in the physiological condition may be a great candidate as a gene delivery vector to electrostatically interact with miR-21i and Apt. The miR-21i and Apt loading capability of PSeSeD was evaluated via agarose gel (0.8 %) electrophoresis and compared to that of PEI25k and PEI800. In Figure 5.1C, PSeSeD

is able to achieve full loading of miR-21i and Apt at an N/P of 6.0 to form the PSeSeD/miR-21i/Apt polyplexes. The miR-21i and Apt loading capacity of PSeSeD is lower than that of PEI25k with full retardation of gene at an N/P ratio of 2.0, but far higher than that of PEI800 with no retardation even at an N/P of over 10.0 in [Figure 5.1D](#).

The hypothesis on zeta potential dependent gene loading capacity of microgels was further confirmed in the other synthesized microgels. Gene of miR-21i and Apt is completely loaded to PSeSeD2X (a higher concentration of DOX than PSeSeD) with zeta potential of 31.5 ± 4.5 mV at 10.0 N/P ([Figure 5.S8A](#)), whereas PSeSeDBHQ with a slightly higher zeta potential (39.3 ± 5.9 mV) than PSeSeD2X shows full loading at an N/P of 8.0 ([Figure 5.S8B](#)). In addition, PSeSe with the highest zeta potential (68.3 ± 0.7 mV) among synthesized microgels presents an outstanding loading capacity at an N/P of 3.0 ([Figure 5.S8C](#)). These results demonstrate the gene loading capacity of microgels by electrostatic interaction is directly proportional to the zeta potential of the microgels and the amount of gene is manipulatable through tuning the zeta potentials of delivery vectors.

Release of miR-21i and Apt from PSeSeD/miR-21i/Apt polyplexes was evaluated via the agarose gel retardation after 72 h incubation in the mimicking cytosol condition of pH 7.4 and 20 mM GSH. In [Figure 5.1E](#), the gene band of PSeSeD/miR-21i/Apt polyplexes with full retardation at 10.0 N/P moves in the presence of GSH, indicating miR-21i and Apt releases in the mimicking cytosol. Reduction of diselenide crosslinkers in the mimicking cytosol allows PSeSeD microgels to be converted to Degrade-P with size of 3.7 ± 1.9 nm and zeta potential of 0.96 ± 3.9 mV ([Table 5.S1](#)), weakening electrostatic interaction with miR-21i and Apt to release them. Therefore, the smart nanomedicine of PSeSeD/miR-21i/Apt with effective loading and selective release of DOX, miR-21i and Apt being triggered by intracellular cytosol is achieved.

5.3.4 HA surface coating to produce PSeSeD/miR-21i/Apt/HA

Drug conjugated or gene-complexed therapeutic products are often accumulated in tumor site by the enhanced permeability and retention (EPR) effect. Prolonging their systemic circulation may increase the accumulation efficiency in tumor site, and reduce undesired distribution in other organs as well as systemic toxicity. Drug or gene delivery products to prolong blood circulation are often designed to be in a size range of 10 to 200 nm to avoid renal and reticuloendothelial system (RES) clearance and have negative surface charges to prevent protein serum adsorption [32, 44]. In this study, anionic hyaluronic acid (HA) was coated on the cationic surface of PSeSeD/miR-21i/Apt at a weight ratio of HA to PSeSeD of 1.5 by electrostatic interaction to produce the PSeSeD/miR-21i/Apt/HA. Successful HA surface coating is confirmed by zeta potential measurement, i.e., the zeta potential of 58.3 ± 1.4 mV for PSeSeD; 51.3 ± 2.5 mV after miR-21i and Apt loading and -30.2 ± 0.23 mV after HA coating (Figure 5.S7). The negative charged nanomedicines after HA coating have been demonstrated to minimize protein adsorption during circulation (Chapter 3), and the hydrodynamic size of PSeSeD/miR-21i/Apt/HA was measured to be 140.9 ± 18.4 nm, falling into the range for EPR effect.

5.3.5 Cellular uptake of PSeSeD/FAM-miR/Apt/HA and release of therapeutic agents

5.3.5.1 Cellular uptake of PSeSeD/FAM-miR/Apt/HA

Monitoring drug-conjugated and gene-complexed therapeutic products during administration provides great insights into intracellular transportation and mechanisms in a qualitative and quantitative manner. PSeSeD/miR-21i/Apt/HA possesses DOX fluorescence at 580 nm. On the other hand, FAM-miR was used instead of miR-21i to prepare the PSeSeD/FAM-miR/Apt/HA with fluorescence at 530 nm. The intracellular transportation of PSeSeD/FAM-miR/HA with two fluorescent emissions can be traced under a confocal laser scanning microscopy (CLSM) and a flow cytometer. HA coating is also operated to allow metastatic cancer cells uptake via

HA receptor mediated endocytosis, but the HA receptors of CD44 and RHAMM are not present on the surface of non-invasive cancer cells and normal cells [45]. All metastatic breast cancer MDA-MB-231 cell membrane was stained with CellMaskTM Deep Red. While only red color MDA-MB-231 cells without PSeSeD/FAM-miR/HA is seen in [Figure 5.2A](#), green (FAM-miR), blue (DOX), and red (MDA-MB-231 cells) are overlapped to produce a pink color in the merged images in [Figure 5.2B](#), indicating successful cellular uptake of PSeSeD/FAM-miR/HA. To confirm whether HA receptor mediate endocytosis is the dominant pathway for cellular entry of PSeSeD/FAM-miR/HA, HA pretreated MDA-MB-231 cells by blocking all surface HA receptors prepared via incubation cells with HA for 24 h were exposed to PSeSeD/FAM-miR/HA. In [Figure 5.2C](#), weak green and blue signals are seen to overlap with red color in HA pretreated cells. Therefore, PSeSeD/FAM-miR/Apt/HA is endocytosed via HA receptor mediation to selectively enter to metastatic cancer cells.

Cellular uptake of PSeSeD/FAM-miR/HA to metastatic cancer cells was quantitatively traced via a flow cytometer. In [Figure 5.2D](#), control cells without PSeSeD/FAM-miR/HA displays FAM (0.29%) and DOX (0.86%) fluorescence intensity, similar to background. After 4 h incubation of cells with PSeSeD/FAM-miR/HA, 99.53 and 100 % of cells have displayed bright fluorescence of FAM and DOX than the control, indicating cells have uptaken PSeSeD/FAM-miR/HA ([Figure 5.2E](#)). Such quantitative information demonstrates traceability of PSeSeD/FAM-miR/Apt/HA and is consistent with the qualitative CLSM results of HA receptor-mediated endocytosis.

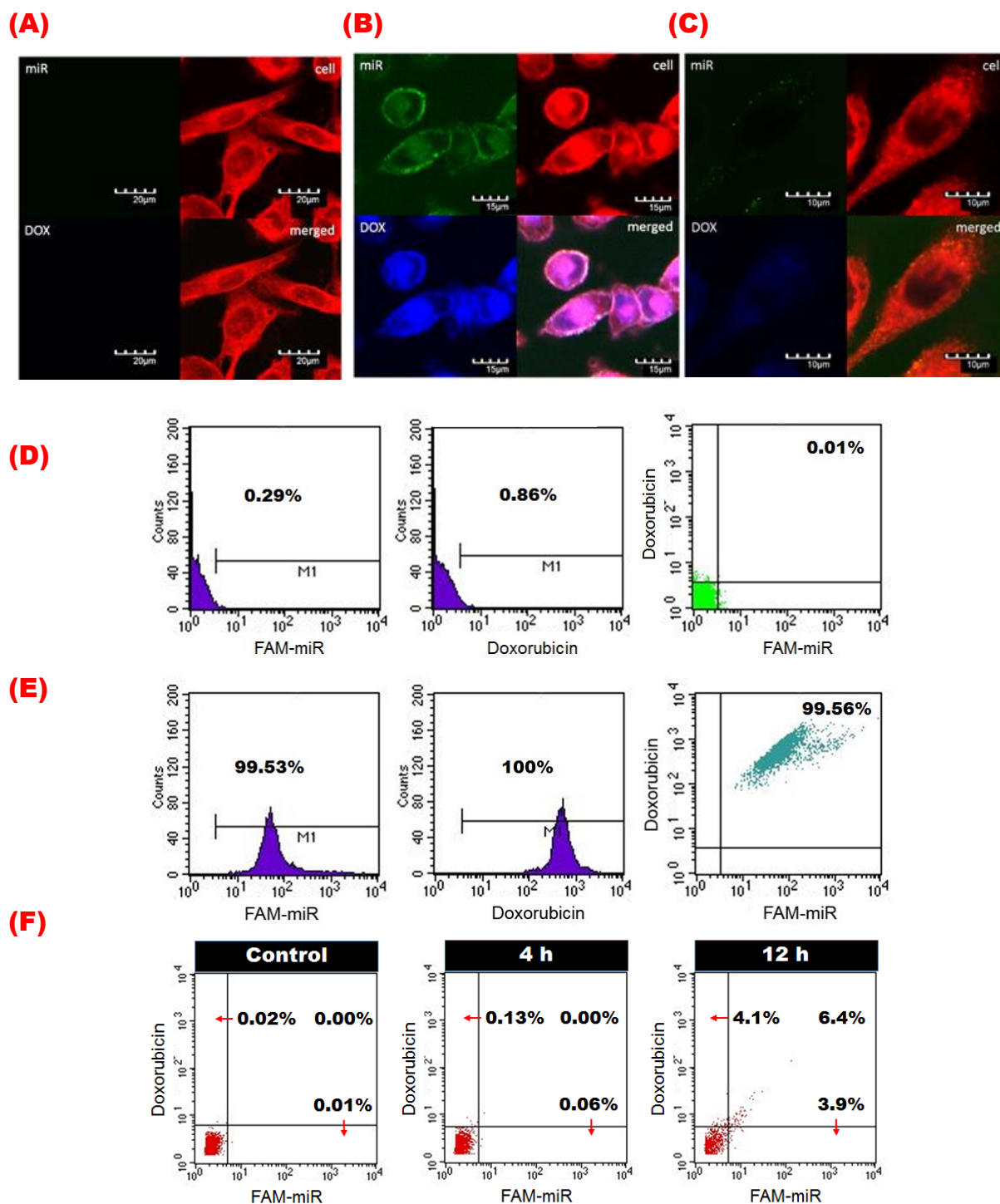


Figure 5.2 Tracing cell intake of PSeSeD/FAM-miR/HA via CLSM imaging of (A) MDA-MB-231 cells without PSeSeD/FAM-miR/HA (scale bar 20 μm), (B) MDA-MB-231 cells with PSeSeD/FAM-miR/HA (scale bar 15 μm), (C) HA pre-treated MDA-MB-231 cells with PSeSeD/FAM-miR/HA (scale bar 10 μm). Cellular uptake tracing via flow cytometer of (D) MDA-MB-231 cells without PSeSeD/FAM-miR/HA as a control and (E) MDA-MB-231 cells with PSeSeD/FAM-miR/HA. (F) Tracing DOX release from PSeSeDBHQ/FAM-miR/HA to MDA-MB-231 cells via flow cytometer over 4 and 12 h, (MDA-MB-231 cells without PSeSeDBHQ/FAM-miR/HA as a control).

5.3.5.2 Release of DOX and FAM-miR

Therapeutic agents exert their therapeutic effects in different intracellular locations after entry into cells. Identification of location of released drugs from delivery carriers allows rational design of the carrier for targeting release of drugs at specific organelles. To trace the released of DOX and FAM-miR from PSeSeD/FAM-miR/HA, PSeSeD was replaced by PSeSeDBHQ to quench the intrinsic fluorescence from DOX and FAM-miR due to the distance between BHQ (quencher) and DOX and/or FAM-miR (donor) within 10 nm [42]. After intracellular release of DOX and FAM-miR from PSeSeDBHQ /FAM-miR/HA, DOX and FAM-miR are far from BHQ conjugated delivery carriers so that their fluorescence can be detectable. The fluorescence signals from DOX and FAM-miR were quantified at a pre-determined time via a flow cytometer. In [Figure 5.2F](#), control of MDA-MB-231 cells without PSeSeDBHQ /FAM-miR/HA has a background intensity with 0.02 and 0.01 % of DOX and FAM-miR fluorescence signals. After cells were incubated with PSeSeDBHQ/FAM-miR/HA for 4 h, the percentage of cells with fluorescence from DOX and FAM-miR slightly increased to 0.13 and 0.06 % and further to 10.5 and 10.3 % over 12 h of incubation. Comparing to the cellular uptake of PSeSeD/FAM-miR/HA with 100 and 99.53 % of DOX and FAM-miR over 4 h incubation ([Figure 5.2E](#)), DOX and FAM-miR are gradually released from PSeSeDBHQ/FAM-miR/HA and traced since being away from the delivery carriers.

5.3.6 Cytotoxicity of PSeSeD/miR-21i/Apt/HA with normal cells

Inherent toxicity of drug delivery carriers to normal cells often hinders their clinical application. Ideal drug carrier should be biocompatible with normal cells before loading therapeutic agents. Often designed carriers with high molecular weight to increase systemic circulation time should be decomposed to fragments with size less than 10 nm for renal clearance to avoid its buildup in body. These fragments should be biocompatible to prevent damage to the kidney

during the clearance. In the absence of DOX, human kidney cell viability assays of PSeSe and Degrade-P (debris of PSeSe) were executed on HEK293T cells with PEI25k and PEI800 as negative and positive control. In [Figure 5.3A](#), PEI25k shows its strong cytotoxicity with a significant drop in cell survival rate from 94.4 ± 4.6 % at a PEI25k concentration of $1.0 \mu\text{g mL}^{-1}$ to less than half at a concentration of $50 \mu\text{g mL}^{-1}$. However, low molecular PEI800 displays excellent biocompatibility with a survival rate of 86.5 ± 5.01 % at a concentration of $50 \mu\text{g mL}^{-1}$. For PSeSe and Degrade-P, HEK293T cells have exceptionally high survival rates of 95.0 ± 1.4 % and 99.1 ± 3.8 % up to their concentrations of $50 \mu\text{g mL}^{-1}$, indicating their outstanding biocompatibility with insignificant inherent toxicity before and after degradation.

In addition to the ideal drug carrier before loading therapeutics, the delivery carrier after loading the therapeutics should be non-toxic to normal cells. Delivery systems of PSeSeD/miR-21i/Apt/HA was incubated with HEK293T cells for 48 h to evaluate its side effect to normal cells with free-DOX as a reference. After treatment with PSeSeD/miR-21i/Apt/HA, HEK293T cells exhibit a high survival rate of 99.2 ± 2.4 % at a DOX concentration of $2.5 \mu\text{g mL}^{-1}$, whereas free-DOX as a negative control, shows its severe cytotoxicity with more than half of HEK293T cell death at a DOX concentration of $0.5 \mu\text{g mL}^{-1}$ ([Figure 5.3B](#)). In PSeSeD/miR-21i/Apt/HA, DOX releasing is highly dependent on the GSH concentration in the cytosol ([Figure 5.1A](#)) and the GSH concentration in HEK293T cells is not high enough to cleave the diselenide crosslinker for releasing DOX, as the GSH concentration in normal cells is normally 2.8 folds lower than that in cancer cells [46, 47].

Besides, HA surface coating may impede cellular uptake of PSeSeD/miR-21i/Apt/HA to HEK293T cells. To confirm the effect of HA surface coating on the HEK293T cell survivals, PSeSeD and HA surface coated PSeSeD/HA were *in vitro* evaluated. The cell survival rate of 96.8 ± 2.1 % is found for HEK 293T cells after exposure to PSeSeD/HA, higher than that of 89.4 ± 1.3 % for PSeSeD at an equivalent DOX concentration of $50 \mu\text{g mL}^{-1}$ ([Figure 5.3B](#)).

This demonstrates the effects of HA surface coating reduces cellular uptake to HEK293T with lack of HA receptors. Therefore, minimal side effects of PSeSeD/miR-21i/Apt/HA to healthy cells are an outstanding impact of our nanomedicines.

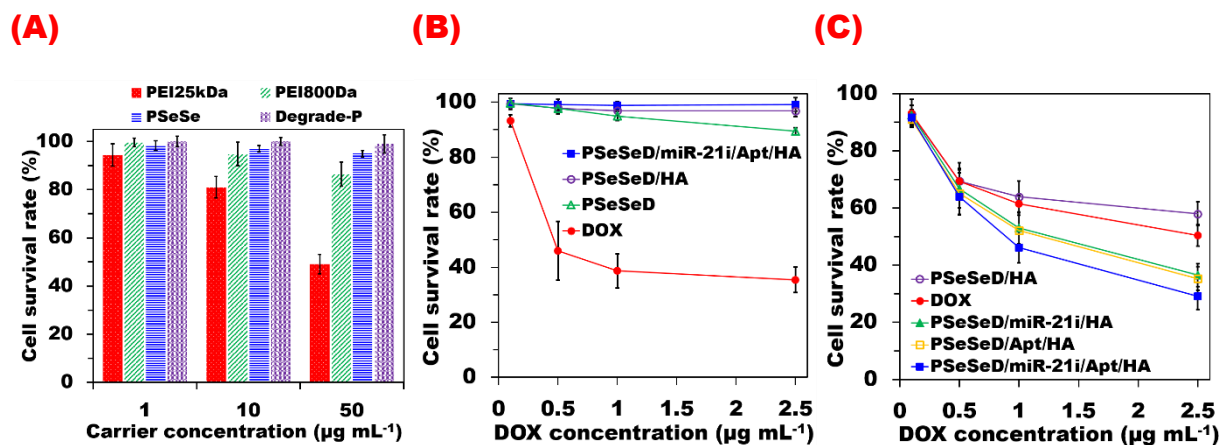


Figure 5.3 (A) Cell viability assays of PEI25k as negative control, PEI800 as positive control, PSeSe and Degrade-P on HEK293T cells after administration for 48 h (n = 4). (B) Cell viability assays of PSeSeD/miR-21i/Apt/HA on HEK293T after 48 h administration (n = 8) with free-DOX as negative control. (C) Anticancer effects of PSeSeD/miR-21i/Apt/HA on MDA-MB-231 after 48 h administration (n = 12)

5.3.7 Therapeutic effect of PSeSeD/miR-21i/Apt/HA on metastatic breast cancer cells

The synergistic therapeutic function of PSeSeD/miR-21i/Apt/HA was evaluated on a metastatic breast cancer cell line, MDA-MB-231, via the cell viability assay after 48 h incubation. The cell viability after treatment with PSeSeD/HA, PSeSeD/miR-21i/HA and PSeSeD/Apt/HA was also measured to compare with that of PSeSeD/miR-21i/Apt/HA. The cell survival rate after treatment with free-DOX, as a native control, and all four PSeSe derived nanomedicines displays a decreasing pattern as DOX concentration increases from 0.1 to 2.5 µg mL⁻¹. However, the degree of such decreases varies, and a significant drop in cell survival rate after PSeSeD/HA is incorporated with miR-21i and Apt indicates the synergistic effects (Figure 5.3C). PSeSeD/HA without miR-21i compared to free-DOX shows slightly lower performance. That is, at a DOX concentration of 2.5 µg mL⁻¹, the cell survival rate is 57.9 ±

4.2 % for PSeSeD/HA and 50.5 ± 3.8 % for free-DOX. Lower than a half amount of the loaded DOX released from PSeSeD/HA over 48 h (Figure 5.1A) to cytosol may be less than the amount of free-DOX localized within the cells. For the PSeSeD/miR-21i/HA, the anticancer effect is enhanced with a drop in the survival rate to $36.6 \pm 4.0\%$ at the same DOX concentration of $2.5 \mu\text{g mL}^{-1}$. Blocking the miR-21 activity by miR-21i can upregulate PDCD4 which activates apoptosis [48]. To isolate ATP by Apt, the PSeSeD/Apt/HA also shows good anticancer effect with a cell survival rate of 35.3 ± 4.1 %. ATP depletion by Apt can activate adenosine monophosphate-activated protein kinase (AMPK) which leads to cancer cell cycle arrest via p27 and apoptosis via p53 [49]. The anticancer synergy effect is amplified when DOX is delivered together with miR-21i and Apt via PSeSeD/miR-21i/Apt/HA with a minimum cell survival rate of 29.1 ± 4.7 % at a DOX concentration of $2.5 \mu\text{g mL}^{-1}$.

5.3.8 Effect of ATP on therapeutic effects on multidrug resistant cancer cells

5.3.8.1 DOX resistance of MDA-MB-231-R

Multidrug resistance of cancer cells enables exporting DOX from intracellular to extracellular environment using ABC transporters with consumption of ATP. Delivery of Apt into cancer cells allows inactivation of the ABC transporters by depletion of ATP with Apt. PSeSeD/miR-21i/Apt/HA was designed to enhance the anticancer effect on cancer cells with multidrug resistance. We cultured MDA-MB-231 cells in the presence of DOX for 12 weeks to produce the drug-resistance MDA-MB-231 cells (MDA-MB-231-R). DOX resistance of MDA-MB-231-R was evaluated via the cell viability assay at DOX concentrations from 0.1 to $2.5 \mu\text{g mL}^{-1}$ in every four weeks for 12 weeks, and indicated 4 weeks (4 W), 8 weeks (8 W), and 12 weeks (12 W) with DOX-sensitive MDA-MB-231 (0 W) as a control. In Figure 5.4A, the survival rate of cells displays an ascending pattern as increasing the incubation time from 0 to 12 W, while viable cells decrease as DOX concentration increases. Half of the MDA-MB-231 cells are viable at 0 W at a DOX concentration of $2.5 \mu\text{g mL}^{-1}$, the number of viable cells rises up to

two third at 8 W and further climbs to 70.7 ± 7.9 % at 12 W, confirming that cells become more resistant to DOX. The resistance of MDA-MB-231-R cells to DOX may be caused by upregulated expression of ABC transporters on the cell membrane due to an increasing efflux of DOX, supported by Saxena et al. via reverse transcription-polymerase chain reaction (RT-PCR) and by Dordal et.al via kinetic analysis of DOX efflux by the exporters [11, 50]. In addition to upregulated expression of ABC transporters, DNA damage of the breast cancer cells by DOX induces NF-kB activation to upregulate oncogenic microRNA-21 expression which can helps the cancer cells avoiding DNA-damage-derived apoptosis by DOX, increasing DOX resistance to the cells [9].

5.3.8.2 ATP assay depending on Apt treatment

ATP directly influences cancer cell survival and MDR via activation of AMPK and ABC transporters [49, 51]. To clarify ATP creation and depletion by MDR and Apt treatment, ATP in MDA-MB-231 (231-S) and MDA-MB-231-R (231-R) cells was quantified depending on Apt treatment with PSeSe/Apt/HA as Apt presence and PSeSe/HA as Apt absence.

The ATP contents in these cells was determined using an ATP bioluminescent somatic cell assay kit and a fluorophotometer (ex. 350 nm wavelength) with a correlation of the intensity of luciferin fluorescence at 530 nm with the mole of ATP from a calibration curve (Figure 5.S9). In the presence of ATP in the mixture of luciferin and luciferase, the intensity of luciferin fluorescence is decreased (Figure 5.S10) as ATP reacts with luciferin via luciferase to produce adeny-luciferin and reduce the amount of luciferin associated with fluorescence [52]. In the absence of Apt, the ATP quantity of 0.418 ± 0.021 pmol in a 231-S cell increases to 0.555 ± 0.019 pmol in a 231-R (Figure 5.4B), indicating that cells with MDR requires 33 % more ATP than cells without MDR, and the ATP may be consumed for ABC transporters. On the other hand, 231-R after Apt treatment display ATP depletion by more than 36 % to an ATP amount

of 0.353 ± 0.027 pmol per cell (Figure 5.4B). Therefore, the Apt treatment from PSeSe/Apt/HA depletes ATP inside cells.

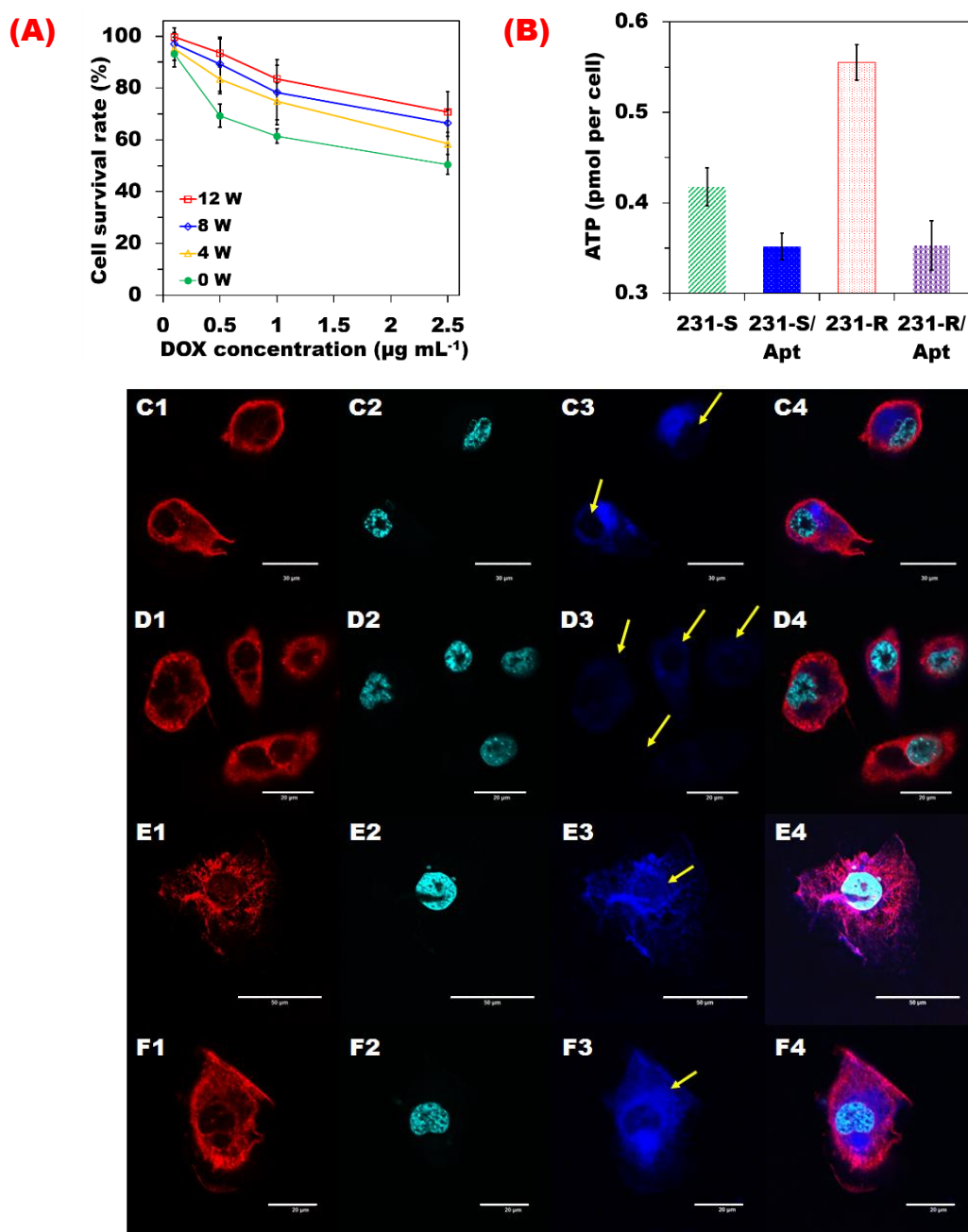


Figure 5.4 (A) Cell viability assay of DOX with diverse concentrations on multidrug-resistant MDA-MB-231-R cells with various culturing periods of 4 weeks (4 W), 8 weeks (8 W) and 12 weeks (12 W), and DOX-sensitive MDA-MB-231 cells (0 W) as a control ($n = 4$), (B) ATP content assays on DOX-sensitive MDA-MB-231 (231-S) cells, DOX-resistant MDA-MB-231-R (231-R) cells and those cells with ATP aptamer treatment (231-S/Apt and 231-R/Apt), via a spectrofluorophotometer, ($n = 3$). Tracing MDA-MB-231-R cell localization of DOX released from (C) PSeSeDBHQ/HA for 24 h (scale bar 30 μm), (D) PSeSeDBHQ/HA for 48 h (scale bar 20 μm), (E) PSeSeDBHQ/Apt/HA for 24 h (scale bar 50 μm), (F) PSeSeDBHQ/Apt/HA

for 48 h (scale bar 20 μm). Colors of red, cyan, blue and overlaps in the low from 1 to 4 of CLSM images are cell membrane, cell nucleus, DOX and the merged.

5.3.8.3 Apt effects on MDA-MB-231-R via tracing DOX intracellular localization

To confirm whether delivery of Apt into cancer cells affects the ABC transporters of MDA-MB-231-R cells, intracellular localization of DOX released from PSeSeDBHQ/Apt/HA (in the presence of Apt) and PSeSeDBHQ/HA (in the absence of Apt) were traced via detecting fluorescence of DOX (blue), membrane (red) and nucleus (cyan) under a CLSM after incubation of cells with two therapeutics for 24 and 48 h. As loaded DOX is quenched by BHQ of both therapeutics (Figure 5.2F), a blue color appearing in the images is associated with released DOX from the therapeutics. In the absence of Apt, a strong blue color is located between red and cyan in Figure 5.4C at 24 h after incubation of cells with PSeSeDBHQ/HA, indicating DOX is released intracellularly into cytosol. However, the blue color becomes dim in cells after 24-h incubation in Figure 5.4D, which may be due to expulsion of intracellularly localized DOX into an extracellular environment via ABC transporters. However, in the presence of Apt, strong blue color overlaps red and cyan colors in both Figures 5.4E and 5.4F for 24 and 48 h incubation, indicating DOX is localized inside nuclei and sustainably released from PSeSeDBHQ/Apt/HA for 48 h. Therefore, MDA-MB-231-R cells consumes more ATP for activation of ABC transporters to expel intracellularly localized DOX to an extracellular environment, however, Apt treatment by PSeSeDBHQ/Apt/HA depletes ATP in the multidrug resistant cells and inhibits the DOX exporters, thereby enhancing localization of DOX in nuclei to trigger DNA damage and apoptosis.

5.3.9 Therapeutic synergy on multidrug resistance cancer cells by PSeSeD/miR-21i/Apt/HA

PSeSeD/miR-21i/Apt/HA was designed to maximize therapeutic effects on multidrug resistant cancer cells. The therapeutic efficacy of PSeSeD/miR-21i/Apt/HA was evaluated by the cell viability of MDA-MB-231-R at DOX concentrations from 0.1 to 2.5 $\mu\text{g mL}^{-1}$ in comparison with free-DOX, PSeSeD/HA, PSeSeD/Apt/HA, and PSeSeD/miR-21i/HA.

Figure 5.5A shows the survival rate of MDA-MB-231-R cells has a descending trend as increasing DOX concentration for all samples. The anticancer effect of DOX-incorporated therapeutic products on the cells with MDR outweighs that of free-DOX for the entire DOX concentrations investigated. The cell survival rate of more than 70 % treated by free-DOX at a DOX concentration of 2.5 $\mu\text{g mL}^{-1}$ is decreased by around 30 % to 41.5 ± 6.8 % after treatment with PSeSeD/HA. DOX sustainably released from PSeSeD/HA in cytosol is expelled by ABC transporters in the transmembrane of multidrug resistant cells [11], while the amount of DOX from PSeSeD/HA may be far lower than that from free-DOX which is permeated in the cells through their transmembrane. More DOX from PSeSeD/HA remains in cells than free-DOX, leading to a higher anticancer effect on the cells.

Comparing to PSeSeD/HA, PSeSeD/Apt/HA, co-delivery of Apt with DOX, has an improved therapeutic efficacy with two-third of the cell death at a DOX concentration of 2.5 $\mu\text{g mL}^{-1}$. Apt depletes ATP in the MDA-MB-231-R (Figure 5.4B), inhibiting ABC transporters to expel the released DOX from inside of the cells, and thereby prolonging intracellular localization of the released DOX (Figure 5.4F). In addition, ATP depletion can induce the cell cycle arrest and apoptosis by upregulating AMPK [49]. Beside, treatment with MDA-MB-231-R cells with PSeSeD/miR-21i/HA, co-delivery of miR-21i with DOX, significantly reduces the amount of viable multidrug resistant cells to 20.6 ± 3.2 % at a DOX concentration of 2.5 $\mu\text{g mL}^{-1}$. Inhibition of miR-21 activity by miR-21i from PSeSeD/miR-21i/HA may re-sensitize the

cancer cells with MDR to DOX with upregulation of PTEN and activate apoptosis with upregulation of PDCD4 [18, 53, 54].

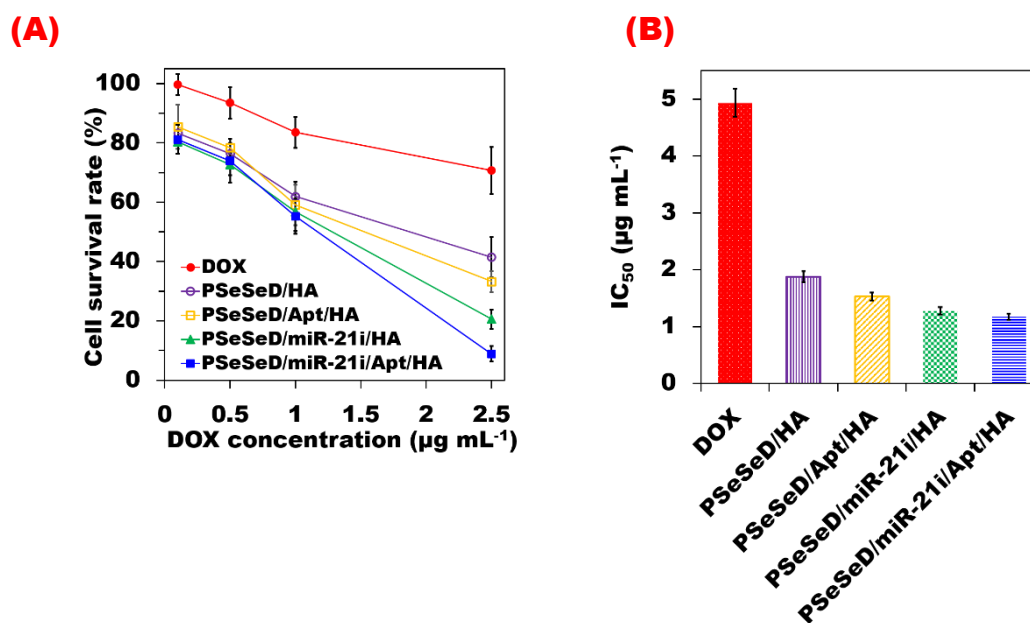


Figure 5.5 Cell viability assay on anticancer effects of free-DOX, PSeSeD/HA, PSeSeD/Apt/HA, PSeSeD/miR-21i/HA and PSeSeD/miR-21i/Apt/HA on multidrug resistant MDA-MB-231-R cells with (A) the cell survival rate to DOX loaded concentrations (n = 12) and (B) DOX concentration for one half cell death, IC₅₀ value.

The most effective therapeutic treatment on MDA-MB-231-R cells is achieved by administration of DOX, miR-21i, and Apt using PSeSeD/miR-21i/Apt/HA, as 8.9 ± 2.6 % of the cell survival is detected at a DOX concentration of $2.5 \mu\text{g mL}^{-1}$. The DOX concentration at which one half of MDA-MB-231-R cells are viable, IC₅₀, is $4.93 \mu\text{g mL}^{-1}$ for free-DOX and it remarkably reduces to $1.17 \mu\text{g mL}^{-1}$ for PSeSeD/miR-21i/Apt/HA (Figure 5.5B). PSeSeD/miR-21i/Apt/HA displays its therapeutic effects on the cancer cells with MDR 4.2-times higher than free-DOX, which means the dose of DOX from PSeSeD/miR-21i/Apt/HA required to achieve the identical anti-cancer effect 4.2-folds less than that from free-DOX. The IC₅₀ values of PSeSeD/Apt/HA and PSeSeD/miR-21i/HA (co-delivery of DOX with Apt or miR-21i) and PSeSeD/HA (mono-delivery of DOX) are 1.1 to 1.6 times higher than that of

PSeSeD/miR-21i/Apt/HA. Therefore, administration of PSeSeD/miR-21i/Apt/HA enhances the therapeutic efficacy of DOX on multidrug resistant cancer cells than nanomedicines with mono-drug or co-drug. PSeSeD/miR-21i/Apt/HA with significantly improved anticancer effects on both DOX sensitive and resistant cells has great promise in therapeutic applications to patients with a multidrug resistant cancer.

5.4 Conclusion

We have successfully demonstrated a nanomedicine for tri-delivery of DOX, miR-21i, and Apt with significantly improved anticancer effect on metastatic cancer cells with multidrug resistance but minimized side effects. The nanomedicine was produced via crosslinking PEI800 and DOX by diselenide crosslinkers, electrostatically interacting with miR-21i and Apt, and finally surface coating with HA. Great biocompatibility of the nanomedicine is achieved from benign PEI800 PSeSeD microgels and their degraded-products, as well as minimal leakage during blood circulation due to its stability in the physiological environment and reduced accumulation in normal cells due to HA coating. Its therapeutic efficacy of the nanomedicine on multidrug resistant cancer cells is realized through structure features with negative charges and a size of 140 nm for reduced systemic clearance and the EPR effect in the tumor site, HA receptor-mediated endocytosis for accurate target on cancer cells, inhibition of miR-21 by miR-21i for re-sensitizing the multidrug resistant cells to DOX, inactivation of ABC transporters via depleting ATP by Apt, and control release of DOX intracellularly due to its specific response to intracellular tumor microenvironment. This nanomedicine will be explored for its therapeutic application in eradicating multidrug resistant cancer cells in the animal model as well as patients.

Acknowledgement

We are grateful for the research grant of the Australian Research Council DP110102877 and DP140104062. SY would like to appreciate the APA scholarship provided by the University of Adelaide. We also thank Byeongjun An for assisting scheme design.

References

- [1] C. Porta, C. Paglino, A. Mosca, Targeting PI3K/Akt/mTOR Signaling in Cancer, *Front. Oncol.*, 4 (2014) 64-64.
- [2] P. Blume-Jensen, T. Hunter, Oncogenic kinase signalling, *Nature*, 411 (2001) 355-365.
- [3] E. Austreid, S. Knappskog, P.E. Lonning, H.P. Eikesdal, The influence of doxorubicin on PTEN and PI3K-Akt-mTOR signaling in human breast cancer, *Cancer Res.*, 73 (2013) P5-08-05-P05-08-05.
- [4] N. Kumar, N. Wethkamp, L.C. Waters, M.D. Carr, K.H. Klempnauer, Tumor suppressor protein Pcd4 interacts with Daxx and modulates the stability of Daxx and the Hipk2-dependent phosphorylation of p53 at serine 46, *Oncogenesis*, 2 (2013) e37.
- [5] N. Pilco-Ferreto, G.M. Calaf, Influence of doxorubicin on apoptosis and oxidative stress in breast cancer cell lines, *Int. J. Oncol.*, 49 (2016) 753-762.
- [6] R.W. Lin, C.J. Ho, H.W. Chen, Y.H. Pao, L.E. Chen, M.C. Yang, S.B. Huang, S. Wang, C.H. Chen, C. Wang, P53 enhances apoptosis induced by doxorubicin only under conditions of severe DNA damage, *Cell Cycle*, 17 (2018) 2175-2186.
- [7] J. Deng, D. Coy, W. Zhang, M. Sunkara, A.J. Morris, C. Wang, L. Chaiswing, D. St Clair, M. Vore, P. Jungsuwadee, Elevated glutathione is not sufficient to protect against doxorubicin-induced nuclear damage in heart in multidrug resistance-associated protein 1 (Mrp1/Abcc1) null mice, *J. Pharmacol. Exp. Ther.*, 355 (2015) 272-279.
- [8] C. Leontiou, J.H. Lakey, C.A. Austin, Mutation E522K in Human DNA Topoisomerase II β Confers Resistance to Methyl N-(4'-(9-acridinylamino)-phenyl)carbamate hydrochloride and Methyl N-(4'-(9-acridinylamino)-3-methoxy-phenyl) methane sulfonamide but Hypersensitivity to Etoposide, *Mol. Pharmacol.*, 66 (2004) 430-439.
- [9] J. Niu, Y. Shi, G. Tan, C.H. Yang, M. Fan, L.M. Pfeffer, Z.-H. Wu, DNA Damage Induces NF- κ B-dependent MicroRNA-21 Up-regulation and Promotes Breast Cancer Cell Invasion, *J. Biol. Chem.*, 287 (2012) 21783-21795.
- [10] D.R. Gutsaeva, M. Thounaojam, S. Rajpurohit, F.L. Powell, P.M. Martin, S. Goei, M. Duncan, M. Bartoli, STAT3-mediated activation of miR-21 is involved in down-regulation of TIMP3 and neovascularization in the ischemic retina, *Oncotarget*, 8 (2017) 103568-103580.
- [11] M. Saxena, M.A. Stephens, H. Pathak, A. Rangarajan, Transcription factors that mediate epithelial-mesenchymal transition lead to multidrug resistance by upregulating ABC transporters, *Cell Death Dis.*, 2 (2011) e179.
- [12] K.P. Locher, Review. Structure and mechanism of ATP-binding cassette transporters, *Philos. Trans. R. Soc. Lond. B Biol. Sci.*, 364 (2009) 239-245.
- [13] Z. Liu, A.C. Fan, K. Rakhra, S. Sherlock, A. Goodwin, X. Chen, Q. Yang, D.W. Felsher, H. Dai, Supramolecular Stacking of Doxorubicin on Carbon Nanotubes for In Vivo Cancer Therapy, *Angew. Chem. Int. Ed.*, 48 (2009) 7668-7672.

- [14] S.M. Swain, F.S. Whaley, M.S. Ewer, Congestive heart failure in patients treated with doxorubicin, *Cancer*, 97 (2003) 2869-2879.
- [15] E.C. Bredahl, K.B. Pfannenstiel, C.J. Quinn, R. Hayward, D.S. Hydock, Effects of Exercise on Doxorubicin-Induced Skeletal Muscle Dysfunction, *Med. Sci. Sports Exerc.*, 48 (2016) 1468-1473.
- [16] C.-C. Peng, C.-L. Hsieh, Y.-B. Ker, H.-Y. Wang, K.-C. Chen, R.Y. Peng, Selected nutraceutical screening by therapeutic effects on doxorubicin-induced chronic kidney disease, *Mol. Nutr. Food Res.*, 56 (2012) 1541-1558.
- [17] G. Damodar, T. Smitha, S. Gopinath, S. Vijayakumar, Y. Rao, An evaluation of hepatotoxicity in breast cancer patients receiving injection Doxorubicin, *Ann. Med. Health Sci. Res.*, 4 (2014) 74-79.
- [18] Z.-X. Wang, B.-B. Lu, H. Wang, Z.-X. Cheng, Y.-M. Yin, MicroRNA-21 Modulates Chemosensitivity of Breast Cancer Cells to Doxorubicin by Targeting PTEN, *Arch. Med. Res.*, 42 (2011) 281-290.
- [19] S. Zhang, L. Han, J. Wei, Z. Shi, P. Pu, J. Zhang, X. Yuan, C. Kang, Combination treatment with doxorubicin and microRNA-21 inhibitor synergistically augments anticancer activity through upregulation of tumor suppressing genes, *Int. J. Oncol.*, 46 (2015) 1589-1600.
- [20] A.V. Lakhin, V.Z. Tarantul, L.V. Gening, Aptamers: problems, solutions and prospects, *Acta Naturae*, 5 (2013) 34-43.
- [21] W.D. Pu, L. Zhang, C.Z. Huang, Graphene oxide as a nano-platform for ATP detection based on aptamer chemistry, *Anal Methods-Uk*, 4 (2012) 1662-1666.
- [22] P. Yu, X. He, L. Zhang, L. Mao, Dual Recognition Unit Strategy Improves the Specificity of the Adenosine Triphosphate (ATP) Aptamer Biosensor for Cerebral ATP Assay, *Anal. Chem.*, 87 (2015) 1373-1380.
- [23] H. Wang, Y. Li, M. Zhang, D. Wu, Y. Shen, G. Tang, Y. Ping, Redox-Activatable ATP-Depleting Micelles with Dual Modulation Characteristics for Multidrug-Resistant Cancer Therapy, *Adv. Healthc. Mater.*, 6 (2017).
- [24] S.M. Moghimi, P. Symonds, J.C. Murray, A.C. Hunter, G. Debska, A. Szewczyk, A two-stage poly(ethylenimine)-mediated cytotoxicity: implications for gene transfer/therapy, *Mol. Ther.*, 11 (2005) 990-995.
- [25] S.P. Mukherjee, H.J. Byrne, Polyamidoamine dendrimer nanoparticle cytotoxicity, oxidative stress, caspase activation and inflammatory response: experimental observation and numerical simulation, *Nanomed. Nanotechnol. Biol. Med.*, 9 (2013) 202-211.
- [26] M. Thiersch, M. Rimann, V. Panagiotopoulou, E. Öztürk, T. Biedermann, M. Textor, T.C. Lühmann, H. Hall, The angiogenic response to PLL-g-PEG-mediated HIF-1 α plasmid DNA delivery in healthy and diabetic rats, *Biomaterials*, 34 (2013) 4173-4182.
- [27] B. Zhang, H. Zhang, S. Dai, J. Bi, Cell-penetrating peptide-labelled smart polymers for enhanced gene delivery, *Eng. Life Sci.*, 17 (2017) 193-203.

- [28] W. Gao, C.M. Hu, R.H. Fang, L. Zhang, Liposome-like Nanostructures for Drug Delivery, *J. Mater. Chem. B*, 1 (2013) 6569-6585.
- [29] C.F. van Nostrum, Covalently cross-linked amphiphilic block copolymer micelles, *Soft Matter*, 7 (2011) 3246-3259.
- [30] Q. Zhao, Y. Lin, N. Han, X. Li, H. Geng, X. Wang, Y. Cui, S. Wang, Mesoporous carbon nanomaterials in drug delivery and biomedical application, *Drug Deliv.*, 24 (2017) 94-107.
- [31] S. Shen, D. Jiang, L. Cheng, Y. Chao, K. Nie, Z. Dong, C.J. Kuttyreff, J.W. Engle, P. Huang, W. Cai, Z. Liu, Renal-Clearable Ultrasmall Coordination Polymer Nanodots for Chelator-Free ⁶⁴Cu-Labeling and Imaging-Guided Enhanced Radiotherapy of Cancer, *ACS Nano*, 11 (2017) 9103-9111.
- [32] S.H. Ku, K. Kim, K. Choi, S.H. Kim, I.C. Kwon, Tumor-Targeting Multifunctional Nanoparticles for siRNA Delivery: Recent Advances in Cancer Therapy, *Adv. Healthc. Mater.*, 3 (2014) 1182-1193.
- [33] T. Wang, J.R. Upponi, V.P. Torchilin, Design of multifunctional non-viral gene vectors to overcome physiological barriers: Dilemmas and strategies, *Int. J. Pharm.*, 427 (2012) 3-20.
- [34] H. Wang, Y. Jiang, H. Peng, Y. Chen, P. Zhu, Y. Huang, Recent progress in microRNA delivery for cancer therapy by non-viral synthetic vectors, *Adv. Drug Del. Rev.*, 81 (2015) 142-160.
- [35] E. Ball, J. McDermott, J. Griffin, F. Davey, R. Davis, C. Bloomfield, Expression of the three myeloid cell-associated immunoglobulin G Fc receptors defined by murine monoclonal antibodies on normal bone marrow and acute leukemia cells, *Blood*, 73 (1989) 1951-1956.
- [36] L. Otvos, Jr., J.D. Wade, Current challenges in peptide-based drug discovery, *Front. Chem.*, 2 (2014) 62.
- [37] S. Misra, V.C. Hascall, R.R. Markwald, S. Ghatak, Interactions between Hyaluronan and Its Receptors (CD44, RHAMM) Regulate the Activities of Inflammation and Cancer, *Front. Immunol.*, 6 (2015) 201.
- [38] M.C. Tan, G.M. Chow, L. Ren, Q. Zhang, Inorganic Nanoparticles for Biomedical Applications, in: D. Shi (Ed.) *NanoScience in Biomedicine*, Springer Berlin Heidelberg, Berlin, Heidelberg, 2009, pp. 272-289.
- [39] Z. Medarova, W. Pham, C. Farrar, V. Petkova, A. Moore, In vivo imaging of siRNA delivery and silencing in tumors, *Nat. Med.*, 13 (2007) 372.
- [40] I.A. Rahman, P. Vejayakumaran, C.S. Sipaut, J. Ismail, C.K. Chee, Size-dependent physicochemical and optical properties of silica nanoparticles, *Mater. Chem. Phys.*, 114 (2009) 328-332.
- [41] V. De Matteis, Exposure to Inorganic Nanoparticles: Routes of Entry, Immune Response, Biodistribution and In Vitro/In Vivo Toxicity Evaluation, *Toxics*, 5 (2017) 29.

- [42] S.A. Marras, F.R. Kramer, S. Tyagi, Efficiencies of fluorescence resonance energy transfer and contact-mediated quenching in oligonucleotide probes, *Nucleic Acids Res.*, 30 (2002) e122.
- [43] Y. Zhang, T.-H. Wang, Quantum Dot Enabled Molecular Sensing and Diagnostics, *Theranostics*, 2 (2012) 631-654.
- [44] H. Yin, R.L. Kanasty, A.A. Eltoukhy, A.J. Vegas, J.R. Dorkin, D.G. Anderson, Non-viral vectors for gene-based therapy, *Nat. Rev. Genet.*, 15 (2014) 541-555.
- [45] S.R. Hamilton, S.F. Fard, F.F. Paiwand, C. Tolg, M. Veiseh, C. Wang, J.B. McCarthy, M.J. Bissell, J. Koropatnick, E.A. Turley, The hyaluronan receptors CD44 and Rhamm (CD168) form complexes with ERK1,2 that sustain high basal motility in breast cancer cells, *J. Biol. Chem.*, 282 (2007) 16667-16680.
- [46] L. Lusini, S.A. Tripodi, R. Rossi, F. Giannerini, D. Giustarini, M.T. del Vecchio, G. Barbanti, M. Cintorino, P. Tosi, P. Di Simplicio, Altered glutathione anti-oxidant metabolism during tumor progression in human renal-cell carcinoma, *Int. J. Cancer*, 91 (2001) 55-59.
- [47] M. Pljesa-Ercegovac, J. Mimic-Oka, D. Dragicevic, A. Savic-Radojevic, M. Opacic, S. Pljesa, R. Radosavljevic, T. Simic, Altered antioxidant capacity in human renal cell carcinoma: role of glutathione associated enzymes, *Urol. Oncol.*, 26 (2008) 175-181.
- [48] L. Frankel, N. Christoffersen, A. Jacobsen, M. Lindow, A. Krogh, A. Lund, Programmed cell death 4 (PDCD4) is an important functional target of the microRNA miR-21 in breast cancer cells, *J. Biol. Chem.*, 283 (2008) 1026 - 1033.
- [49] N. El Mjiyad, A. Caro-Maldonado, S. Ramírez-Peinado, C. Muñoz-Pinedo, Sugar-free approaches to cancer cell killing, *Oncogene*, 30 (2010) 253.
- [50] M.S. Dordal, J.N. Winter, A.J. Atkinson, Kinetic analysis of P-glycoprotein-mediated doxorubicin efflux, *J. Pharmacol. Exp. Ther.*, 263 (1992) 762-766.
- [51] B. Baguley, Multiple Drug Resistance Mechanisms in Cancer, *Mol. Biotechnol.*, 46 (2010) 308-316.
- [52] C. Sørensen, I. Novak, Visualization of ATP Release in Pancreatic Acini in Response to Cholinergic Stimulus, *J. Biol. Chem.*, 276 (2001) 32925-32932.
- [53] W. Hu, C. Tan, Y. He, G. Zhang, Y. Xu, J. Tang, Functional miRNAs in breast cancer drug resistance, *Onco Targets Ther.*, 11 (2018) 1529-1541.
- [54] P.M. Costa, A.L. Cardoso, C. Nóbrega, L.F. Pereira de Almeida, J.N. Bruce, P. Canoll, M.C. Pedroso de Lima, MicroRNA-21 silencing enhances the cytotoxic effect of the antiangiogenic drug sunitinib in glioblastoma, *Hum. Mol. Genet.*, 22 (2013) 904-918.

Supporting information

Developing traceable nanomedicines of doxorubicin, miR-21 inhibitor and ATP aptamer for enhanced therapeutic treatment on multidrug resistant cancers

*Seonho Yun, Mahdhir Bin Amat Tugiman, Jiabin Zhang, Hu Zhang, Jingxiu Bi, Sheng Dai**

Table 5.S1 Characterizations of synthesized microgels of PSeSeD, PSeSeD2X, PSeSeDBHQ, PSeSe, and Degrade-P.

Name of microgels	Hydrodynamic size (d.nm)	Zeta potential (mV)	Absorbance wavelength (nm)	DOX loading (wt. %)	miR-21i full loading (N/P)
PSeSeD	218.7 ± 13.4	58.3 ± 1.4	488.0	9.35	6
PSeSeD2X	136.8 ± 24.3	31.5 ± 4.5	482.0	16.5	10
PSeSeDBHQ	249.6 ± 18.3	39.3 ± 5.9	541.5	N/A	8
PSeSe	260.0 ± 22.9	68.3 ± 0.68	N/A	N/A	3
Degrade-P	3.7 ± 1.9	0.96 ± 3.9	N/A	N/A	N/A

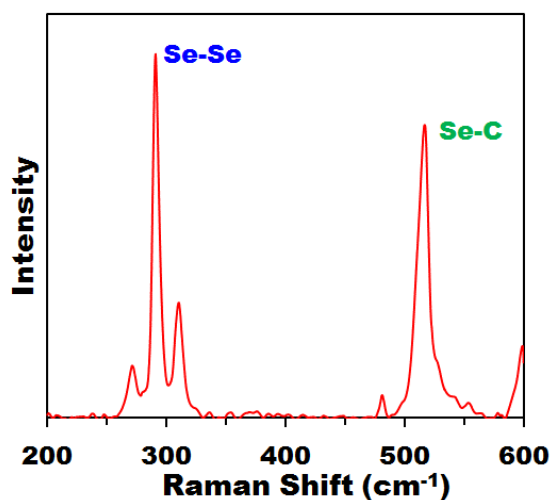


Figure 5.S1 Raman spectrum of diselenide crosslinker of $-\text{SeSe}-$

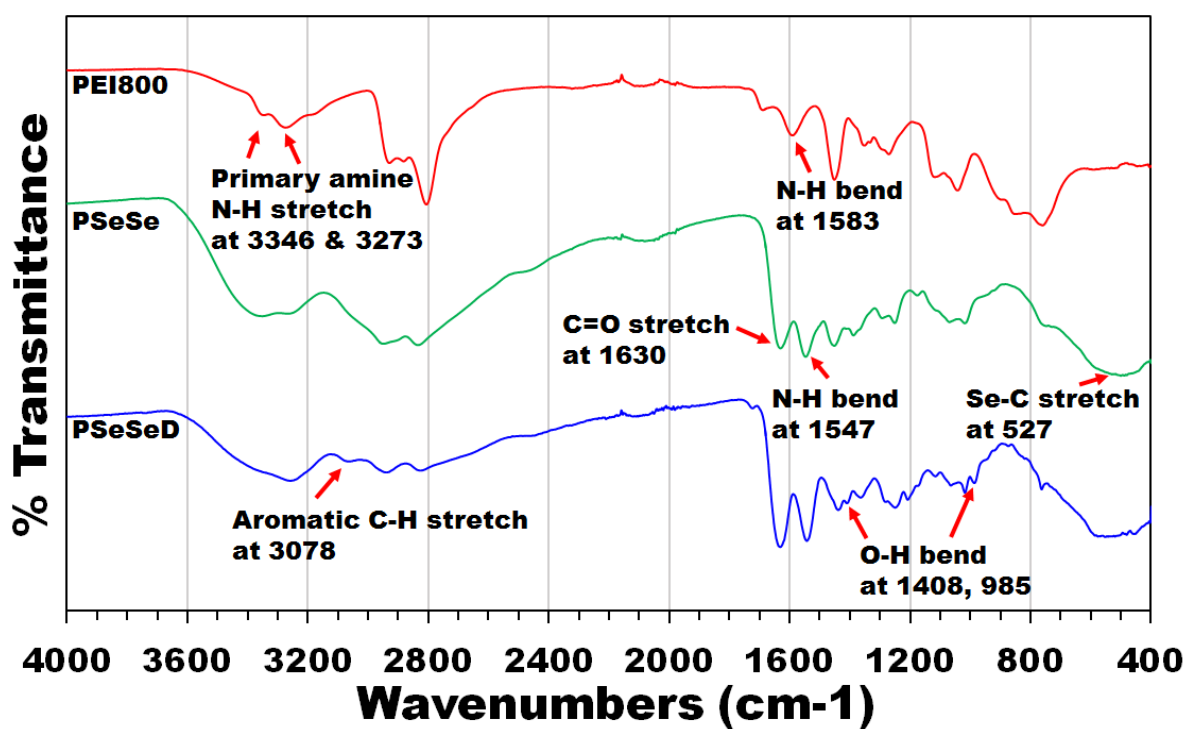


Figure 5.S2 FTIR spectra of PEI800, synthesized microgels of PSeSe and PSeSeD

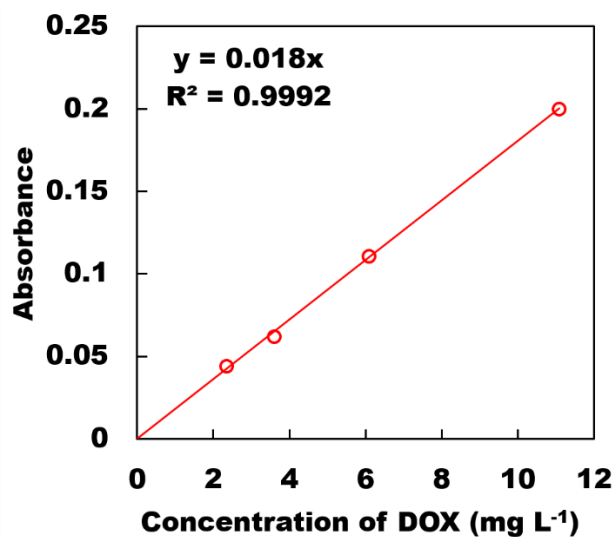


Figure 5.S3 Calibration curve of DOX at 479.5 nm, observed in a UV-vis spectrophotometer

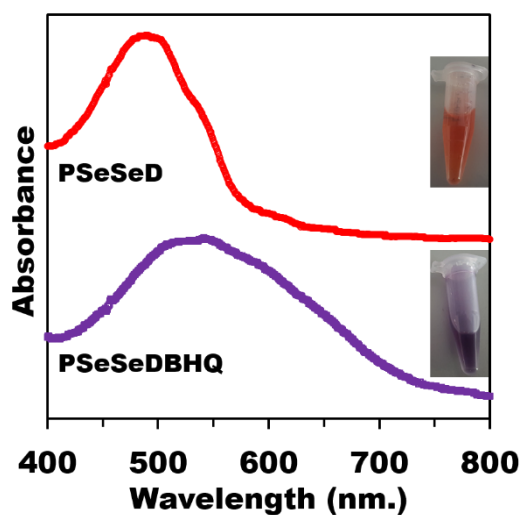


Figure 5.S4 Absorbance spectra of PSeSeD and PSeSeDBHQ from 400 to 800 nm wavelength, and their aqueous solution colors.

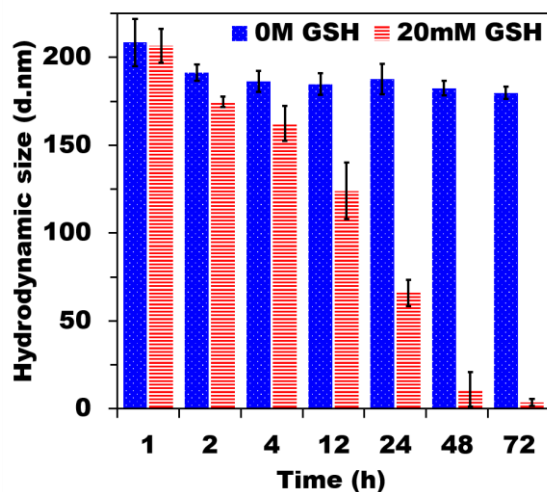


Figure 5.S5 Hydrodynamic size profiles of PSeSe microgels in pH 7.4 and 20 mM GSH over 72 h with 0 M GSH as a negative control.

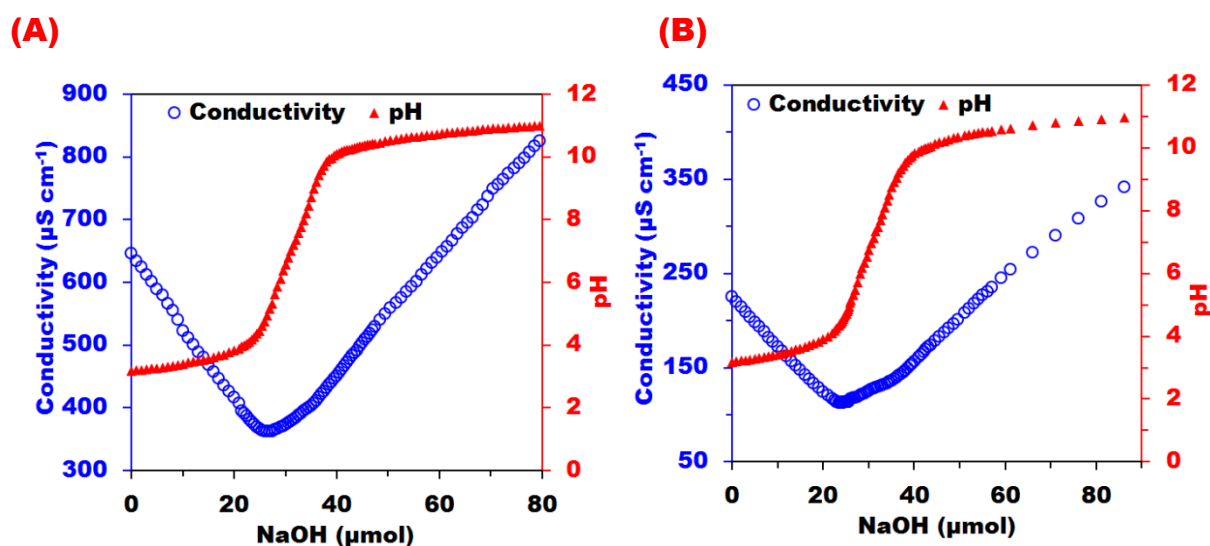


Figure 5.S6 Amine content assays via conductivity and pH titration of (A) PSeSeD microgels (2.5 mg) and (B) PSeSe microgels (2.4 mg)

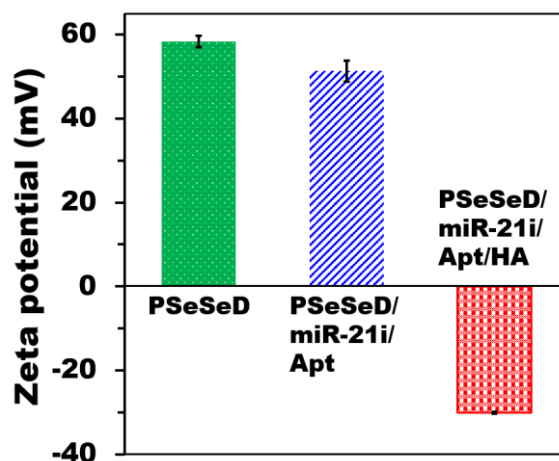
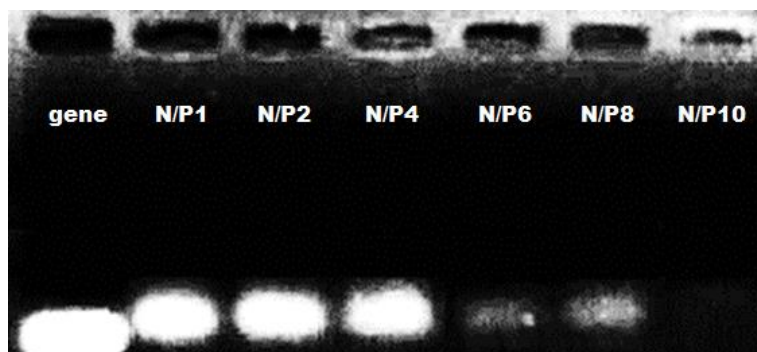
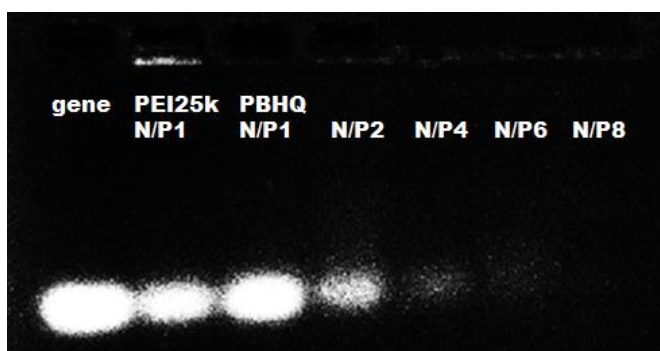


Figure 5.S7 Zeta potentials of PSeSeD, PSeSeD/miR-21i/Apt (N/P 10) and PSeSeD/miR-21i/Apt/HA (N/P 10 and 1.5 wt. of HA to PSeSeD) in 10 mM NaCl solution at pH 7.4.

(A)



(B)



(C)

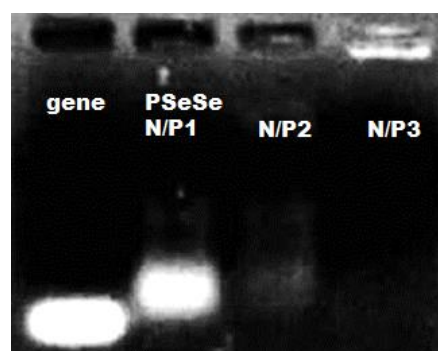


Figure 5.S8 miR-21i and Apt loading assay via agarose gel electrophoresis for (A) PSeSeD2X at N/P ratios from 1 to 10, (B) PSeSeDBHQ at N/P ratios (1, 2, 4, 6 and 8) with PEI25k at N/P 1 as positive control, (C) PSeSe microgels at N/P ratios (1, 2 and 3). Naked gene (miR-21i) in the left-end lane as a control.

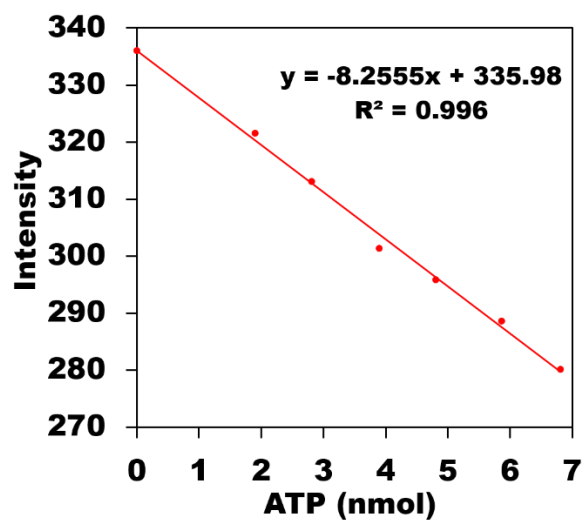


Figure 5.S9 Calibration curve of fluorescence intensity of luciferin (ex. 350 and em. 530 nm wavelength) to ATP concentrations, which is detected from a spectrofluorophotometer.

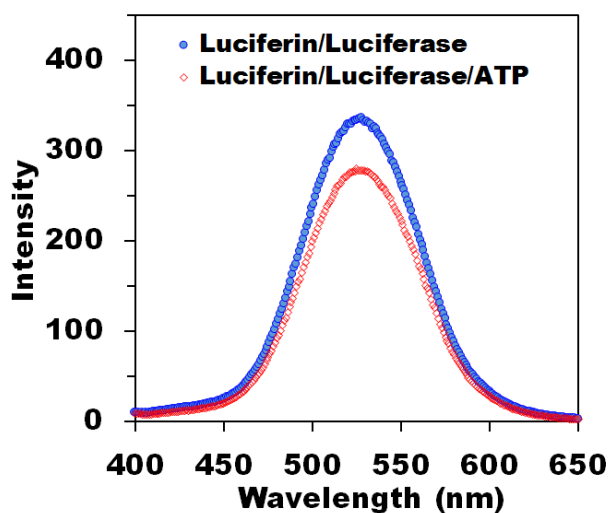


Figure 5.S10 Fluorescence spectra of luciferin with/without ATP in presence of luciferase, measuring a spectrofluorophotometer with excitation at 350 nm wavelength.

Chapter 6 DEVDC peptide conjugated microgels for intracellular-responsive sequential releasing of miRNA-21 inhibitor and doxorubicin for enhanced therapy to multidrug resistant cancers

*Seonho Yun, Jiabin Zhang, Hu Zhang, Jingxiu Bi, Sheng Dai**

S. Yun, J. Zhang, Prof. H. Zhang, Prof. J. Bi, Prof. S. Dai

School of Chemical Engineering, the University of Adelaide, Adelaide, SA 5005, Australia

Prof. H. Zhang

Amgen Bioprocessing Centre, Keck Graduate Institute, 535 Watson Drive, Claremont, CA 91711, United States

Prof. S. Dai

Department of Chemical Engineering, Brunel University London, Uxbridge, UB8 3PH, United Kingdom

sheng.dai@brunel.ac.uk

Statement of Authorship

Title of Paper	DEVDC peptide conjugated microgels for intracellular-responsive sequential releasing of miRNA-21 inhibitor and doxorubicin for enhanced therapy to multidrug resistant cancers
Publication Status	<input type="checkbox"/> Published <input type="checkbox"/> Accepted for Publication <input type="checkbox"/> Submitted for Publication <input checked="" type="checkbox"/> Unpublished and Unsubmitted work written in manuscript style
Publication Details	In preparation for submission

Principal Author

Name of Principal Author (Candidate)	Seonho Yun		
Contribution to the Paper	Mainly designed the experiment, material synthesis, evaluation, and manuscript writing		
Overall percentage (%)	80 %		
Certification:	This paper reports on the original research I conducted during the period of my Higher Degree by Research candidature and is not subject to any obligations or contractual agreements with a third party that would constrain its inclusion in this thesis. I am the primary author of this paper.		
Signature		Date	20/05/2019

Co-Author Contributions

By signing the Statement of Authorship, each author certifies that:

- i. the candidate's stated contribution to the publication is accurate (as detailed above);
- ii. permission is granted for the candidate to include the publication in the thesis; and
- iii. the sum of all co-author contributions is equal to 100% less the candidate's stated contribution.

Name of Co-Author	Jiabin Zhang		
Contribution to the Paper	Helped to operate evaluation part of the experiment		
Signature		Date	21/02/2019

Name of Co-Author	Hu Zhang		
Contribution to the Paper	Supervised the experiment design, data interpretation, manuscript correction		
Signature		Date	24/02/2019

Name of Co-Author	Jingxiu Bi		
Contribution to the Paper	Proof read the manuscript and evaluation		
Signature		Date	25/02/2019

Name of Co-Author	Sheng Dai		
Contribution to the Paper	Supervised the experiment design, data interpretation, manuscript correction, and corresponding author		
Signature		Date	20/05/2019

Abstract

Doxorubicin (DOX) chemotherapy can actively suppress cancers, but simultaneously develop multidrug resistance (MDR) by upregulating miRNA-21 and DOX exporters, causing serious dose-dependent side-effects. Herein, we introduce a fully degradable microgel-based nanomedicine with the ability of initial releasing miRNA-21 inhibitor (miR-21i) to multidrug-resistant cancer cells and sequential DOX release to these re-sensitized cells for enhancing therapeutic efficiency. Glutathione (GSH)-cleavable polyethyleneimine (PEI) microgel carriers were prepared, DOX was loaded to the carriers via a caspase-3-cleavable DEVDC peptide linker through click chemistry, miR-21i was then loaded through electrostatic interaction with PEI moieties, and finally hyaluronic acid (HA) surface coating was applied to promote HA receptor-mediated endocytosis to target cancer cells. The diselenide crosslinker of PEI microgel carriers can be cleaved in GSH-concentrated cytosol to release miR-21i, followed by miR-21 inhibition, MDR reverse, caspase-3 activation, DEVDC cleavage and cysteine-tailed DOX release. The intracellular microenvironment triggered sequential release profiles can be visually traced using the black hole quencher2 (BHQ2)-labeled microgels together with fluorescence quenching technique. Such a system minimizes DOX efflux to healthy cells and achieves 7.3-folds higher anticancer efficiency to cancer cells than free DOX. Obviously, our reported nanomedicines enable sequential release of miR-21i and DOX to multidrug resistant cells with maximal anticancer efficacy and minimal side-effects.

Keywords: sequential release, DEVDC, caspase-3, DOX, miR-21 inhibitor, multidrug resistance, co-delivery

6.1 Introduction

Doxorubicin as an anthracycline is one of the most effective anticancer chemo-drugs with two apoptotic pathways of topoisomerase II (Topo II) intercalation and reactive oxygen species (ROS) production [1, 2]. On the one hand, DNA replication damage by the isolation of the Topo II activates a tumor suppressor nuclear p53, which initiates apoptotic signaling pathway via upregulating Bcl-2-associated X protein (Bax), releasing cytochrome c from mitochondria, activating caspase-9 and caspase-3 and generating apoptosis [1, 3]. The DNA damage can activate inhibitors in the apoptotic pathway. One of the inhibitors is B-cell lymphoma 2 (Bcl-2) that represses Bax activation in mitochondria [2]. In addition, the phosphoinositide 3-kinase (PI3K) pathway, including protein kinase B (Akt) and mammalian target of rapamycin (mTOR) (PI3K/Akt/mTOR), promotes tumor progression and survivals [4]. Moreover, nuclear factor kappa-light-chain-enhancer of activated B cells (NF- κ B) expresses its downstream gene of microRNA-21 (miR-21) as an inhibitor of phosphatase and tensin homolog (PTEN), which restricts the PI3K pathway [5, 6]. At the same time, oxidative stress by the induction of the ROS from DOX triggers tumor necrosis factor alpha (TNF α)-induced apoptotic pathway via activating caspase-8 and caspase-3 [3]. However, the external apoptotic pathway executes N-terminal phosphorylation of Jun (JNK) signaling pathway including c-Jun [7]. JNK/c-Jun pathway promotes cell survivals by expressing vascular endothelial growth factor (VEGF) for angiogenesis and executing epithelial to mesenchymal transition (EMT) for metastasis [8, 9]. In addition, JNK/c-Jun pathway downregulates p53 for inhibition of mitochondrial apoptosis [10]. The oxidative stress upregulates NF- κ B and VEGF-related signal transducer and activator of transcription 3 (STAT3) for overexpression of miR-21, which inhibits programmed cell death 4 (PDCD4), as an inhibitor of the JNK/c-Jun pathway [2, 9, 11]. Taken together, administration of DOX for anticancer chemotherapy leads to apoptosis by activating caspase-3, but simultaneously enhances resistance to the chemotherapy by overexpressing miR-21.

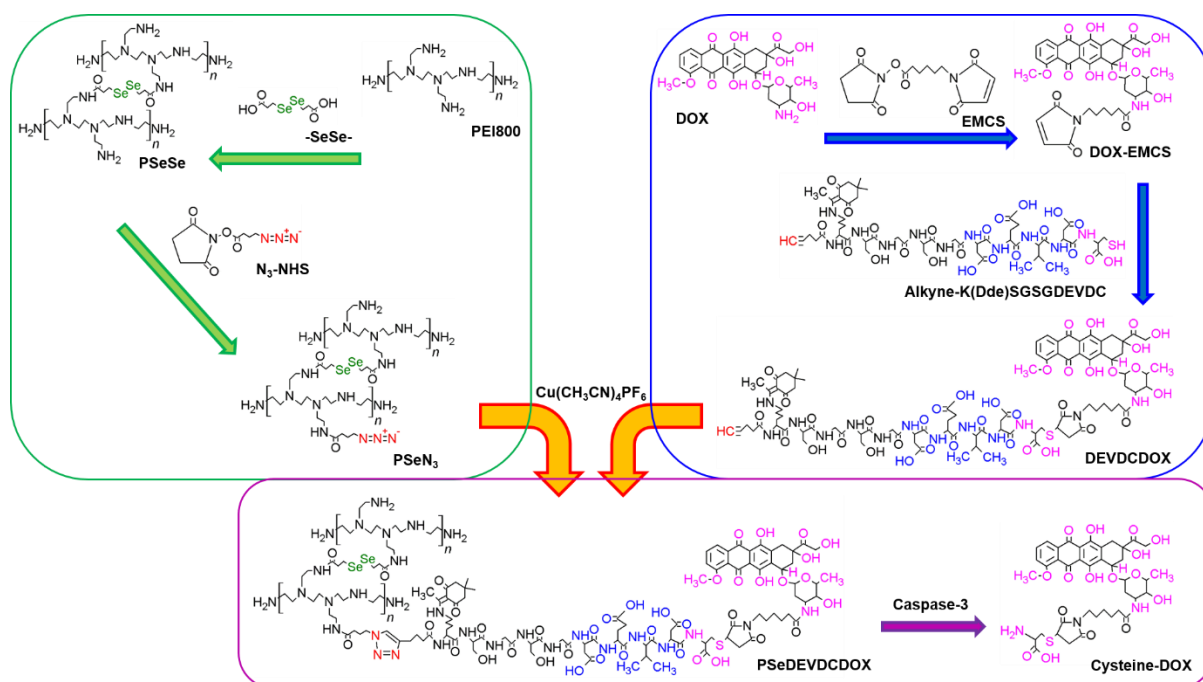
Such simultaneous resistance of cancer cells to chemotherapeutic agents is referred to as multidrug resistance (MDR) [12]. MDR includes inhibition of apoptosis by miR-21 upregulation, ROS detoxification by GSH cytosol level enhancement and reduction of intracellular DOX accumulation by a hydrophobic drug exporter of ATP-binding cassette (ABC) transporter overexpression [13-15]. MDR requires high dose of DOX for high efficacy, which directly induces dose-dependent side effects, such as cardiotoxicity, nephrotoxicity and hepatotoxicity, due to higher cellular uptake of free DOX by normal cells than tumors [16-21]. To overcome MDR and significant side effects, co-drug therapy with DOX and miRNA-21 inhibitor (miR-21i) is required for selective and secure delivery to target cancer cells.

Co-delivery carriers for DOX and supplementary gene drugs, including pDNA, siRNA and miRNA, have been developed with diverse mechanisms of DOX loading and release, while a fixed method of electrostatic interaction of anionic genes with cationic polymer moieties in the systems. Physical adsorption has been utilized to load DOX to co-delivery carriers, such as polymer micelles, polymeric core-shell nanoparticles, hyaluronic acid (HA)-chitosan nanoparticles and polymer modified mesoporous silica nanoparticles, while expressing less controlled releasing of DOX [22-25]. For better controlled release, DOX has been conjugated to polyethyleneimine 25 kDa (PEI25k) via acidic-cleavable hydrazone bond, and gene drugs electrostatically interacted with PEI25k [26, 27]. The formed polyplexes were additionally assembled with polyethylene glycol (PEG) and active target ligands (e.g., folate or Asn-Gly-Arg (NGR) peptide) to prevent serum adsorption and deliver selectively to cancer cells. However, these polyplexes are therapeutically less effective than free DOX without showing clear release mechanism of genes from PEI25k. Polymer-based gene vectors have conventional issues of cytotoxicity and accumulation in patient body due to their strong positive charge and non-degradability although the properties allow effective polyplex formation, durable structure in systemic circulation and active endosomal-escape [28]. To achieve the merits of polymer-

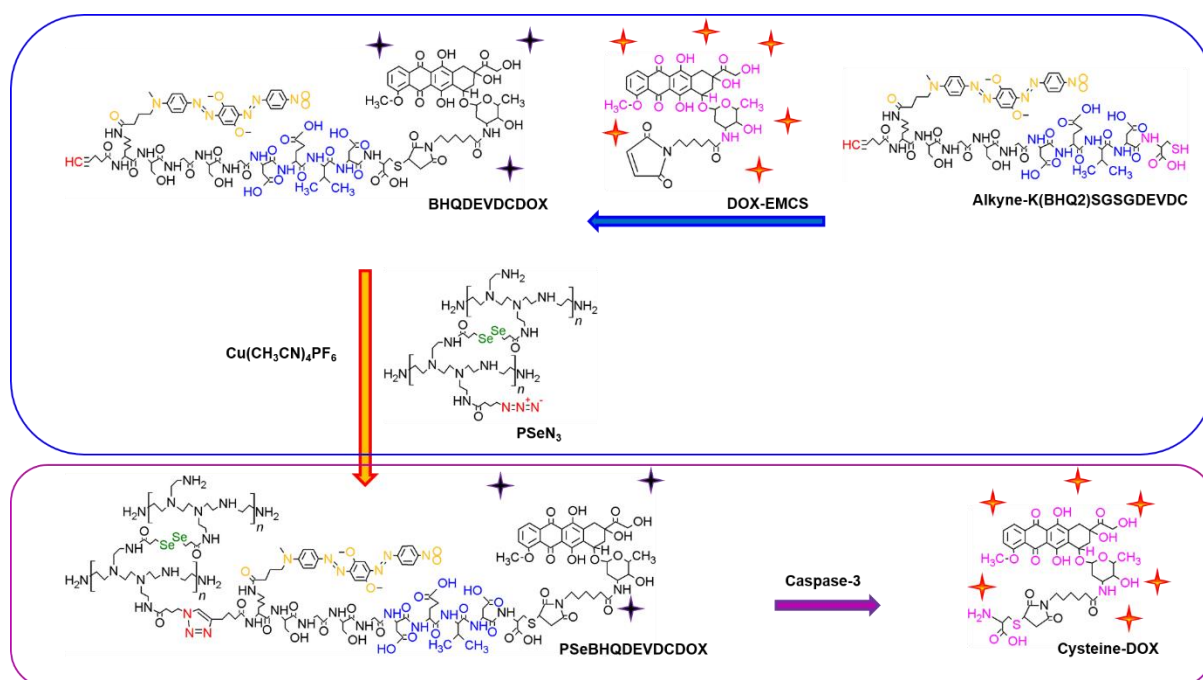
based vectors and eliminate their weakness, our team has introduced fully biodegradable microgels by crosslinking low molecular weight of PEI800 with cytosol level glutathione (GSH)-cleavable diselenide crosslinkers (Chapters 3, 4 and 5). DOX conjugation to the PEI microgels via hydrazone or/and diselenide bonds enables selective release into endosome/lysosome or cytosol of cancer cells regardless of releasing sequence of DOX and miR-21i. Ren et al. employed an external stimulus of near infrared-pulsed (NIR) laser to release DOX at predetermined time, and found that sequential release of DOX following miR-21i amplifies anticancer performance than simultaneous release [29].

In this study, we developed an intracellular microenvironment-triggered system with the ability of sequential release of miR-21i and DOX using fully biodegradable microgels as co-delivery carriers to aim remarkably efficient and effective therapeutic performance in targeting multidrug resistant cells with negligible side effects to healthy cells. DOX was covalently bonded to cysteine through an alkyne-ended peptide linker containing caspase-3-cleavable DEVDC moiety for copper-catalyzed azide-alkyne cycloaddition with azide-conjugated microgels consisting of PEI800 and GSH-cleavable diselenide crosslinkers (Scheme 6.1A), and miR-21i and HA were electrostatically interacted with the microgel carriers. Suppression of DOX release in the absence of caspase-3 and HA surface coating for selective delivery to target cancer cells via HA receptor-mediated endocytosis give rise to negligible side effect to healthy cells. BHQ2-labeled co-delivery system (Scheme 6.1B) can be used to confirm the sequential release of miR-21i and DOX through the fluorescence quenching effect.

(A)

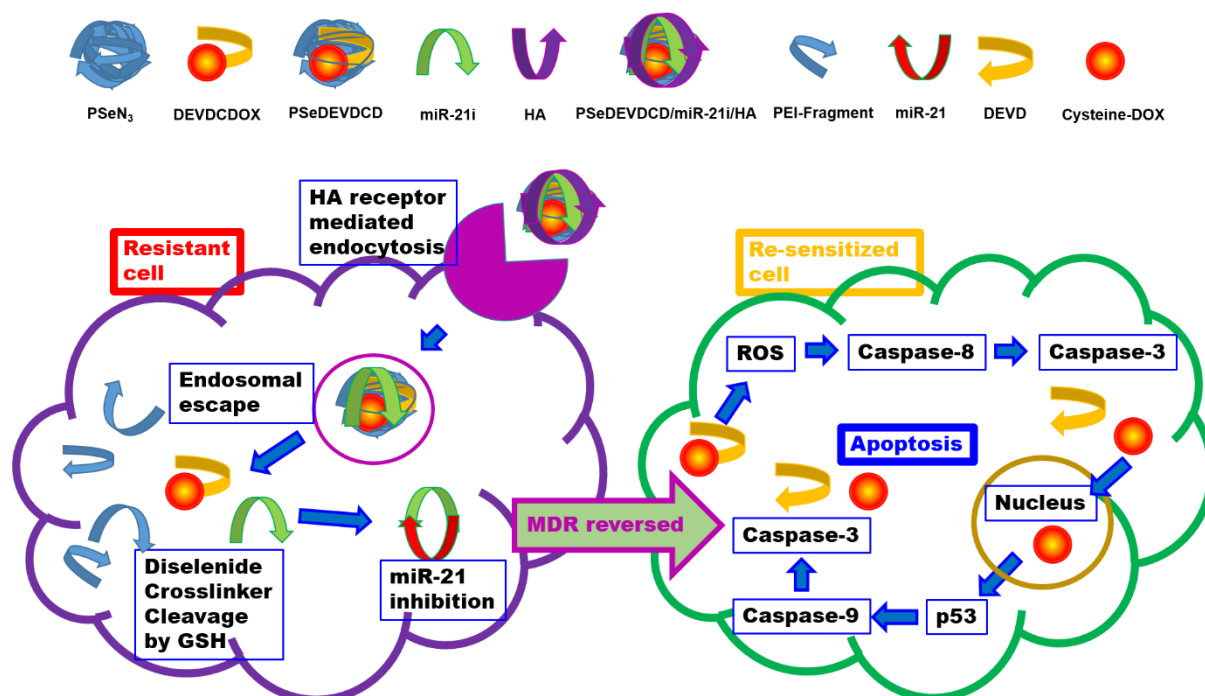


(B)



Scheme 6.1 (A) Scheme on the synthesis of PSeDEVDCDO as a co-delivery carrier of DOX and miR-21i and the release of cysteine-DOX in the presence of caspase-3, (B) Scheme on the synthesis of PSeBHQDEVDCDO as a traceable co-delivery carrier before and after releasing cysteine-DOX, where DOX fluorescence is quenched before release and is recovered after release.

The co-delivery system can be fully degraded by cleavage of diselenide crosslinkers in multidrug-resistant cancer cytosol level GSH and release loaded miR-21i, followed by inhibiting miR-21 and reversing MDR (Scheme 6.2). For the re-sensitized cells, part of DOX can be released by ROS-triggered caspase-3, followed by an accelerated burst DOX release via nucleus p53-induced caspase-3 after cleaving DEVDC moieties in the peptides. As a result, remarkable anticancer effect over simultaneous co-drug release and free DOX are achieved, and the reported sequential release system should have great potentials as effective anticancer nanomedicines in therapeutically complicated applications.



Scheme 6.2 Schematic representation of PSeDEVDCD/miR-21i/HA as effective nanomedicines for intracellular sequential release of miR-21i being triggered by the cytosol GSH of MDR cells and DOX release to re-sensitized MDR cells with activated caspase-3. MDR cell is reversed to re-sensitized cells through the inhibition of miR-21 by miR-21i.

6.2 Experimental

6.2.1 Materials

Branched polyethylenimine M_w 800 (PEI800), 1-ethyl-3-(3-dimethyl-laminopropyl) carbodiimide (EDC) and N-hydroxysulfosuccinimide (NHS) were purchased from Sigma-Aldrich. Doxorubicin hydrochloride (DOX) was obtained from Wuhan Wang Lianshang Biotechnology. (5-Hexynoic acid)-K(Dde)SGSGDEVDC M_w 1254.27 and (5-Hexynoic acid)-K(BHQ2)SGSGDEVDC M_w 1593.58 were synthesized in ChinaPeptides. Azidobutyric acid NHS ester (N₃-NHS) was provided from Lumiprobe. N-Succinimidyl-6-maleimidohexanoate (EMCS) was purchased from Tokyo Chemical Industry. MicroRNA-21 inhibitor (sequence 5'-GUCCACUCUUGUCCUCAUG-3') (miR-21i) and FAM-labelled miRNA inhibitor single stranded negative control (sequence 5'-CAGUACUUUUGUGUAGUACAA-3') (FAM-miR) were prepared by Shanghai GenePharma. Sodium Hyaluronate M_w 60k (HA) was purchased from Lifecore Biomedical. L-glutathione reduced (GSH), human caspase-3 enzyme, triethylenetetramine technical grade (Trien), 1,4-dithiothreitol (DTT), 4-(2-hydroxyethyl)piperazine-1-ethanesulfonic acid (HEPES), ethylenediaminetetraacetic acid (EDTA), 3-[(3-Cholamidopropyl)dimethylammonio]-1-propanesulfonate (CHAPS) hydrate, glycerol, tetrakis(acetonitrile)copper(I) hexafluorophosphate ((Cu(CH₃CN)₄)PF₆), 2,5-dihydroxybenzoic (gentisic) acid, Leibovitz's Medium (L-15), and cell counting Kit-8 (CCK-8) were all purchased from Sigma-Aldrich. Dulbecco modified eagle medium (DMEM), fetal bovine serum (FBS), penicillin-streptomycin (PS), trypsin-EDTA 0.25%, and CellMask™ Deep Red Plasma membrane stain were obtained from Life Technologies. HEK293T and MDA-MB-231 cell lines were kindly gifted by Professor Andrew Zannettino from South Australia Health and Medical Research Institute (SAHMRI) and Dr. Qian Tang from School of Pharmacy at University of South Australia. Deionised water was obtained from a Milli-Q water purification system (18.2 MΩ·cm. Spectra/Por®, Spectrum Laboratories, Inc.)

6.2.2 Synthesis of PSeDEVDCD complexes

6.2.2.1 Synthesis of PSeN₃ microgels

Diselenide crosslinker of 3,3'-diselanediyldipropanoic acid (-SeSe-) and diselenide bond crosslinked PEI microgels (PSeSe) were prepared based on our previous study (Chapter 3). Dried -SeSe- (112.9 mg, 0.37 mmol) was dissolved in 0.8 mL of DMSO with NHS (170.9 mg, 1.48 mmol) and EDC (427 mg, 2.23 mmol) under nitrogen protection and the mixture was stirred at room temperature for 45 min. PEI800 (297 mg, 0.37 mmol), after pH being adjusted to 8.0 by 3 M HCl and freeze dried, was dissolved in 0.6 mL DMSO and injected to the mixture for further 2 days stirring. The black color mixture was transferred to a dialysis tube with the MWCO of 7 kDa and dialyzed against deionized water for 1 week with daily changing water. After filtration and freeze drying, **PSeSe** microgels were produced.

PSeSe (300 mg, 1488 μ mol amine) dissolved in 4 mL of DMSO was mixed with N₃-NHS (13.6 mg, 60 μ mol) and stirred under nitrogen protection at room temperature for 24 h. After dialysis and freeze drying, **PSeN₃** microgel was obtained, and characterized on its zeta potential and hydrodynamic size with a zeta sizer (Malvern Nano ZS ZEN 3600). Fourier-transform infrared spectroscopy (FTIR) was used to confirm azide conjugation.

6.2.2.2 Synthesis of DEVDCDOX and BHQDEVDCDOX

DOX was covalently bonded to alkyne-ended DEVDC peptide to produce the DEVDCDOX via a modified method from previous work [30]. DOX (75 mg, 129.31 μ mol) dissolved in 5 mL of dimethylformamide (DMF) was stirred with 50 μ L of triethylamine (TEA) under darkness for 30 min. EMCS (31.7 mg, 103.45 μ mol) was added to the mixture for further 2 h stirring under nitrogen protection at room temperature. The mixture was diluted in 10 volumes of dichloromethane (DCM) and filtered to remove precipitated DOX. The filtrate was diluted with 10 times in diethyl ether to precipitate the product of **DOX-EMCS**.

Dried DOX-EMCS was re-dissolved in 5 mL DMF with (5-hexynoic acid)-K(Dde)SGSGDEVDC (59.7 mg, 86.2 μmol) and stirred at 4 °C under light protection for 16 h. The mixture was diluted in 10 volumes of DCM and kept at -20 °C for overnight. After centrifuge and 3 times washing with cold DCM, precipitates of alkyne-K(Dde)SGSGDEVDCDOX (**DEVDCDOX**) were collected with the presence of alkyne and aromatic groups being confirmed from FTIR.

DOX calibration curve was constructed via a UV-vis spectrophotometer by measuring absorbance at 479.5 nm against DOX concentrations (mg L^{-1}). DEVDCDOX calibration curve was constructed with same method as the DOX calibration curve.

For BHQDEVDCDOX preparation, DOX-EMCS (2.0 mg, 2.71 μmol) and (5-hexynoic acid)-K(BHQ2)SGSGDEVDC (2.9 mg, 1.82 μmol) were dissolved in 2 mL of DMF and stirred at 4 °C under darkness for 16 h. Black hole quencher2 (BHQ2)-labeled DEVDCDOX (**BHQDEVDCDOX**) was precipitated in cold DCM with centrifuge and obtained after washing.

6.2.2.3 Click chemistry for PSeDEVDCD and PSeBHQDEVDCD

Alkyne-ended peptides with DOX (DEVDCDOX and BHQDEVDCDOX) were covalently bonded to azide-conjugated microgels (PSeN₃) via click reaction of azide-alkyne cycloaddition [31]. Cu(CH₃CN)₄PF₆ (75 mg, 200 μmol) was dissolved in 2.5 mL of acetonitrile (CH₃CN) in a three-necked flask at 60 °C under nitrogen protection with gentle stirring. DEVDCDOX (9.94 mg, 5.0 μmol of alkyne) dissolved in the mixed solvent of 3 mL of DMSO and 0.5 mL of ethanol was instantly injected to the flask. At the same time, gentisic acid (250 mg, 2.0 mmol) in 12.5 mL of sodium phosphate buffer solution (100 mM, pH 7.0) with gentle heating and neutralization by 2 M NaOH, was injected to the flask. Then, PSeN₃ (25.52 mg, 5.0 μmol of azide) dissolved in a solvent of 3 mL of DMSO and 0.5 mL of ethanol was added to the flask.

The mixture in the flask was stirred in an oil bath at 60 °C under nitrogen and light protection for 10 min and further stirred at room temperature overnight. The green-colored mixture in the flask was moved to a cool room at 4 °C for cooling down with gentle stirring under light protection. Trien after pH 7.0 adjustment by 6 volumes of 3 M HCl (1.05 mL, 1mmol) was injected to the flask and the darkish purple-colored mixture was ultrasonicated in an ice bath for 3 min with following overnight stirring at 4 °C under darkness. After filtration to remove copper precipitates, the darkish purple-colored mixture was transferred to a dialysis tube (MWCO 3.5 kDa) with another 1.05 ml of Trien at pH 7.0 inside the tube for dialysis against deionized water at 4 °C for 3 days with daily change of water. After filtration and lyophilization, DOX-conjugated microgels via DEVDC peptide linker (**PSeDEVDCD**) was produced. Successful synthesis of PSeDEVDCD was confirmed via FTIR and UV-Vis spectrophotometric measurement. Zeta potential and hydrodynamic size of PSeDEVDCD were measured via a zeta sizer. DOX loading to PSeDEVDCD (wt. %) was determined with DOX calibration curve (Figure 6.S2A) at 479.5 nm from a UV-vis spectrophotometer. Amine content in PSeDEVDCD ($\mu\text{mol mg}^{-1}$) was measured via conductivity and pH titration (Figure 6.S6). To produce BHQ2-labeled complex of PSeBHQDEVDCD, BHQDEVDCDOX (11.64 mg, 5.0 μmol of Alkyne) was fed instead of DEVDCDOX and the other methods were identical as the PSeDEVDCD production.

6.2.3 *Ex vivo* release of DOX and miR-21i

6.2.3.1 DOX releasing

PSeDEVDCD complex in 1 mL deionized water (2 mg mL^{-1}) was mixed with caspase-3 enzyme ($1 \mu\text{g}$, 0.031 nmol) in 1 mL of the caspase assay buffer (10 % (w/v) glycerol containing 50 mM HEPES, pH 7.4, 100 mM NaCl, 10 mM DTT, 1 mM EDTA, and 0.1 % CHAPS). The mixture of PSeDEVDCD and 15.6 nM caspase-3 was transferred to a dialysis tube (MWCO 3.5) and dialyzed against 13 mL of the caspase assay buffer in a horizontal shaker with a speed

of 100 rpm at room temperature over 48 h. 1 mL of the assay buffer was collected to measure absorbance at 479.5 nm via a UV-vis spectrophotometer at pre-determined time intervals and 1 mL of the fresh buffer was refilled. The released DOX from PSeDEVDCD was quantified with a DOX calibration curve. Dialysis experiment of PSeDEVDCD aqueous solution mixing with 1 mL of the caspase assay buffer but without presence caspase-3 enzyme was chosen as a control.

6.2.3.2 miR-21i loading

PSeDEVDCD complex was incubated with miRNA-21 inhibitor (miR-21i) in RNase free (DEPC) water at room temperature for 20 min to form the **PSeDEVDCD/miR-21i** polyplex. The miR-21i loading capability of PSeDEVDCD was evaluated at various N/P molar ratios (1, 2, 4, 6 and 8), nitrogen (N) in the complex ($3.0 \mu\text{mol mg}^{-1}$) and phosphate (P) in $1 \mu\text{L}$ of miR-21i ($0.42 \text{ nmol } \mu\text{L}^{-1}$), via agarose gel (0.8 %) retardation assay at 100 volts for 1 h. Naked miR-21i and the polyplex of PEI25k and miR-21i at 1 N/P were used as negative and positive controls. The migrated gene images in the gel were fluorescent imaged under UV excitation and captured with a Gene-BOX.

6.2.3.3 Biodegradability

Biodegradability of PSeDEVDCD was *ex vivo* evaluated via measuring its hydrodynamic sizes in 50 mM HEPES buffer solution at pH 7.4 with various GSH concentrations of 0 M, 10 μM and 20 mM. The size changes of PSeDEVDCD in those solutions with stirring at 100 rpm and 37 °C were monitored with dynamic light scattering (DLS) from a zeta sizer at pre-designed time over 120 h.

6.2.3.4 miR-21i releasing

Releasing of miR-21i from the PSeDEVDCD/miR-21i polyplex at 10 N/P was evaluated via agarose gel electrophoresis. The polyplex was incubated in HEPES buffer solution at pH 7.4

and 37 °C with 20 mM GSH for 72 h, and then run in an agarose gel (0.8 %) at 100 volts for 1 h with following photographs in a Gene-BOX. Naked miR-21i and the polyplex at 10 N/P before incubation with GSH were run as negative and positive controls.

6.2.4 HA receptor mediated endocytosis

6.2.4.1 HA surface coating and characterizations

Hyaluronic acid (HA) was coated on the surface of PSeDEVDCD/miR-21i polyplex (10 N/P) at 4 weights of HA to miR-21i in DEPC water at room temperature for 20 min, producing the **PSeDEVDCD/miR-21i/HA** nanomedicines. Zeta potential of PSeDEVDCD/miR-21i/HA in 10 mM NaCl solution at pH 7.4 was measured via a zeta sizer. Hydrodynamic size of PSeDEVDCD/miR-21i/HA in HEPES buffer solution at pH 7.4 was obtained via DLS measurements.

6.2.4.2 Cell culture

Kidney cell line (HEK293T), breast cancer cell line (MDA-MB-231), and multidrug resistant breast cancer cell line (MDA-MB-231-R) were cultured in an incubator (Contherm Scientific) under 5 % CO₂ and a moisturized environment at 37 °C with correspondent culture media. Mixture of Dulbecco modified eagle medium (DMEM), 10 (vol. %) of fetal bovine serum (FBS) and 1 (vol. %) of penicillin-streptomycin (PS) (DMEM-based medium) was consumed by HEK293T, while Leibovitz's medium (L-15) supplemented with 10 % FBS and 1 % PS (L-15-based medium) was used for MDA-MB-231. To culture the MDA-MB-231-R from MDA-MB-231, DOX was incorporated in the L-15-based medium with stepwise increasing DOX concentrations ($\mu\text{g mL}^{-1}$), such as 0.01 for the first 8 weeks, 0.02 for further 8 weeks, and 0.03 for week 17th to 24th. DOX resistance to MDA-MB-231-R cells was evaluated with cell viability assay during the cell culture in 0 week (W), 4 W, 8 W, 12 W and 24 W against DOX concentrations from 0.1 to 2.5 ($\mu\text{g mL}^{-1}$). MDA-MB-231-R cells in the certain week were recovered using trypsin-EDTA (0.25 %) in a 96-well plate for 24 h incubation with L-15-based

medium without DOX. Subsequently, varied concentrations of DOX were administrated to the cells with fresh L-15-based medium. After another incubation for 48 h, the cells with fresh DMEM-based medium were incubated in the presence of Cell Counting Kit-8 (CCK-8) for further 4 h. Absorbance from the well plate was read at 450 nm wavelength in a microplate reader (ELx808 BioTek) and cell survival rate (%) was calculated with following equation:

$$\text{Cell survival rate (\%)} = \frac{\text{Sample} - \text{Background}}{\text{Control} - \text{Background}} \times 100 \quad (1)$$

where sample, control and background indicate the absorbance from the well with toxicant-incorporated cells, only cells, and neither cells nor toxicants respectively.

6.2.4.3 Cellular uptake

HA receptor-mediated endocytosis of PSeDEVDCD/miR-21i/HA into MDA-MB-231 cells was qualitatively monitored via a confocal laser scanning microscope (CLSM), Olympus FV3000. MDA-MB-231 cells were seeded on each glass cover slip in 3 wells of a 6-well plate. The cells in each well were incubated with L-15-based culture medium for 24 h, while the cells in one well were incubated with additional HA (10 mg mL⁻¹) to block HA receptors. FAM-labeled miRNA negative control with a random sequence (FAM-miR) was loaded to PSeDEVDCD at a 10 N/P, and 4 weights of HA to the FAM-miR were coated on the surface of polyplex to produce the PSeDEVDCD/FAM-miR/HA for cellular uptake assays. PSeDEVDCD/FAM-miR/HA was applied to two wells: one with MDA-MB-231 cells and the other with HA receptor-blocked MDA-MB-231 cells, and further incubated for 4 h. At the same time, MDA-MB-231 cells without PSeDEVDCD/FAM-miR/HA in the third well were used as a control. After staining cell membrane with CellMaskTM Deep Red for 5 min, fixing with formaldehyde (4 %) for 10 min, and washing 3 times with PBS, fluorescence from DOX, FAM-miR, and cell membrane in different wells was imaged with colors of blue, green and red via the CLSM.

6.2.5 *In vitro* cell viability assays on normal and cancer cells

6.2.5.1 Biocompatibility of PSeDEVDCD/miR-21i/HA on HEK293T cells

Biocompatibility of the PSeDEVDCD/miR-21i/HA was evaluated via viability assays on a kidney cell line of HEK293T with CCK-8 treatment. HEK293T cells were seeded in a 96-well plate with DMEM-based medium for 24 h incubation. PSeDEVDCD/miR-21i/HA were prepared at various DOX concentrations, 0.1, 0.5, 1.0 and 2.5 ($\mu\text{g mL}^{-1}$), at 10 N/P and 4 times of HA to miR-21i (w/w). With subsequent administration of PSeDEVDCD/miR-21i/HA to the HEK293T cells with fresh culture medium and incubation for 48 h, the cells were treated with CCK-8 for 4 h for absorbance reading at 450 nm via a microplate reader. HEK293T cell survival rates (%) against PSeDEVDCD/miR-21i/HA were obtained from Equation 1. PSeDEVDCD/HA and free DOX at equivalent DOX concentrations were chosen as references.

6.2.5.2 Anticancer effect of PSeDEVDCD/miR-21i/HA on MDA-MB-231 cancer cells

Therapeutic effect of the PSeDEVDCD/miR-21i/HA on a model breast cancer cell line (MDA-MB-231) was evaluated via viability assays together with CCK-8 treatment. The anticancer effects of PSeDEVDCD/miR-21i/HA (10 N/P, 4 weights of HA to miR-21i) with different concentrations of loaded DOX (0.1, 0.5, 1.0 and 2.5 ($\mu\text{g mL}^{-1}$)) were compared to PSeDEVDCD/HA and free DOX at equivalent DOX concentrations as references. Pre-cultured MDA-MB-231 cells in a 96-well plate with L-15-based medium for 24 h were further incubated with those delivery systems for 48 h. After CCK-8 treatment for 4 h in DMEM-based medium, cell survival rates (%) were obtained via absorbance measurement at 450 nm from a microplate reader.

6.2.6 *In vitro* trace of miR-21i and DOX sequential release

To trace releasing patterns of miR-21i and DOX in a multidrug-resistant breast cancer cell line (MDA-MB-231-R), an equivalent amount of FAM-miR and miR-21i mixture was electrostatically interacted with PSeBHQDEVDCD instead of PSeDEVDCD at a 10 N/P. 4

weight of HA to the mixture of FAM-miR and miR-21i was further coated to prepare the PSeBHQDEVDCD/FAM-miR/miR-21i/HA.

The release profiles of quenched fluorescence from FAM-miR and DOX in the PSeBHQDEVDCD/FAM-miR/miR-21i/HA were observed via the CLSM. 24 h pre-incubated MDA-MB-231-R cells in glass slips in a 6-well plate were further incubated with PSeBHQDEVDCD/FAM-miR/miR-21i/HA for 4 h, 8 h and 12 h. Fluorescent signals from FAM-miR, DOX and cell membrane were monitored via a CLSM after cell membrane being stained with CellMaskTM Deep Red and fixed with 4 % formaldehyde.

Releasing of FAM-miR and DOX from the PSeBHQDEVDCD/FAM-miR/miR-21i/HA was further quantified via a flow cytometer (BD FACSCaliburTM). Pre-cultured MDA-MB-231-R cells in a 24-well plate for 24 h were further incubated with PSeBHQDEVDCD/FAM-miR/miR-21i/HA for different time intervals of 4, 8, 12 and 24 h, and the cells without the PSeBHQDEVDCD/FAM-miR/miR-21i/HA were used as a control. Cells in each well at the pre-determined incubation time were collected after trypsin-EDTA treatment, and the fluorescent intensity of DOX and FAM-miR being released from the PSeBHQDEVDCD/FAM-miR/miR-21i/HA was quantified via a flow cytometer with FL-2 (excitation at 488, emission at 585 nm) and FL-1 (excitation at 488, emission at 530 nm).

6.2.7 Therapeutic effect of PSeDEVDCD/miR-21i/HA on multidrug-resistant MDA-MB-231-R cancer cells

Anticancer effect of sequentially releasable PSeDEVDCD/miR-21i/HA on a multidrug-resistant cancer cell line (MDA-MB-231-R) was evaluated via cell viability assays with identical method as previous MDA-MB-231. Survival rates of MDA-MB-231-R cells against the PSeDEVDCD/miR-21i/HA were compared to PSeDEVDCD/HA and free DOX at the equivalent DOX concentrations (0.1, 0.5, 1.0 and 2.5 $\mu\text{g mL}^{-1}$).

6.3 Results and Discussion

6.3.1 Synthesis of PSeDEVDCD

PEI microgels by crosslinking PEI800 by GSH-cleavable diselenide crosslinkers were prepared to load DOX and miR-21i (Chapters 3, 4 and 5). The biocompatible PEI microgels are positively charged and be able to be smartly decomposed with intracellular microenvironment for effective miR-21i loading and release. However, our previous co-delivery systems, which simultaneously release miR-21i and DOX, motivate us the development of novel systems with intracellular microenvironment responsive sequential release of miR-21i and DOX to maximize therapeutic efficiency and efficacy to multidrug resistant cancer cells. To achieve sequential release of miR-21i and DOX, it is considered to conjugate DOX to PEI microgels via a peptide linker containing DEVDC that could be cleaved by caspase-3 enzyme of intracellular stimuli produced after the release of miR-21i (Scheme 6.1A). The activation of caspase-3 enzyme in apoptotic pathways can be inhibited under conditions of anti-apoptotic miR-21 overexpression [3]. However, mitigation of miR-21 activity by miR-21i can facilitate caspase-3 enzyme activation [32].

6.3.1.1 PSeN₃ microgel

PEI microgels with azide groups (PSeN₃) were synthesized to electrostatically interact with miR-21i and conjugate DOX via the cycloaddition with alkyne-ended caspase-3 enzyme-cleavable DEVDC peptide linkers (Scheme 6.1A) for sequential release of miR-21i and DOX to multidrug-resistant cancer cells. After producing PEI microgel (PSeSe), azidobutyric acid NHS ester (N₃-NHS) was introduced to the amine of PSeSe to produce PSeN₃ microgels with a yield of 73.7 %. Successful synthesis of PSeN₃ can be identified by shifts in zeta potentials and hydrodynamic sizes, which decrease from 68.3 ± 0.7 mV and 260.0 ± 1.9 nm of PSeSe

(Chapter 5) to 42.7 ± 1.6 mV (Figure 6.S7) and 242.5 ± 20.8 nm due to the consumption of primary amines of PEI. As further evidence for successful synthesis, FTIR peak of PSeN₃ at 2096 in Figure 6.S1 represents the N₃ stretching.

6.3.1.2 Pro-drugs of caspase-3 enzyme cleavable DEVDCDOX and BHQDEVDCDOX

To produce DOX-bound pro-drug of DEVDCDOX, DOX was chemically bonded to the thiol group in cysteine of the peptides containing DEVDC using a linker of the EMCS containing NHS ester and maleimide ends. The use of cysteine, C, moiety in peptide to conjugate DOX is to protect the functions of amide and carboxylic acid groups in the DEVD moiety of the peptide linker as hydrolysis target sites by caspase-3. Also, the reason for using cysteine moiety in DOX conjugation is to release cysteine-tailed DOX through hydrolysis of DEVD moiety in the peptide (Scheme 6.1A). Cysteine-tailed DOX containing carboxylic acid can reduce the probability of export from cancer cells as it can minimize the affinity to hydrophobic sites of ABC transporters of a DOX exporter in multidrug resistant cells [15].

FTIR spectrum (Figure 6.S1) confirms that the DEVDCDOX pro-drug is successfully produced with peaks at 3255, 3068, 984 and 621 cm⁻¹, representing C≡C-H stretching, aromatic C-H stretching, O-H bending and C≡C-H bending. UV-vis spectrum of DEVDCDOX further reinforces the successful DOX integration due to the absorbance peaks at wavelengths of 292.0 and 479.5 nm identical to DOX (Figure 6.S3A and 6.S3B). DOX ratio (wt.) of the DEVDCDOX pro-drug can be obtained via a UV-vis calibration curve of DOX (Figure 6.S2A) and DEVDCDOX adsorption (Figure 6.S2B) at 479.5 nm, indicating 25 wt. %.

Since we use static fluorescence quenching technique to trace intracellular release of DOX, DOX was covalently bonded to BHQ2-labeled DEVDC peptide (BHQDEVDC) via an EMCS linker to produce the pro-drug of BHQDEVDCDOX containing the fluorophore of DOX and the quencher of BHQ2. BHQDEVDC with a broad band absorption from 500 to 600 nm (Figure

6.S4) can effectively quench the fluorescence of DOX emitted at 580 nm by forming the BHQDEVDCDOX as a ground-state non-fluorescent quencher-fluorophore complex. Ground-state quencher-fluorophore complex formation can quench fluorescence intensity of fluorophore and can be confirmed by shifts in the absorption spectrum of the fluorophore by adding quencher [33]. The shift in UV-vis absorbance peak from DOX (479.5 nm) to BHQDEVDCDOX (536 nm) (Figure 6.S4) indicates that BHQDEVDCDOX pro-drug is a quencher-fluorophore complex with DOX fluorescence quenching function.

6.3.1.3 Production of PSeDEVDCD and PSeBHQDEVDCD

To react azide-containing PSeN₃ microgels and alkyne end-capped DOX-containing pro-drug of DEVDCDOX, copper (I) catalyzed azide-alkyne cycloaddition was operated to produce the PSeDEVDCD (Scheme 6.1A). After the click chemistry reaction and dialysis against deionized water, the product solution with UV-vis absorbance peaks of 543.5 and 577.5 nm (Figure 6.S3H) due to incomplete copper removal [34]. Triethylenetetramine (Trien) is used for copper (I) removal since it shows 10⁸ times higher chelation capability with copper (I) than branched PEI [35]. After dialysis against deionized water, the color of mixture changes to orange associated with an UV-vis absorbance peak at 491.0 nm (Figure 6.S3O), which is well matched with DOX (Figure 6.S3A). Besides, successful production of PSeDEVDCD can be further confirmed by the FTIR peaks at 3068 and 984 cm⁻¹ for aromatic C-H stretching and O-H bending (Figure 6.S1). In addition, zeta potential and hydrodynamic size of the PSeDEVDCD are changed to 30.9 ± 2.3 mV (Figure 6.S7) and 261.2 ± 24.8 nm compared to PSeN₃ microgels by conjugating the DEVDCDOX pro-drug containing carboxylic group. From UV-vis measurement, the DOX loading in PSeDEVDCD is found to be 3.1 wt. %.

At the same time, PSeBHQDEVDCD was also prepared to trace *in vitro* sequential release of FAM-miR and DOX. PSeBHQDEVDCD can be produced using similar azide-alkyne cycloaddition between PSeN₃ and BHQDEVDCDOX (Scheme 6.1B). After azide-alkyne

reaction, the UV-vis absorbance peak of PSeBHQDEVDCD (544.5 nm) shifts from BHQDEVDCDOX pro-drug (536 nm) (Figure 6.S4) and also differs from DOX (479.5 nm). These indicate DOX fluorescence quenching in the PSeBHQDEVDCD is protected in the azide-alkyne reaction.

6.3.2 *Ex vivo* releasing of DOX and miR-21i

6.3.2.1 DOX releasing

DOX was conjugated to the PSeN₃ microgels via a caspase-3 cleavable peptide linker containing DEVDC. Active caspase-3 hydrolyzes the amide bonds between aspartic acid (D) and cysteine (C) of the peptide and release cysteine-DOX (Scheme 6.1A) [30]. To verify *ex vivo* DOX release in the presence of active caspase-3, PSeDEVDCD was mixed with 15.6 nM caspase-3 enzyme and dialyzed against the caspase assay buffer at pH 7.4 over 48 h, while that without caspase-3 was evaluated as a control. Figure 6.1A confirms the apoptotic enzyme-driven controlled release of loaded DOX from PSeDEVDCD with 40.2 ± 2.2 % over 48 h in the presence of caspase-3, while 12.2 ± 0.87 % in the control. DOX releasing from the PSeDEVDCD is due to the cleavage of DEVDC moieties of the peptide linkers by caspase-3 [36]. Caspase-3 can be activated by caspase-8 or caspase-9 in the condition of mitigation of apoptotic pathway inhibitors, such as microRNA-21 (miR-21), and can indiscriminately generate apoptosis [3]. Based on the *ex vivo* DOX releasing assessment, it can be inferred that PSeDEVDCD releases DOX to multidrug resistant cancer cells after activity of miR-21 is inhibited and MDR reverses.

6.3.2.2 miR-21i loading

The strategy to reverse the MDR is to impede the activity of miR-21 in cancer cells with its inhibitor miR-21i [37]. Therefore, it is important to co-deliver DOX and mi-21i together. The miR-21i loading capability to positively charged PSeDEVDCD by electrostatic interaction was

evaluated via agarose gel (0.8 %) retardation assays. At a N/P of 6 (Figure 6.1C), miR-21i can be fully loaded to the PSeDEVDCD.

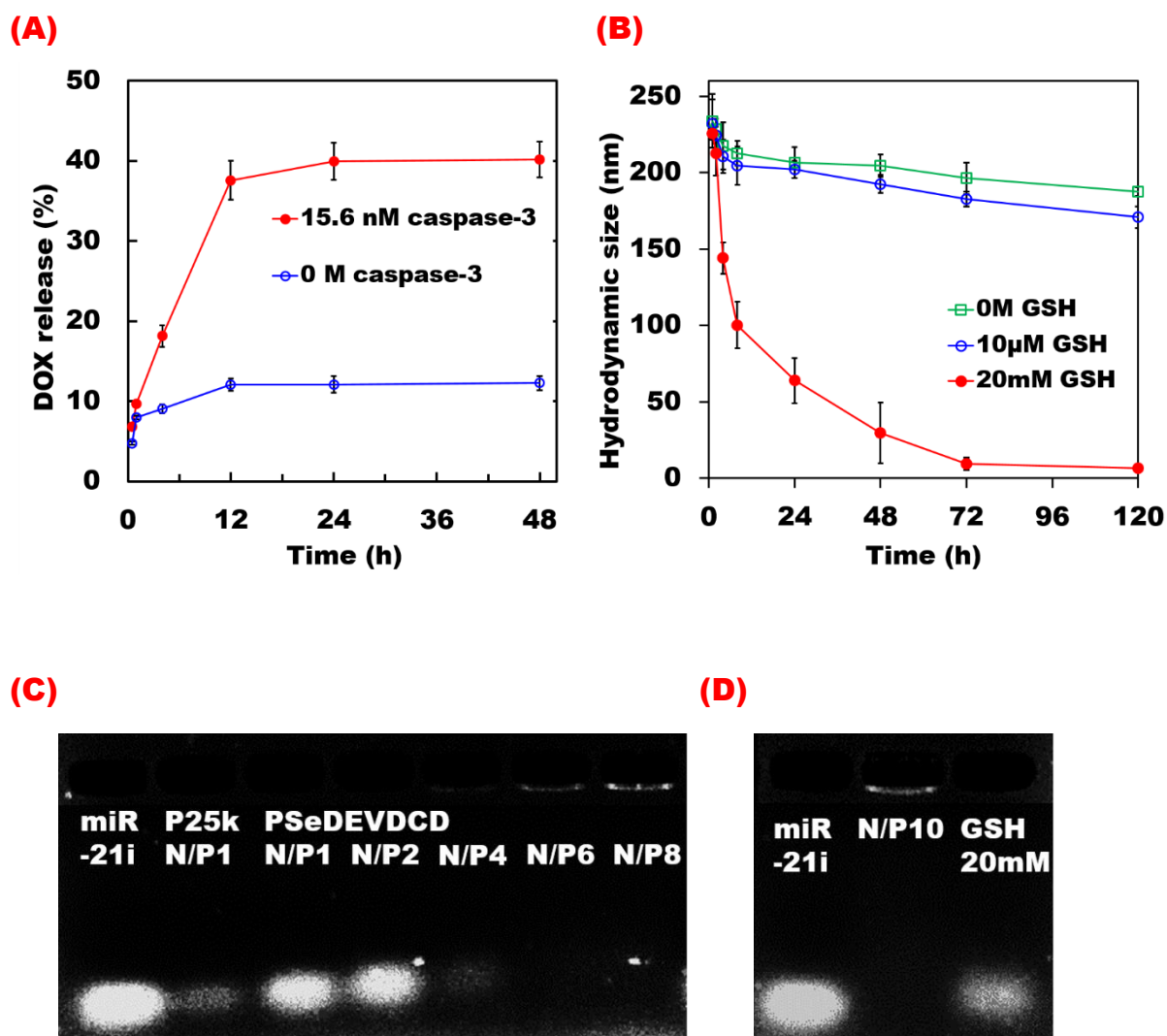


Figure 6.1 (A) DOX release from the PSeDEVDCD in the presence/absence of caspase-3 ($n = 3$), (B) *ex vivo* degradation of PSeDEVDCD via hydrodynamic size measurement in HEPES buffer at pH 7.4 and 0 M GSH, 10 μ M and 20 mM GSH ($n = 3$), (C) miR-21i loading to PSeDEVDCD at various N/P ratios (1, 2, 4, 6 and 8), PEI25k (P25k) N/P of 1 as a positive control and naked miR-21i as a negative control, (D) miR-21i release from the PSeDEVDCD/miR-21i at a 10 N/P in 20 mM GSH after 72 h incubation (right), PSeDEVDCD/miR-21i at a 10 N/P without GSH as positive control (middle) and naked miR-21i as negative control (left).

6.3.2.3 Biodegradability and miR-21i releasing

The loaded miR-21i in the PSeDEVDCD/miR-21i might be released in cancer cytosol due to the presence of high level GSH. GSH can degrade the PSeDEVDCD via cleaving diselenide crosslinkers, and these low charged PSeDEVDCD fragments cannot interact with miR-21i. The PSeDEVDCD biodegradation was *ex vivo* evaluated in a mimicking cancer cytosol (20 mM GSH) through size measurement and compared to imitated extracellular environment (10 μ M GSH) and physiological state (0 M GSH) in an equivalent 50 mM HEPES buffer at pH 7.4 (Figure 6.1B). In 20 mM GSH, the size of PSeDEVDCD at 261.2 ± 24.8 nm drops to 100 nm over 8 h, and further decreases to less than 10 nm over 72 h and 6.5 ± 1.2 nm over 120 h. However, the PSeDEVDCD show structural stability in 0 M and 10 μ M GSH with slight size decreasing to 187.6 ± 2.7 and 170.8 ± 7.0 nm over 5 days. Such study not only strongly confirms the fully decomposition of PSeDEVDCD in mimicking cytosol condition for potential release of pre-loaded miR-21i, but also identifies the structural stability of PSeDEVDCD in simulated physiological and extracellular environment.

To further verify the release of pre-loaded miR-21i in mimicking cytosol condition, the migration image of miR-21i from PSeDEVDCD/miR-21i (10 N/P) in the presence of 20 mM GSH for 72 h was monitored via agarose gel electrophoresis, while the PSeDEVDCD/miR-21i without GSH was run as a control. Figure 6.1D shows that the miR-21i in the PSeDEVDCD/miR-21i with full retardation at 10 N/P is stable in the absence of GSH, but migrates in the presence of GSH. That confirms the release of miR-21i in the simulated cancer cytosol condition. From *ex vivo* study, we can conclude that PSeDEVDCD can fully load miR-21i at a 10 N/P and stably pass through mimicking physiological and extracellular environment conditions with limited pre-leakage of DOX and miR-21i. PSeDEVDCD/miR-21i can be degraded to small fragments in a mimicking cancer cytosol and release the pre-loaded miR-21i. As miR-21 consequently impairs the activity of intracellular caspase-3, the released miR-21i

can assist caspase-3 activation by inhibiting miR-21 [38]. The activated caspase-3 enzymes will then cleave the DEVDC moieties in the peptide linkers of PSeDEVDCD/miR-21i, and subsequently facilitate the release of the conjugated DOX. The reported PSeDEVDCD/miR-21i with functions of sequential release of pre-loaded miR-21 and DOX can minimize DOX side-effects and increase therapeutic efficiency.

6.3.3 HA receptor mediated endocytosis

6.3.3.1 HA surface coating and characterization

Positive charged PSeDEVDCD/miR-21i (zeta potential of 16.8 ± 1.5 mV in Figure 6.S7) trends to interact with serum proteins in the delivery course. To avoid serum protein adsorption, anionic hyaluronic acid (HA) was coated on the surface of PSeDEVDCD/miR-21i (10 N/P) via electrostatic interaction at a 4 weight ratio of HA to miR-21i to produce the PSeDEVDCD/miR-21i/HA. Zeta potential and hydrodynamic size of the PSeDEVDCD/miR-21i/HA are -30.1 ± 1.9 mV (Figure 6.S7) and 190.5 ± 26.1 nm, and negative charged systems show negligible protein adsorption in our previous study (Chapter 3). In addition, the particle size of PSeDEVDCD/miR-21i/HA between 10 and 200 nm is ideal for enhanced tumor accumulation without renal and reticuloendothelial system clearance [39].

6.3.3.2 HA receptor-mediated endocytosis

HA coating on the surface of PSeDEVDCD/miR-21i also allows HA receptor-mediated endocytosis to metastatic cancer cells due to the over-expression of HA receptors, CD44 and RHAMM [40]. HA receptor-mediated endocytosis of PSeDEVDCD/miR-21i/HA to a metastatic cancer cell line of MDA-MB-231 was qualitatively evaluated via a CLSM. To monitor fluorescence of FAM-miR (green), DOX (blue), cell membrane (red) and merged images (purple) via CLSM, PSeDEVDCD/FAM-miR/HA was prepared and MDA-MB-231 cells were stained. Control cells without PSeDEVDCD/FAM-miR/HA are shown in only red in Figure 6.2A, but MDA-MB-231 cells with PSeDEVDCD/FAM-miR/HA are displayed in

all four colors in [Figure 6.2B](#) to indicate excellent cellular uptake. To determine whether the pathway of PSeDEVDCD/FAM-miR/HA endocytosis to MDA-MB-231 is via HA receptors, the HA receptors on the surface of the MDA-MB-231 cells were first blocked before the cellular uptake evaluation. [Figure 6.2C](#) shows limited green and blue colors on the red of merged images, indicating that HA receptor-blocked MDA-MB-231 cells are impaired to uptake PSeDEVDCD/FAM-miR/HA. These results confirm PSeDEVDCD/FAM-miR/HA enter MDA-MB-231 cells via the HA receptor mediation.

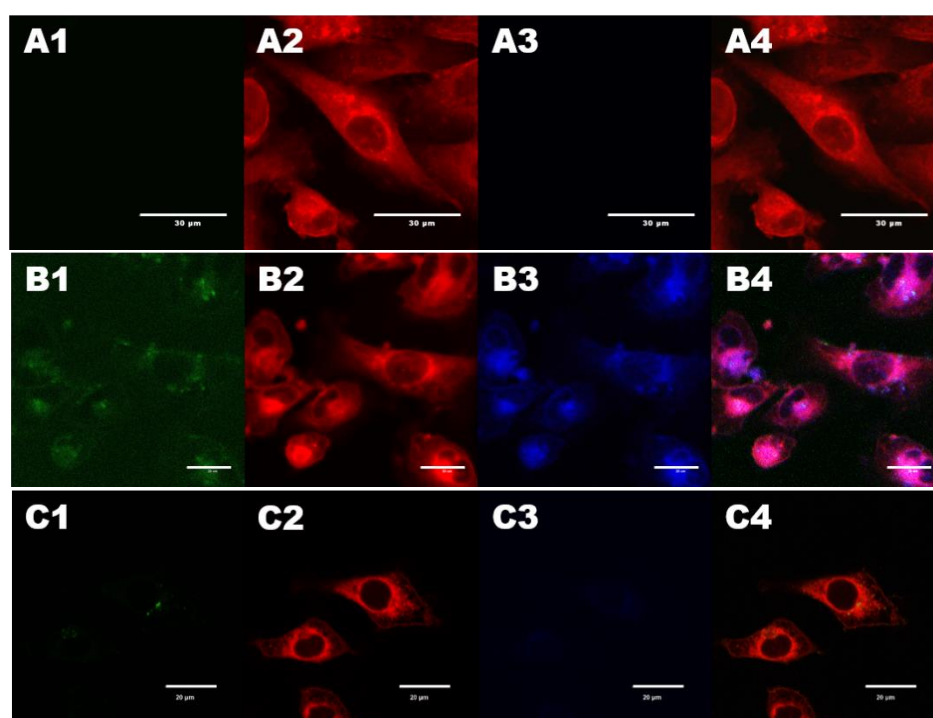


Figure 6.2 Cellular uptake images from a CLSM: (A) MDA-MB-231 cells without PSeDEVDCD/FAM-miR/HA (scale bar 30 μm), (B) MDA-MB-231 cells with PSeDEVDCD/FAM-miR/HA (scale bar 20 μm), (C) HA receptor-blocked MDA-MB-231 cells with PSeDEVDCD/FAM-miR/HA (scale bar 20 μm). The low from 1 to 4 are FAM-miR, cell membrane, DOX and the merged.

Besides, HA receptors of CD44 and RHAMM are rarely expressed on normal cells [40]. Due to the lack of HA receptors of normal cells, *in vitro* cellular uptake evaluation confirms that

the HA coated PSeDEVDCD/FAM-miR/HA selectively enter metastatic cancer cells but not normal cells.

6.3.4 *In vitro* cell viability assays on normal and DOX sensitive cancer cells

6.3.4.1 Biocompatibility

Key advantage of the PSeDEVDCD/miR-21i/HA is the function of targeting sequential release together with minimal side effects to healthy cells. To verify its low toxicity to normal cells, viability of human kidney cell line HEK293T in the presence of PSeDEVDCD/miR-21i/HA (10 N/P and 4 weights of HA to miR-21i) was *in vitro* evaluated at various loaded DOX concentrations from 0.1 to 2.5 $\mu\text{g mL}^{-1}$. For comparison, HEK293T cell viability in the presence of PSeDEVDCD/HA and free DOX was also evaluated at the equivalent DOX concentrations. PSeDEVDCD/miR-21i/HA and PSeDEVDCD/HA show exceptionally high cell survival rates of 94.8 ± 1.9 and 99.6 ± 3.9 % at a DOX concentration of 2.5 $\mu\text{g mL}^{-1}$, whereas free DOX as a negative control presents 35.5 ± 4.6 % of cell survival at the same DOX concentration (Figure 6.3A). The cell viability difference between free DOX and PSeDEVDCD/miR-21i/HA or PSeDEVDCD/HA is due to DOX accumulation in the HEK293T cells. By penetrating cell membrane, free DOX can accumulate enough to induce such severe apoptosis in HEK293T cells where anti-apoptotic gene of miR-21 is rarely expressed [41, 42]. However, HA surface coated PSeDEVDCD/miR-21i/HA and PSeDEVDCD/HA have negligible side-effects due to their ineffective HA receptor-mediated endocytosis to HEK293T cells where HA receptors are limitedly expressed [40]. In addition, DOX releasing from the delivery systems of PSeDEVDCD/miR-21i/HA and PSeDEVDCD/HA is suppressed in the absence of active caspase-3 enzyme (Figure 6.1A). Lack of ROS production or DNA damage in HEK293T cells by ineffective cellular uptake of PSeDEVDCD/miR-21i/HA and PSeDEVDCD/HA cannot trigger to activate caspase-3 and release DOX, resulting in such high survival rate of the cells.

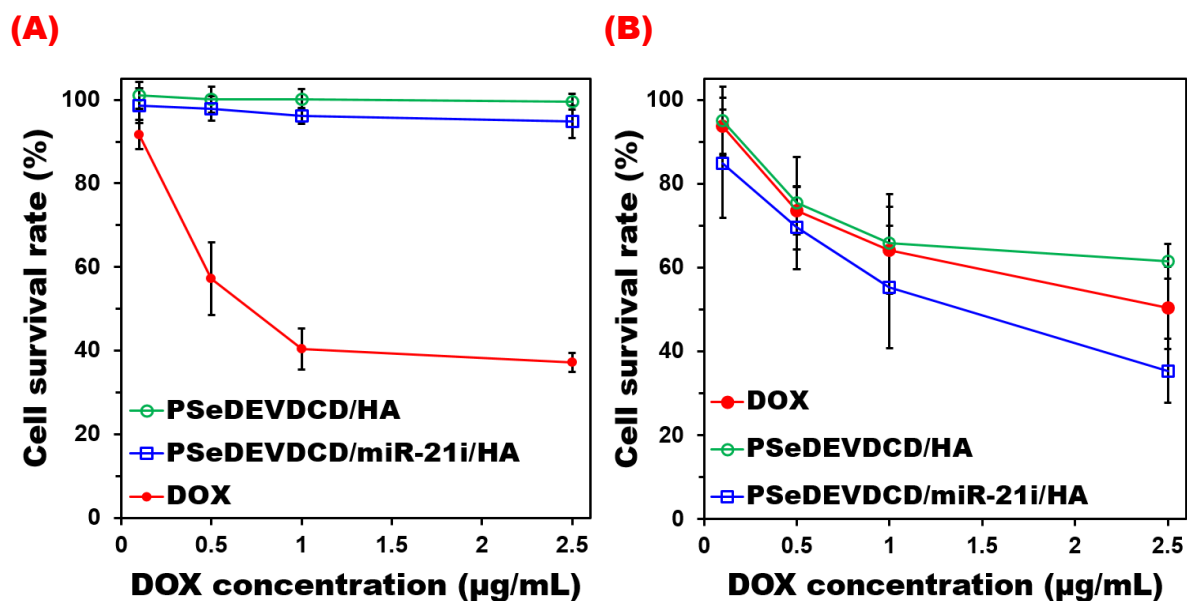


Figure 6.3 Cell viability against free DOX, PSeDEVDCD/HA and PSeDEVDCD/miR-21i/HA (10 N/P) (A) HEK293T survival rates (n = 12) and (B) MDA-MB-231 survival rates (n = 8).

6.3.4.2 Anticancer effect on DOX sensitive cancer cells

Anticancer effect of the PSeDEVDCD/miR-21i/HA was evaluated via viability assay on a DOX sensitive metastatic breast cancer cell line (MDA-MB-231) after 48 h incubation at various loaded DOX concentrations from 0.1 to 2.5 $\mu\text{g mL}^{-1}$. Cell viability assays of PSeDEVDCD/HA and free DOX were also *in vitro* conducted on MDA-MB-231 cells for comparison. Figure 6.3B shows descendent profiles of cell survival rates for all PSeDEVDCD/miR-21i/HA, PSeDEVDCD/HA and free DOX as increasing DOX concentrations. However, the anticancer efficacy of PSeDEVDCD/miR-21i/HA outweighs PSeDEVDCD/HA and free DOX. The cell survival rate for PSeDEVDCD/HA at a DOX concentration of 2.5 $\mu\text{g mL}^{-1}$ is 61.4 \pm 4.2 %, while that for free DOX is 50.5 \pm 9.8 %. The lesser anticancer effect of PSeDEVDCD/HA than free DOX can be explained with the limitedly released DOX from the PSeDEVDCD/HA in the absence of caspase-3 (Figure 6.1A). Highly expressed in the metastatic cancer cells, miR-21 can suppress the release of DOX from the PSeDEVDCD/HA by down-regulating PTEN and inhibiting caspase-3 activation [3, 43].

The PSeDEVDCD/miR-21i/HA show 35.3 ± 7.7 % cancer cell survival. The accompanying miR-21i can inhibit the activity of the apoptosis path suppressor miR-21 so that caspase-3 is activated to release DOX (Figure 6.1A) [3, 44]. In addition, the impeding miR-21 activity by miR-21i can upregulate PDCD4, as an inhibitor of JNK/c-Jun pathway, which protects p53 and accelerates apoptosis [9, 10]. Therefore, synergistic anticancer effects on the metastatic cancer cells is achieved by using PSeDEVDCD/miR-21i/HA.

6.3.5 MDR reverse-triggered sequential releasing

6.3.5.1 Multidrug resistance of MDA-MB-231-R

PSeDEVDCD/miR-21i/HA is prepared to sequentially deliver miR-21i and DOX to MDR metastatic cancer cells to enhance anticancer efficacy. For the evaluation of *in vitro* sequential releasing and therapeutic efficacy, MDA-MB-231 cells were cultured into multidrug resistant metastatic cancer cells of MDA-MB-231-R in the presence of DOX for 24 weeks. During the MDA-MB-231-R cell culture period at pre-determined time, 0, 4, 8, 12, and 24 weeks (W), the resistance of the cells to DOX was evaluated via cell viability assay at various free DOX concentrations from 0.1 to $2.5 \mu\text{g mL}^{-1}$. Figure 6.S8 shows ascending profiles of cell survival rate with prolonging culture time. The fact that initial cell survival of 50.4 ± 3.8 % at a DOX concentration of $2.5 \mu\text{g mL}^{-1}$ increases continuously to 77.3 ± 6.4 % after culturing over 24 W proves the successful incubation process of multidrug resistant cancer cell line, MDA-MB-231-R.

6.3.5.2 Tracing of sequential release of miR-21i and DOX *in vitro*

The sequential release of miR-21i and DOX from PSeDEVDCD/miR-21i/HA has been *ex vivo* evaluated in pH 7.4 buffers under various caspase-3 and 20 mM GSH levels. To verify the ability of PSeDEVDCD/miR-21i/HA to sequentially release miR-21i and DOX in order to maximize therapeutic efficiency and efficacy to multidrug resistant cancer cells, its intracellular release profiles should be tracked, where FAM-miR with its emission at 530 nm

is used together with miR-21i and DOX can emit fluorescence at 580 nm. As FAM-miR has the function of fluorescence but no miR-21 suppression, miR-21i is co-loaded to inhibit the activity of miR-21 for MDR reverse and caspase-3 activation. In addition, the fluorescence of FAM-miR and DOX in PSeBHQDEVDCD is quenched (Figure 6.S4) since the FAM-miR and DOX are close to the BHQ2 moiety within 10 nm [45]. After FAM-miR and DOX being released from the microgel carriers, their fluorescence will be visible.

Prior to FAM-miR and DOX release, BHQ2 quenching the intrinsic fluorescence of FAM-miR and DOX is observed via a CLSM after incubating MDA-MB-231-R cells with PSeBHQDEVDCD/FAM-miR/HA for 4 h, where Figure 6.4A shows overlap of little green (FAM-miR) and no blue (DOX) in the merged image in contrast to the Figure 6.2B for cellular uptake of PSeDEVDCD/FAM-miR/HA. Although MDA-MB-231-R cells can uptake PSeBHQDEVDCD/FAM-miR/HA, quenching of DOX and FAM-miR makes them almost invisible via a CLSM. Besides, the intensity of green from FAM-miR monitored in Figure 6.4B for 8h incubation of MDA-MB-231-R cells with PSeBHQDEVDCD/FAM-miR/HA is further strengthened after incubating for 12 h (Figure 6.4C), where the blue color of DOX is also observed to confirm the sequential release of FAM-miR and DOX.

At the same time, intracellular release of the FAM-miR (FL-1) and DOX (FL-2) from PSeBHQDEVDCD/FAM-miR/miR-21i/HA to MDA-MB-231-R cells was further quantified via flow cytometer at different incubation intervals of 4, 8, 12, and 24 h. Figure 6.4D shows the fluorescence intensity in the sections of upper/left for FAM only, lower/right for DOX only and upper/right for FAM and DOX. The fluorescence intensity of 0.2 % for control MDA-MB-231-R cells without delivery systems of PSeBHQDEVDCD/FAM-miR/miR-21i/HA in those sections displays 4.0, 3.1 and 2.9 % for the cells with the delivery system at incubation time of 4 h. The fluorescence intensity for FAM only, DOX only and both FAM and DOX is further increased to 13.5, 4.0 and 9.7% over 24 h incubation. These indicate that the release of FAM-

miR and DOX from their delivery system of PSeBHQDEVDCD/FAM-miR/miR-21i/HA are traced and continuously increased in volume.

The fluorescence of FAM and DOX quenched by BHQ can be recovered after the FAM-miR and DOX are released from PSeBHQDEVDCD/FAM-miR/miR-21i/HA. Thus, the quantified fluorescence intensity of FAM and DOX through flow cytometer is expressed as the cumulative release of FAM-miR, miR-21i and DOX from PSeBHQDEVDCD/FAM-miR/miR-21i/HA over 24 h, at [Figure 6.4E](#). The releasing amount of FAM-miR and miR-21i increases straightforwardly to 37.8 % over 12 h and further inclines to 45.6 % over 24 h. Such cumulative releasing profile of FAM-miR and miR-21i from PSeBHQDEVDCD/FAM-miR/miR-21i/HA can be explained when the PSeBHQDEVDCD is decomposed in GSH-intensive MDA-MB-231-R cells and loses interaction with FAM-miR and miR-21i, as similar to [Figure 6.1B](#) and [6.1D](#). Therefore, it is confirmed that FAM-miR and miR-21i are released as prolonging time of PSeBHQDEVDCD/FAM-miR/miR-21i/HA positioned in cancer cytosol. However, the cumulative release of DOX shows an unexpected profile to the *ex vivo* DOX releasing assay in 0 M caspase-3 ([Figure 6.1A](#)). The cumulative release of DOX from PSeBHQDEVDCD/FAM-miR/miR-21i/HA in MDA-MD-231-R cells increases moderately to 7.1 % over 8 h, but suddenly escalates to 10.8 % over 12 h and further to 13.3 % over 24 h ([Figure 6.4E](#)). The sudden increase in the speed of DOX release at the incubation time from 8 to 12 h is distinguished from the continuous decrease of DOX releasing speed over 24 h in [Figure 6.1A](#). It can be inferred that the burst release of DOX from PSeBHQDEVDCD/FAM-miR/miR-21i/HA in MDA-MD-231-R cells over 8 - 12 h is triggered by cleaving DEVDC moieties of the peptide linkers in the presence of an active caspase-3. Caspase-3 activation in multidrug resistant cells is hindered by overexpressed miR-21 as an inhibitor of apoptotic pathway [29].

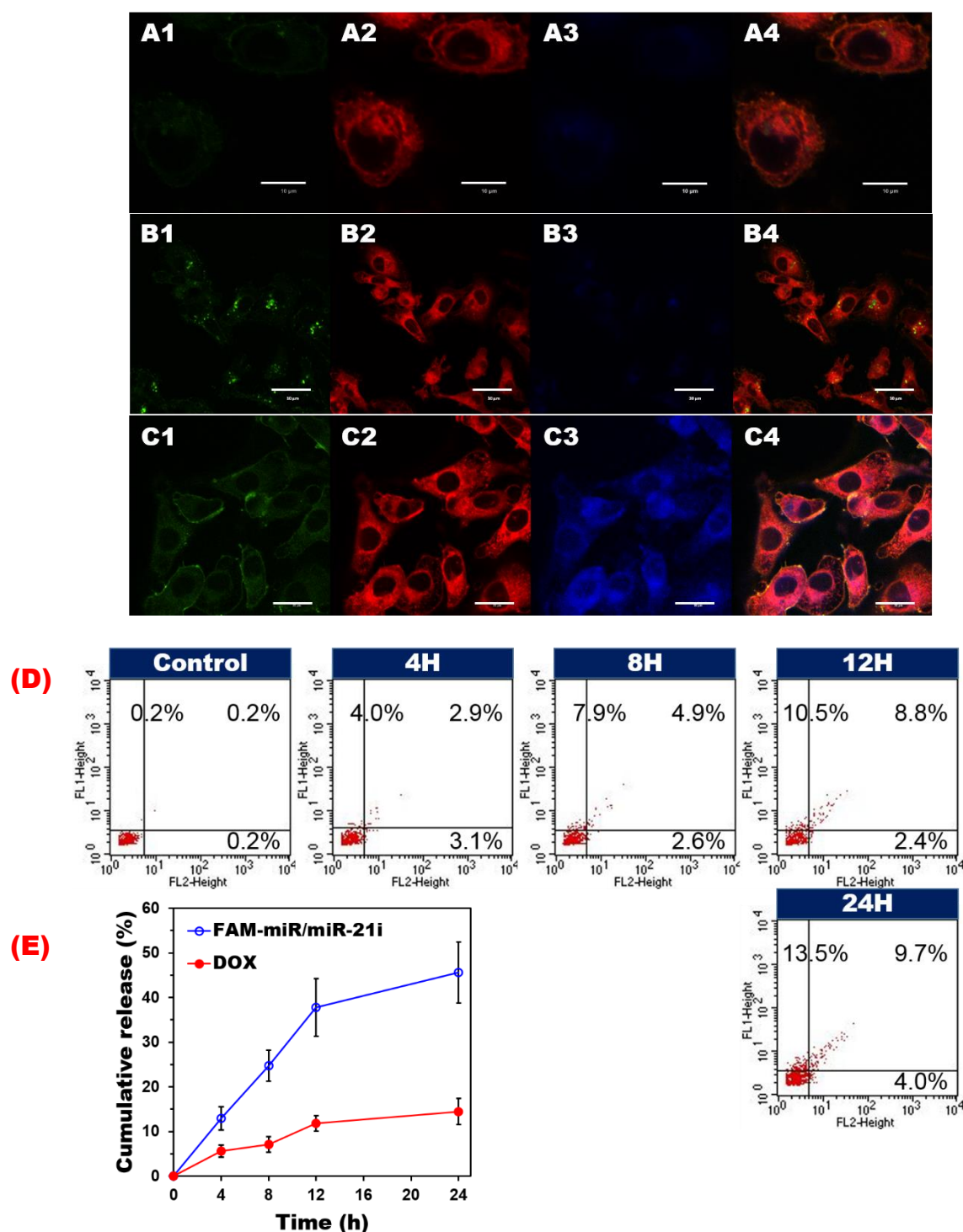


Figure 6.4 Tracing release of quenched FAM-miR and DOX from PSeBHQDEVDCD/FAM-miR/miR-21i/HA to MDA-MB-231-R cells: (A) CLSM images after 4 h incubation (scale bar 10 μ m), (B) CLSM images after 8 h incubation (scale bar 30 μ m), and (C) CLSM images after 12 h incubation (scale bar 20 μ m). The low from 1 to 4 are FAM-miR, cell membrane, DOX and the merged. (D) quantitative release via flow cytometer, MDA-MB-231-R without PSeBHQDEVDCD/FAM-miR/miR-21i/HA as a control, and MDA-MB-231-R incubated with PSeBHQDEVDCD/FAM-miR/miR-21i/HA for 4, 8, 12 and 24h (FL1 for FAM and FL2 for DOX), (E) graphic presentation of cumulative release of FAM-miR, miR-21i and DOX from PSeBHQDEVDCD/FAM-miR/miR-21i/HA to MDA-MB-231-R cells for 24 h incubation (n = 3).

However, the steeply released miR-21i from PSeBHQDEVDCD/FAM-miR/miR-21i/HA over 12 h can inhibit the activity of miR-21 to reverse MDR and activate caspase-3 for DOX burst release. Therefore, it is found that PSeBHQDEVDCD/FAM-miR/miR-21i/HA releases FAM-miR and miR-21i first in GSH-enriched MDA-MB-231 cells, and intensively releases DOX sequentially in the presence of active caspase-3.

6.3.6 Therapeutic effects on multidrug-resistant cancer cells

Sequential releasing of miR-21i and DOX using PSeDEVDCD/miR-21i/HA is able to enhance therapeutic efficiency and efficacy to metastatic cancer cells with MDR. The anticancer effect was evaluated via viability assays to MDA-MB-231-R cells after incubation with PSeDEVDCD/miR-21i/HA, PSeDEVDCD/HA or free DOX with equivalent loaded DOX concentrations from 0.1 to 2.5 $\mu\text{g mL}^{-1}$ for 48 h. [Figure 6.5A](#) shows a dose-dependent but remarkably different therapeutic effects of those systems to cells.

Free DOX is ineffective to treat multidrug-resistant cancer cells since these multidrug resistant cells have self-defensive functions, such as overexpressed ABC transporters to reduce intracellular DOX accumulation, increased GSH levels to detoxify ROS from the remained DOX, and over-activated miR-21 to inhibit apoptosis [13, 14, 46]. The undermined anticancer performance of free DOX can be relatively enhanced by using the PSeDEVDCD/HA system with a cell survival rate of $45.8 \pm 3.8\%$ at a loaded DOX concentration of 2.5 $\mu\text{g mL}^{-1}$. The better therapeutic effect of the PSeDEVDCD/HA than free DOX can be due to its higher intracellular accumulation. HA surface coating of PSeDEVDCD/HA promotes selective endocytosis to MDA-MB-231-R cells through HA receptor mediation. Although DOX releasing from the PSeDEVDCD/HA in the absence of activated caspase-3 is limited ([Figure 6.1A](#)), the amount of DOX from PSeDEVDCD/HA in cytoplasm is still larger than that of permeated free DOX crossover cell transmembrane, in which ABC transporters are installed [46, 47]. DOX loaded in the PSeDEVDCD can generate ROS via the quinone moieties of DOX

in a metabolic process of the cells [48]. The resulting ROS can initiate apoptosis signaling pathways that activate caspase-3 to release DOX from PSeDEVDCD/HA [1]. In addition, the released cysteine-DOX with carboxylic moiety that improves hydrophilicity than free DOX can reduce affinity with a pair of transmembrane domains (TMDs) of the ABC transporters, which hydrophobic materials can bind to [15]. Thus, the released cysteine-DOX from PSeDEVDCD/HA can accumulate in the cytoplasm rather than being exported out, leading to apoptosis in MDA-MB-231-R24w cells. However, the anticancer effect of PSeDEVDCD/HA on the multidrug resistant MDA-MB-231-R24w cells is moderately limited as DOX-induced oxidative stress activates apoptosis signals as well as anti-apoptotic factors of c-Jun and NF- κ B [2, 7]. The apoptotic inhibition of MDA-MB-231-R24w occurs by suppressing the pro-apoptotic gene of p53 by c-Jun and expressing the anti-apoptotic gene of miR-21 by NF- κ B [5, 10].

On the other hand, PSeDEVDCD/miR-21i/HA is more effective in killing cancer cells as evident from a low cell surviving of 1.6 ± 1.1 % at a DOX concentration of $2.5 \mu\text{g mL}^{-1}$. The released miR-21i from PSeDEVDCD/miR-21i/HA impedes miR-21, which targets tumor suppresser genes of PTEN and PDCD4 [37]. Upregulation of PTEN can downregulate PI3K, as an inhibitor of apoptotic pathway, and reverse MDR [44]. The reversing MDR allows to transmit successfully the apoptosis signals initiating from the DOX-induced oxidative stress to activate the caspase-3 [2]. The activated caspase-3 brings cell rupture and apoptotic body formation followed by cell death, as well as stimulating burst DOX-releasing to the re-sensitized MDA-MB-231-R24w cells to accelerate apoptosis [2]. In addition, the upregulated PDCD4 can protect a DNA damage-induced tumor suppresser protein, p53, via downregulating oxidative stress-induced c-Jun, to successively signal to caspase-3 activation for the accelerating DOX release and apoptosis [10, 49]. Besides, the therapeutic efficacy of the PSeDEVDCD/miR-21i/HA to multidrug-resistant MDA-MB-231-R24w cells is even higher

than that to DOX-sensitive MDA-MB-231 cells (Figure 6.3B). As GSH is more enriched in multidrug-resistant cells than DOX-sensitive cells [14], more diselenide crosslinkers of PSeDEVDCD/miR-21i/HA can be cleaved in the GSH-intensive MDA-MB-231-R24w to release extra miR-21i (Figure 6.1B). The amount of miR-21i released from PSeDEVDCD/miR-21i/HA in the multidrug-resistant cells leads to better therapeutic efficacy to DOX-sensitive MDA-MB-231 cells, as well as to the other therapeutics of PSeDEVDCD/HA and free DOX.

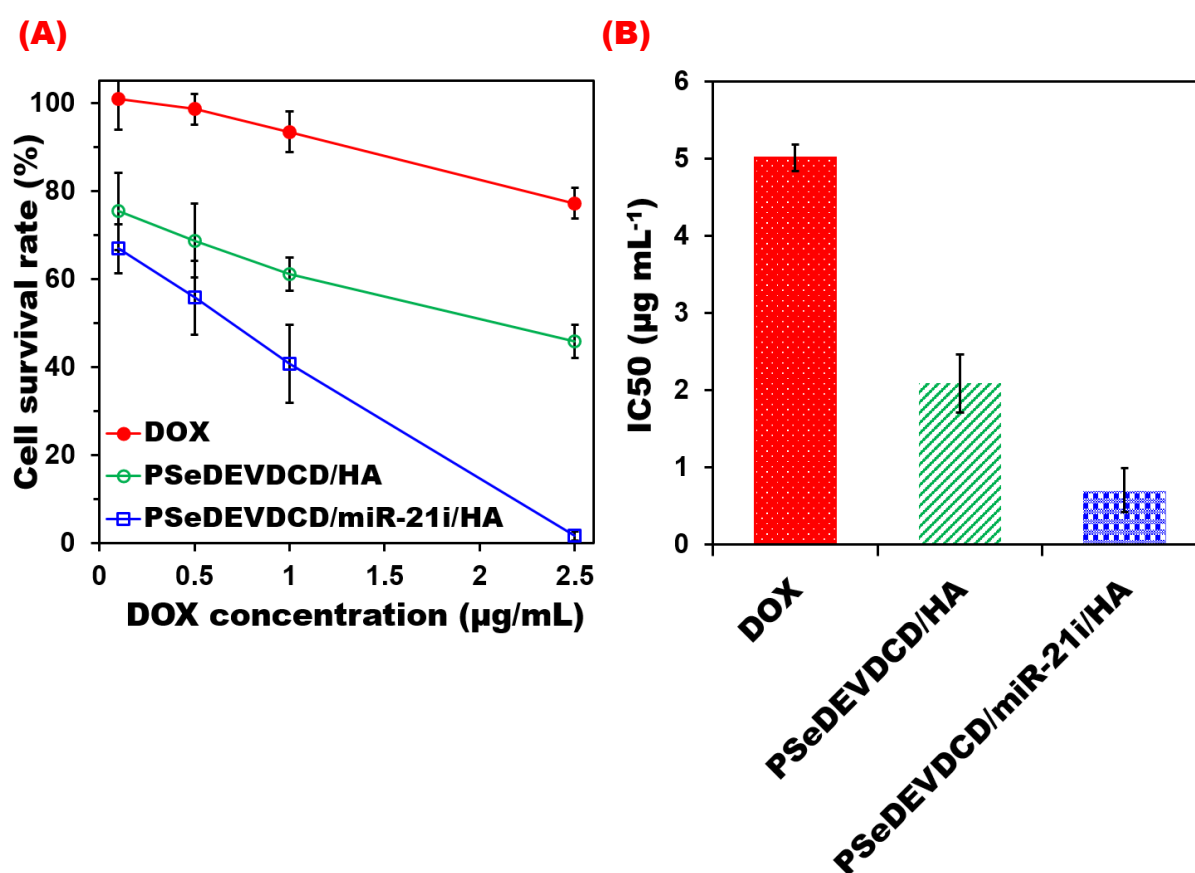


Figure 6.5 Viability of multidrug resistant cancer cells MDA-MB-231-R24w in the presence of free DOX, PSeDEVDCD/HA and PSeDEVDCD/miR/HA: (A) cell survival rate (n = 12) (B) IC₅₀ values (n = 12).

To easily compare therapeutic efficiency, DOX concentration for half cell death IC₅₀ is depicted in Figure 6.5B, where PSeDEVDCD/miR-21i/HA requires 3 times lesser DOX than PSeDEVDCD/HA and 7.3 times lesser than free DOX for half cell death. . In addition, high

therapeutic efficiency can also be achieved by controlling DOX release time to minimize the amount of DOX that ABC transporter can expel. The PSeDEVDCD/miR-21i/HA release DOX at the most appropriate time when caspase-3 is activated and MDR is reversed for high therapeutic efficiency. The therapeutic efficiency for sequential releases of miR-21i and DOX from PSeDEVDCD/miR-21i/HA is compared with those simultaneous release of miR-21i and DOX in our previous studies and traditional therapeutic systems (Tables 6.S1 and 6.S2). Taking the IC_{50} value of free DOX as a reference, the relative IC_{50} values for sequential release of miR-21 and DOX to multidrug resistant cells represent notably higher than concurrent release and conventional therapeutic systems. That suggests the GSH and caspase-3-cleavable PSeDEVDCD/miR-21i/HA system for sequential releasing of miR-21i and DOX has a great potential in effective multidrug resistance cancer therapeutic applications.

6.4 Conclusion

A smart PSeDEVDCD/miR-21i/HA nanomedicine system with the ability of sequential release of miR-21i and DOX to multidrug resistant cancer cells was developed and evaluated to provide maximal therapeutic efficacy together with minimal side-effects. Biodegradable microgels of PSeN₃ by crosslinking PEI800 with diselenide crosslinkers enable to release miR-21i to cancer cytoplasm at a high GSH level. DOX is conjugated to the microgels through a DEVDC-containing peptide linker through azide-alkyne cycloaddition to control DOX release in the presence of active caspase-3. HA surface coating prevents serum protein adsorption and promotes HA receptor-mediated endocytosis to metastatic cancer cells. The intensive release of miR-21i to MDR cancer cells promotes the sequential DOX release of associated with the activation of caspase-3 and re-sensitizing MDR cancer cells. The PSeDEVDCD/miR-21i/HA is fully biodegradable in intracellular microenvironment of cancer cells and low toxic to normal cells. *In vitro* cell viability assays demonstrate the targeting sequential release of miR-21i and

DOX from PSeDEVDCD/miR-21i/HA, giving rise to high therapeutic efficacy and efficiency to multidrug resistant MDA-MB-231-R cells. The presence of this smart PSeDEVDCD/miR-21i/HA nanomedicine system possesses a bright promise for the treatment of final stage cancers.

Acknowledgement

We are grateful for the research grant of the Australian Research Council DP110102877 and DP140104062. SY would like to appreciate the APA scholarship provided by the University of Adelaide.

References

- [1] G. Minotti, P. Menna, E. Salvatorelli, G. Cairo, L. Gianni, Anthracyclines: Molecular Advances and Pharmacologic Developments in Antitumor Activity and Cardiotoxicity, *Pharmacol. Rev.*, 56 (2004) 185-229.
- [2] N. Pilco-Ferreto, G.M. Calaf, Influence of doxorubicin on apoptosis and oxidative stress in breast cancer cell lines, *Int. J. Oncol.*, 49 (2016) 753-762.
- [3] L. Ouyang, Z. Shi, S. Zhao, F.-T. Wang, T.-T. Zhou, B. Liu, J.-K. Bao, Programmed cell death pathways in cancer: a review of apoptosis, autophagy and programmed necrosis, *Cell Prolif.*, 45 (2012) 487-498.
- [4] C. Porta, C. Paglino, A. Mosca, Targeting PI3K/Akt/mTOR Signaling in Cancer, *Front. Oncol.*, 4 (2014) 64-64.
- [5] J. Niu, Y. Shi, G. Tan, C.H. Yang, M. Fan, L.M. Pfeffer, Z.-H. Wu, DNA Damage Induces NF- κ B-dependent MicroRNA-21 Up-regulation and Promotes Breast Cancer Cell Invasion, *J. Biol. Chem.*, 287 (2012) 21783-21795.
- [6] V. Grünwald, L. DeGraffenried, D. Russel, W.E. Friedrichs, R.B. Ray, M. Hidalgo, Inhibitors of mTOR Reverse Doxorubicin Resistance Conferred by PTEN Status in Prostate Cancer Cells, *Cancer Res.*, 62 (2002) 6141-6145.
- [7] N. Tobar, M. Toyos, C. Urra, N. Méndez, R. Arancibia, P.C. Smith, J. Martínez, c-Jun N terminal kinase modulates NOX-4 derived ROS production and myofibroblasts differentiation in human breast stromal cells, *BMC Cancer*, 14 (2014) 640-640.
- [8] M.M. Vleugel, A.E. Greijer, R. Bos, E. van der Wall, P.J. van Diest, c-Jun activation is associated with proliferation and angiogenesis in invasive breast cancer, *Hum. Pathol.*, 37 (2006) 668-674.
- [9] J. Liu, R. Zhai, J. Zhao, F. Kong, J. Wang, W. Jiang, Q. Xin, X. Xue, Y. Luan, Programmed cell death 4 overexpression enhances sensitivity to cisplatin via the JNK/c-Jun signaling pathway in bladder cancer, *Int. J. Oncol.*, (2018).
- [10] M. Schreiber, A. Kolbus, F. Piu, A. Szabowski, U. Möhle-Steinlein, J. Tian, M. Karin, P. Angel, E.F. Wagner, Control of cell cycle progression by c-Jun is p53 dependent, *Genes Dev.*, 13 (1999) 607-619.
- [11] D.R. Gutsaeva, M. Thounaojam, S. Rajpurohit, F.L. Powell, P.M. Martin, S. Goei, M. Duncan, M. Bartoli, STAT3-mediated activation of miR-21 is involved in down-regulation of TIMP3 and neovascularization in the ischemic retina, *Oncotarget*, 8 (2017) 103568-103580.
- [12] R. Krishna, L.D. Mayer, Multidrug resistance (MDR) in cancer: Mechanisms, reversal using modulators of MDR and the role of MDR modulators in influencing the pharmacokinetics of anticancer drugs, *Eur. J. Pharm. Sci.*, 11 (2000) 265-283.
- [13] W. Hu, C. Tan, Y. He, G. Zhang, Y. Xu, J. Tang, Functional miRNAs in breast cancer drug resistance, *Onco Targets Ther.*, 11 (2018) 1529-1541.

- [14] J. Deng, D. Coy, W. Zhang, M. Sunkara, A.J. Morris, C. Wang, L. Chaiswing, D. St Clair, M. Vore, P. Jungsuwadee, Elevated glutathione is not sufficient to protect against doxorubicin-induced nuclear damage in heart in multidrug resistance-associated protein 1 (Mrp1/Abcc1) null mice, *J. Pharmacol. Exp. Ther.*, 355 (2015) 272-279.
- [15] K.P. Locher, Review. Structure and mechanism of ATP-binding cassette transporters, *Philos. Trans. R. Soc. Lond. B Biol. Sci.*, 364 (2009) 239-245.
- [16] J. Greene, B. Hennessy, The role of anthracyclines in the treatment of early breast cancer, *J. Oncol. Pharm. Pract.*, 21 (2015) 201-212.
- [17] N.M. Elsherbiny, M. El-Sherbiny, Thymoquinone attenuates Doxorubicin-induced nephrotoxicity in rats: Role of Nrf2 and NOX4, *Chem. Biol. Interact.*, 223 (2014) 102-108.
- [18] G. Damodar, T. Smitha, S. Gopinath, S. Vijayakumar, Y. Rao, An evaluation of hepatotoxicity in breast cancer patients receiving injection Doxorubicin, *Ann. Med. Health Sci. Res.*, 4 (2014) 74-79.
- [19] E.C. Bredahl, K.B. Pfannenstiel, C.J. Quinn, R. Hayward, D.S. Hydock, Effects of Exercise on Doxorubicin-Induced Skeletal Muscle Dysfunction, *Med. Sci. Sports Exerc.*, 48 (2016) 1468-1473.
- [20] C.-C. Peng, C.-L. Hsieh, Y.-B. Ker, H.-Y. Wang, K.-C. Chen, R.Y. Peng, Selected nutraceutical screening by therapeutic effects on doxorubicin-induced chronic kidney disease, *Mol. Nutr. Food Res.*, 56 (2012) 1541-1558.
- [21] Z. Liu, A.C. Fan, K. Rakhra, S. Sherlock, A. Goodwin, X. Chen, Q. Yang, D.W. Felsher, H. Dai, Supramolecular Stacking of Doxorubicin on Carbon Nanotubes for In Vivo Cancer Therapy, *Angew. Chem. Int. Ed.*, 48 (2009) 7668-7672.
- [22] X. Qian, L. Long, Z. Shi, C. Liu, M. Qiu, J. Sheng, P. Pu, X. Yuan, Y. Ren, C. Kang, Star-branched amphiphilic PLA-b-PDMAEMA copolymers for co-delivery of miR-21 inhibitor and doxorubicin to treat glioma, *Biomaterials*, 35 (2014) 2322-2335.
- [23] W. Kai, H. Qida, Z. Wei, Z. Mengmeng, P. Yuan, T. Guping, Structure-Invertible Nanoparticles for Triggered Co-Delivery of Nucleic Acids and Hydrophobic Drugs for Combination Cancer Therapy, *Adv. Funct. Mater.*, 25 (2015) 3380-3392.
- [24] X. Deng, M. Cao, J. Zhang, K. Hu, Z. Yin, Z. Zhou, X. Xiao, Y. Yang, W. Sheng, Y. Wu, Y. Zeng, Hyaluronic acid-chitosan nanoparticles for co-delivery of MiR-34a and doxorubicin in therapy against triple negative breast cancer, *Biomaterials*, 35 (2014) 4333-4344.
- [25] L. Han, C. Tang, C. Yin, Dual-targeting and pH/redox-responsive multi-layered nanocomplexes for smart co-delivery of doxorubicin and siRNA, *Biomaterials*, 60 (2015) 42-52.
- [26] D.-W. Dong, B. Xiang, W. Gao, Z.-Z. Yang, J.-Q. Li, X.-R. Qi, pH-responsive complexes using prefunctionalized polymers for synchronous delivery of doxorubicin and siRNA to cancer cells, *Biomaterials*, 34 (2013) 4849-4859.

- [27] M. Wang, T. Liu, L. Han, W. Gao, S. Yang, N. Zhang, Functionalized O-carboxymethyl-chitosan/polyethylenimine based novel dual pH-responsive nanocarriers for controlled co-delivery of DOX and genes, *Polym. Chem.*, 6 (2015) 3324-3335.
- [28] H. Wang, Y. Jiang, H. Peng, Y. Chen, P. Zhu, Y. Huang, Recent progress in microRNA delivery for cancer therapy by non-viral synthetic vectors, *Adv. Drug Del. Rev.*, 81 (2015) 142-160.
- [29] Y. Ren, R. Wang, L. Gao, K. Li, X. Zhou, H. Guo, C. Liu, D. Han, J. Tian, Q. Ye, Y.T. Hu, D. Sun, X. Yuan, N. Zhang, Sequential co-delivery of miR-21 inhibitor followed by burst release doxorubicin using NIR-responsive hollow gold nanoparticle to enhance anticancer efficacy, *J. Control. Release*, 228 (2016) 74-86.
- [30] S.W. Chung, B.S. Lee, J.u. Choi, S.W. Kim, I.-S. Kim, S.Y. Kim, Y. Byun, Optimization of a Stable Linker Involved DEVD Peptide-Doxorubicin Conjugate That Is Activated upon Radiation-Induced Caspase-3-Mediated Apoptosis, *J. Med. Chem.*, 58 (2015) 6435-6447.
- [31] H.S. Gill, J. Marik, Preparation of 18F-labeled peptides using the copper(I)-catalyzed azide-alkyne 1,3-dipolar cycloaddition, *Nat. Protoc.*, 6 (2011) 1718.
- [32] P.M. Costa, A.L. Cardoso, C. Nóbrega, L.F. Pereira de Almeida, J.N. Bruce, P. Canoll, M.C. Pedroso de Lima, MicroRNA-21 silencing enhances the cytotoxic effect of the antiangiogenic drug sunitinib in glioblastoma, *Hum. Mol. Genet.*, 22 (2013) 904-918.
- [33] L.K. Fraiji, D.M. Hayes, T.C. Werner, Static and dynamic fluorescence quenching experiments for the physical chemistry laboratory, *J. Chem. Educ.*, 69 (1992) 424.
- [34] R.S. Kumar, S. Arunachalam, V.S. Periasamy, C.P. Preethy, A. Riyasdeen, M.A. Akbarsha, DNA binding and biological studies of some novel water-soluble polymer-copper(II)-phenanthroline complexes, *Eur. J. Med. Chem.*, 43 (2008) 2082-2091.
- [35] S. Kobayashi, K. Hiroishi, M. Tokunoh, T. Saegusa, Chelating properties of linear and branched poly(ethylenimines), *Macromolecules*, 20 (1987) 1496-1500.
- [36] B.B. Wolf, M. Schuler, F. Echeverri, D.R. Green, Caspase-3 Is the Primary Activator of Apoptotic DNA Fragmentation via DNA Fragmentation Factor-45/Inhibitor of Caspase-activated DNase Inactivation, *J. Biol. Chem.*, 274 (1999) 30651-30656.
- [37] Y.H. Feng, C.J. Tsao, Emerging role of microRNA-21 in cancer, *Biomed Rep*, 5 (2016) 395-402.
- [38] H. Wu, J. Wang, H. Ma, Z. Xiao, X. Dong, MicroRNA-21 inhibits mitochondria-mediated apoptosis in keloid, *Oncotarget*, 8 (2017) 92914-92925.
- [39] S.H. Ku, K. Kim, K. Choi, S.H. Kim, I.C. Kwon, Tumor-Targeting Multifunctional Nanoparticles for siRNA Delivery: Recent Advances in Cancer Therapy, *Adv. Healthc. Mater.*, 3 (2014) 1182-1193.
- [40] S.R. Hamilton, S.F. Fard, F.F. Paiwand, C. Tolg, M. Veiseh, C. Wang, J.B. McCarthy, M.J. Bissell, J. Koropatnick, E.A. Turley, The hyaluronan receptors CD44 and Rhamm (CD168) form complexes with ERK1,2 that sustain high basal motility in breast cancer cells, *J. Biol. Chem.*, 282 (2007) 16667-16680.

- [41] M. Dalmark, Characteristics of doxorubicin transport in human red blood cells, *Scand. J. Clin. Lab. Invest.*, 41 (1981) 633-639.
- [42] W. Tian, X. Dong, X. Liu, G. Wang, Z. Dong, W. Shen, G. Zheng, J. Lu, J. Chen, Y. Wang, Z. Wu, X. Wu, High-Throughput Functional MicroRNAs Profiling by Recombinant AAV-Based MicroRNA Sensor Arrays, *PLoS One*, 7 (2012) e29551.
- [43] S. Zhu, H. Wu, F. Wu, D. Nie, S. Sheng, Y.-Y. Mo, MicroRNA-21 targets tumor suppressor genes in invasion and metastasis, *Cell Res.*, 18 (2008) 350-359.
- [44] S. Zhang, L. Han, J. Wei, Z. Shi, P. Pu, J. Zhang, X. Yuan, C. Kang, Combination treatment with doxorubicin and microRNA-21 inhibitor synergistically augments anticancer activity through upregulation of tumor suppressing genes, *Int. J. Oncol.*, 46 (2015) 1589-1600.
- [45] S.A. Marras, F.R. Kramer, S. Tyagi, Efficiencies of fluorescence resonance energy transfer and contact-mediated quenching in oligonucleotide probes, *Nucleic Acids Res.*, 30 (2002) e122.
- [46] M. Saxena, M.A. Stephens, H. Pathak, A. Rangarajan, Transcription factors that mediate epithelial-mesenchymal transition lead to multidrug resistance by upregulating ABC transporters, *Cell Death Dis.*, 2 (2011) e179.
- [47] M.A. Islam, T.E. Park, B. Singh, S. Maharjan, J. Firdous, M.H. Cho, S.K. Kang, C.H. Yun, Y.J. Choi, C.S. Cho, Major degradable polycations as carriers for DNA and siRNA, *J. Control. Release*, 193 (2014) 74-89.
- [48] D.W. Edwardson, R. Narendrula, S. Chewchuk, K. Mispel-Beyer, J.P.J. Mapletoft, A.M. Parissenti, Role of Drug Metabolism in the Cytotoxicity and Clinical Efficacy of Anthracyclines, *Curr. Drug Metab.*, 16 (2015) 412-426.
- [49] N. Kumar, N. Wethkamp, L.C. Waters, M.D. Carr, K.H. Klempnauer, Tumor suppressor protein Pdc4 interacts with Daxx and modulates the stability of Daxx and the Hipk2-dependent phosphorylation of p53 at serine 46, *Oncogenesis*, 2 (2013) e37.

Supporting Information

DEVDC peptide conjugated microgels for intracellular-responsive sequential releasing of miRNA-21 inhibitor and doxorubicin for enhanced therapy to multidrug resistant cancers

*S. Yun, J. Zhang, Prof. H. Zhang, Prof. J. Bi, Prof. S. Dai**

Table 6.S1 Comparison on the therapeutic efficiency of sequential and simultaneous release of miR-21i and DOX in various co-drug delivery systems via relative IC₅₀ value of free DOX to co-delivery system on MDA-MB-231-R cells.

Co-delivery system	Linkers for DOX conjugation	Driving force for DOX release	Releasing sequence	Relative IC ₅₀	Chapter
Free DOX				1	Control
PSeDEVDCD /miR-21i/HA	DEVDC peptide	Activated capase-3	miR-21i then DOX	7.3	This Chapter
PSeSeD /miR-21i/HA	Diselenide bond	Cytosol GSH	Simultaneous	3.8	Chapter 5
PSeHD-SeSeP /miR-21i/HA	Hydrazone and diselenide bonds	Acidic pH and Cytosol GSH	Simultaneous	3.2	Chapter 4

Table 6.S2 Comparison on the anticancer efficiency of various therapeutic systems via relative IC₅₀ value of free DOX to therapeutic system on MDA-MB-231-R cells

Therapeutic system	Relative IC ₅₀	Reference
Free DOX	1	Control
PSeDEVDCD/miR-21i/HA	7.3	This Chapter
DOX/Ac-aCD NP	3.5	[1]
ALN-MA-hyd-DOX	2.5	[2]
LPNs-1	5.4	[3]
DOX-S-S-PTX	6.7	[4]

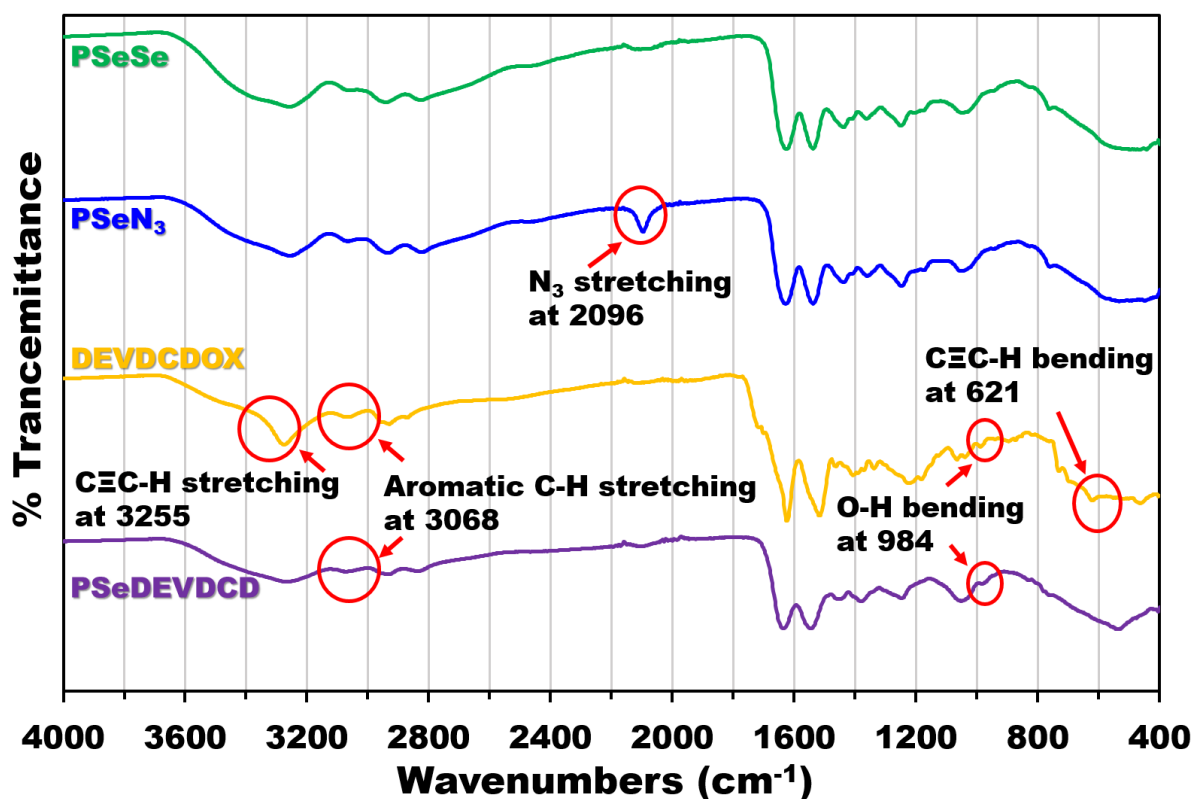


Figure 6.S1 FTIR spectra of diselenide crosslinked PEI microgels (PSeSe), azide group modified PEI microgels (PSeN₃), DOX conjugated alkyne-ended peptide linker (DEVDCDOX), and DOX conjugated to microgels via DEVDC peptide linker (PSeDEVDCD)

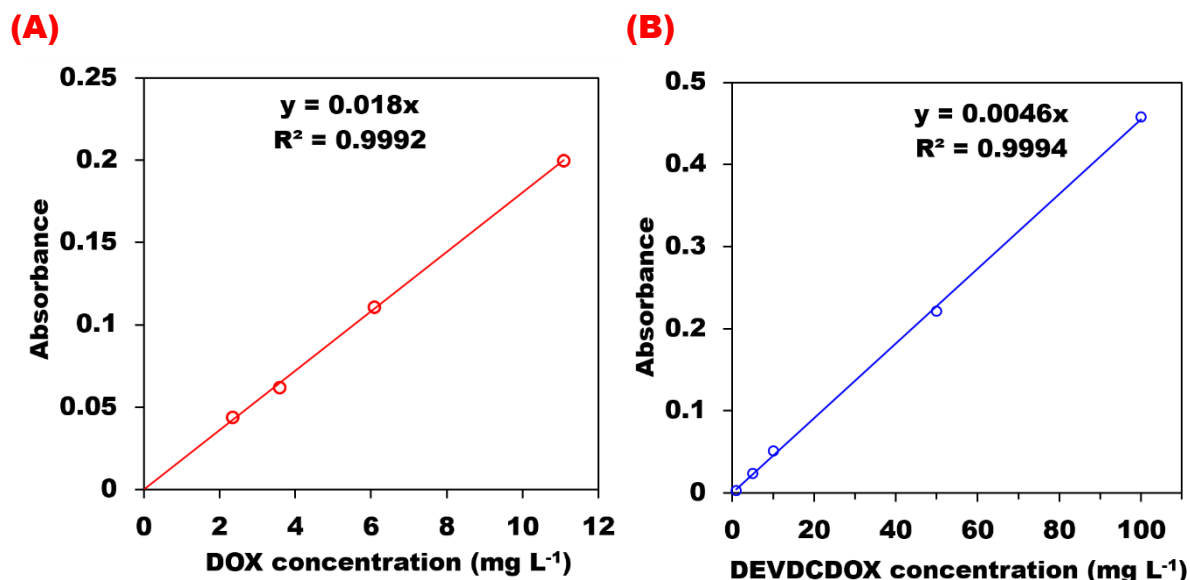


Figure 6.S2 UV-vis calibration curve of (A) DOX and (B) DEVDCDOX in aqueous solution at the wavelength of 479.5 nm and room temperature

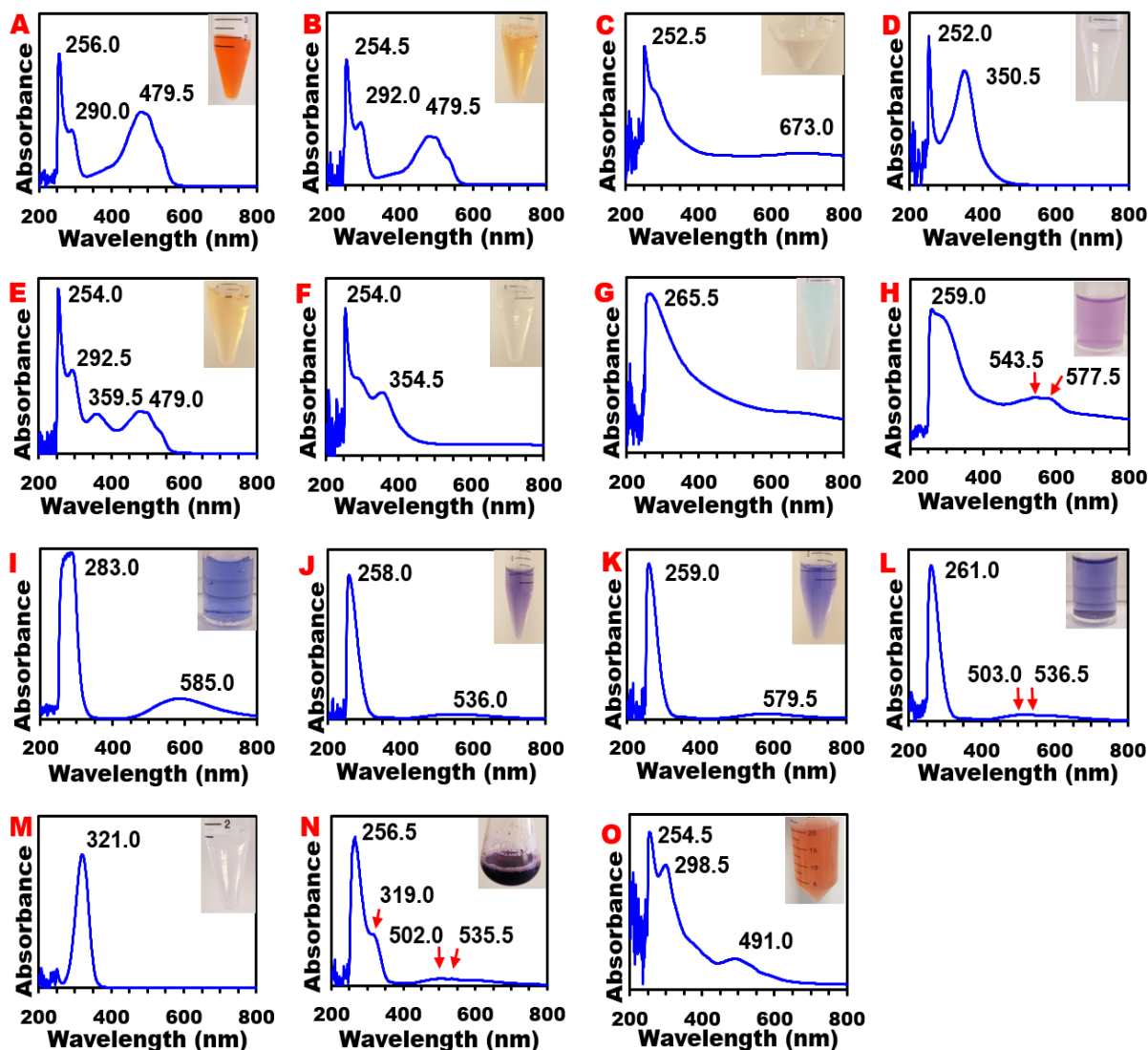


Figure 6.S3 UV-vis spectra and aqueous solution colors of (A) DOX·HCl, (B) DEVDCDOX, (C) PSeN₃ microgels, (D) Triethylenetetramine (Trien), (E) mixture of Trien and DEVDCDOX, (F) mixture of Trien and PSeN₃, (G) copper, (H) mixture of copper and PSeDEVDCD, (I) mixture of copper and Trien, (J) mixture of copper, Trien and DEVDCDOX, (K) mixture of copper, Trien and PSeN₃, (L) mixture of copper, Trien and PSeDEVDCD, (M) gentisic acid, (N) mixture of copper, Trien, gentisic acid and PSeDEVDCD, and (O) PSeDEVDCD at room temperature

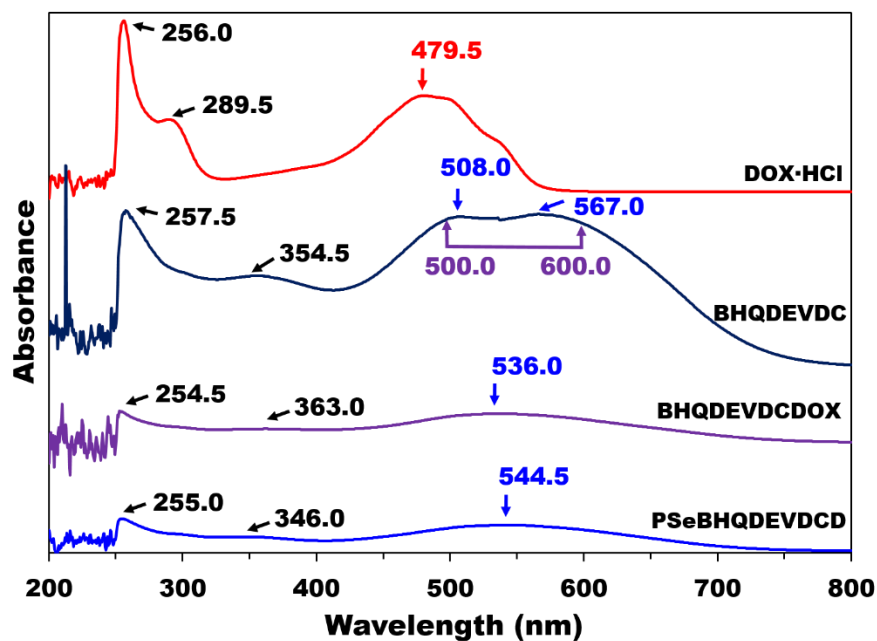


Figure 6.S4 UV-vis spectra of DOX·HCl, BHQ2 conjugated peptide (BHQDEVDC), DOX and BHQ2 conjugated peptide linker (BHQDEVDCDOX), and DOX and BHQ2 conjugated PEI microgels (PSeBHQDEVDCD) at room temperature

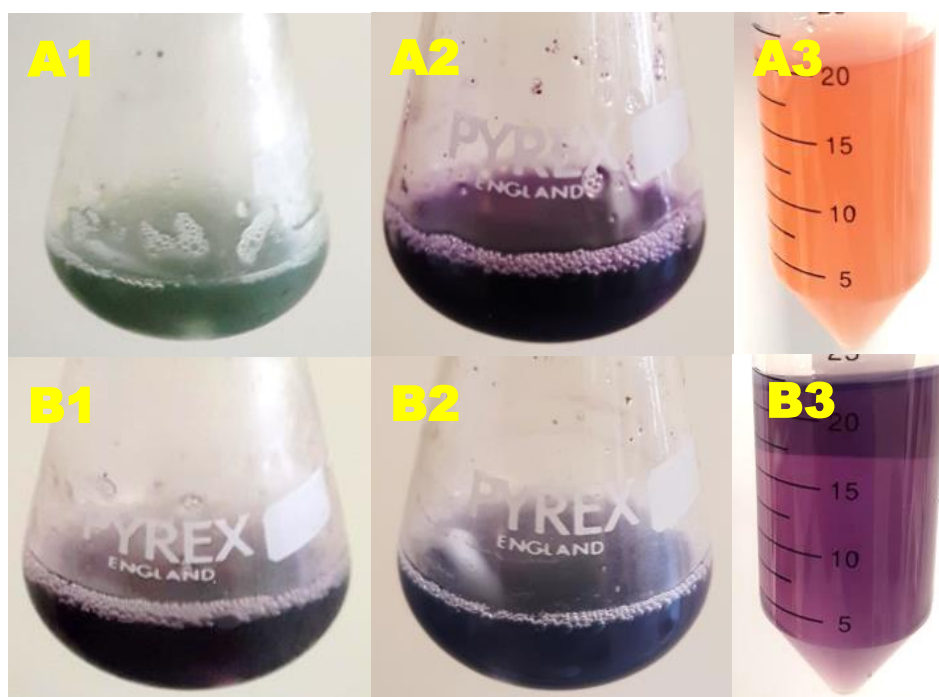


Figure 6.S5 Colors of the aqueous solutions of (A) PSeDEVDCD and (B) PSeBHQDEVDCD. (1) after copper catalyzed click reaction, (2) after adding Trien, and (3) after purification

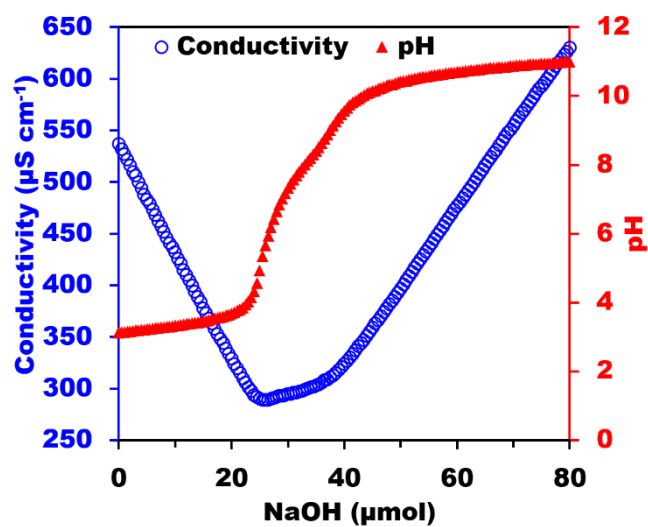


Figure 6.S6 Conductivity and pH titration of PSeDEVDCD (4.5 mg) at room temperature

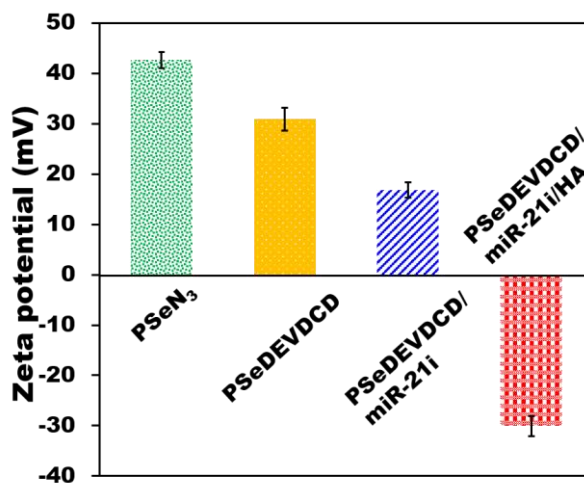


Figure 6.S7 Zeta potentials of PSeN₃, PSeDEVDCD, PSeDEVDCD/miR-21i at a 10 N/P and PSeDEVDCD/miR-21i/HA with a 4-folds weight of HA to miR-21i (n = 3)

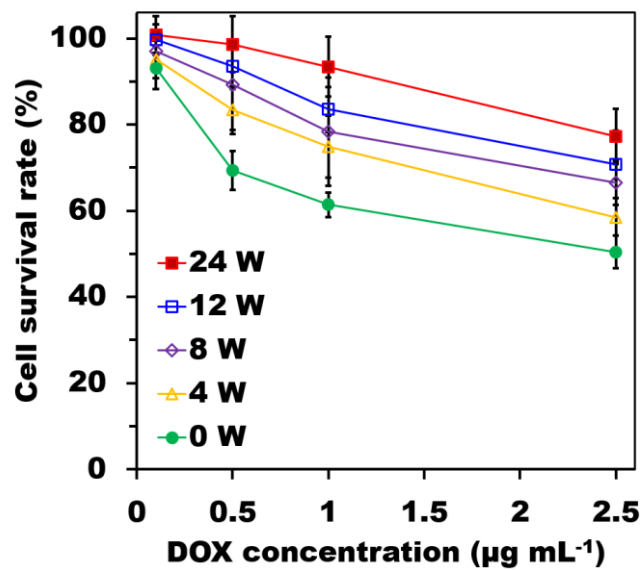


Figure 6.S8 DOX resistance of various MDA-MB-231-R cells as evident from their cell viabilities against free DOX concentrations, where MDA-MB-231 cells were pre-cultured in DOX-incorporated culture medium for 0, 4, 8, 12 and 24 weeks to produce these MDA-MB-231-R cells. (n = 12)

References

- [1] Q. Shi, L. Zhang, M. Liu, X. Zhang, X. Zhang, X. Xu, S. Chen, X. Li, J. Zhang, Reversion of multidrug resistance by a pH-responsive cyclodextrin-derived nanomedicine in drug resistant cancer cells, *Biomaterials*, 67 (2015) 169-182.
- [2] W.L. Ye, Y.P. Zhao, R. Na, F. Li, Q.B. Mei, M.G. Zhao, S.Y. Zhou, Actively targeted delivery of doxorubicin to bone metastases by a pH-sensitive conjugation, *J. Pharm. Sci.*, 104 (2015) 2293-2303.
- [3] J.B. Du, Y.F. Song, W.L. Ye, Y. Cheng, H. Cui, D.Z. Liu, M. Liu, B.L. Zhang, S.Y. Zhou, PEG-detachable lipid-polymer hybrid nanoparticle for delivery of chemotherapy drugs to cancer cells, *Anticancer Drugs*, 25 (2014) 751-766.
- [4] X. Ma, E. Ozliseli, Y. Zhang, G. Pan, D. Wang, H. Zhang, Fabrication of redox-responsive doxorubicin and paclitaxel prodrug nanoparticles with microfluidics for selective cancer therapy, *Biomater. Sci.*, 7 (2019) 634-644.

Chapter 7. Conclusion and Recommendation

7.1 Conclusion

The aim of this thesis is to develop novel multifunctional co-delivery systems of doxorubicin (DOX) and miRNA-21 inhibitor (miR-21i) to achieve both maximal anticancer performance and minimal side effects. Based on the understating of DOX as an active anticancer drug in the apoptotic signaling pathways, accompanied by serious multidrug resistance (MDR) and side effects, we developed a series of novel synergetic co-drug therapy protocols of DOX with miR-21i on mitigation MDR by impeding the activity of miRNA-21 (miR-21) and investigated rational design of co-delivery systems to satisfy essentially required factors in the delivery course. Key conclusions are outlined below:

Multifunctional PEI microgel-based co-delivery system (PSeHD/miR-21i/HA) was firstly prepared to meet all the essential factors in the delivery course in lieu of conflicts to achieve high anticancer effects and low side effects. The functions of PSeHD/miR-21i/HA include hydrazone for DOX conjugation and release in acidic cancer environment, diselenide crosslinking for microgel formation and degradation in reductant cytosol condition, size control from 161 nm for prolonged blood circulation to 10 nm for miR-21i release and complete urinary excretion, surface charge conversion from + 30 mV for miR-21i loading and HA coating to – 26.1 mV for the prevention of serum protein adsorption, HA surface coating for HA receptor-mediated endocytosis, positive charged PEI moieties for rapid endosomal escape, and DOX chemical conjugation for tracing the delivery course. This nano-drug system results in 4.4-fold higher anticancer effects on breast cancer cell line MDA-MB-231 than free DOX. It also demonstrates biocompatibility with kidney cell line HEK293T, as opposed to severe cytotoxic free DOX.

Biocompatible co-delivery systems was further developed by improving DOX loading by conjugation through a dual hydrazone and diselenide lock together with miR-21i and HA loading through electrostatic interaction (PSeHD-SeSeP/miR-21i/HA). The dual-lock for DOX conjugation fully suppresses premature leakage under physiological conditions and promotes intensive DOX release in reductant cytosol of cancer cells. The PSeHD-SeSeP/miR-21i/HA also demonstrates a remarkable biocompatibility with HEK293T cells and a 3.2-fold increase in anticancer effects on the MDR cell line of MDA-MB-231-R12w compared with free DOX.

We further enhanced the anticancer effects on cancer cells with MDR together with real-time monitoring of DOX release by synthesizing traceable nanomedicines incorporated with DOX, miR-21i, HA, and ATP aptamer (Apt) (PSeSeD/miR-21i/Apt/HA). The microgels are synthesized in one pot with PEI800, DOX and diselenide crosslinkers to ensure microgel fully degraded and release all cargoes (DOX, miR-21i, and Apt) to cytosol. Apt administration in MDA-MB-231-R12w cells demonstrates ATP depletion, which hinders the role of ATP-binding cassette (ABC) transporters in exporting DOX across the cell membrane. The use of BHQ2 quenching technology enables the visualization of DOX release profiles. As opposed to the lack of intracellular DOX accumulation in the absence of Apt, the amount of DOX in the nucleus of the cells is monitored in the presence of Apt. With the aid of ABC transporter inhibition, PSeSeD/miR-21i/Apt/HA demonstrates a 4.2-fold higher anticancer effect on MDA-MB-231-R12w compared with free DOX and minimal side effects on an HEK293T cells.

Finally, we developed the strategy of sequential therapy of miR-21i and DOX by synthesizing intracellular stimuli-triggered co-delivery systems (PSeDEVDCD/miR-21i/HA) for maximal its anticancer effects. DOX conjugation to the systems via peptide linkers containing DEVDC moieties is cleaved by activated caspase-3 enzyme. miR-21i being loaded to the diselenide-crosslinked PEI microgels will be initially released into the cytosol by reducing crosslinkers, and thus reverses MDR of cancer cells. The ROS production from DOX can stimulate apoptotic

pathways for the activation of caspase-3 that cleaves DEVDC moieties of the peptide linker and triggers a burst release of DOX in the re-sensitized cells. PSeDEVDCD/miR-21i/HA resultantly demonstrates a 7.3-fold increase in anticancer effects on multidrug-resistant breast cancer cell line MDA-MB-231-R24w compared with free DOX and minimal adverse side effects on HEK293T cells.

In summary, combination therapy of DOX and sub-drugs (miR-21i or Apt) together with their sequential release protocol can effectively enhance therapeutic efficacy against multidrug-resistant cancer cells via the MDR reversal by inhibiting miR-21 or ABC transporters. The advent of smart intercellular microenvironment responsive crosslinkers or linkers renders to achieve controlled release drugs together with decreasing cytotoxicity and premature release. On the other hand, targeting delivery through surface HA coating further improves therapeutic efficiency and circulate stability.

7.2 Future directions

In this thesis, a series of novel multifunctional microgel-based delivery systems with multi-drugs of DOX, miR-21i and Apt have achieved DOX's maximal anticancer effects and minimal side effects, contributing to advanced design. The following guidelines may be potential to explore in the future:

Although the performance of the proposed co-delivery systems for anticancer effects and adverse side effects has been demonstrated *in vitro*, but furthermore, *in vivo* assessments of the delivery systems will provide more feasibility in clinical applications.

The proposed co-delivery systems selectively targets metastatic cancer cells to induce apoptosis, but the cancer cells can spread through cancer vasculature to other organs and interfere with comprehensive chemotherapy. The use of extracellular tumor enzyme-cleavable

peptide linkers will facilitate the connecting of different types of carriers in one system to deliver multiple drugs to different cancer targets, such as solid cancer and cancer vasculature for integrated cancer treatment.